η^8-Permethylpentalene Titanium Chemistry

by

Robert Thomas Cooper

A thesis submitted in part fulfilment of the requirements for the degree of Doctor of Philosophy at the University of Oxford

Lincoln College
Oxford

November 2012

The work described in this thesis was carried out in the Chemistry Research Laboratory, Mansfield Road, Oxford between October 2007 and November 2012 under the supervision of Professor Dermot O'Hare. All the work is my own unless stated to the contrary, and has not been previously submitted for any degree at this or any other university.

Robert Thomas Cooper

Lincoln College

November 2012

ABSTRACT

η^8-Permethylpentalene Titanium Chemistry

Robert Thomas Cooper **D.Phil Thesis**

Lincoln College **Michaelmas Term 2012**

The focus of this thesis is the synthesis of organometallic complexes incorporating the η^8-permethylpentalene titanium moiety (η^8-Pn*Ti), their characterisation, and their reactivity with small molecules. **Chapter One** summarises the chemistry of the pentalene molecule, from its instability in the free state to the incorporation of the hydrocarbon into organometallic complexes. The chapter continues with a review of the coordination modes available to Pn and concludes with a brief discussion on the effects of permethylation of hydrocarbon ligands and the advent of permethylpentalene (Pn*).

Chapter Two documents the improved synthesis of $[Pn^*TiCl(\mu\text{-}Cl)]_2$ utilising isomeric control imparted on the Pn* synthon, $Pn^*(SnMe_3)_2$. This protocol permits access to a variety of methylated compounds through metathesis chemistry, of which five have been crystallographically elucidated, revealing the fold angle to be reliant on an interplay between steric and electronic factors. Mono-, bi- and trimetallic {Pn^*TiMe_2, $[Pn^*TiMe(\mu\text{-}Cl)]_2$ and $[Pn^*Ti(\mu\text{-}Me)]_2(\mu\text{-}CH_2)$, and $[Pn^*TiMe(\mu\text{-}Me)_2]_2Mg$ respectively} species were synthesised dependent on the methylating agent employed and they displayed varying thermal stabilities, with the dimeric nature of $[Pn^*TiMe(\mu\text{-}Cl)]_2$ proving crucial in the formation of $[Pn^*Ti(\mu\text{-}Cl)]_2(\mu\text{-}CH_2)$.

Chapter Three describes the incorporation of classical organometallic ligands into the Pn*Ti moiety, including the first examples of benzyl, alkyl, aryl, allyl and η^1-Cp bound to a PnTi fragment. Seven complexes have been structurally characterised including the first ever crystal structure of a π-hydrocarbon bound Ti species bearing two $CH_2{}^tBu$ groups, $Pn^*Ti(CH_2{}^tBu)_2$, and the fluxional mixed hapticity complex $Pn^*Ti(\eta^5\text{-}Cp)(\eta^1\text{-}Cp)$, whose η^1-Cp rearranges *via* a 1,2-sigmatropic shift.

Chapter Four investigates the reactivity of the monomeric dialkyls, Pn^*TiR_2 (R = Me, CH_2Ph, CH_2SiMe_3 and $CH_2{}^tBu$) with CO_2, CO and H_2. All four compounds demonstrate "normal" insertion of the CO_2 moiety into both Ti-R bonds, revealing a symmetrical bidentate coordination of the RCO_2 units. Computational studies have highlighted two competing pathways for their reaction with CO, dependent on the concentration of CO and size of R, which results either in formation of an enediolate or a titanoxirane. The reaction with H_2 yields the fascinating trimeric mixed valence, $[Pn^*Ti(\mu_2\text{-}H)]_3(\mu_3\text{-}H)$, the first structurally characterised example of a trimeric Ti-H species and the first to include a Ti-(μ_3-H) moiety. $(Pn^*TiCl)_2(\mu\text{-}O)$ is formed by the action of adventitious H_2O and possesses a linear Ti-O-Ti bridge with a degree of Ti-O double bond character, supported by crystallographic data and DFT calculations.

Chapter Five discusses ethylene polymerisation studies on the monomeric dialkyl complexes Pn^*TiR_2 (R = Me, CH_2Ph, CH_2SiMe_3 and $CH_2{}^tBu$) using the activators $[Ph_3C][B(C_6F_5)_4]$, $[PhNMe_2H][B(C_6F_5)_4]$, Al^iBu_3 and H_2.

Chapter Six presents full experimental procedures for all of the syntheses and reactions outlined in Chapters Two to Five. **Chapter Seven** details characterising data for all novel compounds, and crystallographic data in the form of CIF files may be found in the electronic **Appendix**, found on the compact disc at the back of this thesis.

ACKNOWLEDGEMENTS

First of all I would like to thank Dermot for all of his help and support throughout my time in his group. Thanks must also go to Dr. Nick Rees for the modelling of NMR data, Dr. Muhsen Al-Ibadi for running the DFT calculations and Colin Sparrow for running mass spectrometry.

I am hugely indebted to Dr. Ashley for his guidance, support, help and friendship. I must also thank Mark 'crystal' Chadwick, for taking his time to run scores of my crystals and Tom, for all of his meticulous proof reading.

Thanks must also go to group members, past and present, including my fellow DPhil and running partner Mr Moorhouse, I'm looking forward to discussing your thesis on our outings, Sam for the emergency laptop loan, Henry for the 'rum-gins', and everyone else for making my time so enjoyable. Paul, Paulina, Gowrie and Yi, you haven't been forgotten.

A mention should also to go to Dr. Cushion, for his defection from the Mountford group and numerous comical nights in the PT, and also to the friends and housemates that I've known throughout this time. I'd like to thank my family for their constant support and vague interest in my work, and yes this does mean I'm no longer a student!

Last but by no means least I'd like to thank T, for all your support throughout this process. It's been one hell of an achievement for team C&T and many more will follow x.

Table of Contents

CHAPTER ONE: Introduction

CHAPTER TWO: Synthesis of Permethylpentalene Titanium-Methyl Derivatives

CHAPTER THREE: Synthesis of Permethylpentalene Titanium Complexes

CHAPTER FOUR: Reactivity Studies of Novel Permthypentalene Titanium Dialkyls with Small Molecules

CHAPTER SEVEN: Characterising Data

APPENDIX: Crystal Data (.CIF files on attached CD)

RTC2_2	Crystal data for **2.2**
RTC2_3	Crystal data for **2.3**
RTC2_4	Crystal data for **2.4**
RTC2_5	Crystal data for **2.5**
RTC2_7	Crystal data for **2.7**
RTC3_1	Crystal data for **3.1**
RTC3_2	Crystal data for **3.2**
RTC3_3	Crystal data for **3.3**
RTC3_4	Crystal data for **3.4**
RTC3_5	Crystal data for **3.5**
RTC3_6	Crystal data for **3.6**
RTC3_7	Crystal data for **3.7**
RTC4_1	Crystal data for **4.1**
RTC4_2	Crystal data for **4.2**
RTC4_3	Crystal data for **4.3**
RTC4_5	Crystal data for **4.5**
RTC4_7	Crystal data for **4.7**
RTC4_8	Crystal data for **4.8**
RTC4_9	Crystal data for **4.9**

Abbreviations

Å	Ångstrom
Ac	Acetyl (CH_3CO)
acac	Acetylacetonate
Br	Broad
^{n}Bu	*n*-Butyl
^{t}Bu	*tert*-Butyl
°C	Degrees Celsius
cm^{-1}	Wavenumber
$^{13}C\{^{1}H\}$	Proton Decoupled ^{13}C
CH_2Cl_2	Dichloromethane
COD	Cycloocta-1,4-diene
COSY	Correlated Spectroscopy
COT	Cyclooctatetraene
Cp	Cyclopentadienyl
Cp*	Pentamethylcyclopentadienyl
Cent	Centroid
CSD	Cambridge Structural Database
d	Doublet
DFT	Density Functional Theory
DME (DEE)	1,2-Dimethoxyethane (-Diethoxyethane)
DMF	Dimethylformamide
DMSO	Dimethyl Sulphoxide
EI	Electron Impact
ESD	Estimated Standard Deviation
Et	Ethyl
Et_2O	Diethyl Ether
g	Gram(s)
GC	Gas Chromatography
GPC	Gel-Permeation Chromatography
HMBC	Heteronuclear Multiple Bond Correlation
HMQC	Heteronuclear Multiple Quantum Coherence
Hz	Hertz
^{i}Pr	*iso*-Propyl
IR	Infrared
m	Multiplet (NMR); Medium (IR)
MAO	Methylaluminoxane
Me	Methyl
MHz	Megahertz
MO	Molecular Orbital
MS	Mass Spectrometry
NMR	Nuclear Magnetic Resonance
NOESY	Nuclear Overhauser Effect Spectroscopy
NWT	Non-wingtip

Abbreviations (continued)

PE	Polyethylene
Ph	Phenyl
Pn	Pentalene
Pn*	Hexamethylpentalene
Ppm	Parts Per Million
Q	Quartet
RT	Room Temperature
s	Singlet (NMR); Strong (IR)
t	Triplet
THF	Tetrahydrofuran
TMEDA	N,N,N’,N’-Tetramethylethylenediamine
vs.	Versus
VT	Variable temperature
WT	Wingtip
°	Degrees

Chapter One

Introduction

1.1 Overview

This thesis constitutes a study of the synthesis and characterisation of η^8-permethylpentalene titanium complexes, along with an investigation into their reactivity with small molecules. The first section of this chapter introduces pentalene as a molecule and details the diverse bonding modes available to this fascinating ligand with a review of metal complexes that have previously been documented, organised by increasing hapticity. The remainder of the introduction focuses on the effects of permethylation of hydrocarbon ligands in organometallic chemistry including the advent and subsequent chemistry of permethylpentalene.

1.2 Pentalene as an organic molecule

Pentalene [C_8H_6, Pn; Figure 1.1 (a)], is an unsaturated hydrocarbon, which can be related to cyclooctatetraene (COT) by transannular 'pinching' across the eight-membered ring, or to cyclopentadiene (Cp) by the edge-sharing ring-fusion of two cyclopentadienyl fragments.[1] The molecule itself is of fundamental interest with regard to the aromaticity of non-alternant unsaturated systems; it was first mentioned in 1922 and was postulated to be an aromatic system[2] with a delocalisation energy as high as 170 kJ mol^{-1} (the value estimated for benzene is 150 kJ mol^{-1}).[3] Initial efforts towards pentalene synthesis were unsuccessful,[4] for example the attempted platinum induced dehydrogenation of bicyclo[3.3.0]octane did not afford pentalene although naphthalene is formed upon similar treatment of decalin.[5] 1-Methylpentalene was generated by thermolysis of a complex fulvene system and was found to be very unstable, reacting rapidly at −196 °C to give [2+2] dimers [one isomer is shown as (a) in Figure 1.2].[6] A dibenzannulated pentalene was also found to be very reactive, polymerising readily at room temperature and UV-visible spectroscopy indicated this molecule has a non-delocalised, conjugated diene-like electronic structure.[7]

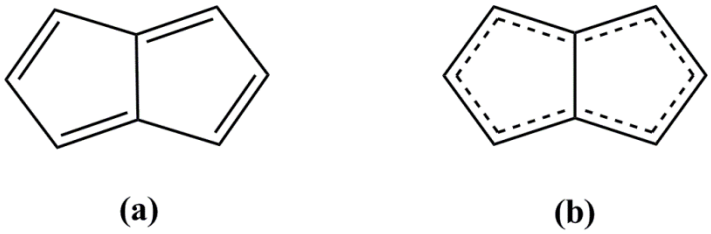

(a) **(b)**

Figure 1.1: The (a) C_{2h} and (b) D_{2h} structures of the pentalene molecule.

Calculations on pentalene itself suggest the molecule has a bond-alternant, C_{2h} structure [rather than the delocalised, D_{2h}-symmetric possibility, Figure 1.1 (b)] as the result of a pseudo Jahn-Teller effect;[8, 9] however, pentalene in now commonly considered an 8π-Hückel *anti*-aromatic system.[10, 11] Unsubstituted pentalene was finally synthesised in 1973 by Hafner *et al.*;[12] like the 1-methyl analogue it is unstable with respect to dimerisation. Relatively recently, the monomer has been studied in an Ar/N_2 matrix (formed by photocleavage of the parent dimer).[13] Data obtained through UV-visible and IR experiments confirm the predicted C_{2h} structure, ascribed to influence of the antiaromatic π-system on the molecular geometry. Furthermore, the study also showed that the photocleavage proceeds in a stepwise fashion, presumably *via* a bis(vinylcyclopentadienyl) biradical. These results clearly highlight the hurdle faced by early organic chemists; Pn was indeed far too unstable an entity to obtain using conventional techniques. The monocyclic analogue, cyclooctatetrene, is also an 8π system and therefore should suffer from the same instability bestowed upon Pn, yet it is a relatively stable liquid at room temperature. However, the molecule is able to adopt a 'tub-shaped' geometry[14] [Figure 1.2 (b)], which distorts the network of electrons away from planarity and thus avoids antiaromaticity.[15] Pentalene cannot distort in this manner due to the constraints imposed by its central C-C bond, forcing the molecule to be planar and hence pentalene is more reactive, forming the [2+2] cycloadduct even at low temperature.

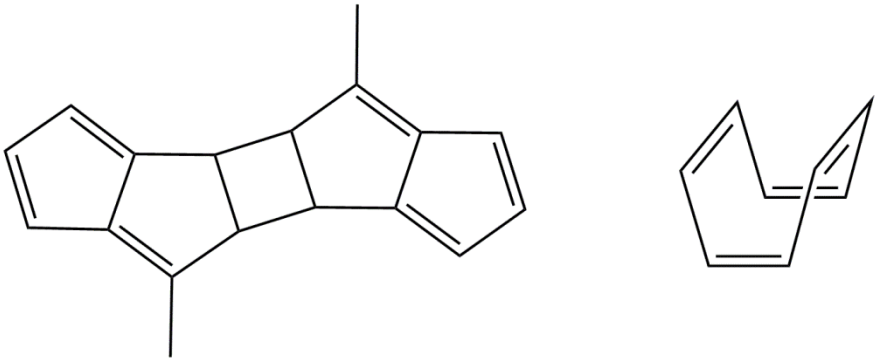

(a) **(b)**

Figure 1.2: (a) One isomer of the [2+2] dimer of 1-methylpentalene and (b) the 'tub' geometry of COT.

A variety of pentalenes have been synthesised that show greater longevity; these are stabilised either electronically [e.g. 1,3-bis(N,N-dimethylamino)pentalene,[16] Figure 1.3 (a)], sterically [by preventing dimerisation through the use of bulky substituents e.g. 1,3,5-tris-*tert*-butylpentalene,[17] Figure 1.3 (b)] or by both means [e.g. hexaphenylpenatalene,[18] Figure 1.3 (c)]. The latter was the first non ring-fused pentalene to have been made, using a Michael-Knoevenagel condensation between 1,2,3-triphenylcyclopentadiene and 1,2,3-triphenylpropenone followed by oxidation. Here, electronic delocalisation onto the aryls dissipates antiaromatic destabilisation in combination with the steric bulk of the Ph groups shielding the Pn nucleus from dimerisation. These bulky systems are often crystalline solids; X-ray crystallographic studies[19] of 1,3,5-tris-*tert*-butylpentalene and 1,2-bis(carboxymethyl)-4,6-bis(*tert*-butyl)pentalene, the first crystalographically characterised pentalenes, provide clear evidence for the bond-alternate structure calculated for the unsubstituted molecule. This is also suggested by the UV-visible spectra of these stabilised species.[20]

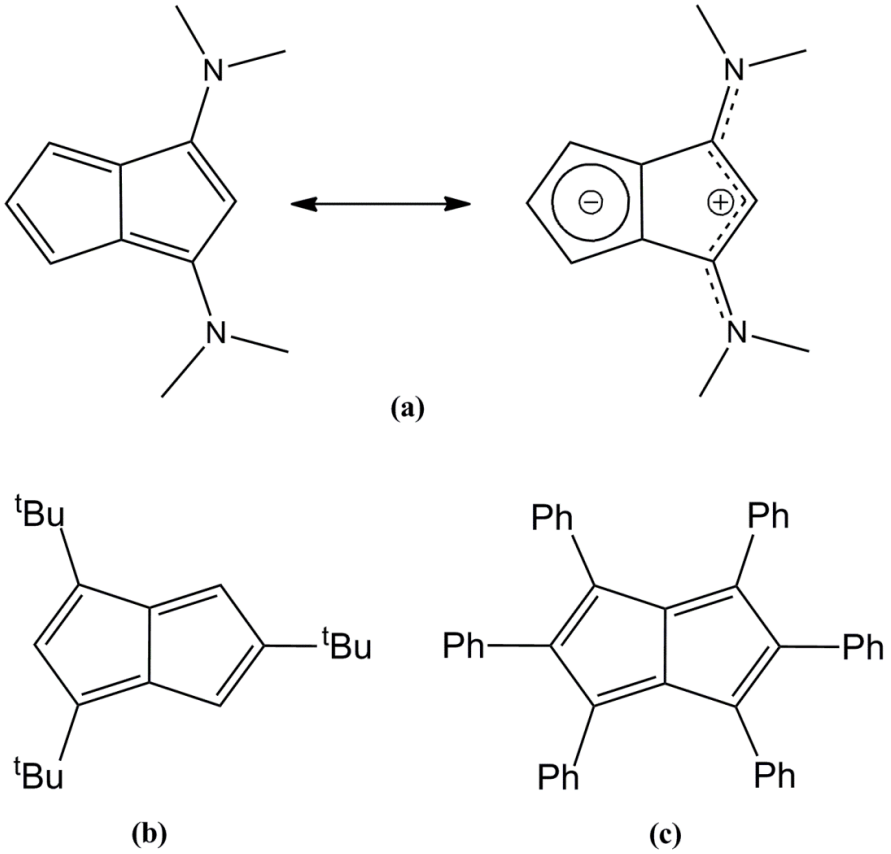

Figure 1.3: (a) Canonical forms of 1,3-bis(N,N-dimethylamino)pentalene demonstrating 'push-pull' stabilisation; (b) 1,3,5-tris-*tert*-butylpentalene and (c) hexaphenylpentalene.

Very recently a number of groups have employed Rh, Pd, Au and Li catalysts in the cyclisation of alkynes to good effect, forming a number of series of substituted, annulated and di-pentalene derivatives.[21–26] These exciting new routes have opened up the possibility of the selective formation of substituted pentalene derivatives that have thus far eluded synthetic chemists.

1.3 Pentalene as a ligand in organometallic complexes

While neutral pentalene is unstable, the formal two electron reduction product, Pn^{2-}, is a 10π-Hückel stable aromatic system that may be considered the lower homologue of naphthalene; indeed Pn^{2-} [Figure 1.4 (a)] is related to the Cp^{-} anion as naphthalene is to benzene. The isoelectronic cyclooctatetraene dianion may be formed from the reduction of COT;[27] this prompted Katz *et al.* to attempt the synthesis of the pentalene dianion as a route into the chemistry of the pentalene system.

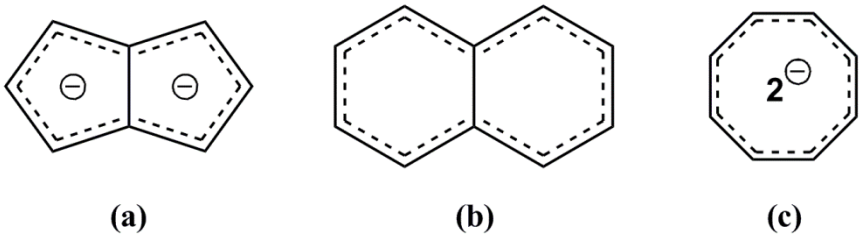

Figure 1.4: 10π-Hückel aromatic systems (a) pentalene dianion; (b) naphthalene and (c) COT dianion.

Due to the extreme thermolability of Pn, Katz's synthesis of Pn^{2-} proceeded not *via* direct reduction of pentalene but by the double deprotonation of dihydropentalenes,[28, 29] analogous to the formation of Cp^- from CpH. The reaction of ^nBuLi with PnH_2 in DME solvent resulted in the formation of $Pn[Li(DME)]_2$ as a crystalline solid, from which a structural characterisation could be made.[30] It demonstrates the dianionic pentalene system to be planar and of D_{2h} symmetry, with no significant bond length alternation between the carbon atoms; hence the dianion is a delocalised system as predicted by Hückel theory. The lithium ions are located on opposite faces of the ligand, each coordinated in a η^5- fashion, comparable to the geometry found in the crystal structure of the dilithum salt of naphthalene.[31] Photolysis of the dianion affords the pentalene radical anion,[32] which has been studied by EPR and the dilithium salt undergoes oxidation upon reaction with $CuCl_2$ to form a diasteromeric mixture of pentalene dimers discussed previously.[33, 13] Dihydropentalenes may also be singly deprotonated to give the hydropentalenyl anion as a 6π aromatic system delocalised around one half of the molecule, allowing the molecule to function, effectively as a substituted Cp^- anion.[34]

Transition metals are known to form stable organometallic complexes with organic molecules that are themselves unstable under normal conditions, for example cyclobutadiene,[35] trimethylenemethane[36] and heptafulvene.[37] These reactive organic groups may sometimes be removed from the metal and used in subsequent reactions, such as by oxidation with Ce^{4+}.[38] The origin of the use of pentalene as a ligand in organometallic chemistry can be traced to the attempts of Katz *et al.* to stabilise the molecule by coordination to transition metals. Organometallic pentalene chemistry remains relatively unexplored, chiefly due to difficulties in the synthesis of dihydropentalene precursors to the pentalene dianion, which is the starting material for the majority of metal-pentalene complexes.

1.4 Nomenclature

In this thesis, substituted pentalene ligands are written as $Pn^{n\text{-}R}$ where n is the position of substitution and R is the substituent. The numbering scheme for the pentalene ring is given below [Figure 1.5 (a)] hence, for example, 1,3,5-tris(trimethylsilyl)pentalene [Figure 1.5 (b)] is abbreviated $Pn^{1,3,5\text{-}(SiMe_3)}$.

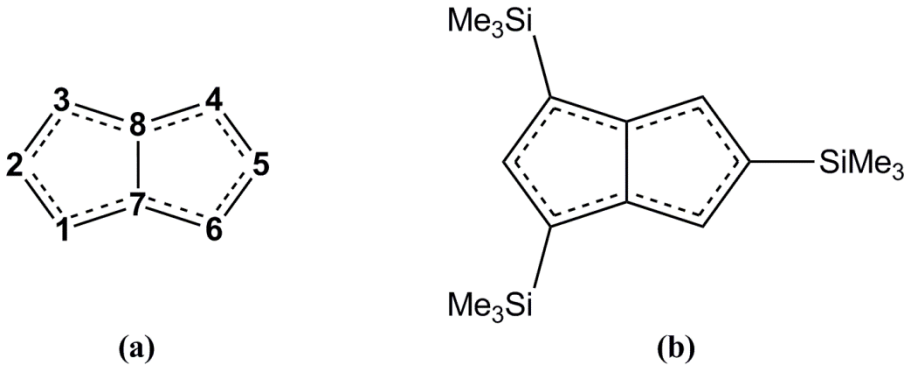

Figure 1.5: Nomenclature for substituted pentalene ligands.

The carbon atoms 7 and 8 are referred to as the 'bridgehead' carbons, 2 and 5 as the 'wingtip' (WT) carbons and lastly 1, 3, 4 and 6 as the 'non-wingtip' (NWT) carbons. The coordination mode of a ligand is specified where there is possible ambiguity; cyclopentadienyl and substituted Cp ligands are assumed to be bound in an η^5-manner unless specified otherwise. Similarly, all pentalene complexes referred to from Chapter Two are assumed to be bound in an η^8-fashion unless otherwise stated.

1.5 Coordination modes of pentalene

If regarded as a neutral moiety, pentalene has up to eight electrons available for donation towards a single metal centre in an organometallic complex,[39] bonding through the π-orbitals of the ring in an analogous fashion to cyclopentadiene, arenes and other conjugated ligands (considered as a dianion Pn^{2-} is a ten electron ligand, as Cp^- is a six electron donor). Only 'covalent' organometallic pentalene complexes are considered here; lithium and potassium salts of the dianion are presumed to have ionic, carbanion-like character and are only mentioned as a source of 'Pn^{2-}' in synthesis.

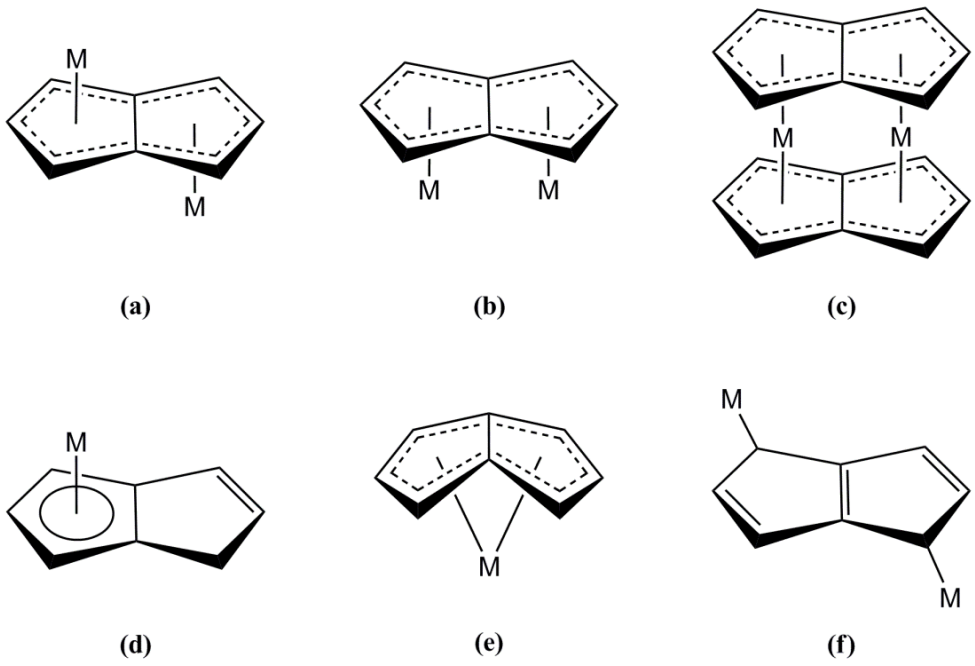

Figure 1.6: Known coordination modes of the pentalene ring system.

Pentalene offers a wide variety of coordination modes[40] – it can form bimetallic species with either an *anti*- or *syn*-disposition [Figure 1.6 (a) and (b) respectively], where the metals are bound in an η^5-type fashion to each ring of the bicyclic system. This allows the ligand to act as a bridging platform that can facilitate the possibility of electronic communication between the metal centres. In order to satisfy electron counting and coordinative saturation of the metal centres, auxiliary ligands are usually attached. In the *syn* case, this may be by an additional pentalene molecule, thus forming a homoleptic 'double-sandwich' structure [Figure 1.6 (c)]. Analogous to the metallocenes of the cyclopentadienyls, this 'double-sandwich' structure can be regarded as a ring-fused derivative between two of these monomers. A 'ring slippage' from these geometries may also lead to a favoured η^3-cordination over η^5, akin to an 'ene-allyl' distortion seen in indenyl and other Cp complexes,[41, 42] and combinations of these types can be envisaged for heterobimetallics, where the metals can have differing modes of coordination to each ring. The possibilities are not restricted to dinuclear species as the hydropentalenyl ligand (PnH^-) [Figure 1.6 (d)], formed from the mono-deprotonation of PnH_2, can form mononuclear complexes that may be regarded as functionalised Cp derivatives. Nor is this flexibility restricted to η^5-coordination, as all eight atoms may coordinate to a single metal centre in an η^8-mode [Figure 1.6 (d)], with strong folding about the bridgehead bond, resulting in the ligand effectively capping an entire face of

the metals coordination sphere. All of these binding modes (and others) have been observed for organometallic pentalene species and will be reviewed in the following sections. The diametric extreme to η^8-coordination, and arguably the simplest mode, is η^1-bonding where metals are bound in an η^1-'alkyl-like' fashion, and these will be considered first.

1.5.1 η^1-coordinated pentalene complexes

Stannylated pentalene derivatives have been prepared from the deprotonation of dihydropentalene with either one or two equivalents of $Sn(NEt_2)Me_3$ yielding the mono and bimetallic species, $(SnMe_3)PnH$ and $(SnMe_3)_2Pn$ respectively.[43, 44] The metals are bound in a η^1-fashion *via* a σ-bond to the pentalene molecule and the solid state structure of *anti*-$(SnMe_3)_2(\eta^1{:}\eta^1\text{-Pn})$ reveals isolated single and double bonds within the pentalene framework. η^1-'alkyl-like' coordination of Sn is typical for Sn^{IV} organometallics[45] and the molecule is fluxional with the $SnMe_3$ groups undergoing rapid [1,5]-sigmatropic shifts around the rings periphery as shown by NMR spectroscopy (this behaviour is commonplace for Sn^{IV} species bound to an unsaturated carbocyclic ring system).[45] However, the $SnMe_3$ fragments do not bind to the bridgehead atoms and consequently cannot 'cross over' to an adjacent five-membered ring. A *syn*-isomer is also co-produced in the synthesis but has not been crystallographically characterised.

1.5.2 η^3-coordinated pentalene complexes

The first transition metal pentalene complex to be structurally elucidated by single crystal X-ray diffraction was $[Ni(\eta^3\text{-allyl})]_2Pn$ reported by Miyake and Kanai in 1971 from the reaction of $[Ni(\eta^3\text{-allyl})Cl]_2$ and Li_2Pn.[46] The structure shows an *anti*-disposition of $Ni(\eta^3\text{-allyl})$ units with considerably longer Ni-C bridgehead distances compared to the remainder, consistent with an 'allyl-like' $(\mu{:}\eta^3{:}\eta^3\text{-Pn})$ bonding description (Figure 1.7). This would give each metal an electron count of 16, which is rational given that $Ni(\eta^3\text{-allyl})_2$ is known to be a stable entity.[47] $[Cr(\eta^3\text{-allyl})]_2Pn$ and $[Zr(\eta^3\text{-allyl})]_3Pn$ were also reported in the same publication but with limiting characterising data; the former was shown to be paramagnetic and data indicate a *trans*-geometry of the metals. Both were found to decompose above −20 and −10 °C respectively.

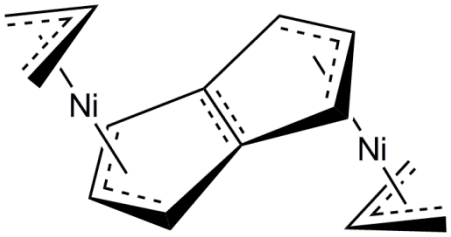

Figure 1.7: anti-[Ni(η^3-allyl)]$_2$(μ:η^3:η^3-Pn).

One of the first homoleptic metal pentalene species to be synthesised was Ni_2Pn_2 by Katz *et al.* with the reaction of Li_2Pn and either $NiCl_2$·DME or $NiCp_2$, albeit in very low yield (4%).[48] The sandwich compound is analogous to a 'double' parent metallocene. However, in contrast to the monomer, Ni_2Pn_2 was found to be diamagnetic, whereas $NiCp_2$ (S = 1) is paramagnetic. NMR studies demonstrated D_{2h} symmetry in solution, although no structural characterisation has been undertaken and initial analysis predicted a π-allyl-π-cyclopentadienyl structure in order for Ni to obtain an 18 electron configuration, although this was thought to be too strained. Much later a bis(η^3-allyl) coordination to the pentalenes was postulated by Burdett and Canadell, who carried out extended Hückel type calculations for the M_2Pn_2 complexes (M = Co and Ni).[49] Calculations revealed the overlap population of the metal atom with the bridgehead atoms of the pentalene to be very small while the values for the exterior atoms were considerable. Further evidence was obtained fortuitously through the structure determination of its permethylated analogue $Ni_2Pn^*_2$ synthesised by O'Hare *et al.*, which was confirmed as possessing a $Ni_2(\mu:\eta^3:\eta^3\text{-}Pn^*)_2$ bonding motif.[50] Care must be taken, as such a description camouflages the fact that the two 'allyl' units are intimately linked electronically.[49]

1.5.3 η^5-coordinated pentalene complexes

1.5.3.1 Monometallic η^5-Pn complexes

The main source of monometallic η^5-Pn coordination complexes are derived from the hydropentalenyl ligand (PnH^-), formed by the deprotonation of PnH_2, however, this was not the source for the pioneering M-PnH species. Mn(η^5-PnH)$(CO)_3$ was formed in 1960 by the cyclotetramerisation of acetylene with $Mn_2(CO)_{10}$.[51, 52] It was shown that the isolated double bond may be hydrogenated with H_2 to give the corresponding trihydropentalenyl species containing three methylene groups in the

uncoordinated ring.[52] A rational synthesis was later achieved in this laboratory from the salt metathesis reaction of $Mn(CO)_3(pyr)_2Br$ with TlPnH.[53] The Re congener [$Re(\eta^5$-PnH$)(CO)_3$] was formed in an analogous manner by the reaction of $[Re(CO)_3(THF)Br]_2$ with two equivalents of TlPnH in 60% yield and the η^5-coordination was confirmed by X-ray diffraction.[54] In addition to this, a corresponding Re trihydropentalenyl species was formed by the transannular dehydrogenation of 1,3- or 1,5-COD on combination with $Re_2(CO)_{10}$, whose coordination was again confirmed by X-ray diffraction.[55] Jones has also formed the alkylated hydropentalenyl analogue [$Re(\eta^5$-$Pn^{Me}H)(CO)_3$] in an analogous manner from the $TlPn^{Me}H$ salts.[54] ^{1}H NMR spectroscopy reveals the compound to exist as a mixture of isomers, similar to the Tl starting material, which differed in the position of the Me group relative to the C=C bond in the uncoordinated ring ($Pn^{1\text{-}Me}H$ or $Pn^{3\text{-}Me}H$).

The first rational synthesis of hydropentalenyl complexes was reported by Katz *et al.* who used LiPnH in combination with $FeCl_2$ to produce the ferrocene equivalent $Fe(\eta^5$-PnH$)_2$.[29, 34] The structure was initially assigned because of its similarities to NMR data for ferrocene. The presence of two allylic proton peaks suggested that diasteromers were present, which was later confirmed by X-ray crystallography and revealed a 50:50 mixture of isomers in the crystal, dependant on the relative positions of the double bonds.[56] Reaction of LiPnH with 'half-sandwich' precursors Fe(Cp*)(acac) and $[Ru(Cp^*)Cl]_4$ gave the mixed ring complexes M(η^5-PnH)(Cp*) [M = Fe and Ru, Figure 1.8 (a)].[57, 58] These species are useful in the construction of higher order metallocene oligomers or polymers due to the possible deprotonation of the pendant allylic groups in the uncoordinated ring. Indeed, deprotonation of $Fe(\eta^5$-PnH$)_2$ with either one equivalent of ^{n}BuLi or several of ^{t}BuLi, leads to the formation of ferrocenyl anion Li[$Fe(\eta^5$-PnH$)(\eta^5$-Pn$)$] or the dianion $Li_2[Fe(\eta^5$-Pn$)_2]$ respectively.[34] These are valuable monomer building blocks for extended polymetallic arrays and will be discussed further in Section 1.5.3.3.

The aforementioned PnH^- transfer reagent, TlPnH, precipitates from the reaction of Tl_2SO_4 with $NaOH_{(aq)}$ and PnH_2.[59] The decreased basicity of the *in situ* formed TlOH compared to organolithium reagents ensures only mono deprotonation is effected and benefits include increased stability to oxygen and moisture. It was subsequently used in the synthesis of Rh(η^5-PnH)(η^4-COD) [Figure 1.8 (b)] and Pt(η^5-PnH)Me_3 by salt

elimination reactions with $[Rh(\eta^4\text{-COD})Cl]_2$ and $PtMe_3I$ respectively,[59] with the latter being the only platinum pentalene complex known.

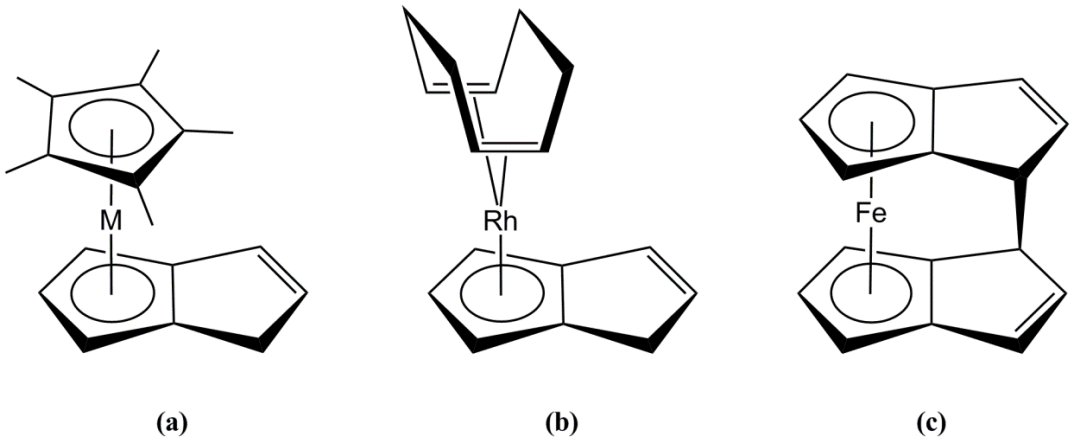

Figure 1.8: Monometallic η^5-pentalene complexes (a) mixed ring hydropentalenyl complexes (M = Fe and Ru); (b) $Rh(\eta^5\text{-PnH})(\eta^4\text{-COD})$ and (c) bis(pentalenyl)iron.

In an attempt to parallel results already observed for Ni[48] and Co[60] (*vide infra*), Katz *et al.* found the reaction of Li_2Pn with one equivalent of $FeCl_2$ does not give the target bimetallic sandwich compound, but instead affords a compound, in which only one iron atom is present, coordinated to two pentalene rings.[60] NMR spectroscopy and X-ray diffraction[61] show the structure to be ferrocene-like with a C-C between the uncoordinated pentalene rings giving a C_2-symmetric molecule [Figure 1.8 (c)]; calculations suggest that the bimetallic sandwich structure is unstable when M = Fe.[49]

Jonas *et al.* have described the existence of another coordination mode for pentalene mononuclear complexes. In this geometry, the ligand is bound through only five of the eight carbon atoms to the metal centre, leaving an uncoordinated 'naked' allyl anion on the remainder.[62–64] A number of known examples have a formal positive charge on the metal centre aiding stabilisation, and resulting in the novel zwitterionic structure. An isostructural series of these compounds may be synthesised from $[M(Cp^*)Cl_2]_2$ (M = Cr, Co and Rh) and Li_2Pn [Figure 1.9 (a)]. η^8-coordinate precursors can also react to form this bonding mode, exemplified by the double nucleophilic addition of MeLi to the bis-homoleptic $Zr(\eta^8\text{-Pn})_2$, which forms the dianionic complex $Li_2[Zr(\eta^5\text{-Pn})_2Me_2]$ [Figure 1.9 (b)], which may be reacted with $[NH^nBu_3]^+Cl^-$ to form the hydropentalenyl complex $Zr(\eta^5\text{-PnH})_2Cl_2$. The zwitterionic molecules display interesting chemistry, with investigations into $Co(Cp^*)(\eta^5\text{-Pn})$ demonstrating their

ability to 1,3,4,6-tetra substitute the pentalene ring before removing CoCp* in the form of its η^4-COD adduct, *via* the addition of 1,5-COD/Li, permitting isolation of the dilithium salts of the substituted pentalenes. These salts can then be used in synthesis, which leads to the structural elucidation of the highly alkylated Zr(η^8-Pn')(η^8-Pn'') (Pn' = Pn'' = $Pn^{1,3,4,6\text{-}Me}$; Pn' = $Pn^{1,3,4,6\text{-}Me}$, Pn'' = $Pn^{1,3\text{-}Me}$ or $Pn^{1,3\text{-}iPr}$), exhibiting D_2 symmetry of the molecules.

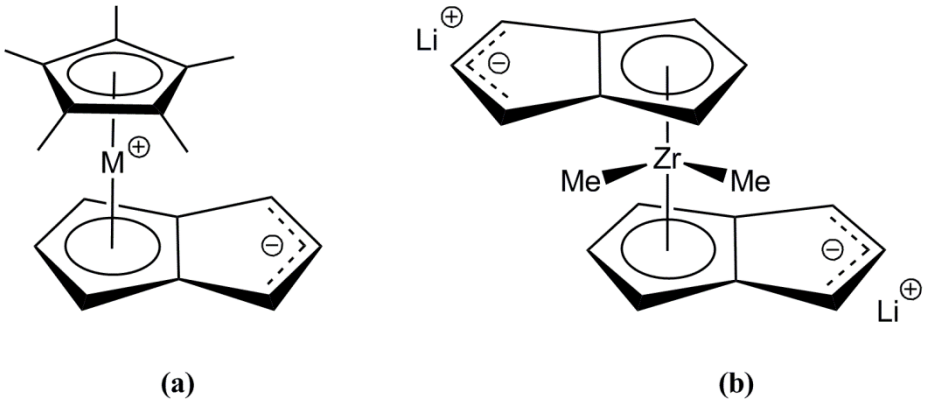

Figure 1.9: Monometallic η^5-pentalene complexes (a) Zwitterionic η^5-coordinated pentalene species (M = Cr, Co and Rh) and (b) the dianion adduct of MeLi and Zr(η^8-Pn)$_2$.

1.5.3.2 Bimetallic η^5-Pn complexes

Manriquez *et al.* have reported a series of homo- and hetero-bimetallic pentalene complexes [M(Cp*)](μ:η^5:η^5-Pn)[M'(Cp*)] (M = M' = Fe, Co, Ni, Ru; M = Fe, M' = Co, Ru) by reaction of Li_2Pn or Li[Fe(η^5-Pn)(Cp*)] with a 'half-sandwich' source of the metal atom.[65, 66] The homobimetallics of Fe and Co have been structurally characterised and have an *anti*-arrangement of MCp* units, revealing a planar pentalene ring system with no bond-alternation evident. The Fe analogue reveals a distortion from an ideal η^5-coordination of the pentalene ligand, which may be due to the symmetry of the pentalene π orbital contributions.[40] The ability of the pentalene ligand to promote spin-spin interactions is demonstrated by the homonuclear complexes M = Co, Ni which are diamagnetic; the 'parent' metallocenes MCp_2, however are paramagnetic with one and two unpaired electrons respectively.[45] A variety of techniques have been used to determine the extent of electronic delocalisation in their mixed-valent forms; Mössbauer spectroscopy of the iron monocations shows valence-averaged Fe environments down to 1.5 K and all homonuclear species exhibit two oxidation processes in their electrochemistry. For the first row metals these exhibit very large $\Delta E_{1/2}$ values (between

460 and 1000 mV, indicative of extremely strong metal-metal electronic coupling mediated by the ligand). However, the existence of complicating factors, such as solvent and counterion effects inherent with the technique, suggest that these values should be used with caution.[40]

Cloke *et al.* have synthesised lanthanide analogues of Manriquez's *anti*-$[M(Cp^*)]_2(\mu{:}\eta^5{:}\eta^5\text{-Pn})$, using the silylated pentalene derivative, $Pn^{1,4\text{-}Si^iPr_3}$.[67] The one pot reaction involving $MI_2(THF)_x$ and KCp* followed by half an equivalent of $K_2Pn^{1,4\text{-}Si^iPr_3}$ afforded $[M(Cp^*)(THF)]_2(\mu{:}\eta^5{:}\eta^5\text{-}Pn^{1,4\text{-}Si^iPr_3})$ (M = Eu and Yb) [Figure 1.10 (a)] in 27% and 34% yields respectively.[68] The complexes displayed poor solubility in a variety of solvents and while they could not be desolvated even at 180 °C/10^{-6} mbar, they were found to be stable under these conditions. X-ray diffraction studies reveal an anti-arrangement of divalent lanthanide centres across a planar pentalene with the metal centres slipped towards the WT-carbons analogous to their transition metal analogues.[65] Electronic spectroscopy revealed a smaller f-d band gap in comparison with their COT analogues and suggests a greater degree of through ligand metal-metal interaction for the pentalene complexes.

O'Hare and co-workers have prepared the double cymantrene and cyrhetrene analogues for pentalene. The binuclear pentalene equivalents, *anti*-$[M(CO)_3]_2(\mu{:}\eta^5{,}\eta^5\text{-Pn})$ (M = Mn, Re) [Figure 1.10 (b)], have been synthesised by the combination of either $Mn(CO)_3(pyr)_2Br$ or $[Re(CO)_3(THF)Br]_2$ and Li_2Pn in the correct stoichiometric ratio.[53, 69] Crystallographic data confirm an *anti*-arrangement and an isomorphous nature, with the pentalene ligand essentially planar, as seen for other *anti*-bimetallic species reported previously. The Mn bimetallic may be chemically and electrochemically reduced; the latter displays two quasi-reversible events, separated by 410 mV, exemplifying the stabilising effects of the bridging ligand upon the reduced forms. The former permits isolation of both the green mono-anionic salt, and was achieved using $Fe(Cp)(\eta^6\text{-}C_6Me_6)$ as the reductant, and the purple dianion as its dipotassium salt using KC_8. Both are extremely air sensitive solids with rapid oxidation to the neutral species observed upon exposure to air. The IR spectra and UV-Vis-NIR show that the mixed-valence species exhibits extremely strong electronic delocalisation, belonging to Class III in the Robin-Day classification, which corresponds to two completely equivalent $Mn^{0.5}$ centres. The value calculated for electronic coupling between the metals, 6400 cm^{-1} is

the largest reported value for a hydrocarbon-bridged bimetallic mixed-valence species, approaching those seen for delocalised Class III organic radical cations, claimed to be the most delocalised mixed-valence systems known. Mono-alkylated pentalene derivatives of the Mn homobimetallic, substituted in the 1-position (R = Me, Et, ^{i}Pr),[54] have also been made, along with the heteronuclear bimetallic, *anti*-$[Mn(CO)_3][Re(CO)_3](\mu{:}\eta^5{:}\eta^5\text{-Pn})$, from the reaction of half an equivalent of $[Re(CO)_3(THF)Br]_2$ with $Li[Mn(CO)_3(\eta^5\text{-Pn})]$ (formed *via* the combination of $Mn(CO)_3(\eta^5\text{-PnH})$ and Li^{t}Bu).

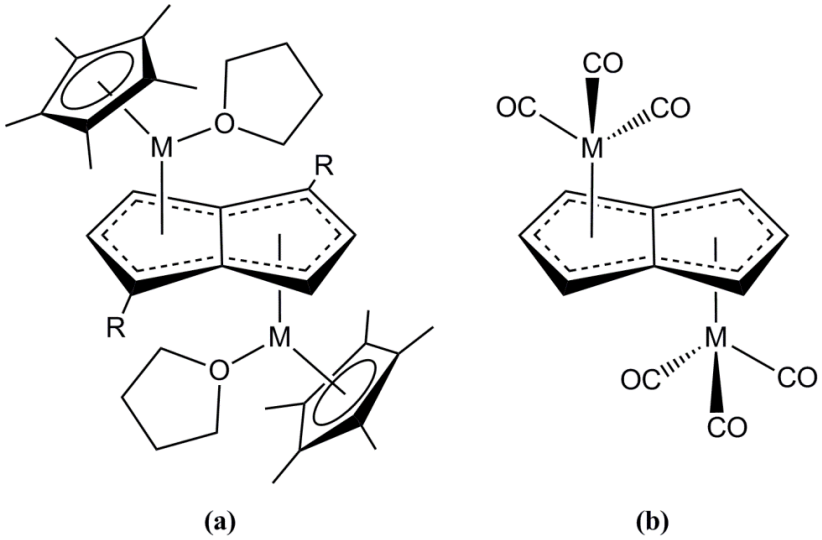

Figure 1.10: *anti*-Bimetallic $\mu{:}\eta^5{:}\eta^5$-pentalene complexes (a) $[M(Cp^*)(THF)]_2Pn^{1,4\text{-}Si^iPr_3}$ (M = Eu and Yb) and (b) $[M(CO)_3]_2Pn$ (M = Mn and Re).

The isomer, *syn*-$[Re(CO)_3]_2(\mu{:}\eta^5{:}\eta^5\text{-Pn})$ was simultaneously prepared under the same reaction conditions as the minor component, alongside *anti*-$[Re(CO)_3]_2(\mu{:}\eta^5{:}\eta^5\text{-Pn})$, mentioned above. Investigations revealed the *syn*:*anti* ratio to be inversely proportional to the temperature the reaction was conducted at, since it was found that the two isomers did not interconvert, even when heated to 100 °C. It was postulated that the *syn*-isomer was the kinetic product, which is thought to arise due to the dimeric nature of the Re starting material. The solid state structure reveals a non-planar pentalene ligand with a significant 'hinge-angle' (angle between the two five membered rings, 13.1°), away from the Re centres, which are at a distance greater than the value estimated for a metal-metal bond. The negligible overlap between the metal centres has been supported by DFT studies, which also calculates the energy difference between the *syn*- and *anti*-isomers to be 7 kJ mol^{-1}, in favour of the latter.

Similar *syn*-bimetallic pentalene complexes of Fe carbonyls have been prepared by Hunt and Russel *via* $Fe(CO)_5$-induced dehydrogenation of 1-phenyldihydropentalene[70] and 1-(N,N-dimethyl)aminodihydropentalene.[71] The unsubstituted Fe complex was synthesised by Weidemüller and Hafner through fission of the [2+2] dimer of neutral pentalene with $Fe_2(CO)_9$.[72] This parallels the initial discovery of unsubstitued cyclobutadiene by Pettit *et al.* by means of its complexation to an Fe tricarbonyl centre,[35] and is reminiscent of the procedure used to prepare $[Fe(Cp)(CO)_2]_2$ from the C-H activation of CpH using $Fe(CO)_5$.[73] The 1-methyl derivative is formed likewise, from the [2+2] dimer of 1-methylpentalene. All of these Fe carbonyl species show bridging and terminal CO absorptions in their IR spectra, and the metal carbonyl structure is thought to parallel that of the isoelectronic $Fe_2(CO)_5(\mu{:}\eta^5{:}\eta^5\text{-COT})$,[74] as shown in Figure 1.11 (a), although these structures have not been confirmed by X-ray diffraction.

The first structurally characterised *syn*-bimetallic was reported by Stone *et al.* in 1973, for *syn*-$[Ru(CO)_2(GeMe_3)]_2Pn$, where each Ru centre is η^5-coordinated by pentalene with a metal-metal bond between Ru atoms [Figure 1.11 (b)].[75, 76] It was formed by refluxing *cis*-$Ru(CO)_4(GeMe_3)_2$ with COT in heptanes, and was isolated in low yield (11%). An analogous trimethylsilyl complex was also obtained when $GeMe_3$ was exchanged for $SiMe_3$.[77] The pentalene ligand is non-planar, with a hinge-angle of 7° between the two five-membered rings as a result of complexation of two metal centres to the same face. This was the first example of a pentalene complex, formed *via* a dehydrogenative transannular ring closure of COT within the metals coordination sphere.[77] The mechanism of this pentalene forming reaction has been the subject of several studies,[78, 79] and the use of substituted COT ligands, C_8H_7R (R = Me, Ph and $SiMe_3$), has been exploited, affording substituted pentalene complexes.[78]

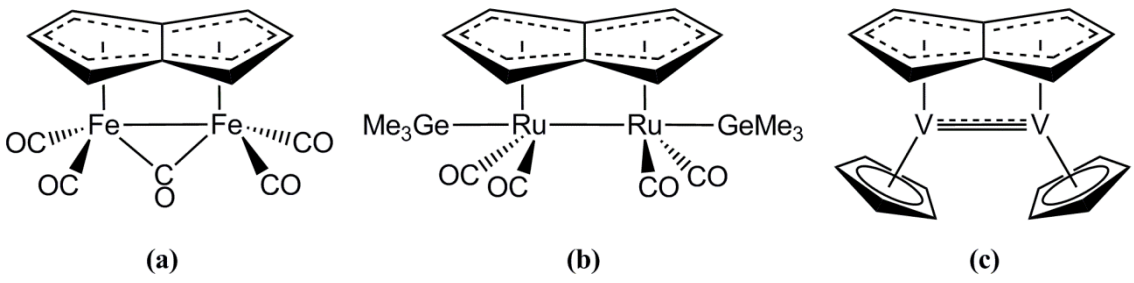

Figure 1.11: *syn*-Bimetallic $\mu{:}\eta^5{:}\eta^5$-pentalene complexes (a) $[Fe(CO)_2]_2(\mu\text{-CO})Pn$; (b) $[Ru(GeMe_3)(CO)_2]_2Pn$ and (c) $[VCp]_2Pn$.

The only example of *syn*-configuration of Cp-metal fragments to a pentalene moiety, is for the divanadium compound *syn*-$[V(Cp)]_2(\mu{:}\eta^5{:}\eta^5\text{-Pn})$ [Figure 1.11 (c)], reported by O'Hare *et al.* from the reaction of Li_2Pn and the 'half-sandwich' equivalent $[V(Cp)Cl(THF)]_n$.[80] X-ray diffraction studies reveal a vanadium-vanadium triple bond, similar to that found in the isoelectronic *syn*-$[V(Cp)]_2(\mu{:}\eta^5{:}\eta^5\text{-COT})$,[81] and DFT calculations supporting the experimental data show a $\sigma^2\pi^2\delta^2$ configuration. It was found to be weakly paramagnetic in solution and did not obey the Curie law, but instead could be successfully modelled as a spin-equilibrium between an S = 0 ground state and a thermally populated S = 1 excited state, shown by DFT to be a low-lying δ* orbital, whose occupation results in the anti-ferromagnetic coupling between electrons. The complex is unstable in solution and disproportionates to the known V^{III} compound $V(Cp)(\eta^8\text{-Pn})$ (*vide infra*), and other unidentified V-containing products. This compound demonstrates a rare example of a multiply bound V-V unit, compared to the plethora of examples in dichromium complexes.[82]

The first structurally characterised example of a bimetallic pentalene sandwich compound was $Mo_2(\mu{:}\eta^5{:}\eta^5\text{-}Pn^{1,4\text{-}Si^iPr_3})_2$, reported by Cloke and co-workers from the reaction of $K_2Pn^{1,4\text{-}Si^iPr_3}$ and $Mo_2(OAc)_4$;[83] X-ray crystallography revealed the bimetallic sandwich structure, with planar pentalene ligands and a staggered arrangement of the Si^iPr_3 substituents. This molecule is also diamagnetic with the Mo-Mo bond length found to be between the averages for double and quadruple Mo-Mo bonds. A simplified bonding description of the molecule is provided by the resonance forms shown in Figure 1.12, treating the complex as (a) an 18 electron doubly-bonded species or (b) a 16 electron quadruply-bonded molecule. Investigation by PES and DFT calculations suggests the bonding to resemble that of the simple metallocenes and gives a bond order between Mo atoms as 1.86.[84] Interestingly, the reaction affords two products that could not be separated by standard techniques, the characterised bimetallic sandwich species being isolated through degradation of the other product with oxygen-free water. NMR data of the crude reaction mixture suggests the other component to be an isomer, featuring each pentalene ring coordinated η^8- (*vide infra*) to one Mo centre only, with an unsupported Mo-Mo bond, to give an unusual 'dumbbell'-shaped molecule.

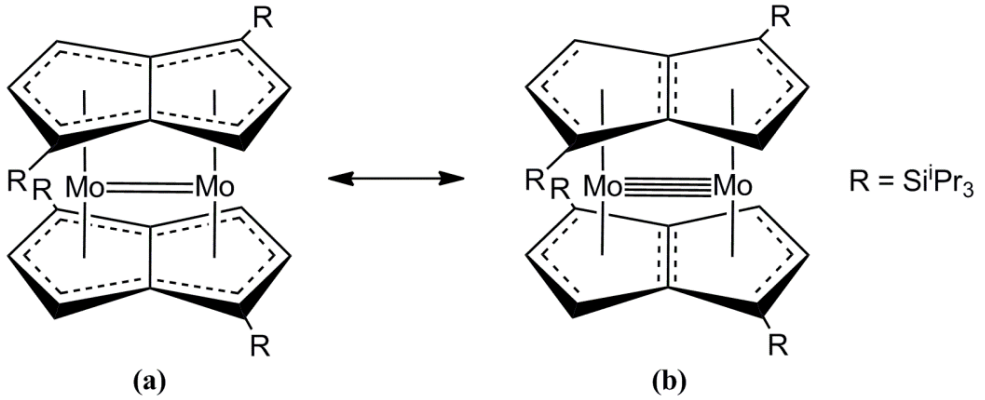

Figure 1.12: Resonance forms of $Mo_2(\mu{:}\eta^5{:}\eta^5\text{-}Pn^{1,4\text{-}Si^{i}Pr_3})_2$.

Synthesised in an analogous manner to its congener above, $Cr_2(\mu{:}\eta^5{:}\eta^5\text{-}Pn^{1,4\text{-}Si^{i}Pr_3})_2$ was formed as the sole organometallic product, as a paramagnetic species in 21% yield. Magnetic studies demonstrate the dimer to be consistent with two S = ½ centres interacting anti-ferromagnetically, with the bonding between the Cr centres best described as a double bond, with a calculated bond order of 1.67; this is in marked contrast to the rigorously diamagnetic Mo analogue. Similar $M_2(\mu{:}\eta^5{:}\eta^5\text{-}Pn^{1,4\text{-}Si^{i}Pr_3})_2$ complexes of Rh and Pd have been reported and crystallographically characterised;[85] these are diamagnetic with formal bond orders of one and zero respectively.

1.5.3.3 Trimetallic η^5-Pn complexes and η^5/η^n-mixed coordination modes

In addition to the work conducted to form Ru carbonyl pentalene bimetallics, Stone and co-workers investigated the reaction of $Ru_3(CO)_{12}$ with COT and formed (in low yield along with previously characterised products)[86, 87] *syn*-$Ru_3(CO)_8Pn$, again mediated by a transannular dehydrogenation of the hydrocarbon starting material.[77, 88] A single crystal X-ray diffraction study revealed two Ru centres coordinated to the pentalene ligand, with *syn*-geometry as shown schematically in Figure 1.13 (a); the third Ru is bound only to CO groups and the other Ru atoms. The pentalene ring is bent away from the metal centres as found for other *syn*-bimetallics; the Ru_3 triangle is not parallel to the mean plane of the pentalene atoms but is instead, inclined to this at an angle of 50°. The structure is found to be fluxional by NMR, the high temperature spectra implying a time-averaged molecular plane of symmetry through the WT-C atoms of the pentalene ring; the fluxional process is thought to be a pendulum-like swing of the $Ru(CO)_4$ group with regard to the ligand [Figure 1.13 (a)]. Derivatisation proved

possible through the use of RC_8H_7 (R = Me, Ph) or multiply silylated cyclooctatrienes precursors, which cyclised during reaction to furnish isomeric mixtures of 1- and 2-R substituted $Ru_3(CO)_8Pn^{1/2\text{-}R}$, $Ru_3(CO)_8Pn^{1,5\text{-}SiMe_3}$ and $Ru_3(CO)_8Pn^{1,3,5\text{-}SiMe_3}$ (R = Me, Ph) complexes that could be chromatographically purified.[89, 90] The 1-alkyl/arylated and bis(trimethylsilyl) compounds were found not to display the aforementioned fluxional behaviour, whereas the more symmetrical remainder do (the two orientations of $Ru(CO)_4$ now being degenerate), and the activation energies for interconversion are independent of the substituent.

Further investigation of the $Ru_3(CO)_8Pn^{1,3,5\text{-}SiMe_3}$ complex exposed the presence of a minor isomer, shown by X-ray diffraction to have all three Ru centres bound to the pentalene ligand in a syn-arrangement as shown in Figure 1.13 (b),[91, 92] with both entities co-planar. The $Ru(CO)_2$ group is η^5-coordinated by pentalene, while the two $Ru(CO)_3$ fragments are bound to only two carbon atoms of the ring; the ligand may be considered akin to a bridging-allyl moiety here in its interaction with the $Ru(CO)_3$ groups and hence the geometry is best described as *syn*-(μ:η^5:η^2:η^2). This isomer is denoted 'face-bound' because the pentalene is bound to the face of the Ru_3 triangle; by analogy, the previously encountered trimetallics [Figure 1.13 (a)] are called 'edge-bound' isomers. Both of these isomers are in equilibrium in solution and can be detected by NMR and IR spectroscopy with the 'edge-bound' form predominating for all $Ru_3(CO)_8Pn^{2\text{-}R}$ (R = H, Me, Ph, $SiMe_3$) compounds.

Interconversion of 'edge-' and 'face-bound' species requires simultaneous CO migration and shift of the ligand from the edge of the metal cluster to the face and vice-versa. Combined with the fluxional nature of the 'edge-bound' isomer discussed above, this can allow migration of the pentalene ligand over all three metal atoms in the Ru_3 cluster, although this is thought only to occur for the unsubstituted complex. Rearrangement in the substituted complexes is restricted to 'edge-face' isomerism and 'edge-isomer' fluxionality detailed in Figure 1.13 (a) (i.e. the $Ru(CO)_2$ group in the 'face-bound' isomer never becomes a $Ru(CO)_4$ fragment); all of these fluxional processes are thought to occur *via* a large number of steps and have been fully described.[90]

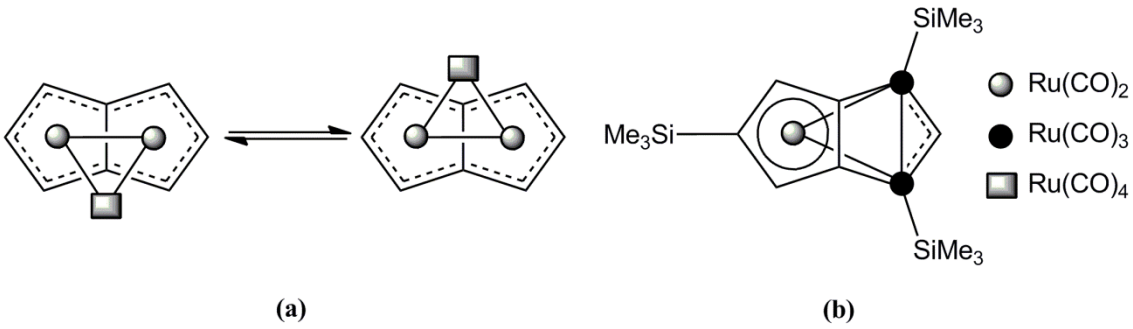

Figure 1.13: Trimetallic η^5-pentalene complexes (a) 'pendulum' isomerisation in $Ru_3(CO)_8Pn$ and (b) the 'face-bound' isomer of $Ru_3(CO)_8Pn^{1,3,5\text{-}SiMe_3}$.

In an attempt to isolate the bimetallic $[CrCp^*]_2Pn$, Jones and O'Hare have discovered an *anti*-analogue of the 'face-bound' geometry in the paramagnetic trichromium species $[CrCp^*](\mu{:}\eta^5{:}\eta^2,\eta^2\text{-}Pn)[(CrCp^*)_2(\mu\text{-}OMe)]$, by the reaction of two equivalents of $[Cr(Cp^*)(\mu\text{-}Cl)]_2$ with $Li_2Pn(DME)_x$.[93] Crystallographic studies reveal two discrete metal containing units, bridged by a planar pentalene ligand. One half is an η^5-coordinated $CrCp^*$ 'chromocene' portion and the other a pentalene/OMe bridged $[Cr^{II}Cp^*]_2$ dimer, with bonding similar to that shown by bimetallic allyl systems. Exchange of the complexing agent from DME to DEE, produced the OEt-bridged trimetallic, and demonstrates that this group is scavenged from the starting material. The alkoxide is also essential for the formation of the complex, as reaction of donor-free Li_2Pn does not give a tractable product. The Cr-Cr distance is consistent with a double bond and this would give each Cr centre a 16 electron configuration, isoelectronic with chromocene. The overall magnetism is consistent with the superposition of a chromocene fragment and an antiferromagnetically coupled Cr^{II}_2 moiety.

The strong coupling and delocalisation of charge between pentalene bridged metals has highlighted the possibility that such materials might show electronic conductivity or long-range magnetic ordering in 1D-organometallic polymers or 'nanowires'.[49, 94] Manriquez has developed an iterative scheme towards this goal[57] (Figure 1.14) using the combination of mono-lithiated ferrocene species with $Fe(Cp^*)(acac)$ to 'cap' one end of the polymer chain.[95, 96] Subsequent lithiation of the remaining hydropentalenyl unit and reaction with the '$[FeCp^*]^+$' synthon allows the formation of the symmetrical 'quadruple-decker' trimetallic. Alternatively reaction of $Li[Fe(\eta^5\text{-}PnH)(\eta^5\text{-}Pn)]$ with $Fe(acac)_2$ produces the analogous species capped with the hydropentalenyl ligand, which is prepared for further chain extension. Unfortunately the

poor solubility of the latter (400 mg l^{-1} of boiling toluene) has prevented the full investigation of any metal-metal interactions using solution-based techniques, or even the characterisation of the material by NMR spectroscopy. Subsequent investigations using 1-methyl and 1,4-Si^iPr_3 substituted pentalenes have been met with success and led to increased solubility in hydrocarbon solvents of the triple- and quadruple-decker Fe^{II} complexes.[40, 53] However, the asymmetry of substitution produced materials that were commonly oils due to the formation of multiple isomers that proved difficult to purify and has precluded any substantial characterisation.

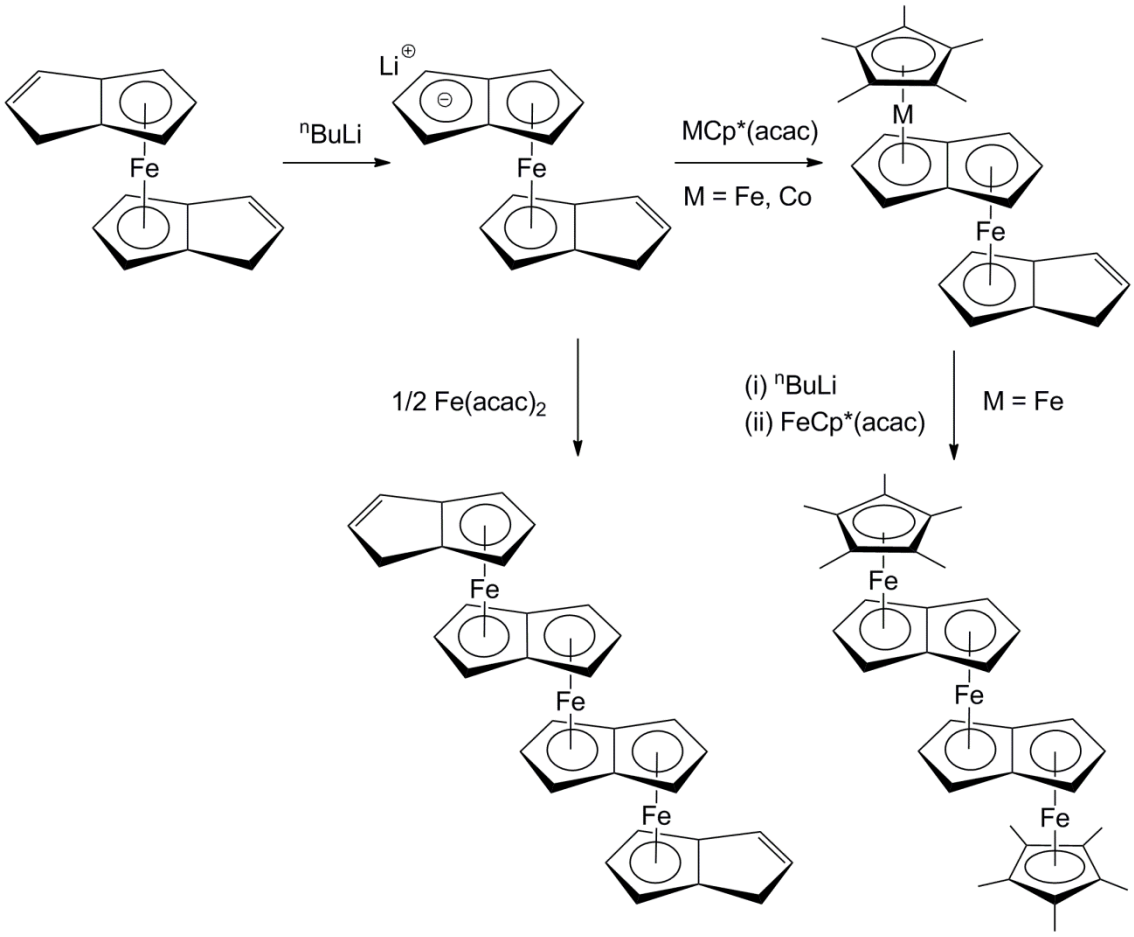

Figure 1.14: Synthetic routes to bi- and trimetallic pentalene complexes.

An extension of the nanowires methodology was used to synthesise the *anti*-heterobimetallic [RuCp*](μ:η^5,η^3-Pn)[Rh(η^4-COD)][97] [Figure 1.15 (a)] from Li[Ru(Cp*)(η^5-Pn)][58] and [Rh(η^4-COD)Cl]$_2$. X-ray crystallography reveals η^3-coordination of the Rh atom is indicative that this compound is an extreme 18/16 electron count for the Ru/Rh centres respectively. The COD ligand can be displaced easily by CO to generate the dicarbonyl species. This heterobimetallic is found to be

one of the most efficient and selective catalysts for the dehydrogenative silylation of styrene (for which organometallic Rh^{I} complexes are common catalysts); the second metal atom may have important influence on the reactivity of the Rh centre, as is also found for heterobimetallic Rh-indenyl complexes.[98]

In 1972 Katz *et al.* proposed that if two metallic centres were *syn*-facial then another pentalene ligand could be used to cap the other side to form a double metallocene analogous to two ring-fused cyclopentadienyl sandwich compounds. Reported at a similar time to Ni_2Pn_2 (*vide supra*), the Co analogue was initially assigned as $Co_2(\mu{:}\eta^5,\eta^5\text{-Pn})_2$, synthesised from Li_2Pn and $CoCl_2$, in very low yield (4-10%).[60] While the mononuclear metallocene $CoCp_2$ (S = ½) is paramagnetic, the pentalene complex displays diamagnetism. Calculations suggest that direct metal-metal overlap is negligible[49] and the interaction is likely to be an antiferromagnetic coupling, mediated through the ligand system. The initial assignment of the ($\mu{:}\eta^5{:}\eta^5$-Pn) pentalene binding modes was proposed from NMR data, which displayed D_{2h} symmetry; however, more recent studies on the electronic structure reveal that a particularly flat potential energy surface lies between two $Co_2(\mu{:}\eta^5,\eta^3\text{-Pn})_2$ canonical forms, with the symmetrical D_{2h} η^5,η^5-species lying as a transition state at the midpoint.[99] This mixed coordination motif was further supported by the synthesis and X-ray diffraction study of its permethylated analogue $Co_2Pn^*_2$ (*vide infra*),[50] which confirmed a $Co_2(\mu{:}\eta^5,\eta^3\text{-Pn}^*)_2$ arrangement, containing inversion symmetry.

Another example of a mixed coordination mode bimetallic sandwich compound is the interesting $Mn_2(\mu{:}\eta^5,\eta^1\text{-Pn}^{1,4\text{-Si}^i\text{Pr}_3})_2$ [Figure 1.15 (b)], synthesised by Cloke *et al.* from the reaction of $K_2Pn^{1,4\text{-Si}^i\text{Pr}_3}$ with $MnCl_2$.[100] A single crystal X-ray diffraction study reveals an asymmetric coordination environment in the molecule, with two distinctly different Mn centres bound to the ligands in different modes. One Mn is bound in a typical metallocene $\eta^5{:}\eta^5$-fashion, while the other is bound $\eta^1{:}\eta^1$-; DFT and magnetic studies demonstrate the former to be low spin and the latter high spin and a resulting weak interaction between the two Mn^{II} centres.

Another example of a silylated pentalene mixed coordination complex is the Sm^{III} sandwich compound $Sm(\eta^8\text{-Pn}^{1,4\text{-Si}^i\text{Pr}_3})(\eta^5\text{-Pn}^{1,4\text{-Si}^i\text{Pr}_3}\text{H})$, which incorporates an η^8-pentalene ligand and an η^5-hydropentalenyl ligand [Figure 1.15 (c)].[101] It was produced

as one of three products from the attempted synthesis of the Sm^{II} pentalene bridged dimer, which has been observed for Eu and Yb[68] [Figure 1.10 (a)] by the reaction of $K_2Pn^{1,4\text{-}Si^iPr_3}$ with $[SmCp^*(\mu\text{-}I)(THF)_2]_2$. The reaction follows a complex pathway, resulting in protonation of some of the pentalene molecules in aprotic conditions, which presumably arises from side reactions following the ring opening of THF, a not uncommon occurrence for low valent f-element compounds.[102–105]

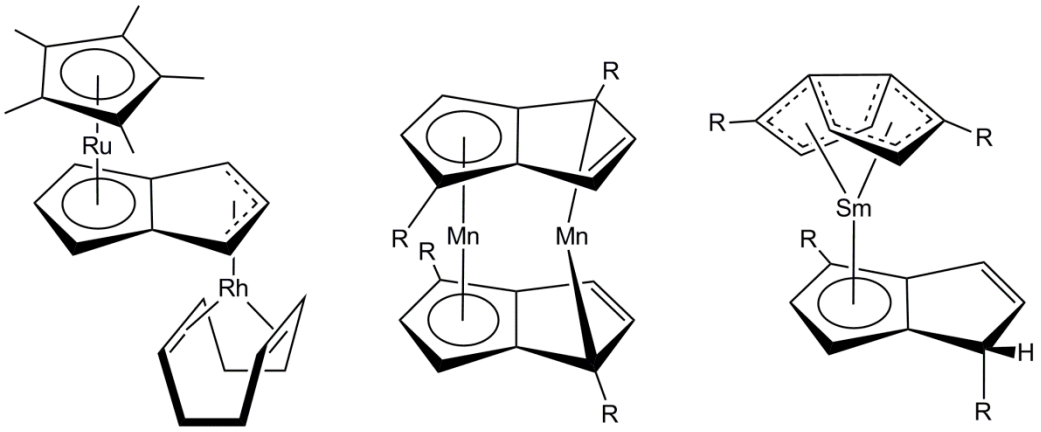

Figure 1.15: Mixed coordination η^5:η^n-pentalene complexes (a) [RuCp*][Rh(COD)]Pn; (b) $Mn_2(Pn^{1,4\text{-}Si^iPr_3)_2}$ and (c) $Sm(Pn^{1,4\text{-}Si^iPr_3})(Pn^{1,4\text{-}Si^iPr_3}H)$.

1.5.4 η^8-coordinated pentalene complexes

One of the most recent discoveries in modern pentalene chemistry is that the ligand can fold about its bridgehead carbon atoms, and thus bring closer together the constituent five-membered rings, when coordinating to a single metal centre. The 'fold-angle' is defined as the angle by which the ligand is found to deviate from planarity[40] (Figure 1.16) and values for crystallographically characterised η^8-Pn complexes are tabulated at the end of this section for reference (Table 1.1). This coordination mode enables all eight carbon atoms of the ligand to participate in M-C bonding; thus Pn acts as an 8π donor, or treated as the dianion, a 10π hydrocarbon.[106] This geometry necessarily contravenes Hückel's rule of aromaticity since the molecule must be planar to remain so. Size and electron-counting considerations indicate that this mode is most likely to be encountered with early metals and f-elements.[85]

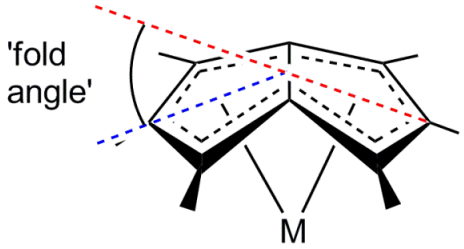

Figure 1.16: The 'fold angle' for an η^8-bound pentalene ligand.

The first example of a metal complex featuring η^8-coordinate pentalene was reported by Cloke *et al.* in 1997; Ta(η^8-Pn$^{1,5\text{-SiMe}_3}$)Cl$_3$ was the unexpected product formed in low yield (10%), upon protonolysis of the cyclooctatetrene complex Ta[η^8-1,4-(SiMe$_3$)$_2$C$_8$H$_6$]Me$_3$ with [NH^{i}Pr$_2$Et]$^+$Cl$^-$.[107] Subsequently the rational synthesis of the analogous trimethyl complex Ta(η^8-Pn$^{1,4\text{-Si}^i\text{Pr}_3}$)Me$_3$ was synthesised from the more symmetrical silylated pentalene dianion and TaCl$_2$Me$_3$.[108] A series of mixed-ligand Ta(η^8-Pn$^{1,4\text{-Si}^i\text{Pr}_3}$)Me$_yX_{3-y}$ (y = 1-3, X = Cl; y = 0, X = I) may be formed by successive reactions with [NHEt$_3$]$^+$Cl$^-$ or BX$_3$ (X = Cl and I). Upon increasing the number of Cl atoms in the coordination sphere of Ta there is a small yet discernible increase in the fold-angle of the pentalene ligand, which correlates with gradual augmentation of electron deficiency at the metal centre and its concomitant alleviation, by shortening Ta-C wing-tip contacts. Interestingly, the methyl in the dichoro complex Ta(η^8-Pn$^{1,4\text{-Si}^i\text{Pr}_3}$)MeCl$_2$, can be deprotonated by Li[N(SiMe$_3$)$_2$] to give the novel dimeric compound [Ta(η^8-Pn$^{1,4\text{-Si}^i\text{Pr}_3}$)Cl($\mu$-CH$_2$)]$_2$, consisting of bridging methylene units; X-ray crystallography uncovers that it exists as a sole diastereomer, with the Si^{i}Pr$_3$ substituents in an eclipsed arrangement.[85]

Around the same time, Jonas *et al.* described η^8-coordination by pentalene in a series of sandwich complexes of Ti, Zr, Hf and V. The V species V(η^8-Pn')(η^5-L) (Pn' = Pn, L = Cp, Cp*, Ind; Pn' = Pn$^{2\text{-Me}}$, L = Cp) are diamagnetic, 18 electron complexes formed by the reaction of Li$_2$Pn' with VL$_2$X (X = halide).[109] These three molecules have been characterised by X-ray crystallography (Pn' = Pn, L = Cp, Cp*;Pn' =Pn$^{2\text{-Me}}$, L = Cp), in each case the pentalene has a fold angle of 43°; this is greater than that found for the Ta complex as may be expected for the smaller metal atom and remains unsurpassed in mononuclear pentalene organometallic chemistry.

Reaction of $Ti(Cp)Cl_2$ with Li_2Pn affords 17 electron $Ti(\eta^8\text{-}Pn)(Cp)$; structural characterisation revealed the fold angle to be 37°, less than in the isomorphous V complex.[110] Oxidation of this complex with XCH_2CH_2X (X = Cl, Br) produces the diamagnetic $Ti(\eta^8\text{-}Pn)(Cp)X$ [Figure 1.17 (a)] that exhibits a decrease in distortion of the Pn unit (33°), which is to be anticipated from the increased steric compression in accommodating an extra ligand within the Ti coordination sphere. The analogous Zr chloride species is formed from $Zr(Cp)_2Cl_2$ and Li_2Pn; it is isostructural and has the same fold-angle, with a concomitant lengthening of the M-C distances to reflect the larger size of the second row element.

Homoleptic organometallic $M(\eta^8\text{-}Pn')$ (M = Ti, Zr, Hf; Pn' = Pn, $Pn^{2\text{-}Me}$) [Figure 1.17 (b)] can be synthesised by reaction of $Ti(\eta^8\text{-}Pn')(Cp)Br$ or $M(Cp)_2Cl_2$ with one or two equivalents of Li_2Pn' respectively.[110] VT-NMR suggests that at low temperature two conformers of $Ti(\eta^8\text{-}Pn^{2\text{-}Me})$ exists in solution, which interconvert through rotation of the ligands about the bridgehead axes, giving the complex a D_{2d} pseudo-tetrahedral geometry. Unfortunately neither of these complexes has been structurally solved and therefore this has not been verified. Formally these $M(\eta^8\text{-}Pn')_2$ compounds are diamagnetic '20 electron species' although DFT calculations have shown that in this symmetry only nine out of ten π-type ligand orbitals match with those on the metal, the remaining one is non-bonding and has no metal character.[111] PES measurements have further elucidated the electronic structure of these molecules and support a D_2 or closely related geometry.[112] However, more recent computational studies have suggested the bis η^8-coordination to be a transition state with the unsymmetrical $Ti(\eta^8\text{-}Pn)(\eta^6\text{-}Pn)$ structure calculated to be lower in energy.[113] Until such time that a structure determination can be made, the true nature of the structure remains elusive.

$Zr(\eta^8\text{-}Pn)_2$ reacts with $ZrCl_4{\cdot}2THF$ to give the 18 electron complex $Zr(\eta^8\text{-}Pn)(THF)_2Cl_2$, which may be considered a 'half-sandwich' equivalent for Zr-Pn chemistry since some or all of the THF or Cl ligands may be replaced by others. This is demonstrated by the high-yielding conversion to $Zr(\eta^8\text{-}Pn)(\eta^3\text{-}C_3H_5)_2$ upon treatment with allyllithium.[114] The compound has been extensively studied by ^1H and ^{13}C NMR spectroscopy, which show a C_2-symmetric molecule that consists of two proposed enantiomers; these are thought to interconvert *via* an η^1-allyl form. Most of these Zr species are active catalysts for ethylene polymerisation, for example $Zr(\eta^8\text{-}Pn)(THF)_2Cl_2$, $Zr(\eta^8\text{-}Pn)(\eta^3\text{-}C_3H_5)_2$ and $Zr(\eta^8\text{-}Pn)(\eta^5\text{-}Ind)Cl$ are maintained to have

activities of 458, 6474 and 31,531 g of polyethene/ g of Zr h^{-1} at 2 bar ethene pressure.[115] Analogues of these Group IV compounds with silylated ligands may also be used as catalysts for the copolymerisation of ethylene with α-olefins.[116]

The pentalene chemistry of the f-elements has been investigated by Cloke *et al.* using bulky silylated ligands. The reaction of $K_2Pn^{1,4\text{-}Si^iPr_3}$ with MCl_4 (M = Th, U)[117, 118] affords the homoleptic complexes $M(Pn^{1,4\text{-}Si^iPr_3})_2$ analogous to thorocene and uranocene, the archetypal sandwich compound of the f-elements. Whereas uranocene and thorocene have parallel and planar COT rings,[119, 120] these complexes have fold-angles about the pentalene bridgehead of 24° and 25° respectively; the much smaller values demonstrating the larger ionic radii of M^{IV} relative to the transition metal η^8-bound species (Table 1.1). The structures also demonstrate that the bulky silyl substituents are bent away from the metal centres, approximately 17° from the planes of the five-membered rings. Presumably, this permits better ring-metal overlap. Two isomers are present both in solution and in the crystal; these differ in the relative rotations of the pentalene rings to give chiral (semi-eclipsed D_2 form) and meso (semi-staggered S_4) arrangements (the ligand is facially enantiotopic), which are not interconverted on the NMR timescale. Hypothetically, interconversion between the two can only occur through complete M-$Pn^{1,4\text{-}Si^iPr_3}$ bond scission, followed by recoordination to the opposite face and unsurprisingly, this process is not borne out in practice.

The cerocene counterpart has also been synthesised by the reaction of two equivalents of $(Pn^{1,4\text{-}Si^iPr_3})^{2-}$ with $CeCl_3$ to provide the anionic complex $KCe(\eta^8\text{-}Pn^{1,4\text{-}Si^iPr_3})_2$, which is oxidised by $Ag[BPh_4]$ to yield the vivid blue $Ce(\eta^8\text{-}Pn^{1,4\text{-}Si^iPr_3})_2$, formally a Ce^{IV} compound.[121] Crystal structure analyses have demonstrated the presence of *meso*- and *rac*-forms in both species with fold angles of 22° and 26° respectively (the former as the 18-crown-6/pyridine solvate). The WT atoms are drawn towards the metal in the latter to compensate for the increased charge on the Ce atom. Much debate exists with regard to the true oxidation state of the metal in $Ce(COT)_2$,[122, 123] with techniques such as XANES spectroscopy[124] indicating a valence closer to Ce^{III} than Ce^{IV}. However, magnetic measurements, PES and DFT calculations are concordant with a tetravalent formulation.[125]

'Half-sandwich' lanthanide and actinide species may also be formed.[85] The reaction of $M(Pn^{1,4\text{-}Si^iPr_3})_2$ with MCl_4 (M = Th, U) gives $M(Pn^{1,4\text{-}Si^iPr_3})Cl_2$ akin to the Zr 'half-sandwich' complex discussed above, although an X-ray study of the Th compound reveals a tetrameric structure, whereas the Zr molecule is a monomer.[110] Y^{III} (dimeric and Yb^{II} [monomeric, Figure 1.17 (c)] complexes are available from the tri- and diiodides respectively, with the latter possessing the smallest fold angle to date (19.5°).[40]

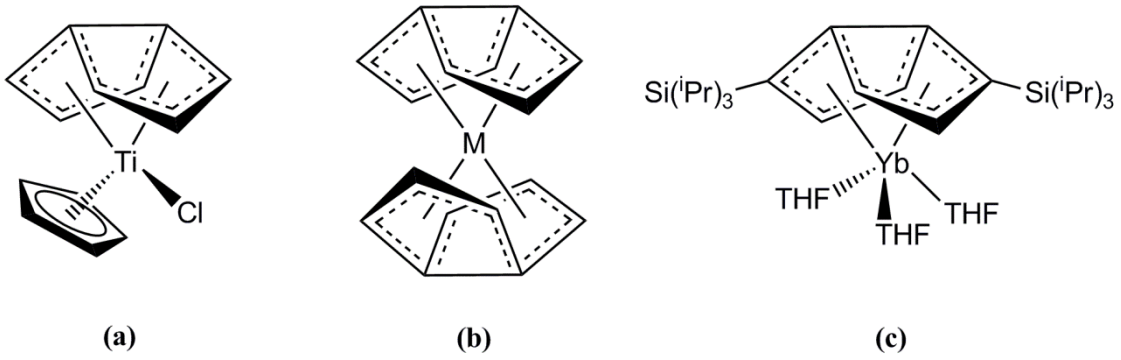

Figure 1.17: η^8-Pn complexes (a) mixed-ring species Ti(Pn)(Cp)Cl; (b) Homoleptics of Ti and Zr and (c) half-sandwich complex $Yb(Pn^{1,4\text{-}Si^iPr_3})(THF)_3$.

The mixed-ring U^{III} complex $U(Pn^{1,4\text{-}Si^iPr_3})(Cp^*)$ can be synthesised from UI_3, KCp* and $K_2(Pn^{1,4\text{-}Si^iPr_3})$ under an Ar atmosphere;[126] the fold angle of the pentalene ligand is 26°, which is smaller than that for the homoleptic U compound and implies a greater steric congestion in the latter. Exposure of this molecule to dinitrogen results in the formation of a new, dimeric species with N_2 bridging the metal centres, bound 'side-on'. The N-N bond is considerably lengthened from that found in dinitrogen, consistent with the oxidation of the metal centres to U^{IV}, later supported through DFT calculations.[127] Two different pentalene fold angles of 26° and 22.5° are present within the molecule, and the U-C distances are remarkably similar to the U^{III} monomer; it is postulated that steric congestion prevents sizeable structural change. Another comparable example of a side-on bound uranium-N_2 complex is the triamidoamine species $\{U[N(CH_2CH_2NSi^tBuMe_2)_3]_2(\mu{:}\eta^2,\eta^2\text{-}N_2)\}$,[128] where the N-N bond length is essentially identical to that found in the free diatomic; the difference in reactivity is thought to arise from different frontier orbital geometries and sterics in the two ligand environments.[129] Both $[U(Pn^{1,4\text{-}Si^iPr_3})(Cp^*)]_2(\mu{:}\eta^2\eta^2\text{-}N_2)$ and

$\{U[N(CH_2CH_2NSi^tBuMe_2)_3]_2(\mu{:}\eta^2,\eta^2\text{-}N_2)\}$ reform the monomeric species upon freeze-pump-thaw degassing of a solution, indicating that the binding of N_2 is reversible; $[U(Pn^{1,4\text{-}Si^iPr_3})(Cp^*)]_2(\mu{:}\eta^2\eta^2\text{-}N_2)$ will also lose N_2 from a solid sample.

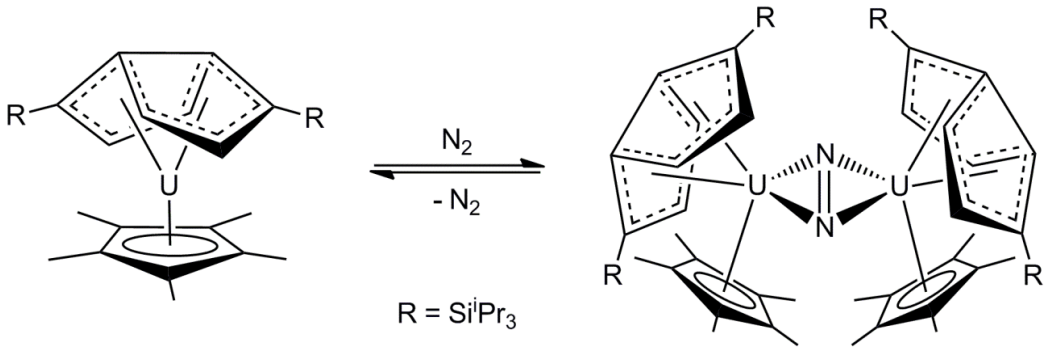

Figure 1.18: Reversible reduction of N_2 by $U(Pn^{1,4\text{-}Si^iPr_3})(Cp^*)$.

Table 1.1: Fold angles for η^8-bound pentalene organometallic complexes.

Complex	Fold angle (°)	Reference
Ti(Pn)Cp	37.0	110
Ti(Pn)CpCl	33.0	110
Zr(Pn)CpCl	33.0	110
$Zr(Pn)Cl_2(THF)_2$	30.0	110
Zr(Pn*)CpCl	30.7	158
V(Pn)Cp	43.0	109
V(Pn)Cp*	43.0	109
$V(Pn^{2\text{-Me}})Cp^*$	43.0	109
$Ta(Pn^{1,4\text{-}Si^iPr_3})Me_3$	29.2	108
$Ta(Pn^{1,4\text{-}Si^iPr_3})Me_2Cl$	31.2	108
$Ta(Pn^{1,4\text{-}Si^iPr_3})MeCl_2$	32.5	108
$Ta(Pn^{1,5\text{-}Si^iPr_3})Cl_3$	33.0	107
$[Y(Pn^{1,4\text{-}Si^iPr_3})(THF)I]$	26.0	40
$Ce(Pn^*)_2$	24.7	159
$Ce(Pn^{1,4\text{-}Si^iPr_3})_2[K(18\text{-crown-}6)(pyr)_2]$	22.0	121
$Ce(Pn^{1,4\text{-}Si^iPr_3})_2$	26.0	121
$Sm(\eta^8\text{-}Pn^{1,4\text{-}Si^iPr_3})(\eta^5\text{-}Pn^{1,4\text{-}Si^iPr_3}H)$	25.5	101
$Sm(\eta^8\text{-}Pn^{1,4\text{-}Si^iPr_3})Cp^*$	25.5	101
$Yb(Pn^{1,4\text{-}Si^iPr_3})(THF)_3$	20.0	40
$Th(Pn^{1,4\text{-}Si^iPr_3})_2$	24.0	117
$[Th(Pn^{1,4\text{-}Si^iPr_3})Cl_2]_4$	28.1, 24.7	85
$U(Pn^*)_2$	25.7	160
$U(Pn^{1,4\text{-}Si^iPr_3})_2$	25.0	118
$U(Pn^{1,4\text{-}Si^iPr_3})_2Cp^*$	26.0	126
$[U(Pn^{1,4\text{-}Si^iPr_3})_2Cp^*]_2(\mu\text{:}\eta^2\text{:}\eta^2\text{-}N_2)$	26.0, 22.5	126

1.6 Heterosubstituted pentalene ligands

Many heterocyclic systems isoelectronic with neutral pentalene or the pentalene dianion are known.[130] The 10π species are often monoanionic and hence are potentially useful starting materials for organometallic complexes; a variety of aza-,[131–135] oxa-[136] and thiapentalene[137, 138] anions are known. However, organometallic derivatives thus far, are scarce. Heteroferrocenes with 2,3-dimethyl-1-(N-methyl)azapentalene [Figure 1.19 (a)][139] and 5-methyl-1-thiapentalene[140] ligands have been synthesised *via* reaction of $FeCl_2$ with the corresponding lithiates. These are coordinated to the metal centre through the carbocyclic ring and electrochemical studies indicate they are somewhat more electron rich than ferrocene, as might be expected. Interestingly, attempts to form the analogous ferrocenes with 2-aza and 2-thiapentalene ligands were unsuccessful.[139, 141] Similar carbocyclic coordination is observed in the cymantrene and ruthenocene analogues, which have been synthesised using an alkyl-substituted 1-thiapentalene.[142]

The use of a pentalene analogue with unit charge may be advantageous in f-element chemistry due to the low oxidation states and large coordination spheres characteristic of these metals. Interest has centred around the 7-azapentalenyl anion, where then heteroatom is substituted in the bridgehead position [Figure 1.19 (b)], may be easily synthesised by the action of alkali metals on 3H-pyrrolizine with the Li, Na and K salts known.[131, 143] Thallium, trimethylsilyl and trimethyltin derivatives have also been synthesised[144] and the crystal structure of the potassium salt of a benzannulated derivative has been determined, demonstrating a 3D polymeric array of linear zig-zag chains and a variety of coordination environments for the K ions.[145] However, no complexes of the d- or f-elements have been reported to date.

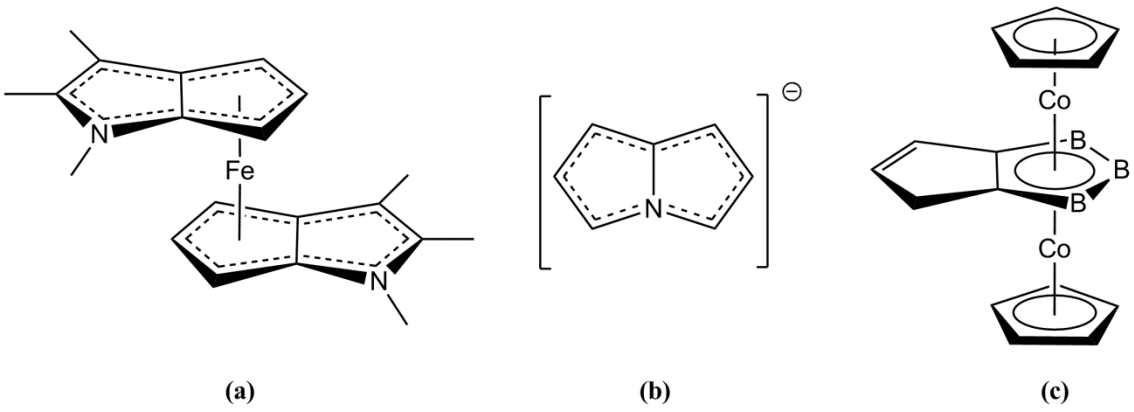

Figure 1.19: Heteropentalenes (a) 2,3-dimethyl-1-(N-methyl)azapentalene; (b) 7-azapentalenyl anion and (c) triple-decker carborane.

An exceptional example of an organometallic complex with a heterosubstituted pentalene skeleton is the triple-decker carborane depicted in Figure 1.19 (c); reaction of NaB_5H_8, $CoCl_2$ and NaCp gives a mixture of products including (in poor yield) the unusual species where the Cp ligand has been inserted into the borane polyhedron.[146, 147] The $C_5B_3H_7^{4-}$ anion is isoelectronic with $C_8H_7^-$, so this molecule could be considered analogous to a hydropentalenyl complex. It is also the only known example of a molecules with a pentalene skeleton having two metal centres coordinated on opposite faces of the same five membered ring.

One final example is of a pentalene mimic, $(RuCp^*)_2(\mu{:}\eta^5{:}\eta^5\text{-}B_8H_{14})$,[148] which contains no carbon atoms and is structurally analogous to Manriquez's $(RuCp^*)_2Pn$. It similarly contains two oxidation waves in its cyclic voltammogram but displays a greater degree of mixed valency, postulated as a better match of frontier orbital energies of the borane and the ruthenium fragment compared to Pn.

1.7 The effects of permethylation and the advent of permethylpentalene

The archetypal example demonstrating the effects of permethylation on hydrocarbon based π-ligands is the substitution of Cp for Cp* in cyclopentadienyl based complexes and the prominent differences in chemical and physical properties of the analogous complexes that occur as a result. Cp* complexes often display greater solubility and crystallisability than their cyclopentadienyl counterparts, as well as stronger metal-ligand interactions. Prototypical examples include the spin crossover from $^6A_{1g}$ to $^2E_{2g}$ on going from Cp_2Mn to Cp^*_2Mn[149, 150] and the observation that Cp_2Ti [Figure 1.20 (a)] spontaneously dimerises, whereas Cp^*_2Ti [Figure 1.20 (b)] is a stable

complex as a result of a combination of steric crowding and a lack of a vinylic α-H, which is thought to be a key deactivation route for Cp complexes.[151, 152]

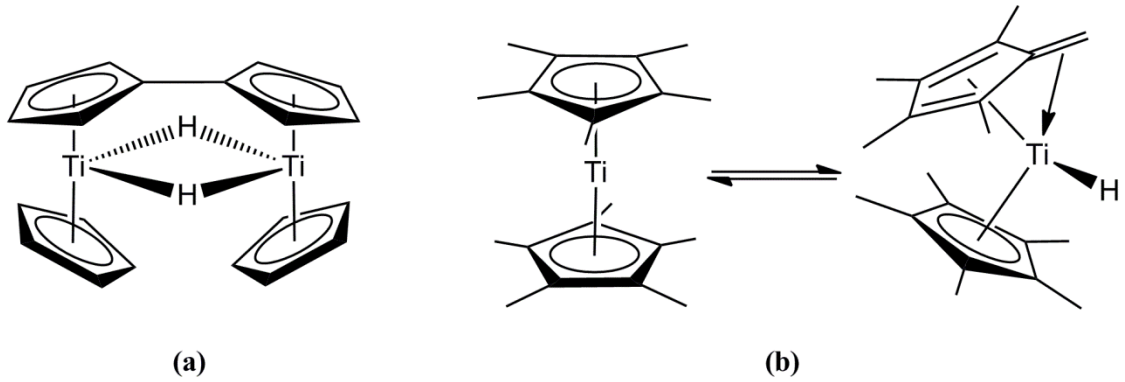

Figure 1.20: Structural differences between (a) '$TiCp_2$' and (b) $TiCp^*_2$.

These differences are often ascribed to the greater electron donating inductive effect of the permethylated ligand, the stronger sp^3 C-H bonds and the steric bulk of Cp*. This bulkier ligand has also been found to stabilise unusual metal oxidation states, exemplified by the isolation of Cp*ZnZnCp*. It is one of only a few examples of Zn^I complexes, and the first reported example of a compound containing a Zn-Zn bond.[153]

On studying the effects of permethylation of Cp, it is logical to assume that permethylation of pentalene would have similar effects on the organic molecule and subsequent organometallic complexes. Preparation of substituted pentalene derivatives has proved difficult, relying on existing protocols for the production of dihydropentalene, which themselves suffer from low yields, expense, and the requirement of specialist equipment.[67] It is these difficulties that have hindered the rapid development of organometallic pentalene chemistry. However, the total synthesis of an organic precursor and its conversion into the dilithium salt of permethylpentalene (C_8Me_6; Pn*) has relatively recently been reported by O'Hare *et al.*.[154, 155] The synthesis employs an entirely solution phase and facile route from readily available starting materials and achieves yields comparable to modern syntheses of the Cp* precursor Cp*H. This breakthrough has enriched the field of organometallic pentalene chemistry even further, and various permethypentalene complexes have since been reported.

The benefit of increased solubility imparted on permethylated systems is apparent from the crystallographic study of *syn*-$[Fe_2(CO)_4(\mu\text{-}CO)](\mu{:}\eta^5,\eta^5\text{-}Pn^*)$,[156] synthesised from the reaction of $Fe_2(CO)_9$ and the Pn* synthon, 1,3,4,5,6-pentamethyl-

2-methylene-1,2-dihydropentalene (Pn*').[155] The study confirmed the structure put forward for the Pn analogue with the presence of a (μ-CO), was assigned on the basis of IR data due to a lack of crystallographic characterisation. Other carbonyl complexes that have been prepared include the triad of isomorphous group IX homonuclear *syn*-bimetallic carbonyls $[M_2(CO)_4](\mu{:}\eta^5,\eta^5\text{-Pn*})$ (M = Co, Rh and Ir). The cobalt complex is synthesised in an analogous manner to the Fe species above using $Co_2(CO)_8$,[156] while the Rh and Ir analogues were synthesised *via* salt elimination using $Pn^*(SnMe_3)_2$ with the dimeric metal precursor $[MCl(CO)_2]_2$ (M = Rh, Ir).[157] They demonstrate a linear trend of increasing slip parameter ($\eta^5 \rightarrow \eta^3$), with increasing metal size on descending the group, as would be expected incorporating two $M(CO)_2$ moieties in a *syn*-facial arrangement.

A systematic range of first row transition metal 'double-metallocenes' $M_2Pn^*_2$ (M = V, Cr, Mn, Co, Ni) has been synthesised and all have been structurally characterised *via* X-ray diffraction;[50] this contrasts earlier observations seen for Katz's M_2Pn_2 (M = Co and Ni). The V and Mn complexes show very short intermetallic distances that are consistent with metal-metal bonding, while Co displays differential bonding to each side of the Pn* ligand consistent with an $\eta^5{:}\eta^3$- formulation [Figure 1.21 (b)]. The Pn* moieties for $Ni_2Pn^*_2$ are best described as $\eta^3{:}\eta^3$-bonded to the Ni centres and all the complexes display D_{2h} symmetry in solution. The temperature variation of the chemical shifts for the resonances of the Cr analogue indicates that the molecule has an S = 0 ground state and a thermally populated S = 1 excited state. Paradoxically, attempts to isolate the 'double ferrocene' equivalent, $Fe_2Pn^*_2$, led only to the isolation of the permethylpentalene dimer, Pn^*_2.

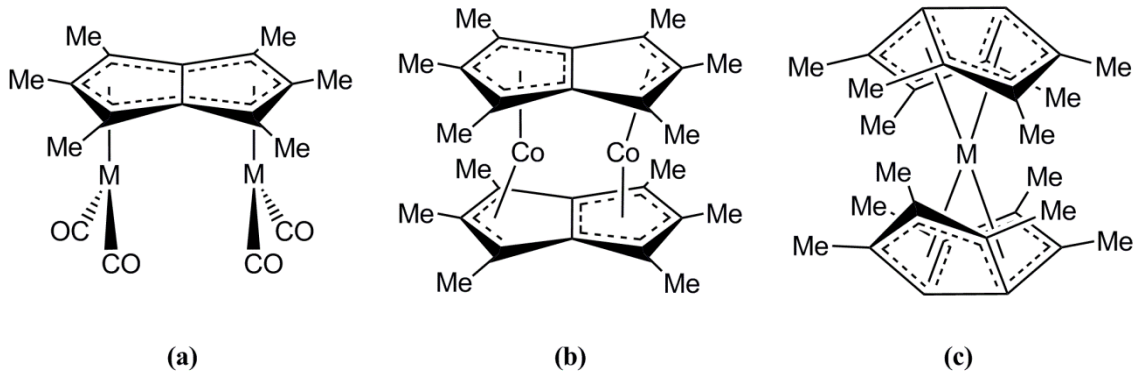

Figure 1.21: Complexes of permethylpentalene (a) $[M_2(CO)_4](\mu{:}\eta^5,\eta^5\text{-Pn*})$ (M = Co, Rh and Ir); (b) $Co_2(\mu{:}\eta^5{:}\eta^3\text{-Pn*})_2$ and (C) $M(\eta^8\text{-Pn*})_2$ (M = Ce and U).

The Pn* analogue of Jonas' Zr(Cp)(η^8-Pn*)Cl has been reported and is, as expected isostructural,[158] however, it does posses a smaller fold angle (30.7 vs. 33.0°) supporting current bonding theory, which suggests that the ligand distortion correlates with electron deficiency at the metal centre.[108] This is this first time that the electronic factors have been manipulated solely *via* the ligand and provides evidence for the greater electron donating inductive effect of the permethylated ligand.

Examples are not solely confined to the transition series, the ligand has also been shown to form f-element complexes by the isolation of the isomorphous cerocene and uranocene equivalents M(η^8-Pn*)$_2$ [M = Ce and U, Figure 1.21 (c)].[159, 160] The Ce analogue has been studied using a variety of techniques, including XANES spectroscopy and DFT calculations; the former gives strong evidence for a formal valency of Ce^{III} and provides an example of the self-contained Kondo effect, whereas the latter ascribes a more covalent description to a Ce^{IV} compound. UPn*$_2$ was similarly found to exist as three stereoisomers in its crystalline form and is a simple Curie-Weiss magnet in the solution phase. Electrochemical studies have indicated the reduced species to react with dinitrogen paralleling the observations for the silylated pentalene species.[126, 127]

1.8 Aims of thesis

The role of carbocyclic ligands in the development of novel organometallic complexes has been colossal, most notably utilising cyclopentadienyl, cyclooctatretraenyl and their substituted analogues, which are now ubiquitous in the field.[45] Comparatively, organometallic pentalene chemistry is still in its infancy, mainly owing to complexities surrounding the synthesis of the ligand. Relatively recent developments towards dianionic trialkylsilylated pentalenes ($Pn^{1,4\text{-}SiR_3}$)$^{2-}$ (R = Me and ^{i}Pr)[67] and the advent of a facile route to the dilithium salt of permethylpentalene (both in multigram scales), may prove to be key in overcoming past difficulties. These are promising signs that the inertia that has impeded the rapid growth of organometallic pentalene chemistry will evaporate into the ether, unleashing the huge potential that this fascinating ligand has to offer.

The aims of this thesis are to gain access and advance the vastly underdeveloped field of η^8-pentalene chemistry, specifically in the area of alkylated

η^8-permethylpentalene titanium derivatives and their reactivity with small molecules. Owing to the substitutional flexibility of the M-Cl bond *via* simple metathesis reactions, an improved synthesis of $[\eta^8\text{-Pn*TiCl}(\mu\text{-Cl})]_2$ will be sought as an entry point into η^8-Pn*Ti-alkyl/aryl chemistry. These complexes will be studied using a wide range of techniques, gaining a wealth of structural and reactivity data, which should complement the myriad chemistry displayed by their bis(cyclopentadienyl) analogues.

1.9 References for Chapter One

1 R. B. King, *Applied Organometallic Chemistry*, 2003, 17, 393–397.

2 J. W. Armit and R. Robinson, *Journal of the Chemical Society, Transactions*, 1922, 121, 827.

3 J. March and M. B. Smith, *Advanced Organic Chemisty: Reactions, Mechanisms, and Structure*, J. Wiley & Son, 5th Editio., 2000.

4 M. Gates and S. Malchick, *Journal of the American Chemical Society*, 1957, 5546–5550.

5 J. W. Barrett and R. P. Linstead, *Journal of the Chemical Society (Resumed)*, 1936, 611.

6 P. De Mayo, R. Bloch, and R. A. Marty, *Journal of the American Chemical Society*, 1971, 93, 3071–3072.

7 C. T. Blood and R. P. Linstead, *Journal of the Chemical Society (Resumed)*, 1952, 2263, 2263.

8 P. C. den Boer-Veenendaal and D. H. W. den Boer, *Molecular Physics*, 1961, 4, 33–38.

9 P. C. den Boer, D. H. W. den Boer, C. A. Coulson, and T. H. Goodwin, *Tetrahedron*, 1963, 19, 2163–2170.

10 M. J. S. Dewar and C. De Llano, *Journal of the American Chemical Society*, 1969, 91, 789–795.

11 B. A. Hess Jr. and L. J. Schaad, *Journal of the American Chemical Society*, 1971, 93, 305–310.

12 K. Hafner, R. Donges, E. Goedecke, and R. Kaiser, *Angewandte Chemie International Edition in English*, 1973, 12, 337–339.

13 T. Bally, Z. Zhu, M. Neuenschwander, and S. Chai, *Journal of the American Chemical Society*, 1997, 119, 1869–1875.

14 H. S. Kaufman, I. Fankuchen, and H. Mark, *Nature*, 1948, 161, 165–165.

15 F. G. Klarner, *Angewandte Chemie-International Edition*, 2001, 40, 3977.

16 K. Hafner, K. F. Bangert, and V. Orfanos, *Angewandte Chemie International Edition in English*, 1967, 6, 451–452.

17 K. Hafner and H. U. Suss, *Angewandte Chemie-International Edition in English*, 1973, 12, 575–577.

18 E. L. Goff, *Journal of the American Chemical Society*, 1962, 84, 3975–3976.

19 B. Kitschke and H. J. Lindner, *Tetrahedron Letters*, 1977, 29, 2511–2514.

20 P. Bischof, R. Gleiter, K. Hafner, K. H. Knauer, J. Spanget-Larsen, and H. U. Süss, *Chemische Berichte*, 1978, 111, 932–938.

21 Y. Shibata, K. Noguchi, and K. Tanaka, *Organic letters*, 2010, 12, 5596–9.

22 Z. U. Levi and T. D. Tilley, *Journal of the American Chemical Society*, 2009, 131, 2796–7.

23 Z. U. Levi and T. D. Tilley, *Journal of the American Chemical Society*, 2010, 132, 11012–4.

24 A. S. K. Hashmi, M. Wieteck, I. Braun, P. Nösel, L. Jongbloed, M. Rudolph, and F. Rominger, *Advanced Synthesis & Catalysis*, 2012, 354, 555–562.

25 M. Saito, M. Nakamura, T. Tajima, and M. Yoshioka, *Angewandte Chemie (International ed. in English)*, 2007, 46, 1504–7.

26 M. Saito, M. Nakamura, and T. Tajima, *Chem. Eur. J.*, 2008, 14, 6062–8.

27 T. J. Katz, *Journal of the American Chemical Society*, 1960, 84, 3784–5.

28 T. J. Katz and M. Rosenberger, *Journal of the American Chemical Society*, 1962, 84, 865–866.

29 T. J. Katz, M. Rosenberger, and R. K. O'Hara, *Journal of the American Chemical Society*, 1964, 86, 249–52.

30 J. J. Stezowski, H. Hoier, D. Wilhelm, T. Clark, and P. von R. Schleyer, *Journal of the Chemical Society, Chemical Communications*, 1985, 1263.

31 J. J. Brooks, W. Rhine, and G. D. Stucky, *Journal of the American Chemical Society*, 1972, 94, 7346–7351.

32 D. Wilhelm, J. L. Courtneidge, T. Clark, and A. G. Davies, *Journal of the Chemical Society, Chemical Communications*, 1984, 810.

33 S. You, S. Chai, N. Schwarz, and M. Neuenschwander, *Helvetica Chimica Acta*, 1997, 80, 1627–1638.

34 T. J. Katz and M. Rosenberger, *Journal of the American Chemical Society*, 1963, 85, 2030–31.

35 G. Emerson, L. Watts, and R. Pettit, *Journal of the American Chemical Society*, 1965, 87, 131–133.

36 G. Emerson, K. Ehrlich, W. P. Giering, and P. C. Lauterbur, *Journal of the American Chemical Society*, 1966, 88, 3172–3173.

37 D. J. Ehntholt and R. C. Kerber, *Journal of the Chemical Society D: Chemical Communications*, 1970, 1451.

38 R. Pettit, *Pure and Applied Chemistry*, 1968, 17, 253–272.

39 J. C. Green, M. L. H. Green, and G. Parkin, *Chemical communications (Cambridge, England)*, 2012, 48, 11481–503.

40 O. T. Summerscales and F. G. N. Cloke, *Coordination Chemistry Reviews*, 2006, 250, 1122–1140.

41 J. M. O'Connor and C. P. Casey, *Chemical Reviews*, 1987, 87, 307–318.

42 M. J. Calhorda, C. C. Romao, and L. F. Veiros, *Chemistry--A European Journal*, 2002, 8, 868–875.

43 Y. A. Ustynyuk, A. K. Shestakova, V. A. Chertkov, N. N. Zemlyansky, I. V. Borisova, A. I. Gusev, E. B. Tchuklanova, and E. A. Chernyshev, *Journal of Organometallic Chemistry*, 1987, 335, 43–57.

44 A. K. Shestakova, V. A. Cherkov, and Y. A. Ustynyuk, *Metalloorganischeskaya Khim*, 1988, 1, 132–6.

45 C. Elschenbroich and A. Salzer, *Organometallics - A concise introduction*, VCH, Second Ed., 1991.

46 A. Miyake and A. Kanai, *Angewandte Chemie International Edition in English*, 1971, 10, 801–802.

47 G. Wilke and B. Bogdanovic, *Angew. Chem.*, 1961, 73, 756.

48 T. J. Katz and N. Acton, *Journal of the American Chemical Society*, 1972, 94, 3281–3283.

49 J. K. Burdett and E. Canadell, *Organometallics*, 1985, 4, 805–815.

50 A. E. Ashley, R. T. Cooper, G. G. Wildgoose, J. C. Green, and D. O'Hare, *Journal of the American Chemical Society*, 2008, 130, 15662–77.

51 T. Coffield, K. Ihrman, and W. Burns, *Journal of the American Chemical Society*, 1960, 82, 1251–1252.

52 T. H. Coffield, K. G. Ihrman, and W. Burns, *Journal of the American Chemical Society*, 1960, 82, 4209–4210.

53 S. C. Jones, D.Phil Thesis, University of Oxford, 2003.

54 S. C. Jones, P. Roussel, T. Hascall, and D. O'Hare, *Organometallics*, 2006, 25, 221–229.

55 K. K. Joshi, R. H. B. Mais, F. Nyman, P. G. Owston, and A. M. Wood, *Journal of the Chemical Society A: Inorganic, Physical, Theoretical*, 1968, 318.

56 E. Molins, W. Maniukiewicz, C. Miravitlles, M. Mas, J. M. Manriquez, I. Chavez, B. Oelckers, J. Farran, and J. L. Brianso, *Acta Crystallographica, Section C: Crystal Structure Communications*, 1996, C52, 2414–2416.

57 B. Oelckers, I. Chavez, J. M. Manriquez, and E. Roman, *Organometallics*, 1993, 12, 3396–3397.

58 F. Burgos, V. Arancibia, J. M. Manríquez, and I. Chávez, *Bol. Soc. Chil. Quím*, 2000, 45, 621–8.

59 T. J. Katz and J. J. Mrowca, *Journal of the American Chemical Society*, 1966, 89, 1105–1111.

60 T. Katz, N. Acton, and J. McGinnis, *Journal of the American Chemical Society*, 1972, 94, 6205–6206.

61 M. R. Churchill and K. K. G. Lin, *Inorganic Chemistry*, 1973, 12, 2274–2279.

62 K. Jonas and K. R. Porschke, in *Abstract of papers, 224th ACS National Meeting, Boston, MA*, 2002.

63 K. Jonas, *Max-Planck-Institut für Kohlenforschung Report for the Period of January 2000 – December 2001*, 2002.

64 K. Jonas, *Max-Planck-Institut für Kohlenforschung Report for the Period of January 2002 – December 2004*, 2005.

65 E. E. Bunel, L. Valle, N. L. Jones, P. J. Carroll, C. Barra, M. Gonzalez, N. Munoz, G. Visconti, A. Aizman, and J. M. Manriquez, *Journal of the American Chemical Society*, 1988, 110, 6596–6598.

66 J. M. Manriquez, M. D. Ward, W. M. Reiff, J. C. Calabrese, N. L. Jones, P. J. Carroll, E. E. Bunel, and J. S. Miller, *Journal of the American Chemical Society*, 1995, 117, 6182–6193.

67 F. G. N. Cloke, M. C. Kuchta, R. M. Harker, P. B. Hitchcock, and J. S. Parry, *Organometallics*, 2000, 19, 5795–5798.

68 O. T. Summerscales, S. C. Jones, F. G. N. Cloke, and P. B. Hitchcock, *Organometallics*, 2009, 28, 5896–5908.

69 S. C. Jones, T. Hascall, S. Barlow, and D. O'Hare, *Journal of the American Chemical Society*, 2002, 124, 11610–11611.

70 D. F. Hunt and J. W. Russell, *Journal of Organometallic Chemistry*, 1972, 46, C22–C24.

71 D. F. Hunt and J. W. Russell, *Journal of the American Chemical Society*, 1972, 94, 7198–7199.

72 W. Weidemüller and K. Hafner, *Angewandte Chemie International Edition in English*, 1973, 12, 925–925.

73 T. S. Piper, F. A. Cotton, and G. Wilkinson, *Journal of Inorganic and Nuclear Chemistry*, 1955, 1, 165–174.

74 E. Fleischer, A. Stone, R. B. K. Dewar, J. D. Wright, C. E. Keller, and R. Pettit, *Journal of the American Chemical Society*, 1966, 88, 3158–3159.

75 A. Brookes, J. Howard, S. A. R. Knox, F. G. A. Stone, and P. Woodward, *Journal of the Chemical Society, Chemical Communications*, 1973, 587–589.

76 J. A. K. Howard and P. Woodward, *Journal of the Chemical Society, Dalton Transactions: Inorganic Chemistry (1972-1999)*, 1978, 412–416.

77 S. A. R. Knox and F. G. A. Stone, *Accounts of Chemical Research*, 1974, 7, 321–328.

78 P. J. Harris, J. A. K. Howard, S. A. R. Knox, R. J. McKinney, R. P. Phillips, F. G. A. Stone, and P. Woodward, *Journal of the Chemical Society, Dalton Transactions*, 1978, 403.

79 M. J. McGlinchey, *Inorganica Chimica Acta*, 1981, 49, 125–127.

80 S. C. Jones and D. O'Hare, *Chemical Communications*, 2003, 321, 2208.

81 C. Elschenbroich, J. Heck, W. Massa, E. Nun, and R. Schmidt, *Journal of the American Chemical Society*, 1983, 105, 2905–2907.

82 F. A. Cotton, C. A. Murillo, and R. A. Walton, *Multiple Bonds Between Metal Atoms*, Springer-Verlag, New York, 2005.

83 M. C. Kuchta, F. G. N. Cloke, and P. B. Hitchcock, *Organometallics*, 1998, 17, 1934–1936.

84 F. G. N. Cloke, J. C. Green, C. N. Jardine, and M. C. Kuchta, *Organometallics*, 1999, 18, 1087–1090.

85 F. G. N. Cloke, *Pure and Applied Chemistry*, 2001, 73, 233–238.

86 M. I. Bruce, M. Cooke, and M. Green, *Journal of Organometallic Chemistry*, 1968, 13, 227–234.

87 F. A. Cotton, A. Davison, T. J. Marks, and A. Musco, *Journal of the American Chemical Society*, 1969, 91, 6598–6603.

88 J. A. K. Howard, S. A. R. Knox, V. Riera, F. G. A. Stone, and P. Woodward, *Journal of the Chemical Society, Chemical Communications*, 1974, 452.

89 J. A. K. Howard, S. A. R. Knox, F. G. A. Stone, A. C. Szary, and P. Woodward, *Journal of the Chemical Society, Chemical Communications*, 1974, 4, 788.

90 S. A. R. Knox, R. J. McKinney, V. Riera, F. G. A. Stone, and A. C. Szary, *Journal of the Chemical Society, Dalton Transactions*, 1979, 1801.

91 J. A. K. Howard, R. F. D. Stansfield, and P. Woodward, *Journal of the Chemical Society, Dalton Transactions*, 1979, 264, 1812.

92 J. A. K. Howard, S. A. R. Knox, R. J. McKinney, R. F. D. Stansfield, F. G. A. Stone, and P. Woodward, *Journal of the Chemical Society, Chemical Communications*, 1976, 557.

93 S. C. Jones, T. Hascall, A. J. Norquist, and D. O'Hare, *Inorganic Chemistry*, 2003, 42, 7707–7709.

94 A. Ceccon, S. Santi, L. Orian, and A. Bisello, *Coordination Chemistry Reviews*, 2004, 248, 683–724.

95 C. Miravitlles, E. Molins, W. Maniukiewicz, M. Mas, J. M. Manríquez, I. Chávez, B. Oelckers, a. Alvarez-Larena, and J. L. Briansó, *Acta Crystallographica Section C Crystal Structure Communications*, 1996, 52, 3047–3049.

96 A. Alvarez-Larena, J. L. Briansó, J. F. Piniella, J. Farran, J. M. Manríquez, I. Chávez, B. Oelckers, E. Molins, and C. Miravitlles, *Acta Crystallographica Section C Crystal Structure Communications*, 1996, 52, 2754–2757.

97 F. Burgos, I. Chávez, J. M. Manriquez, M. Valderrama, E. Lago, E. Molins, F. Delpech, A. Castel, and P. Rivière, *Organometallics*, 2001, 20, 1287–1291.

98 C. Bonifaci, A. Ceccon, A. Gambaro, F. Manoli, L. Mantovani, P. Ganis, S. Santi, and A. Venzo, *Journal of Organometallic Chemistry*, 1998, 557, 97–109.

99 S. Bendjaballah, S. Kahlal, K. Costuas, E. Bevillon, and J.-Y. Saillard, *Chemistry-A European Journal*, 2006, 12, 2048–2065.

100 G. Balazs, F. G. N. Cloke, A. Harrison, P. B. Hitchcock, J. Green, and O. T. Summerscales, *Chemical communications (Cambridge, England)*, 2007, 1, 873–5.

101 O. T. Summerscales, D. R. Johnston, F. G. N. Cloke, and P. B. Hitchcock, *Organometallics*, 2008, 27, 5612–5618.

102 L. R. Avens, D. M. Barnhart, C. J. Burns, and S. D. McKee, *Inorganic Chemistry*, 1996, 35, 537–539.

103 W. J. Evans, J. T. Leman, J. W. Ziller, and S. I. Khan, *Inorganic chemistry*, 1996, 35, 4283–4291.

104 C. P. Larch, F. G. N. Cloke, and P. B. Hitchcock, *Chemical Communications*, 2008, 82.

105 C. Boisson, J. C. Berthet, M. Lance, M. Nierlich, and M. Ephirtikhine, *Chemical Communications*, 1996, 9, 2129.

106 H. Butenschön, *Angewandte Chemie International Edition in English*, 1997, 36, 1695–1697.

107 Q. A. Abbasali, F. G. N. Cloke, P. B. Hitchcock, and S. C. P. Joseph, *Chemical Communications*, 1997, 4, 1541–1542.

108 F. G. N. Cloke, P. B. Hitchcock, M. C. Kuchta, and N. A. Morley-Smith, *Polyhedron*, 2004, 23, 2625–2630.

109 K. Jonas, B. Gabor, R. Mynott, K. Angermund, O. Heinemann, and C. Krüger, *Angewandte Chemie International Edition in English*, 1997, 36, 1712–1714.

110 K. Jonas, P. Kolb, G. Kollbach, B. Gabor, R. Mynott, K. Angermund, O. Heinemann, and C. Krüger, *Angewandte Chemie International Edition in English*, 1997, 36, 1714–1718.

111 K. Costuas and J. Saillard, *Chemical Communications*, 1998, 2047–2048.

112 R. Gleiter, S. Bethke, J. Okubo, and K. Jonas, *Organometallics*, 2001, 20, 4274–4278.

113 H. Li, H. Feng, W. Sun, Y. Xie, R. B. King, and H. F. Schaefer III, *New Journal of Chemistry*, 2011, 35, 1718.

114 B. Gabor, K. Jonas, and R. Mynott, *Inorganica Chimica Acta*, 1998, 270, 555–558.

115 K. Jonas, P. Kolb, and G. Kollbach, Mononuclear and polynuclear transition metal complexes with pentalene ligands bound to a single metal atom, Patent App. US 5,959,132 (1999).

116 F. G. N. Cloke and J. S. Parry, Novel transition metal complexes, Patent App. WO 9,907,716 (1999).

117 F. G. N. Cloke and P. B. Hitchcock, *Journal of the American Chemical Society*, 1997, 119, 7899–7900.

118 F. G. N. Cloke, J. C. Green, and C. N. Jardine, *Organometallics*, 1999, 18, 1080–1086.

119 A. Zalkin and K. N. Raymond, *Journal of the American Chemical Society*, 1969, 91, 5667–5668.

120 A. Avdeef, K. N. Raymond, K. O. Hodgson, and A. Zalkin, *Inorganic Chemistry*, 1972, 11, 1083–1088.

121 G. Balazs, F. G. N. Cloke, J. C. Green, R. M. Harker, A. Harrison, P. B. Hitchcock, C. N. Jardine, and R. Walton, *Organometallics*, 2007, 26, 3111–3119.

122 M. Dolg, P. Fulde, W. Ku□chle, C.-S. Neumann, and H. Stoll, *The Journal of Chemical Physics*, 1991, 94, 3011.

123 M. Dolg, P. Fulde, H. Stoll, H. Preuss, A. Chang, and R. M. Pitzer, *Chemical Physics*, 1995, 195, 71–82.

124 N. M. Edelstein, P. G. Allen, J. J. Bucher, D. K. Shuh, C. D. Sofield, N. Kaltsoyannis, G. H. Maunder, M. R. Russo, and A. Sella, *Journal of the American Chemical Society*, 1996, 118, 13115–13116.

125 A. Streitwieser, S. A. Kinsley, J. T. Rigsbee, I. L. Fragala, and E. Ciliberto, *Journal of the American Chemical Society*, 1985, 107, 7786–7788.

126 F. G. N. Cloke and P. B. Hitchcock, *Journal of the American Chemical Society*, 2002, 124, 9352–9353.

127 F. G. N. Cloke, J. C. Green, and N. Kaltsoyannis, *Organometallics*, 2004, 23, 832–835.

128 P. Roussel and P. Scott, *Journal of the American Chemical Society*, 1998, 120, 1070–1071.

129 P. Roussel, W. Errington, N. Kaltsoyannis, and P. Scott, *Journal of Organometallic Chemistry*, 2001, 635, 69–74.

130 A. Krutosíková and T. Gracza, in *Topics in heterocyclic chemistry*, 2012.

131 W. H. Okamura and T. J. Katz, *Tetrahedron*, 1967, 23, 2941–2957.

132 H. Volz and B. Meßner, *Tetrahedron Letters*, 1969, 10, 4111–4114.

133 H. Volz, U. Zirngibl, and B. Meßner, *Tetrahedron Letters*, 1970, 11, 3593–3595.

134 H. Volz and R. Draese, *Tetrahedron Letters*, 1970, 11, 4917–4920.

135 J. Elguero, R. M. Claramunt, and A. J. H. Summers, *Adv. Heterocycl. Chem.*, 1978, 22, 183–320.

136 T. S. Cantrell and B. L. Harrison, *Tetrahedron Letters*, 1969, 10, 1299–1302.

137 J. Skramstad, *Chemica Scipta*, 1973, 4, 81–84.

138 H. Volz and H. Kowarsch, *Tetrahedron Letters*, 1976, 17, 4375–4376.

139 H. Volz and R. Draese, *Tetrahedron Letters*, 1975, 16, 3209–3212.

140 H. Volz and H. Kowarsch, *Journal of Organometallic Chemistry*, 1977, 136, C27–C30.

141 H. Volz and H. Kowarsch, *Hetercycles*, 1977, 7, 1319–37.

142 D. A. Kisun'ko, M. V. Zabalov, Y. F. Oprunenko, and D. A. Lemenovskii, *Russian Journal of General Chemistry*, 2004, 74, 105–109.

143 E. E. Schweizer and K. K. Light, *The Journal of Organic Chemistry*, 1966, 31, 870–872.

144 D. a Kissounko, N. S. Kissounko, D. P. Krut'ko, G. P. Brusova, D. a Lemenovskii, and N. M. Boag, *Journal of Organometallic Chemistry*, 1998, 556, 145–149.

145 M. J. Bermingham, F. G. N. Cloke, M. G. Gardiner, P. B. Hitchcock, L. E. Wise, and B. F. Yates, *Dalton transactions (Cambridge, England□: 2003)*, 2005, 5, 1157–8.

146 V. R. Miller, R. Weiss, and R. N. Grimes, *Journal of the American Chemical Society*, 1977, 99, 5646–5651.

147 J. R. Pipal and R. N. Grimes, *Inorganic Chemistry*, 1978, 17, 10–14.

148 S. Ghosh, B. C. Noll, and T. P. Fehlner, *Angewandte Chemie (International ed. in English)*, 2005, 44, 6568–71.

149 J. L. Robbins, N. M. Edelstein, S. R. Cooper, and J. C. Smart, *Journal of the American Chemical Society*, 1979, 101, 3853–3857.

150 M. E. Switzer, R. Wang, M. F. Rettig, and A. H. Maki, *Journal of the American Chemical Society*, 1974, 96, 7666–7674.

151 H. Brintzinger and J. E. Bercaw, *Journal of the American Chemical Society*, 1971, 93, 2045–2046.

152 J. E. Bercaw, *Journal of the American Chemical Society*, 1974, 96, 5087–5095.

153 I. Resa, E. Carmona, E. Gutierrez-Puebla, and A. Monge, *Science (New York, N.Y.)*, 2004, 305, 1136–8.

154 A. E. Ashley, A. R. Cowley, and D. O'Hare, *Chemical Communications (Cambridge, England)*, 2007, 1512–4.

155 A. E. Ashley, A. R. Cowley, and D. O'Hare, *European Journal of Organic Chemistry*, 2007, 2007, 2239–2242.

156 A. E. Ashley, G. Balázs, A. R. Cowley, J. C. Green, and D. O'Hare, *Organometallics*, 2007, 26, 5517–5521.

157 L. A. Bennett, Part II Thesis, University of Oxford, 2008.

158 A. E. Ashley, Permethylpentalene Chemistry, Thesis, University of Oxford, 2006.

159 A. Ashley, G. Balazs, A. Cowley, J. Green, C. H. Booth, and D. O'Hare, *Chemical communications (Cambridge, England)*, 2007, 1515–7.

160 F. M. Chadwick, A. Ashley, G. Wildgoose, J. M. Goicoechea, S. Randall, and D. O'Hare, *Dalton Transactions (Cambridge, England: 2003)*, 2010, 39, 6789–93.

Chapter Two

Synthesis of Permethylpentalene Titanium-Methyl Derivatives

2.1 Introduction

Group IV metallocenes have displayed a variety of interesting chemical and physical properties that have engrossed theoretical and practical chemists since their discovery over half a century ago. Synthesis of bright green so-called 'titanocene' Cp_2Ti in 1956, via reaction of $TiCl_2$ and NaCp,[1] and its red 'bent' dichloride analogue Cp_2TiCl_2 two years earlier, *via* a parallel method using $TiCl_4$,[2] marked the discovery of one of the most extensively utilised organotransition metal complex systems. While free Cp_2Ti (formally a 14 electron species) is non-isolable, a brown diamagnetic form was elucidated as the dimeric fulvalene $[Cp(C_5H_4)TiH]_2$,[3–5] whose solid state structure was only confirmed some 36 years after its initial synthesis.[6] Incorporation of additional neutral and/or anionic ligands has led to the isolation of a vast range of derivatives, leading to a more general definition for group IV bent metallocenes as d^0 *pseudo*-tetrahedral organometallic compounds in which the transition metal atom bears two η^5-cyclopentadienyl-type ligands and two σ-ligands.[7] Titanocene complexes have many important and varied applications, ranging from stoichiometric organic reactions to catalytic reactions in the field of polymerisation and fine chemical synthesis.[8, 9]

Generally, formation of cyclopentadienyl-type complexes is achieved *via* salt metathesis; examples include many common group IV derivatives such as Cp_2TiX_2 (X = halide). However, reaction of $TiCl_4$ and LiCp* fails to produce the permethylated analogue $Cp^*_2TiCl_2$, instead producing Cp^*TiCl_3.[10] $Cp^*_2TiCl_2$ was synthesised by oxidation of the Ti^{III} precursor Cp^*_2TiCl by HCl, which proceeded in yields of up to 65%.[11, 12] The more demanding synthetic route to Cp* complexes, as compared to Cp, gives us a slight insight into problems we might face adapting the syntheses for the production of complexes with the more reducing and sterically demanding Pn* framework.

The methyl ligand in organometallic chemistry is unique in that it is a pure σ-binding ligand of moderate electronegativity and is not subject to β-hydrogen elimination, a major decomposition pathway for metal-alkyl species.[13] Discovered in the same decade as 'titanocene', methyltitanium compounds play an important role as catalysts in Ziegler-Natta systems.[14–16] First prepared in 1959 by Clauss and Beerman, the bright yellow homoleptic complex $TiMe_4$ is highly oxygen, moisture and temperature sensitive.[17, 18] The material is found to decompose just above −78 °C in its crystalline form and at around 0 °C as a solution in ether. This extra thermal stability is attributed to the dual action of ether stabilising both the electron deficient titanium centre and alleviating coordinative unsaturation, thus blocking decomposition pathways.[19] This is highlighted further by the correlation of thermal stability and Lewis base strength in the series, $TiMe_4(Me_2PCH_2CH_2PMe_2) > TiMe_4(PMe_3)_2 > TiMe_4$,[20] a trend also observed for $TaMe_5$ Lewis base adducts.[21]

To date only nine titanium compounds bearing any pentalene derivative have been reported in the literature, none of which contain in combination a Ti-Me bond and only three of which have been structurally characterised. This chapter describes the improved synthesis of $[Pn^*TiCl(\mu\text{-}Cl)]_2$, an entry point to permethylpentalene titanium alkyl species, and subsequent reactivity with various methylating agents using salt metathesis reactions.

2.2 Isomeric control of Pn* synthons

High yielding syntheses of η^8-Pn* complexes necessitates the use of *cis*-$Pn^*(SnMe_3)_2$ or *cis*-$Pn^*Li_2(TMEDA)_x$ starting materials, as the Pn* ligand folds about the bridgehead carbons so that both of the constituent rings can bond to, and essentially cap, one face of a metal's coordination sphere. The discovery that isomeric control can be imparted on the Pn* synthon used [Pn^*Li_2 and $Pn^*(SnMe_3)_2$] and subsequently transferred to a target organometallic compound was found to be a sensitive function of the solvent employed. The use of non-polar solvents (e.g. hexane or benzene) in the preparation of $Pn^*(SnMe_3)_2$ from $Pn^*Li_2(TMEDA)_x$ solely produces the *cis* isomer. Conversely, use of a polar solvent in a parallel synthesis selectively produces the *trans* isomer from what is believed to be the *cis*-$Pn^*Li_2(TMEDA)_x$ starting material, isolated from the synthesis of the dianion synthon (Figure 2.1).

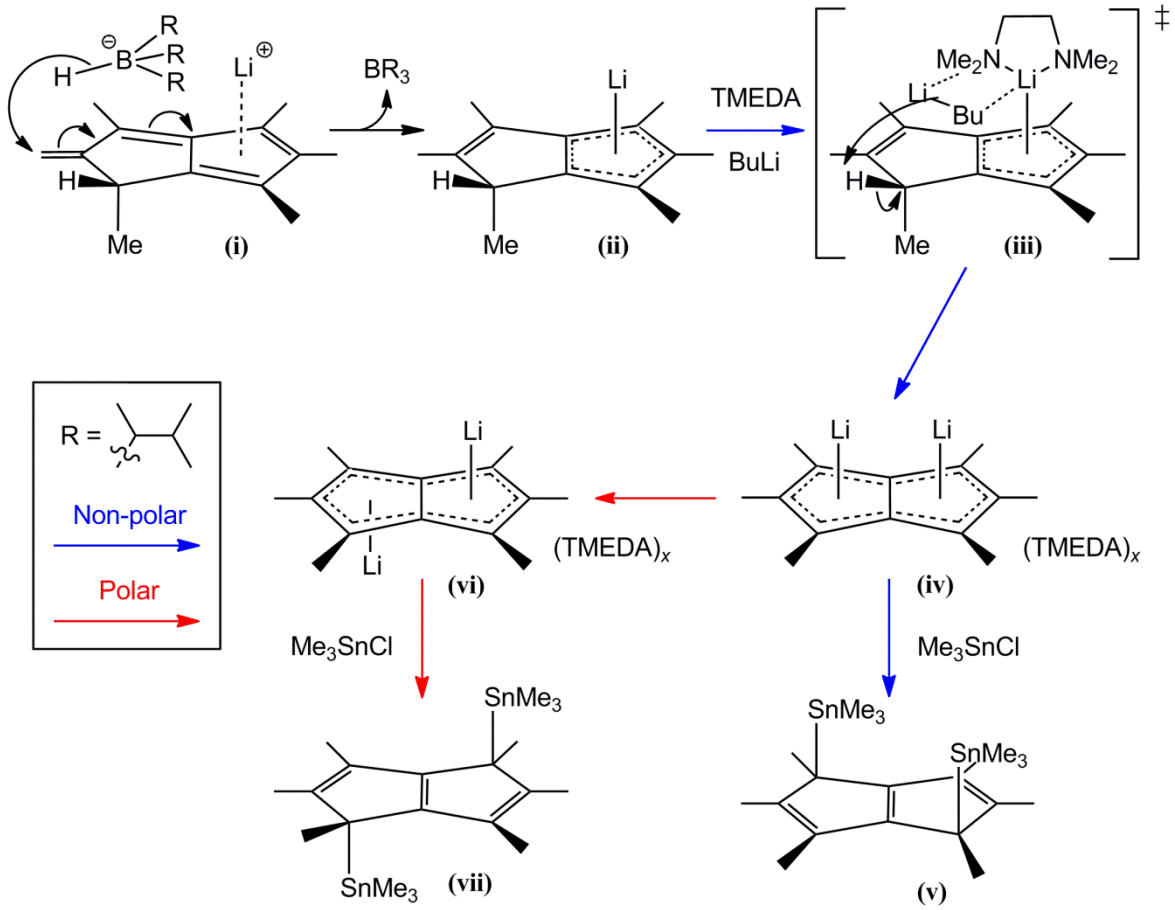

Figure 2.1: Proposed mechanism for isomeric control of Pn* synthons.

The proposed mechanism for this selectivity begins with the elegant formation of LiPn*H from the fulvene, Pn*' and LS-Selectride; the first example of regiospecific conjugate hydride delivery upon a pure hydrocarbon to produce a cyclopentadienyl anionic species.[22] The hydride selectively adds to the exocyclic vinylic bond of the fulvene, Figure 2.1 **(i)** in a similar fashion to 1,4-reduction of α,β-unsaturated carbonyls.[23] This occurs on the least sterically hindered face of the bicyclic ring system due to the bulky R groups employed on the trialkylborohydride reagent. The monolithiate **(ii)** precipitates out under the reaction conditions employed, and as a result, the lithium ion is fixed *anti* to the methyl group on the adjacent ring. The next step involves formation of a ^{n}BuLi·TMEDA complex that coordinates to **(ii)**, followed by proton abstraction as shown in **(iii)**. The second lithium ion therefore necessarily coordinates to the same face due to the prearranged formation of complex **(iii)**, hence chelation ensures that we form *cis*-Pn*Li_2(TMEDA)$_x$, **(iv)**, an effect which can also be seen in the *ortho*-lithiation of N,N-dimethylaniline.[24] Calculations performed on the unsubstituted Pn ligand for the complex Li_2Pn(DME)$_2$ suggest that the *trans* isomer is

more stable than the *cis* by 89.1 kJ mol^{-1}.[25] **(iv)** precipitates from the reaction medium, ensuring the lithium ions are insufficiently soluble to exchange faces and so the kinetic *cis* product is 'trapped out'. When **(iv)** is transmetallated to form Pn*$(SnMe_3)_2$, we can impart stereoselective control on the product *via* solvent selection. If a non-polar solvent is used, a tight ion pair is present and the lithium ions are insufficiently solvated to detach and exchange faces, so the *cis* stereochemistry is locked and transmetallation with Me_3SnCl yields *cis*-Pn*$(SnMe_3)_2$ **(v)**. However, if a donor solvent such as THF is used, **(iv)** becomes sufficiently solvated for the lithium ions to detach and isomerise. This allows formation of the thermodynamically favoured *trans*-Pn*$Li_2(TMEDA)_x$, **(vi)**, subsequent transmetallation of which with Me_3SnCl occurs stereospecifically and exclusively forms *trans*-Pn*$(SnMe_3)_2$, **(vii)**.

2.3 Improved synthesis of [Pn*TiCl(μ-Cl)]$_2$ (2.1)

The synthesis of [Pn*TiCl(μ-Cl)]$_2$ (**2.1**) has previously been reported by the O'Hare group;[26] however, it suffered from very poor yields (maximum achieved 8%) and was unreliable. The reducing power of the Pn* dianion proved a problem in the synthesis, with the standard metathesis route employing $TiCl_3 \cdot 3THF$ and Pn*Li_2 (1:1) followed by $PbCl_2$ oxidation providing unsatisfactory results. In light of the prior research, and the need to avoid the direct combination of the dilithiate with the metal precursor in its highest oxidation state, an alternative route was sought to avoid large losses of the ligand through oxidation. This factor is of utmost importance for Ti species in group IV, since it has the highest ionisation energy (M^{III}/M^{IV}) (Ti - 4175, Zr - 3313, Hf - 3216 kJ mol^{-1}) of the triad.[27] Therefore the use of a softer transmetallation reagent was investigated. Abel *et al.* reported the use of cyclopentadiene-substituted tin compounds for metathesis reactions, using them to prepare monocyclopentadienyl transition metal complexes[28] such as $CpTiCl_3$ and related compounds.[29] Accordingly the selective formation of the precursor *cis*-Pn*$(SnMe_3)_2$ *via* solvent selection (Section 2.2) and subsequent reaction with $TiCl_4 \cdot 2THF$ proved highly successful in synthesising the target compound **2.1**, in a markedly improved yield.

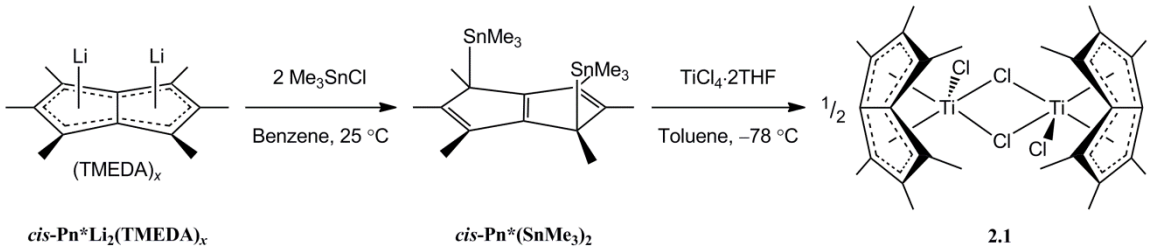

Figure 2.2: Synthesis of [Pn*TiCl(μ-Cl)]$_2$ (**2.1**).

The improved synthesis of **2.1** is detailed in Figure 2.2; equimolar quantities of $TiCl_4$·2THF and *cis*-Pn*($SnMe_3$)$_2$ (generated *in situ*), were combined in toluene at −78 °C, with the solution turning dark brown upon warming to room temperature. Removal of the solvent yielded a very dark brown residue which after washing with pentane, was extracted with hot toluene. Cooling the saturated solution to –35 °C yielded an orange crystalline solid, which was characterised as **2.1** by ^{1}H, ^{13}C NMR and mass spectrometry (EI), and agreed with published data.[26] The method reliably afforded **2.1** in a dramatically improved 70-75% yield, opening up the possibility of greater investigation into the area of permethylpentalene titanium chemistry, due to the substitutional flexibility of the Ti-Cl bond.

2.4 Synthesis and characterisation of [Pn*TiMe(μ-Cl)]$_2$ (2.2)

Reaction of **2.1** with two equivalents of MeLi in Et_2O (Figure 2.3) affords a dark green solution. Subsequent work up and cooling of a toluene solution produces an emerald green microcrystalline solid in moderate yield (57%), which was identified as [Pn*TiMe(μ-Cl)]$_2$ (**2.2**) by elemental analysis and X-ray crystallography. Single crystals suitable for X-ray diffraction were grown by slow cooling of a solution in the same solvent to −35 °C, and two views of the structure are shown in Figure 2.4 and 2.5.

Figure 2.3: Synthesis of [Pn*TiMe(μ-Cl)]$_2$ (**2.2**).

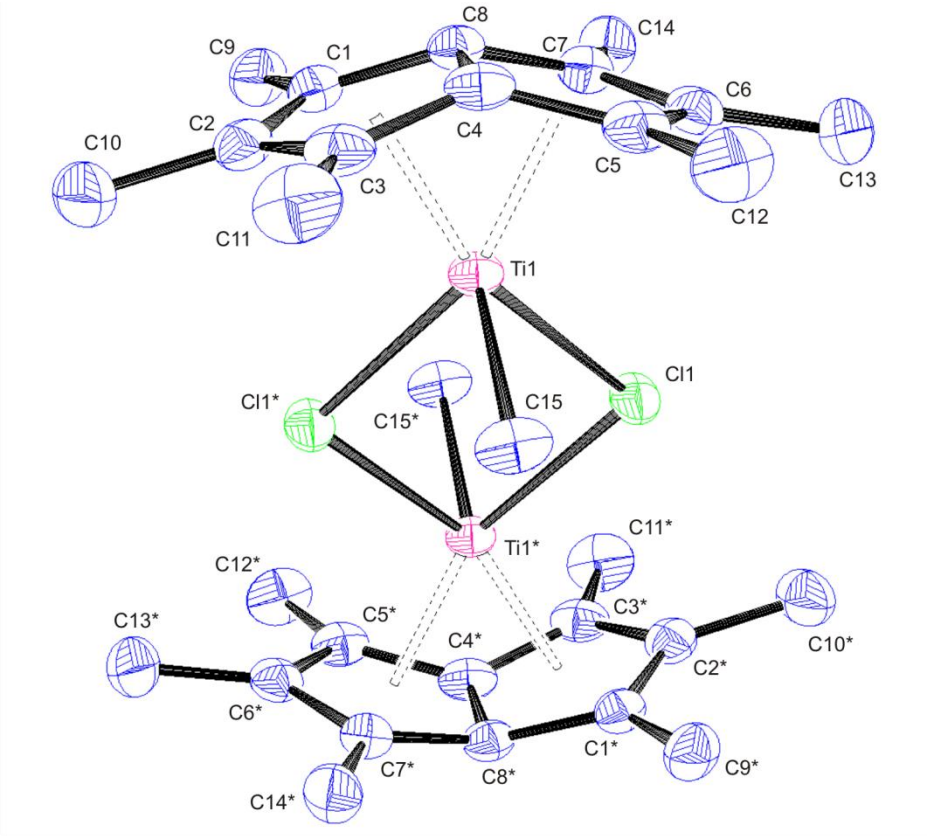

Figure 2.4: Side-on view of **2.2** with thermal ellipsoids at 50%. Hydrogen atoms omitted for clarity, * denotes atoms generated by inversion symmetry.

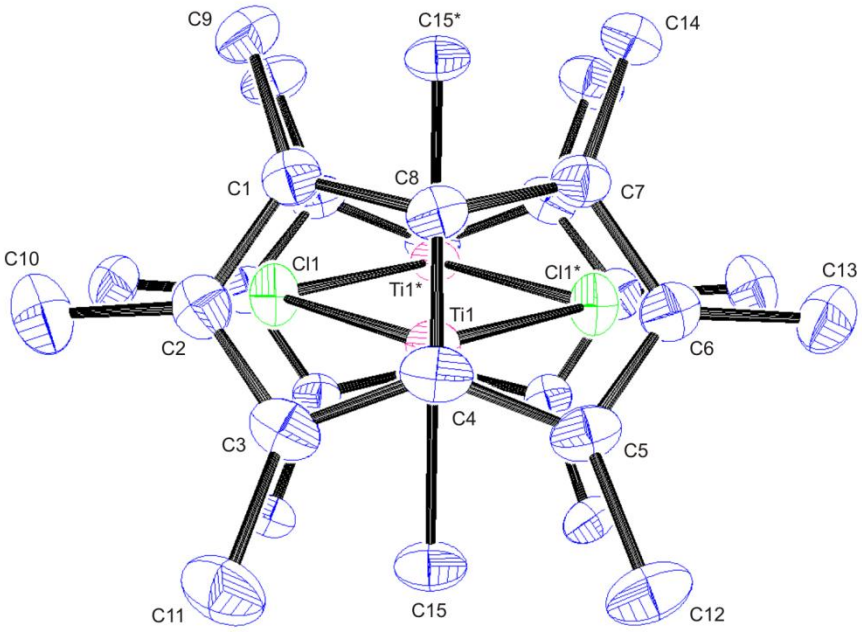

Figure 2.5: Top view of **2.2** with thermal ellipsoids at 50%. Hydrogen atoms omitted for clarity, * denotes atoms generated by inversion symmetry.

2.2 crystallises in the $P\bar{1}$ space group with two independent molecules in the asymmetric unit; both of these are half-molecules of the constituent dimers, possessing inversion symmetry and are geometrically closely related. Through dimerisation the titanium centre has alleviated electron deficiency from a 14 electron monomer to the 16 electron dimer, analogous to **2.1** (Figure 2.6).[26]

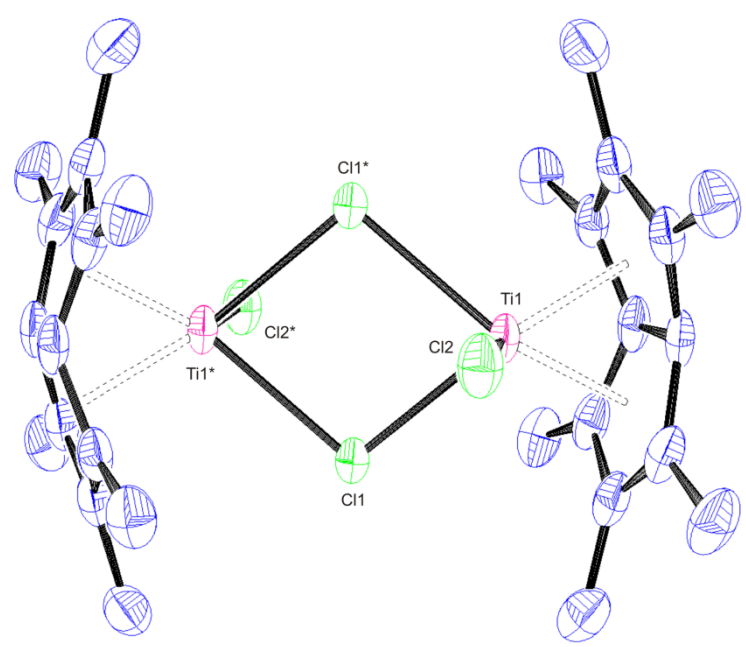

Figure 2.6: Solid state structure of **2.1**, reproduced from ref 26.

2.2 is isostructural with **2.1**, the sole difference being that the former has a terminal methyl whereas the latter a terminal chloride. This leads to slight differences in their observed bond distances and angles and can be attributed to the greater electron donating ability of Me as compared to Cl [Pauling electronegativities: Cl = 3.16, C = 2.55, (Me = 2.55)[30];[27] thus the electron deficient Ti metal centre in **2.2** will be stabilised relative to **2.1**. This is supported by the fact that the fold angle in **2.2** (30.6°) is smaller than the values seen for **2.1** (32.6° and 32.9°)[26] [as demonstrated in the series $Ta(\eta^8\text{-}Pn^{1,4\text{-}Si^iPr_3})Me_yX_{3-y}$ (y = 1-3, X = Cl; y = 0, X = I)][31].

The Ti(1)-C(15) bond length [2.188(5) Å] is substantially longer than the distance seen for the most closely related Ti compound $[Ti(Me)_2(\mu\text{-}Cl)_2]_n$ [2.055(5) Å],[13] which is reasoned to be the result of the reduction of the formal charge on Ti in **2.2** by electron donation from Pn*. It does however, correlate well with the lengths seen in Cp_2TiMe_2 [2.170(2) and 2.181(2) Å],[32] which also contains terminal

Ti-Me bonds. The Pn* ligands are almost eclipsed around the $Ti_2(\mu\text{-}Cl)_2$ core (Figure 2.5), paralleling the structure of **2.1**. The average value for the Ti-(μ-Cl) bonds (2.508 Å) is in good agreement with that seen for **2.1** (2.485 Å),[26] with the slight elongation attributed to the differences in electronegativities (Me *vs.* Cl) of the terminal group, as discussed earlier. Other comparisons to π-hydrocarbon bound titanium chlorides are those for Ti^{III} – $[Ti(Cp)_2(\mu\text{-}Cl)]_2$ (2.543 Å)[33] and the unusual tetrameric $[Ti(\eta^8\text{-}COT)(\mu\text{-}Cl)]_4$ (2.592 Å)[34] – in which the lower oxidation state on the Ti atom exerts less of an electrostatic attraction on the formally anionic chloride ligands and subsequently contacts are lengthened compared to **2.2**.

With a Ti···Ti distance of 3.840 Å, which is slightly larger than seen in **2.1** (3.806 Å), there is no evidence of a titanium-titanium bond present (sum of covalent radii = 2.64 Å).

Table 2.1: Selected bond lengths, angles and structural parameters for one of the symmetric molecules in the asymmetric unit of **2.2**. * denotes atoms generated by inversion symmetry and ESDs are given in parentheses.

Lengths (Å)			
Ti(1) - C(1)	2.355(4)	C(1) - C(2)	1.417(7)
Ti(1) - C(2)	2.531(5)	C(2) - C(3)	1.400(7)
Ti(1) - C(3)	2.404(4)	C(3) - C(4)	1.431(7)
Ti(1) - C(4)	2.132(4)	C(4) - C(5)	1.436(7)
Ti(1) - C(5)	2.412(4)	C(5) - C(6)	1.412(7)
Ti(1) - C(6)	2.534(5)	C(6) - C(7)	1.424(6)
Ti(1) - C(7)	2.339(5)	C(7) - C(8)	1.431(7)
Ti(1) - C(8)	2.121(4)	C(8) - C(1)	1.433(6)
Ti(1) - Ti(1*)	3.8401(11)	C(4) - C(8)	1.456(6)
Ti(1) - C(15)	2.188(5)	Av. C_{ring} - Me	1.502
Ti(1) - Cl(1)	2.494(1)	Ti(1) - Pn^*_{cent}	1.970
Ti(1) - Cl(1*)	2.521(1)	Ti(1) - Pn^*_{cent}	1.967

Angles (°)	
C(15) - Ti(1) - Cl(1)	91.32(14)
C(15) - Ti(1) - Cl(1*)	89.80(14)
Ti(1) - Cl(1) - Ti(1*)	99.95(4)
Cl(1) - Ti(1) - Cl(1*)	80.05(4)
Fold Angle	30.61

The intraligand distances within Pn* do not show a distinct bond alternation pattern and the average value of 1.427 Å is within the range previously established in other η^8-pentalene organometallics; as expected, the bridgehead bond is the longest due to the strain induced by the deformation of the bicyclic framework. The Ti-C(Pn*) lengths can be partitioned into three distinct categories with the shortest contacts to the ring junction (average 2.127 Å), the longest to the wingtip atoms (2.533 Å) and the remainder intermediate (2.378 Å); this pattern is a common feature in other structurally characterised η^8-Pn[35] and η^8-Pn*[26, 36, 37] complexes and indeed is repeated for all crystallographically elucidated species reported in this work. A selection of structural parameters for all crystallographically characterised complexes contained within each chapter are collated and discussed in their respective conclusions.

The room temperature ^{1}H NMR spectrum of **2.2** reveals three sharp singlets in a 6:12:3 intensity ratio and one may conclude that the solution phase structure of the molecule is in contrast to that observed in the solid state (C_{2h}), from which a 6:6:6:3 intensity ratio would be expected. This indicates a fluxional process is operating in solution, which equates all four NWT-Me groups on each Pn* moiety. The singlet of relative intensity three, corresponding to the Me group (δ = 0.40 ppm; C_6D_6), matches well with that seen for $Cp^*_2TiMeCl$ (δ = 0.23 ppm; C_6D_6).[38] The ^{13}C NMR (C_6D_6) spectrum shows five resonances corresponding to the Pn* carbons at the expected values,[26] with the resonance at δ = 37.6 ppm ascribed to the terminal methyl carbon.

It is known that transition metal complexes containing σ-alkyl ligands have a tendency to be thermally and photochemically sensitive, leading to decomposition by a number of pathways, which results in difficulties in characterisation.[19, 39] **2.2** was found to be indefinitely stable in the solid state under an inert atmosphere but decomposed in solution over a matter of days at room temperature, forming a purple solution later identified as $[Pn^*Ti(\mu\text{-}Cl)]_2(\mu\text{-}CH_2)$ (**2.3**). The pattern in thermal stability of **2.2** and **2.7** (*vide infra*) is in contrast to that seen for the related compounds $Cp_2TiClMe$ and Cp_2TiMe_2, where the mono alkylated species is significantly more thermally robust than its dialkylated analogue.[39–41] This is postulated to be the result of **2.2** possessing a dimeric structure which is pre-organised for an intramolecular decomposition pathway with concomitant liberation of CH_4 forming **2.3**, in contrast to the monomeric structure of Pn^*TiMe_2 (**2.7**, *vide infra*).

2.5 Synthesis and characterisation of $[Pn^*Ti(\mu\text{-}Cl)]_2(\mu\text{-}CH_2)$ (2.3)

A benzene solution of **2.2** was heated in a sealed ampoule to 50 °C and the emerald green solution slowly turned dark magenta over a number of days (Figure 2.7). Work up was completed in a glovebox and the slow cooling of a hexane solution furnished $[Pn^*Ti(\mu\text{-}Cl)]_2(\mu\text{-}CH_2)$ (**2.3**), which was identified by X-ray crystallography and mass spectrometry (EI). The latter showed the molecular ion at accurate mass followed by peaks ascribed to the loss of CH_2 and Cl and subsequent scission of the dimer unit. This Pn* complex gave large, dark red X-ray quality crystals upon slow evaporation of a C_6D_6 solution and two views of the solid state structure of $[Pn^*Ti(\mu\text{-}Cl)]_2(\mu\text{-}CH_2)$ (**2.3**) are shown in Figure 2.8 and 2.9.

Figure 2.7: Synthesis of $[Pn^*Ti(\mu\text{-}Cl)]_2(\mu\text{-}CH_2)$ (**2.3**).

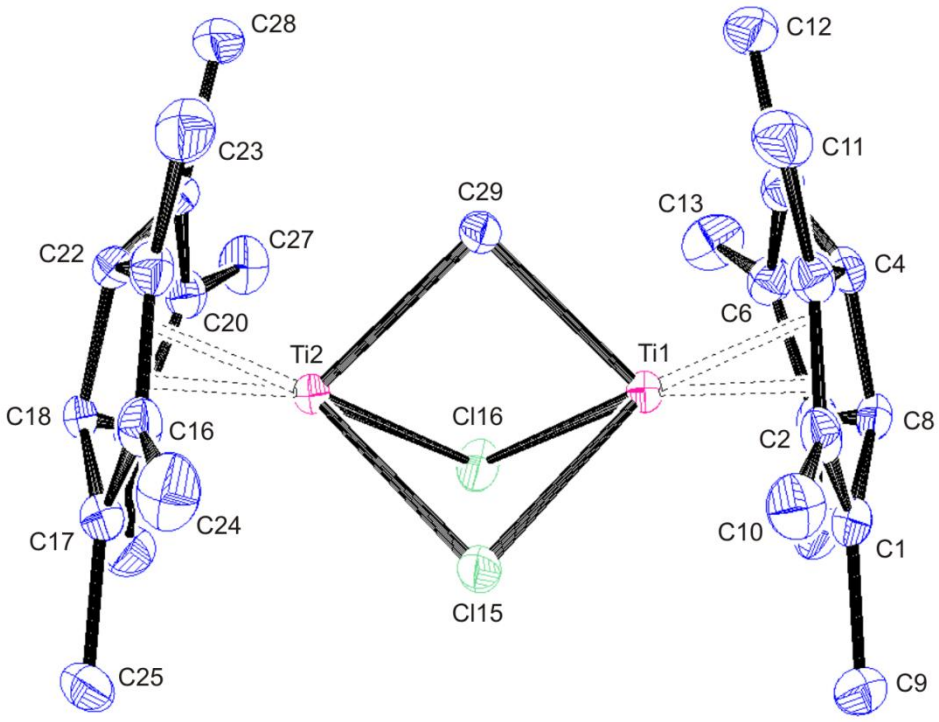

Figure 2.8: Side-on view of **2.3** with thermal ellipsoids at 50%. Hydrogen atoms omitted for clarity.

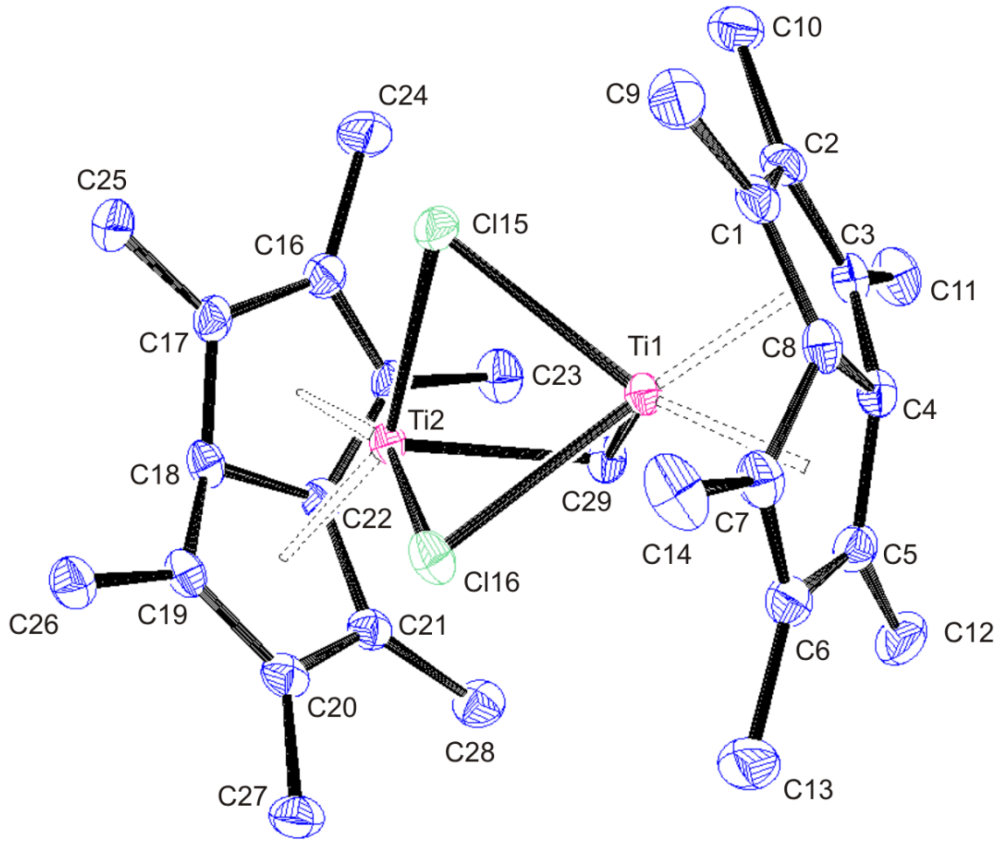

Figure 2.9: Angled view of **2.3** with thermal ellipsoids at 50%. Hydrogen atoms omitted for clarity.

Crystallographic analysis shows **2.3** to crystallise in the $P2_1$ space group with two asymmetric whole molecules in the asymmetric unit. The two molecules are almost identical geometrically, with eclipsed Pn* ligands around a $Ti_2(\mu\text{-}Cl)_2(\mu\text{-}CH_2)$ core and both Pn* moieties 'canting' towards the methylene bridge. In the solid state **2.3** is of C_{2v} symmetry with the principle axis running through C(29) and the point equidistant between Ti(1) and Ti(2). Each titanium centre possesses a stable electron count of 16, paralleling **2.1** and **2.2**.

The most pertinent comparisons would be made with the Tebbe reagent $Cp_2Ti(\mu\text{-}CH_2)(\mu\text{-}Cl)AlMe_2$,[42] the most important source of titanium methylene compounds, which is utilized in the conversion of esters to vinyl ethers, or with that of the dimethylene bridging titanium complex $[Cp_2Ti(\mu\text{-}CH_2)]_2$,[43] but unfortunately analysis of the crystal structure and subsequent bond lengths and angles are not available in the literature.

Table 2.2: Selected bond lengths, angles and structural parameters for one of the whole asymmetric molecules in the asymmetric unit of **2.3**. ESDs are given in parentheses.

Lengths (Å)			
Ti(1) - C(1)	2.324(2)	Ti(2) - C(15)	2.406(2)
Ti(1) - C(2)	2.520(3)	Ti(2) - C(16)	2.517(3)
Ti(1) - C(3)	2.418(2)	Ti(2) - C(17)	2.339(2)
Ti(1) - C(4)	2.146(2)	Ti(2) - C(18)	2.126(2)
Ti(1) - C(5)	2.435(3)	Ti(2) - C(19)	2.323(2)
Ti(1) - C(6)	2.512(3)	Ti(2) - C(20)	2.487(2)
Ti(1) - C(7)	2.318(2)	Ti(2) - C(21)	2.389(2)
Ti(1) - C(8)	2.127(2)	Ti(2) - C(22)	2.137(2)
Ti(1) - C(29)	2.136(2)	Ti(2) - C(29)	2.167(2)
Ti(1) - Cl(15)	2.4858(7)	Ti(2) - Cl(15)	2.4703(7)
Ti(1) - Cl(16)	2.4764(7)	Ti(2) - Cl(16)	2.4935(7)
C(1) - C(2)	1.423(4)	C(15) - C(16)	1.411(4)
C(2) - C(3)	1.400(3)	C(16) - C(17)	1.423(4)
C(3) - C(4)	1.445(4)	C(17) - C(18)	1.436(4)
C(4) - C(5)	1.433(3)	C(18) - C(19)	1.437(4)
C(5) - C(6)	1.408(4)	C(19) - C(20)	1.426(3)
C(6) - C(7)	1.432(4)	C(20) - C(21)	1.406(4)
C(7) - C(8)	1.443(4)	C(21) - C(22)	1.443(3)
C(8) - C(1)	1.446(3)	C(22) - C(15)	1.444(3)
C(4) - C(8)	1.454(3)	C(18) - C(22)	1.461(3)
Av. C_{ring} - Me	1.501	Av. C_{ring} – Me	1.500
Ti(1) - Pn^*_{cent}	1.965	Ti(2) - Pn^*_{cent}	1.964
Ti(1) - Pn^*_{cent}	1.946	Ti(2) - Pn^*_{cent}	1.961
Ti(1) - Ti(2)	3.0391(5)		
Angles (°)			
Ti(1) - C(29) - Ti(2)	89.88(9)		
Ti(1) - Cl(15) - Ti(2)	75.64(2)		
Ti(1) - Cl(16) - Ti(2)	75.39(2)		
Fold Angle	32.51 & 33.26		

The molecular morphology of the solid state structure is identical to that seen in the mixed valence $(Pn^*Ti)_2(\mu\text{-}Cl)_3$ (Figure 2.10), previously synthesised by O'Hare *et al. via* combination of KC_8 and **2.1**.[44] It has the same tripodal disposition of bridging ligands between the Ti centres with the methylene group pointed towards a bridgehead carbon and the chloride ligands pointed towards the non-wingtip carbons on the adjacent side of the ligand when looking end on, with the Pn* ligands eclipsed. The

average Ti-(μ-Cl) distance (2.482 Å) compares well with that seen in the isostructural $Ti^{III/IV}$ complex (2.501 Å) and other Pn*Ti-compounds, **2.1** and **2.2** (2.485 and 2.508 Å respectively).[26, 44]

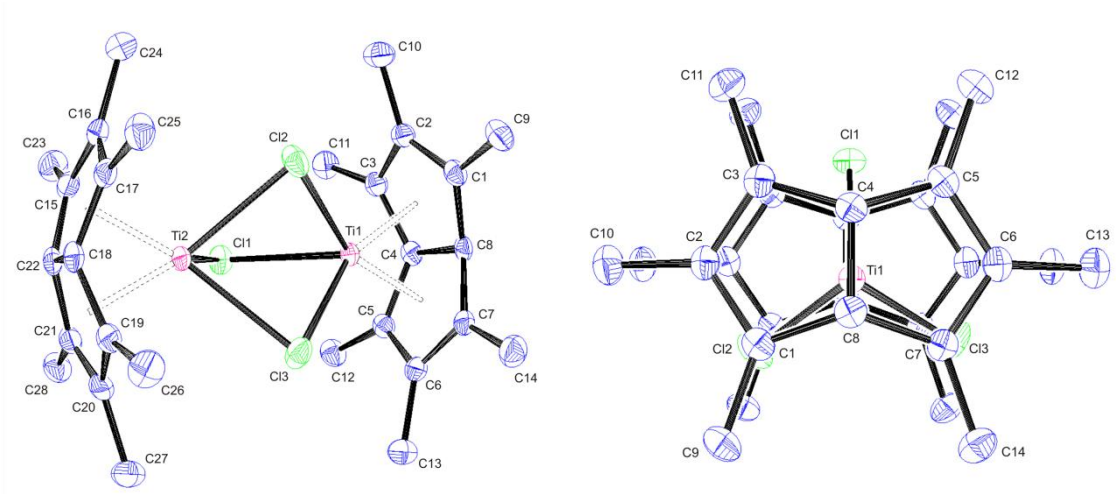

Figure 2.10: Angled and side-on view of solid state structure of $(Pn^*Ti)_2(\mu\text{-}Cl)_3$, reproduced from ref 44.

The fold angles (32.5° and 33.3°) are very similar to those in **2.1** (32.6/32.9°) and with the usual three sets of Ti-C(Pn*) contacts,[35] the average Ti-C(Pn*) distance (2.345 Å) being nearly identical to **2.2** and similar Ti-Pn^*_{cent} distances (1.959 and 1.969 Å respectively), it can be inferred that η^8-bonding is present in each case.

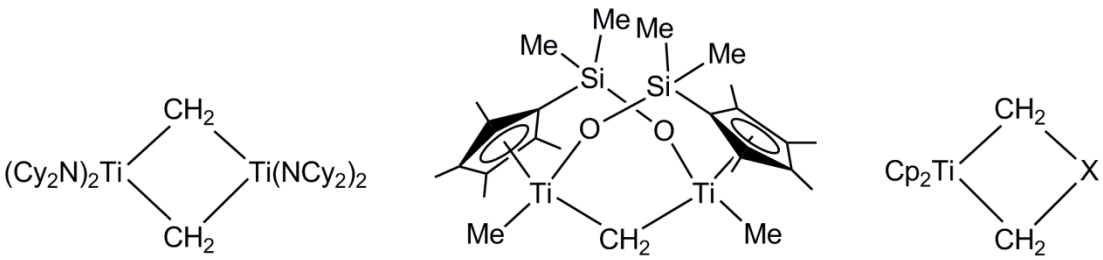

Figure 2.11: Bridging methylene groups in homobimetallics (a) $[(Cy_2N)_2Ti(\mu\text{-}CH_2)]_2$; (b) $\{Ti[\mu\text{-}(\eta^5\text{-}C_5Me_4SiMe_2\text{-}O]Me\}_2(\mu\text{-}CH_2)$ and (c) titanocyclobutanes, $Cp_2Ti(\mu\text{-}CH_2)_2X$ [X = CMe_2, C(Ph)H, C(^{t}Bu)H and $SiMe_2$].

Interestingly, another bridging methylene compound incorporating a pentalene framework, $[Ta(\eta^8\text{-}Pn^{1,4\text{-}Si^iPr_3})Cl(\mu\text{-}CH_2)]_2$ has been reported: However, no detailed structure or characterising data were published.[35] The only information revealed was the eclipsing nature of the (η^8-$Pn^{1,4\text{-}Si^iPr_3}$) ligands, which is paralleled for Pn* in **2.3**.

There are very few fully characterised examples of bridging methylene groups between two titanium centres in the literature: $[(Cy_2N)_2Ti(\mu\text{-}CH_2)]_2$[45] and $\{Ti[\mu\text{-}(\eta^5\text{-}C_5Me_4SiMe_2\text{-}O)]Me\}_2(\mu\text{-}CH_2)$[46] have Ti-($\mu$-$CH_2$) distances of 2.018 and 2.0719(13) Å respectively (Figure 2.11). These are considerably shorter than that seen for **2.3** (2.152 Å), which could be due to the Pn* moiety being comparatively electron rich relative to the corresponding ancillary ligand sets, $(Cy_2N)_2$ and [μ-(η^5-$C_5Me_4SiMe_2$-O)], meaning the Ti centre has less of a desire to gain stability through shorter Ti-(μ-CH_2) contacts. The distance is however, in good agreement with that seen for the titanocyclobutanes $Cp_2TiCH_2C(R)(R')CH_2$ (R = R' = Me; R = Ph, ^{t}Bu R' = H) with values ranging from 2.113-2.160 Å[47] and the silicon analogue $Cp_2TiCH_2Si(Me)_2CH_2$ 2.146-2.169 Å.[48] The Ti(1)-C(29)-Ti(2) angle [89.88(9)°] matches well with that documented for the structurally similar heterobinuclear bridging methylene complex $Cp_2TiRh(COD)(\mu\text{-}CH_2)(\mu\text{-}Cl)$, which has a reported angle of 92.0°.[49]

The room temperature ^{1}H NMR spectrum of **2.3** consists of three resonances in an intensity ratio 2:12:24. The two resonances corresponding to the Pn* moiety fall within their expected range with a notable resonance furthest downfield (δ = 5.18 ppm; C_6D_6) that of μ-CH_2. This low-field value agrees well with that reported for $\{Ti[\mu\text{-}(\eta^5\text{-}C_5Me_4SiMe_2\text{-}O)]Me\}_2(\mu\text{-}CH_2)$ (δ = 5.90 ppm; C_6D_6) as does the ^{13}C resonance (δ = 183.2 and 196.9 ppm respectively).[46] The five other resonances in the ^{13}C NMR correspond to the Pn* ring carbons falling within their usual range.

α-hydrogen abstraction is one of a number of decomposition pathways observed for metal-alkyl complexes. The process can occur via an *inter*- or *intra*-molecular pathway resulting in an alkylidene or carbene complex.[19, 39] The mechanism for formation of **2.3** is postulated to proceed by an intramolecular α-hydrogen abstraction pathway, with the dimeric structure of **2.2** being crucial as a prerequisite for CH_4 elimination and the subsequent formation of **2.3**. Evidence against the mechanism occurring *via* an intermolecular pathway is the thermal stability of **2.7** and its inability to form the analogous structure **2.4** upon prolonged heating (*vide infra*). Bridging methylene formation by homobimetallic systems bearing terminal methyl groups has been reported in the literature, with flexibility of the central core key in allowing both metal atoms to act cooperatively during the course of the process.[46] One of the postulated mechanisms in the formation of $\{Ti[\mu\text{-}(\eta^5\text{-}C_5Me_4SiMe_2\text{-}O)]Me\}_2(\mu\text{-}CH_2)$ from $\{Ti[\mu\text{-}(\eta^5\text{-}C_5Me_4SiMe_2\text{-}O)]Me_2\}_2$ involves direct σ-bond metathesis, in which the

leaving methyl group originates from the adjacent titanium atom. The equivalence of all NWT-Me groups of **2.2** in solution, as demonstrated by NMR spectroscopy conflicts with the solid state structure and indicates a fluxional process occurring. Although mechanistic details of this process are unknown, it is facile on the NMR timescale at room temperature and as such indicates **2.2** may contain the flexibility, described previously as being paramount to such a process. It can be envisaged that one of the conformations in this fluxional process is **(i)** Figure 2.12, which is correctly aligned for CH_4 elimination by α-H abstraction from the methyl group on the neighbouring Ti atom. Since CH_4 is detected when the reaction is conducted on the NMR scale (0.16 ppm; C_6D_6) and in conjunction with the other spectroscopic evidence, it seems reasonable to propose this mechanism for formation of **2.3** (Figure 2.12).

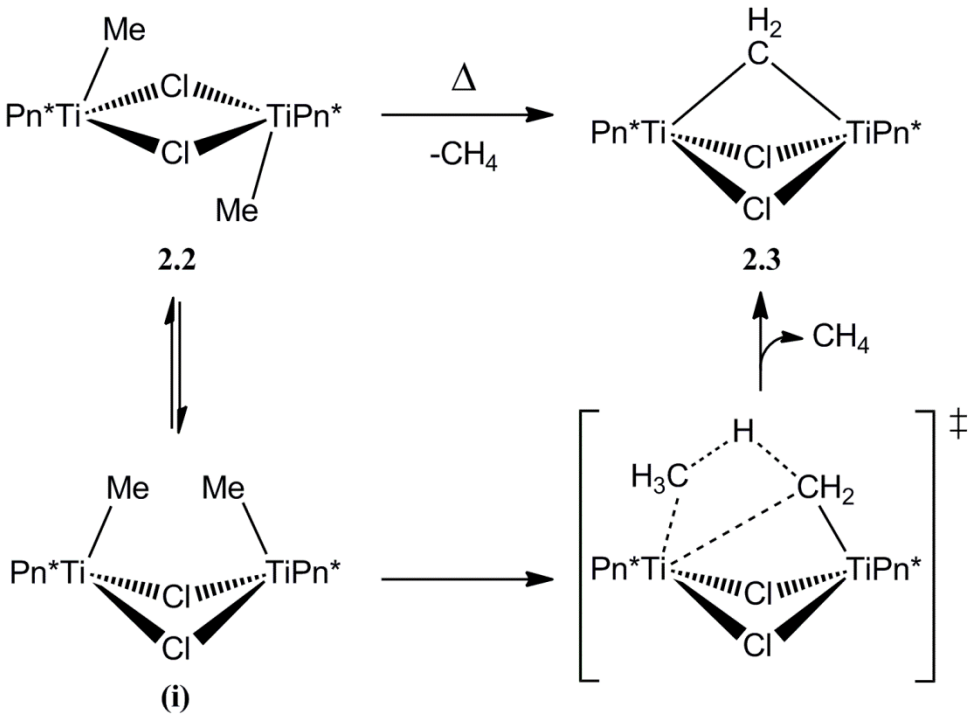

Figure 2.12: Proposed mechanism for the formation of **2.3**.

2.6 Synthesis and characterisation of [Pn*Ti(μ-Me)]$_2$(μ-CH$_2$) (2.4)

It has been documented that bridging chloride ligands show the same substitutional lability as terminal chlorides *via* standard salt metathesis reactions.[49] This can be seen for the heterobinuclear complex $Cp_2TiRh(COD)(\mu\text{-}CH_2)(\mu\text{-}Cl)$, whereby the bridging chloride can exchange for a methyl group on reaction with MeLi or MeMgX, resulting in a compound containing both μ-CH_2 and μ-Me groups.[50] With this in mind,

attempts were made to replicate the reactivity by reaction of **2.3** with the methylating agent Me_2Mg. The two were combined in C_6D_6 with a trace of Et_2O to promote reaction and sonicated for three hours, over which time the purple solution deepened in colour (Figure 2.13).

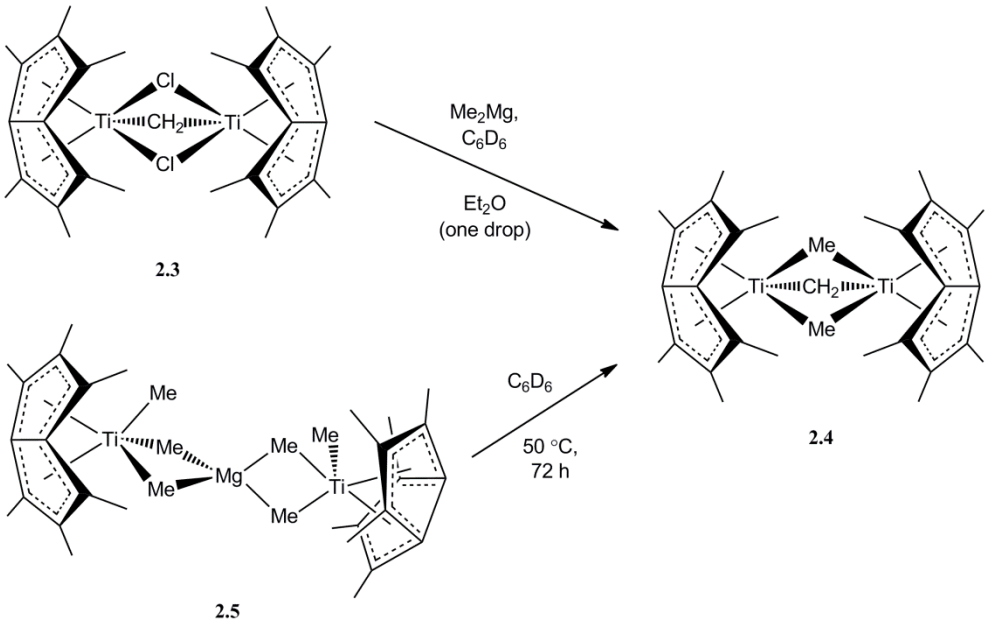

Figure 2.13: Syntheses of $[Pn^*Ti(\mu\text{-}Me)]_2(\mu\text{-}CH_2)$ (**2.4**).

^{1}H NMR analysis demonstrated the complete consumption of **2.3** and the clean formation of a novel species, later confirmed as $[Pn^*Ti(\mu\text{-}Me)]_2(\mu\text{-}CH_2)$ (**2.4**) by X-ray crystallography. The room temperature ^{1}H NMR spectra are almost identical (μ-CH_2 chemical shift: **2.4**, δ = 5.22 ppm; **2.3**, δ = 5.18 ppm) with the addition of an extra resonance at high field for **2.4**, expected on the substitution of Me for Cl. The spectrum consists of four resonances in an intensity ratio 2:12:24:6 with the aforementioned high field resonance corresponding to that of the μ-Me protons (δ = −0.74 ppm, relative intensity six; C_6D_6), which correlates extremely well with the value seen for the cationic species $\{[Cp^*(^tBu_2C{=}N)Ti]_2(\mu\text{-}Me)(\mu\text{-}CH_2)\}[B(C_6F_5)_4]$ (δ = −0.98 ppm).[51] There are seven resonances seen in the room temperature ^{13}C NMR spectrum, with five corresponding to the Pn* ring carbons falling within their usual range. As observed in the ^{1}H NMR, the μ-CH_2 resonance (δ = 180.2 ppm) lies downfield to that of μ-Me (δ = 48.5 ppm), and the latter's chemical shift is downfield relative to the value for the terminal methyl in **2.2** (δ = 37.6 ppm); this is expected as coordination of two electron

deficient Ti^{IV} centres will draw more electron density and deshield the μ-Me carbon to a greater extent.

Single crystals suitable for X-ray diffraction were grown in an identical manner to **2.3** by slow evaporation of a C_6D_6 solution, and the solid state structure of $[Pn^*Ti(\mu\text{-}Me)]_2(\mu\text{-}CH_2)$ (**2.4**) is shown in Figure 2.14.

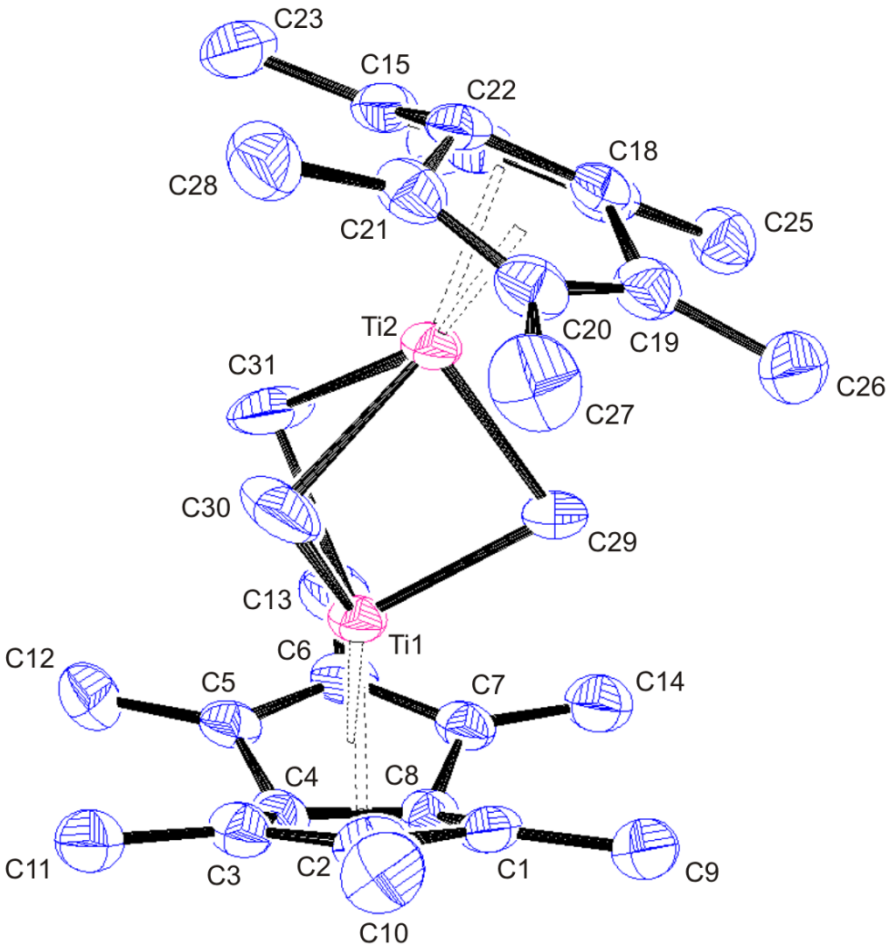

Figure 2.14: Side-on view of **2.4** with thermal ellipsoids at 50%. Hydrogen atoms omitted for clarity.

Crystallographic analysis demonstrates **2.4** to crystallise in the same $P2_1$ space group as **2.3**, and similarly, has two asymmetric whole molecules in the asymmetric unit. The two molecules are almost identical geometrically and are isostructural to **2.3** with both Pn* moieties 'canting' towards the methylene bridge. It also possesses the same C_{2v} solid state symmetry, with the principle axis running through C(29) and the point equidistant between Ti(1) and Ti(2) and the same formal electron count at each titanium

centre, 16.[52] This is the first crystallographically characterised compound containing both bridging methyl and methylene groups between two titanium centres.

As expected, substitution of two highly electronegative chlorides for two methyls yields fold angles (31.6/32.0°) that are smaller than those seen in **2.3** (32.5/33.3°). This trend has been previously noted in series of pentalene compounds where the M-BH carbon bond lengths are consistent but the M-WT carbon distance varies depending on the electronegativity of the co-ligands, the pentalene ligand folds at the bridgehead towards the metal in order to 'restore' the electronic deficiency caused by electron-withdrawing substituents on the metal.[31]

The CH_3 moiety is known to adopt a number of different bridging conformations[53] and although attempts to locate the hydrogens *via* a Fourier difference analysis were unsuccessful, it seems reasonable to assign a symmetric pyramidal arrangement as the Ti-(μ-Me) distances are essentially equivalent within ESDs. Examples containing agostic interactions are usually asymmetric with markedly different distances to each respective metal centre, as found in the dipalladium cationic complex $[(N\text{^}N)_2Pd_2(\mu\text{-}CH_2)(\mu\text{-}Me)]^+$ [N^N = ArN=CMeCMe=NAr, Ar = 2,6-$C_6H_3(^iPr)_2$].[54] Comparisons to other methyl bridged dititanium compounds are limited, with only a handful reported in the CSD, but the average value for the Ti-(μ-Me) distance (2.297 Å) is in good agreement with those documented.[13, 55, 56] It is also longer than observed for the terminal methyl in **2.2** [2.188(5) Å], which is expected since a terminal Me is a two-centre two-electron bonding interaction, in contrast with the three-centre two-electron bonding interaction for a μ-Me, highlighting the comparatively poor bridging nature of the methyl group.

The Ti-(μ-CH_2) distance (2.123 Å) is much shorter than the Ti-(μ-Me) (2.297 Å), which is expected as the attraction between the electron deficient Ti^{IV} centres and the formally dianionic 'CH_2' will be greater than for the monoanionic 'CH_3' and the Ti^{IV} metal centres. The value is also marginally shorter than seen in **2.3** (2.152 Å). A further observation upon methylation is the decreased Ti-C(29)-Ti angle (**2.3**, 89.9°; **2.4**, 83.4°); a trend mirrored in the methylation of the analogous heterobinuclear $Cp_2TiRh(COD)(\mu\text{-}CH_2)(\mu\text{-}Cl)$ to $Cp_2TiRh(COD)(\mu\text{-}CH_2)(\mu\text{-}Me)$, resulting in a comparable decrease from 92.0° to 83.9°.[50] A consequence of the aforementioned reduction of bond lengths and angle is the dramatically shortened Ti-Ti distance in **2.4**

as compared to **2.3** [2.8238(10) and 3.0391(5) Å respectively]. Although there is a striking difference between the two bond lengths, both fall short of the sum of covalent radii (2.64 Å) indicating no significant metal-metal interaction.

Table 2.3: Selected bond lengths, angles and structural parameters for one of the whole asymmetric molecules in the asymmetric unit of **2.4**. ESDs are given in parentheses.

Lengths (Å)			
Ti(1) - C(1)	2.458(5)	Ti(2) - C(15)	2.375(5)
Ti(1) - C(2)	2.539(6)	Ti(2) - C(16)	2.539(6)
Ti(1) - C(3)	2.358(5)	Ti(2) - C(17)	2.413(5)
Ti(1) - C(4)	2.145(5)	Ti(2) - C(18)	2.156(5)
Ti(1) - C(5)	2.362(5)	Ti(2) - C(19)	2.421(5)
Ti(1) - C(6)	2.536(6)	Ti(2) - C(20)	2.513(5)
Ti(1) - C(7)	2.439(5)	Ti(2) - C(21)	2.364(5)
Ti(1) - C(8)	2.170(5)	Ti(2) - C(22)	2.135(5)
Ti(1) - C(29)	2.110(5)	Ti(2) - C(29)	2.135(5)
Ti(1) - C(30)	2.313(6)	Ti(2) - C(30)	2.305(6)
Ti(1) - C(31)	2.290(6)	Ti(2) - C(31)	2.278(6)
C(1) - C(2)	1.405(8)	C(15) - C(16)	1.405(8)
C(2) - C(3)	1.428(8)	C(16) - C(17)	1.431(8)
C(3) - C(4)	1.453(8)	C(17) - C(18)	1.452(8)
C(4) - C(5)	1.418(8)	C(18) - C(19)	1.447(8)
C(5) - C(6)	1.419(8)	C(19) - C(20)	1.413(8)
C(6) - C(7)	1.417(8)	C(20) - C(21)	1.425(7)
C(7) - C(8)	1.438(8)	C(21) - C(22)	1.435(8)
C(8) - C(1)	1.461(8)	C(22) - C(15)	1.451(8)
C(4) - C(8)	1.458(7)	C(18) - C(22)	1.443(7)
Av. C_{ring} - Me	1.491	Av. C_{ring} - Me	1.492
Ti(1) - Pn^*_{cent}	1.992	Ti(2) - Pn^*_{cent}	1.977
Ti(1) - Pn^*_{cent}	1.994	Ti(2) - Pn^*_{cent}	1.983
Ti(1) - Ti(2)	2.8238(10)		

Angles (°)	
Ti(1) - C(29) - Ti(2)	83.39(16)
Ti(1) - C(30) - Ti(2)	75.37(15)
Ti(1) - C(31) - Ti(2)	76.36(16)
Fold Angle	31.63 & 32.03

An alternative synthesis of **2.4** has also been discovered; heating a C_6D_6 solution of **2.5** and residual THF for four days at 50 °C was also found to furnish **2.4**

(Figure 2.13). Unfortunately, this synthetic method was found to be capricious and an unreliable route to the large scale synthesis of **2.4**.

2.7 Synthesis and characterisation of [Pn*TiMe(μ-Me)$_2$]$_2$Mg (2.5)

The syntheses of [Pn*TiMe(μ-Me)$_2$]$_2$Mg (**2.5**) are detailed in Figure 2.15; reaction of **2.1** with a large excess of Me_2Mg in a 2:1 toluene/THF mixture afforded a green-brown solution. Subsequent work up and extraction with hexane yielded a pink solution, which interestingly on cooling to −35 °C precipitated green single crystals suitable for X-ray diffraction. The green crystalline solid was identified as **2.5** by X-ray crystallography and the structure is shown below (Figure 2.16).

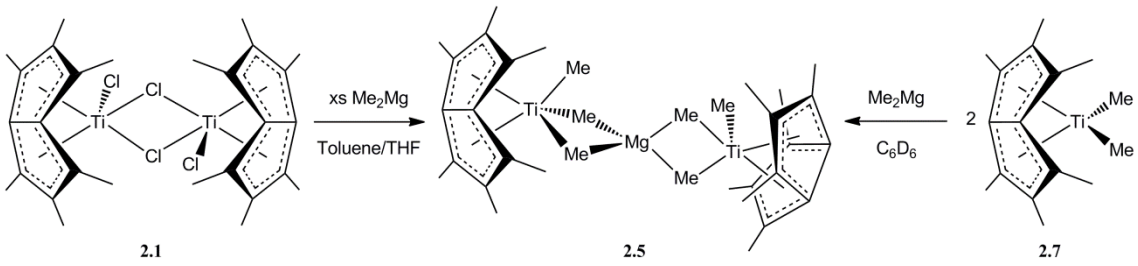

Figure 2.15: Syntheses of [Pn*TiMe(μ-Me)$_2$]$_2$Mg (**2.5**).

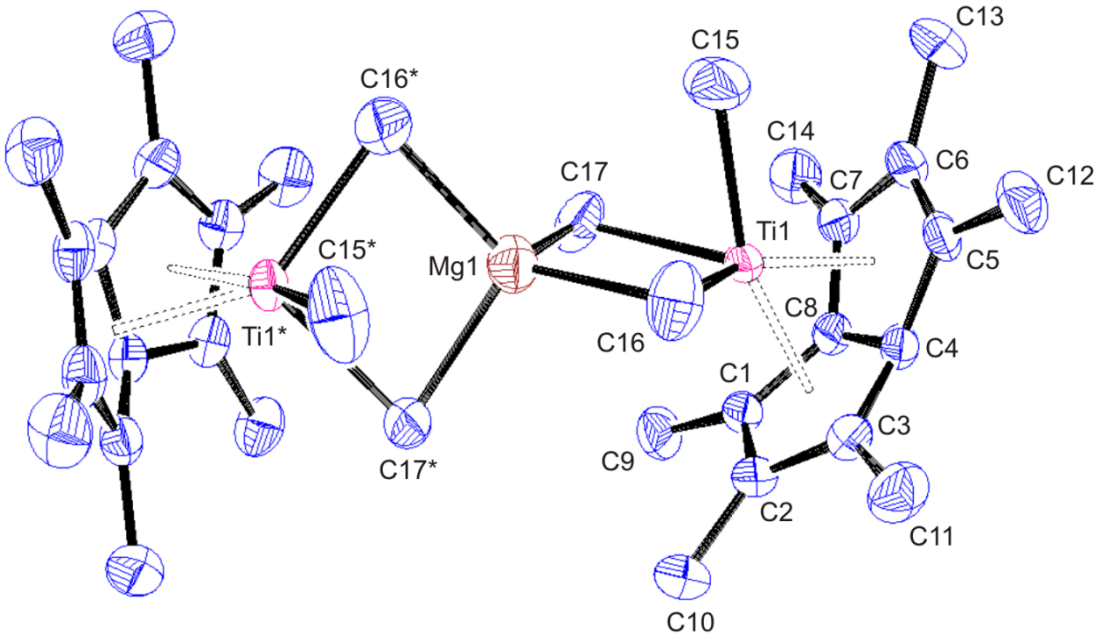

Figure 2.16: Side-on view of **2.5** with thermal ellipsoids at 50%. Hydrogen atoms omitted for clarity, * denotes atoms generated by (S_4) symmetry.

Crystallographic analysis demonstrates **2.5** to crystallises in the chiral $P4_32_12$ space group with one half molecule in the asymmetric unit related by an S_4 symmetry element, with the axis passing through the Ti(1), Mg(1) and Ti(1*) atoms. As the compound possesses an improper rotation axis, it may crystallise in a chiral space group due to crystal packing forces resulting in the spiral nature of the molecules in the unit cell (Figure 2.17); this leads to the possibility of a right and left hand enantiomer. The flack parameter of 0.04(4) demonstrates that the crystal is enantiopure and the absolute configuration is as shown.

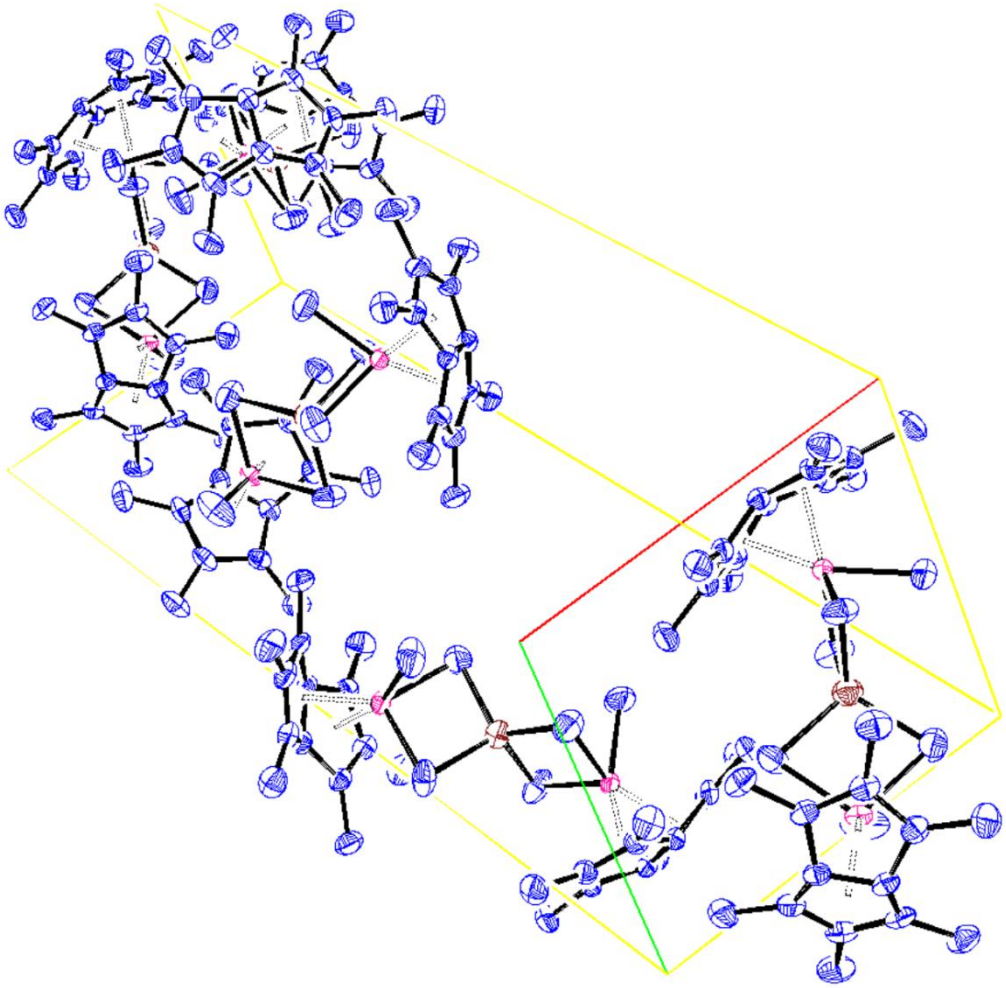

Figure 2.17: Spiral disposition in enantiopure unit cell of **2.5** with thermal ellipsoids at 50%. Hydrogen atoms omitted for clarity.

Similar to **2.1**, **2.2**, **2.3** and **2.4**, each titanium centre possesses a formal electron count of 16.

The solid state structure contains one terminal and two bridging methyls per Pn*Ti, pivoted around a central magnesium atom and can be thought of as a Me_2Mg moiety sandwiched between two Pn^*TiMe_2 units forming the interesting trimetallic **2.5**. This is the first crystallographically characterised example of a double alkyl bridge between a titanium and magnesium centre reported in the literature. The disposition of bridging methyls around the magnesium centre is an archetypal tetrahedron with the average C-Mg-C angle 109.5°, which compares very well with that seen for the structurally similar trimetallic complex $[Li(TMEDA)]_2Me_4Mg$ (109.5°)[57] and that of polymeric $(Me_2Mg)_\infty$ (105.0°).[58] The average Mg-(μ-Me) bond length (2.213 Å) is also in good agreement with the examples above [2.260 and 2.240 Å respectively]. The geometry is emphasised by the angle between the two planes containing C(15)/Ti(1)/Mg(1) and C(15*)/Ti(1*)/Mg(1) being close to perpendicular at 85.1°.

Table 2.4: Selected bond lengths, angles and structural parameters for **2.5**. * denotes atoms generated by (S_4) symmetry and ESDs are given in parentheses.

Lengths (Å)			
Ti(1) - C(1)	2.414(2)	C(1) - C(2)	1.411(4)
Ti(1) - C(2)	2.571(3)	C(2) - C(3)	1.422(4)
Ti(1) - C(3)	2.406(3)	C(3) - C(4)	1.438(4)
Ti(1) - C(4)	2.134(2)	C(4) - C(5)	1.436(3)
Ti(1) - C(5)	2.343(2)	C(5) - C(6)	1.420(4)
Ti(1) - C(6)	2.544(3)	C(6) - C(7)	1.409(4)
Ti(1) - C(7)	2.434(3)	C(7) - C(8)	1.438(4)
Ti(1) - C(8)	2.147(2)	C(8) - C(1)	1.451(3)
Ti(1) - C(15)	2.203(3)	C(4) - C(8)	1.451(4)
Ti(1) - C(16)	2.245(4)		
Ti(1) - C(17)	2.291(3)	Av. C_{ring} - Me	1.503
Ti(1) - Mg(1)	2.8302(4)		
Ti(1) - Pn^*_{cent}	1.997	Mg(1) - C(16)	2.222(4)
Ti(1) - Pn^*_{cent}	1.982	Mg(1) - C(17)	2.203(3)

Angles (°)	
C(15) - Ti(1) - C(16)	81.67(17)
C(15) - Ti(1) - C(17)	79.33(17)
C(16) - Ti(1) - C(17)	99.88(12)
Ti(1) - C(16) - Mg(1)	78.64(12)
Ti(1) - C(17) - Mg(1)	78.06(11)
Av. C - Mg(1) - C	109.51
Fold Angle	29.78

The average Ti-(μ-Me) distance (2.268 Å) is slightly longer than that seen for the terminal Ti-Me distance [2.203(3) Å] (as expected for a three centre, two electron versus a two centre, two electron interaction) and is in good agreement with other Ti-(μ-Me) lengths reported; **2.4** - 2.297 Å; [bis(amidinate)]Ti_2Cp_2(μ-Me)(μ-H) - 2.274(3) Å; Cp_2TiRh(COD)(μ-CH_2)(μ-Me) - 2.294(6) Å. The Ti-(μ-Me)-M (M = Ti, Rh) angle also correlates well; 78.4 and 75.9, 81.9 and 80.0° respectively.[50, 55] The terminal methyl bond [2.203(3) Å] is longer than that observed for **2.2** (2.188 Å), **2.7** [2.132(2) and 2.139(2) Å *vide infra*] and in the related Cp_2TiMe_2 [2.170(2) and 2.181(2) Å].[32] This observation combined with a difference of only 0.065 Å between Ti-(μ-Me) and Ti-Me bond lengths, suggests a fluxional process is operating whereby there is exchange between the bridging and terminal methyl groups, a fact that is supported by a single broad Me resonance in the ^{1}H NMR spectra (*vide infra*).

The fold angle for **2.5** (29.8°) is the smallest reported for any Pn-Ti containing compound to date. This is attributed to the combination of greater steric congestion in the titanium coordination sphere and the increased electron density at the metal from three inductively donating methyl groups. This results in a diminished need to maximise Ti-C(Pn*) contacts, resulting in the longest Ti-WT C(Pn*) distance in the series and consequently, the smallest fold angle.[35]

The Ti-Mg distance [2.8302(4) Å] is longer than the sum of covalent radii (2.68 Å; Ti, 1.32; Mg, 1.36 Å)[27] and is in good agreement with that seen for the related trinuclear Ti-Mg-Ti hydride-bridged complexes [$(C_5H_{5-n}Me_n)_2$Ti(μ-H)$_2$]$_2$Mg (n = 3-5) [2.785(2), 2.784(1) and 2.858(4) Å respectively][59] where no metal-metal bond is postulated.

The room temperature ^{1}H NMR spectrum of **2.5** reveals three resonances, two sharp and one broad in an intensity ratio 12:6:9. The two sharp resonances correspond to the Pn* moiety, while the broad resonance of relative intensity nine (δ = −0.37 ppm, $\nu_{½}$ = 83.5 Hz; toluene-d_8) corresponds to the Me groups bound to titanium. This chemical shift is reasonable and falls between values seen for terminal and bridging Me groups already observed in this series (**2.2**, 0.40; **2.4**, −0.74 ppm respectively). The broad resonance indicates a fluxional process is occurring, with exchange of bridging and terminal Me groups. VT ^{1}H NMR measurements were conducted in an attempt to 'freeze-out' the fluxional process and upon cooling the resonance continued to broaden

to $\nu_{½}$ = 311.7 Hz at −60 °C and essentially coalesce with the baseline at −80 °C. Unfortunately no decoalescence was observed and further measurements were hampered due to the compounds poor solubility at low temperatures. Conversely, upon heating the resonance slowly sharpened to $\nu_{½}$ = 18.8 Hz at 90 °C but the fast exchange limit could not be reached, due to restrictions of the solvent temperature window and the onset of decomposition. At temperatures above 70 °C, CH_4 was evolved and the formation of **2.4** was noted, the exact mechanism is unknown but is thought to be complex and further investigations are required. There are five resonances observed in the room temperature ^{13}C NMR spectrum, all corresponding to the Pn* fragment, the resonance associated with the Ti-Me groups could not be located and this is attributed to the fluxional process operating.

2.8 Synthesis and characterisation of [Pn*TiMe$_3$]Li·(Et$_2$O)$_x$ (2.6)

'Anionic' metal alkyl complexes are known for a number of transition metals and usually contain one or more alkali metal counter ions to obtain complex neutrality.[39] Since lithium alkyl species contain bridging alkyl groups, it is not surprising that 'anionic' metal complexes contain Li-R-M arrangements, which can be observed in the crystallographically characterised $Li_3[CrMe_6]\cdot 3$(1,4-dioxane). Its structure consists of six methyl groups disposed in a slightly distorted octahedral arrangement around Cr and each tetrahedral lithium atom surrounded by two methyls and two dioxanes.[60, 61] 'Anionic' titanium alkyls were first documented in 1972 from the reaction of $TiMe_4$ with MeLi as a dioxane complex,[62, 63] although the structure was not confirmed until much later, when the ether analogue $[Li(Et_2O)_2][Ti(CH_3)_5]$ was characterised in 1999.[13]

Reaction of **2.1** with 6.4 equivalents of MeLi in Et_2O, shown in Figure 2.18, afforded a deep teal solution. Subsequent work up and cooling of saturated solutions in a number of solvents failed to produce a crystalline solid suitable for analysis. **2.6** was assigned the formula [Pn*TiMe$_3$]Li·(Et$_2$O)$_x$ on the basis of $^{1}H/^{13}C/^{7}Li$ NMR spectroscopy, and subsequent reactivity with **2.1** (*vide infra*). Properties of **2.6** include a very high solubility in ethereal, aromatic and to a certain extent, even hydrocarbon solvents, provided a stoichiometric quantity of coordinating solvent is present. Complete removal of coordinating solvent under reduced pressure renders the compound completely insoluble in aromatic and hydrocarbon solvents.

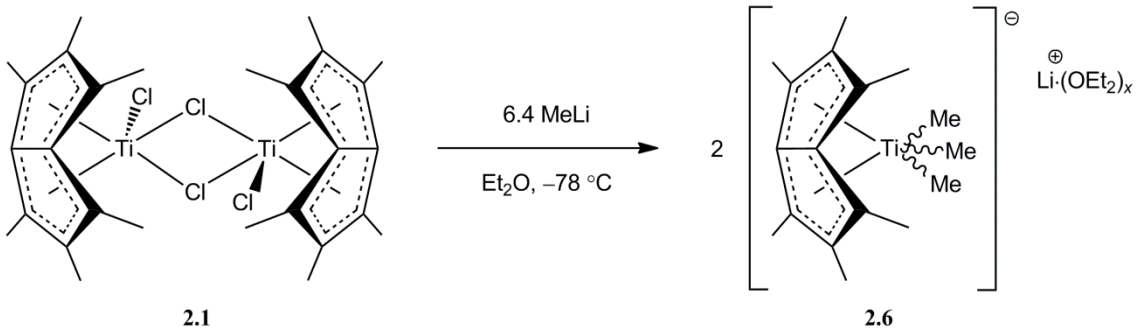

2.1 **2.6**

Figure 2.18: Synthesis of $[Pn^*TiMe_3]Li{\cdot}(Et_2O)_x$ (**2.6**).

The room temperature ^1H NMR spectrum of **2.6** reveals three sharp singlets in an intensity ratio 6:12:9 corresponding to Pn* and Ti-Me resonances, as well as the expected quartet and triplet associated for the coordinating Et_2O. The well defined singlets and ratio of Pn*:Ti-Me intensities (18:9) provides strong evidence of the presence of three methyl groups attached to titanium. The chemical shift corresponding to Ti-Me ($\delta = -0.45$ ppm; C_6D_6) matches reasonably well that seen for related 'anionic' d^0 group IV metal-methyl complexes $[Li(TMEDA)]_2[MMe_6]$ (M = Zr, Hf), ($\delta = 0.24$ and 0.15 ppm respectively; C_7D_8),[64] and similarly the ^{13}C chemical shift correlates equally well (21.8, 32.0 and 31.1 ppm respectively). Also present in the ^{13}C NMR spectrum are five resonances corresponding to the Pn* carbons, at the expected values and two for the coordinated Et_2O.

Further evidence for the assignment of **2.6** stems from its reactivity with **2.1**. Combination of the two aforementioned species in the correct ratio on an NMR scale results in a redistribution reaction, with **2.6** acting as a methylating agent upon **2.1**. The sole protio-NMR active product detected is Pn^*TiMe_2 (**2.7**) (Figure 2.19).

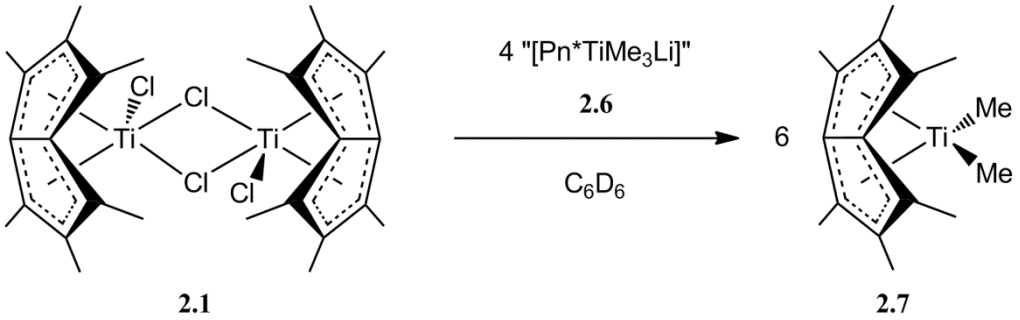

2.1 **2.7**

Figure 2.19: Redistribution reaction of titanium methyls.

Similar redistribution reactions are known in the literature involving chromium(III) phenyl complexes with formation of two equivalents of $Cr(C_6H_5)_3$ on reaction of $Li_3Cr(C_6H_5)_6$ with $CrCl_3$.[65]

Owing to the lack of suitable single crystals, the solid state structure of **2.6** can only be hypothesised, but it seems reasonable to predict the presence of a pseudo piano-stool type structure with an η^8-Pn*Ti moiety bound to three methyl groups bridging a lithium counter ion. The number of methyl groups that bridge is uncertain but the related complexes $[Li(Et_2O)_2][Ti(CH_3)_5]$[13] and $[Li(TMEDA)]_2[ZrMe_6]$[64] both have lithium ions bridged by two methyl groups and this seems a reasonable suggestion for **2.6** [Figure 2.20(a)]. This would mean the interconversion between terminal and bridging methyl groups is very fast on the NMR timescale at room temperature resulting in the equivalence of all groups, as is observed for **2.6**. VT ^{1}H NMR measurements were conducted in an attempt to 'freeze-out' any resonances corresponding to possible fluxionality between bridging and terminal methyl groups and hence determine the number of each present. This was unsuccessful, with negligible line broadening and no splitting of the methyl resonance down to temperatures as low as −80 °C, a phenomenon paralleled in the related $[Li(Et_2O)_2][Ti(CH_3)_5]$ and $[Li(TMEDA)]_2[ZrMe_6]$. Conversely, the lithium may be bridged by all three in a symmetric manner [Figure 2.20(b)].

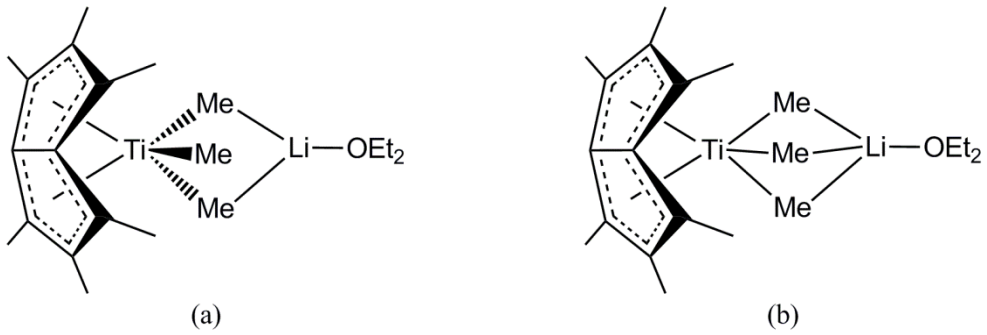

Figure 2.20: Possible solid state structures of $[Pn*TiMe_3]Li\cdot(Et_2O)_x$ (**2.6**).

2.9 Synthesis and characterisation of Pn*TiMe$_2$ (2.7)

The synthesis of $Pn*TiMe_2$ (**2.7**) is detailed in Figure 2.21; combination of 4.2 equivalents of MeMgCl solution with **2.1** in Et_2O afforded a purple solution upon warming to room temperature. Subsequent work up and cooling of a hexane solution produced a pink microcrystalline solid in good yield (77%), which was identified as **2.7** by elemental analysis and X-ray crystallography. Single crystals suitable for X-ray

diffraction were grown by slow cooling of a solution in the same solvent to −80 °C and the structure is given below (Figure 2.22).

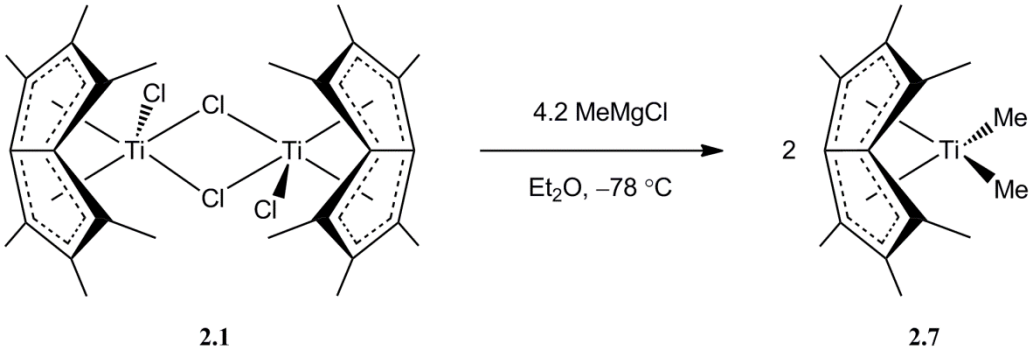

Figure 2.21: Synthesis of Pn*TiMe$_2$ (**2.7**).

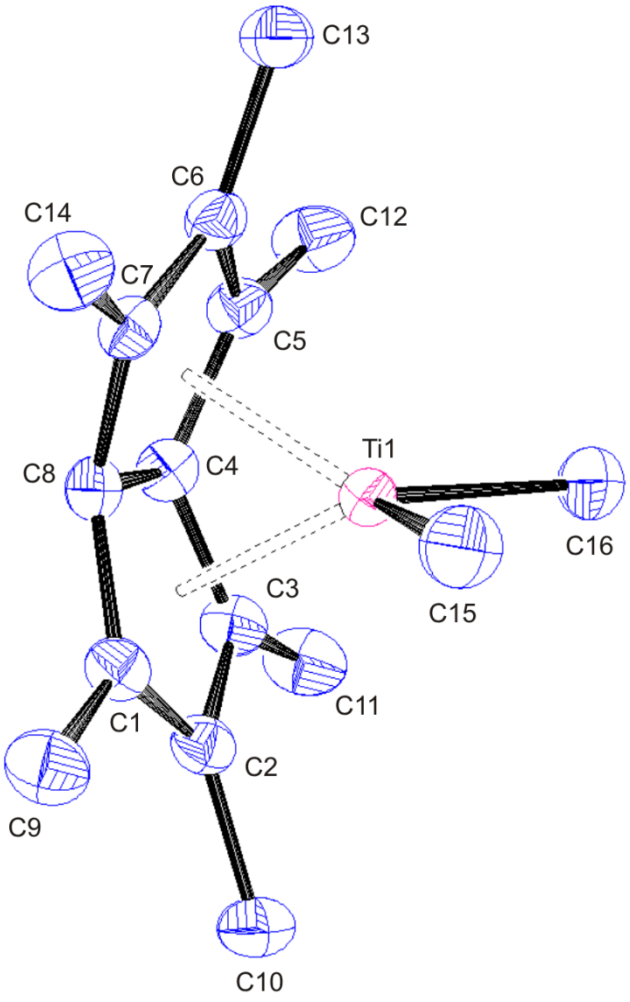

Figure 2.22: Side-on view of **2.7** with thermal ellipsoids at 50%. Hydrogen atoms omitted for clarity.

2.7 crystallises in the $P2_1/n$ space group with one independent molecule in the asymmetric unit. The ligands are coordinated in a pseudo tetrahedral arrangement around Ti as exemplified by the C(15)-Ti(1)-C(16) angle of 104.84(9)°, a feature paralleled for many bis-Cp analogues.[32, 66–68] **2.7** is unique in the series as the only monomeric crystallographically characterised species. This may be due to the relatively poor bridging nature of methyl groups, as on electronic grounds the hypothetical dimer $[Pn^*TiMe(\mu\text{-}Me)]_2$, should be more stable with each Ti centre possessing an electron count of 16 compared to 14 in monomeric **2.7**. Another possible factor, steric congestion should not present a problem due to the existence of **2.4** with two μ-Me and one $\mu\text{-}CH_2$ group bridging the Ti centres.

The monomeric, 14 electron configuration of **2.7** has a large influence on structural parameters, with it possessing the shortest $Ti\text{-}Pn^*_{cent}$ and average Ti-C(Pn*) distances in the series (Table 2.6). It also possesses the largest fold angle (35.7°), nearly 3° larger than any other and 6° greater than that observed for **2.5**, which is justified as being a combination of steric and electronic factors. **2.7** is less sterically congested about the Ti centre with only two additional ligands bound to the Pn*Ti fragment, whereas all other species in this series have three. This enables the pentalene framework to bend more about its bridgehead bond to maximise Ti-C(Pn*) contacts with fewer repulsive steric interactions with ancillary ligands. This, in conjunction with its deficient 14 electron configuration, results in a large fold angle.

The average Ti-Me bond length (2.136 Å) is shorter than the distance seen for the closely related Cp_2TiMe_2 and Ind_2TiMe_2 (2.176 and 2.210 Å respectively),[32, 67] which is rationalised by the electron deficient nature of the Ti centre forming a stronger Ti-Me interaction, thus alleviating its deficiency in comparison to the 16 electron Cp_2TiMe_2 and Ind_2TiMe_2 complexes. The same argument applies for the corresponding distance in the 16 electron **2.2** [2.188(5) Å], which is longer.

Table 2.5: Selected bond lengths, angles and structural parameters for **2.7**. ESDs are given in parentheses.

Lengths (Å)			
Ti(1) - C(1)	2.354(2)	C(1) - C(2)	1.413(2)
Ti(1) - C(2)	2.459(2)	C(2) - C(3)	1.421(2)
Ti(1) - C(3)	2.339(2)	C(3) - C(4)	1.438(2)
Ti(1) - C(4)	2.127(2)	C(4) - C(5)	1.444(2)
Ti(1) - C(5)	2.361(2)	C(5) - C(6)	1.417(2)
Ti(1) - C(6)	2.473(2)	C(6) - C(7)	1.421(2)
Ti(1) - C(7)	2.329(2)	C(7) - C(8)	1.443(2)
Ti(1) - C(8)	2.126(1)	C(8) - C(1)	1.447(2)
Ti(1) - C(15)	2.139(2)	C(4) - C(8)	1.467(2)
Ti(1) - C(16)	2.132(2)		
Ti(1) - Pn^*_{cent}	1.932	Av. C_{ring} - Me	1.502
Ti(1) - Pn^*_{cent}	1.930		
Angles (°)			
C(15) - Ti(1) - C(16)		104.84(9)	
Fold Angle		35.66	

The room temperature ^{1}H NMR spectrum of **2.7** reveals three sharp singlets in a 12:6:6 intensity ratio and one can conclude that the solution phase structure shares the same C_{2v} symmetry observed in the solid state. The two resonances corresponding to the Pn* moiety fall within their expected range with the resonance of relative intensity six furthest upfield (δ = 0.15 ppm; C_6D_6) that of the terminal methyl groups. This high-field value agrees reasonably well with that reported for $Cp^*_2TiMe_2$ (δ = −0.49 ppm; C_6D_6)[69] as does the corresponding ^{13}C resonance (δ = 41.1 and 48.7 ppm respectively). The five other resonances in the ^{13}C NMR spectrum correspond to the Pn* ring carbons falling within their usual range of values. There is no evidence of an agostic interaction present with the methyl coupling constant $^1J_{C\text{-}H}$ = 114.8 Hz much larger than the 75-100 Hz range reported[70] as an indication of such a phenomenon.

Owing to the thermal instability of **2.2** and the relative stabilities of $Cp_2TiClMe$ and Cp_2TiMe_2,[39, 40] it is somewhat surprising to find that **2.7** is thermally stable. **2.7** is stable indefinitely at room temperature in both the solution and solid state and is also found to be stable at elevated temperatures (≤ 60 °C) in solution for a number of days

with little decomposition detected. Full decomposition was found to occur only at temperatures above 100 °C maintained over a 24 hour period. Interestingly, no identifiable decomposition products could be extracted contrasting the generation of **2.3** from **2.2**. The lack of formation of the analogous **2.4** reveals that a parallel decomposition pathway is not available to **2.7**. This has been attributed to the contrasting monomer/dimer formulation, with the latter a prerequisite for an intramolecular α-hydrogen abstraction by the methyl group on the neighbouring Ti atom and the concomitant liberation of CH_4. There is also no evidence for the formation of a carbene species, analogous to the proposed reactive intermediate in the thermolysis of $Cp^*_2TiMe_2$, nor a Pn* equivalent of the observed tuck-in structure with $Cp^*(C_5Me_4CH_2)TiMe$ resulting from hydrogen migration from a ring methyl group to methylidene ligand (Figure 2.23).[71] The latter is unsurprising as this would lead to a large deformation of the Pn* ring system which would be unfavourable.

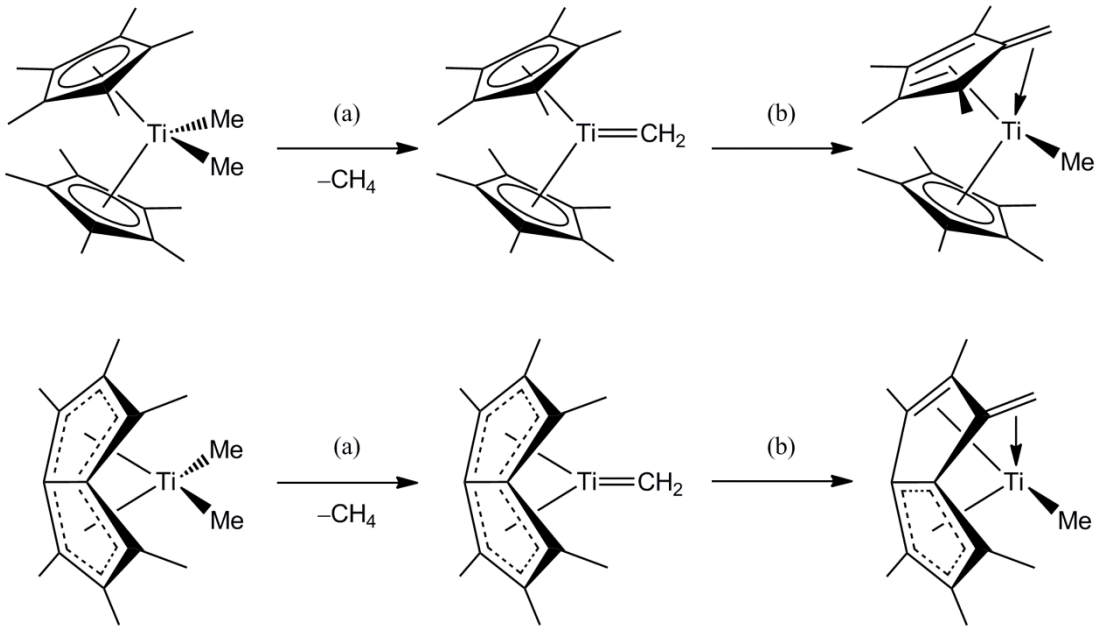

Figure 2.23: Proposed decomposition of $Cp^*_2TiMe_2$ and possible analogous pathway for **2.7**. (a) intramolecular α-H abstraction, (b) H-migration.

An alternative synthesis of **2.7** involving **2.1** and **2.6** is detailed in Section 2.8 (Figure 2.19). The reactivity of **2.7** with small molecules (CO_2, CO, H_2 and C_2H_4) is discussed in detail in chapters four and five.

2.10 Conclusion

A considerably improved synthesis of $[Pn^*TiCl(\mu\text{-}Cl)]_2$ has been developed utilising isomeric control imparted on the Pn* synthon $Pn^*(SnMe_3)_2$. This protocol permits access to a variety of methylated compounds through metathesis chemistry for the first time. All complexes have been characterised including five crystal structures expanding the number of structurally determined η^8-PnTi complexes reported in the literature to eight. Analysis has revealed an array of structural conformations from the electron deficient coordinatively unsaturated monomeric Pn^*TiMe_2, to the dimeric $[Pn^*Ti(\mu\text{-}Me)]_2(\mu\text{-}CH_2)$, with the presence of both bridging methyl and methylene units, and the interesting fluxional trimetallic $[Pn^*Ti(\mu\text{-}Me)_2Me]_2Mg$ incorporating the Me_2Mg methylating reagent. Action of an excess of the powerful MeLi with $[Pn^*TiCl(\mu\text{-}Cl)]_2$ transfers three methyl groups forming $[Pn^*TiMe_3]Li.(Et_2O)_x$ which has shown to act as a methylating agent in the alternative formation of Pn^*TiMe_2. The complexes show varying thermal stabilities with the dimeric nature of $[Pn^*TiMe(\mu\text{-}Cl)]_2$ proving crucial in the elimination pathway for the formation of $[Pn^*Ti(\mu\text{-}Cl)]_2(\mu\text{-}CH_2)$. The fold angles demonstrate a reliance on the interplay between electronic and steric factors and a comparison of the solid state structural properties of all crystallographically characterised complexes throughout this chapter has been performed.

Table 2.6: Collection of pertinent solid state parameters and valence electron counts for Chapter Two.

Compound	Av. Fold Angle (°)	Av. Ti-C Distance (Å)	Av. Ti-Pn^*_{cent} Distance (Å)	Ti-Ti Distance (Å)	Ti Valence Electron Count
2.1[26]	32.75	2.344	1.955	3.8058(7)	16
2.2	30.61	2.354	1.969	3.8401(11)	16
2.3	32.89	2.345	1.959	3.0391(5)	16
2.4	31.83	2.370	1.987	2.8238(10)	16
2.5	29.78	2.374	1.990	5.6448(6)	16
2.7	35.66	2.321	1.931	n/a	14

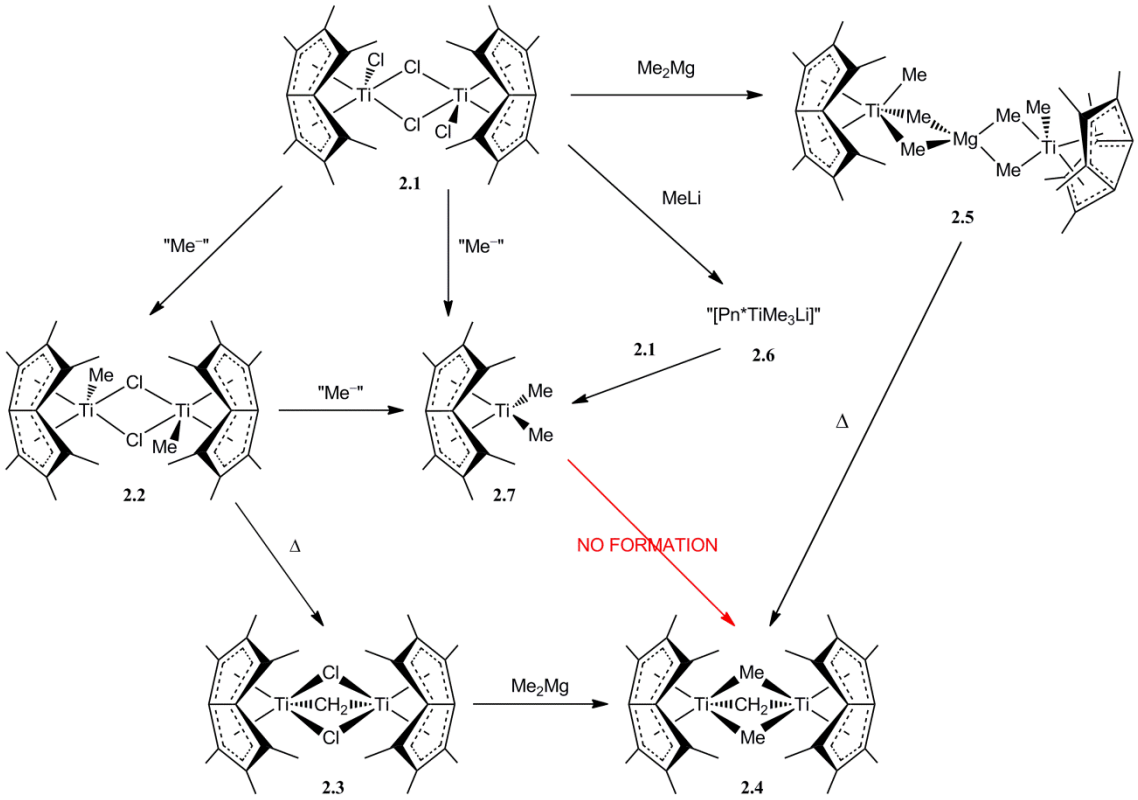

Figure 2.24: Reaction scheme of Pn*Ti-methyl compounds.

2.11 References for Chapter Two

1 A. K. Fischer and G. Wilkinson, *Journal of Inorganic and Nuclear Chemistry*, 1956, 2, 149–152.

2 G. Wilkinson and J. Birmingham, *Journal of the American Chemical Society*, 1954, 76, 4281–4284.

3 H. Brintzinger and J. E. Bercaw, *Journal of the American Chemical Society*, 1970, 92, 6182–6185.

4 A. Davison and S. S. Wreford, *Journal of the American Chemical Society*, 1974, 96, 3017–3018.

5 D. A. Lemenovskii, I. F. Urazowski, Y. K. Grishin, and V. A. Roznyatovsky, *Journal of Organometallic Chemistry*, 1985, 290, 301–305.

6 S. I. Troyanov, H. Antropiusová, and K. Mach, *Journal of Organometallic Chemistry*, 1992, 427, 49–55.

7 L. Resconi, L. Cavallo, A. Fait, and F. Piemontesi, *Chemical Reviews*, 2000, 100, 1253–1346.

8 M. T. Reetz, *Titanium in Organic Synthesis - A Manual in Organometallics in Synthesis*, John Wiley & Sons Ltd, Chichester, 1994.

9 F. Kuber, *Applied Homogeneous Catalysis with Organometallic Compounds*, 1996, 2, 893–902.

10 R. B. King and M. B. Bisnette, *Journal of Organometallic Chemistry*, 1967, 8, 287–297.

11 J. E. Bercaw, R. H. Marvich, L. G. Bell, and H. H. Brintzinger, *Journal of the American Chemical Society*, 1972, 94, 1219–1238.

12 J. E. Bercaw, *Journal of the American Chemical Society*, 1974, 96, 5087–5095.

13 S. Kleinhenz and K. Seppelt, *Chem. Eur. J.*, 1999, 5, 3573–3580.

14 K. Ziegler, E. Holzkamp, H. Breil, and H. Martin, *Angewandte Chemie*, 1955, 67, 541–547.

15 G. Natta, I. Pasquon, and E. Giachetti, *Angewandte Chemie*, 1957, 69, 213–219.

16 C. Beermann and H. Bestian, *Angewandte Chemie*, 1959, 71, 618–623.

17 C. Beermann and K. Clauss, *Angewandte Chemie*, 1959, 71, 627–627.

18 H. J. Berthold and G. Groh, *Zeitschrift für anorganische und allgemeine Chemie*, 1963, 319, 230–235.

19 P. J. Davidson, M. F. Lappert, and R. Pearce, *Chemical Reviews*, 1976, 76, 219–242.

20 J. Müller and K.-H. Thiele, *Zeitschrift für anorganische und allgemeine Chemie*, 1968, 362, 120–128.

21 R. R. Schrock and P. Meakin, *Journal of the American Chemical Society*, 1974, 96, 5288–5290.

22 A. E. Ashley, A. R. Cowley, and D. O'Hare, *Chemical communications (Cambridge, England)*, 2007, 1512–4.

23 B. Ganem, *The Journal of Organic Chemistry*, 1975, 40, 146–147.

24 M. Schlosser, F. Faigl, L. Franzini, H. Geneste, G. Katsoulos, and G.-F. Zhong, *Pure and Applied Chemistry*, 1994, 66, 1439–1446.

25 J. J. Stezowski, H. Hoier, D. Wilhelm, T. Clark, and P. von R. Schleyer, *Journal of the Chemical Society, Chemical Communications*, 1985, 1263.

26 A. E. Ashley, Permethylpentalene Chemistry, Thesis, University of Oxford, 2006.

27 J. Emsley, *The Elements*, Oxford University Press, 2000.

28 E. W. Abel and S. Moorhouse, *Journal of the Chemical Society, Dalton Transactions*, 1973, 1706.

29 P. Jutzi and M. Kuhn, *Journal of Organometallic Chemistry*, 1979, 173, 221–229.

30 R. J. Boyd and S. L. Boyd, *Journal of the American Chemical Society*, 1992, 114, 1652–1655.

31 F. G. N. Cloke, P. B. Hitchcock, M. C. Kuchta, and N. A. Morley-Smith, *Polyhedron*, 2004, 23, 2625–2630.

32 U. Thewalt and T. Wöhrle, *Journal of Organometallic Chemistry*, 1994, 464, C17–C19.

33 R. Jungst, D. Sekutowski, J. Davis, M. Luly, and G. Stucky, *Inorganic Chemistry*, 1977, 16, 1645–1655.

34 H. R. van der Wal, F. Overzet, H. O. van Oven, J. L. de Boer, H. J. de Liefde Meijer, and F. Jellinek, *Journal of Organometallic Chemistry*, 1975, 92, 329–340.

35 O. T. Summerscales and F. G. N. Cloke, *Coordination Chemistry Reviews*, 2006, 250, 1122–1140.

36 A. Ashley, G. Balazs, A. Cowley, J. Green, C. H. Booth, and D. O'Hare, *Chemical communications (Cambridge, England)*, 2007, 1515–7.

37 F. M. Chadwick, A. Ashley, G. Wildgoose, J. M. Goicoechea, S. Randall, and D. O'Hare, *Dalton transactions (Cambridge, England: 2003)*, 2010, 39, 6789–93.

38 G. A. Luinstra and J. H. Teuben, *Organometallics*, 1992, 11, 1793–1801.

39 R. R. Schrock and G. W. Parshall, *Chemical Reviews*, 1976, 76, 243–268.

40 J. A. Waters and G. A. Mortimer, *Journal of Organometallic Chemistry*, 1970, 22, 417–424.

41 J. A. Waters, V. V. Vickroy, and G. A. Mortimer, *Journal of Organometallic Chemistry*, 1971, 33, 41–52.

42 F. N. Tebbe, G. W. Parshall, and G. S. Reddy, *Journal of the American Chemical Society*, 1978, 100, 3611–3613.

43 B. J. J. Van de Heisteeg, G. Schat, O. S. Akkerman, and F. Bickelhaupt, *Organometallics*, 1985, 4, 1141–1142.

44 R. J. West, Part II Thesis, University of Oxford, 2008.

45 L. Scoles, R. Minhas, R. Duchateau, J. Jubb, and S. Gambarotta, *Organometallics*, 1994, 13, 4978–4983.

46 O. Buitrago, C. Ramírez de Arellano, G. Jiménez, and T. Cuenca, *Organometallics*, 2004, 23, 5873–5876.

47 J. B. Lee, G. J. Gajda, W. P. Schaefer, T. R. Howard, T. Ikariya, D. A. Straus, and R. H. Grubbs, *Journal of the American Chemical Society*, 1981, 103, 7358–7361.

48 W. R. Tikkanen, J. Z. Liu, J. W. Egan, and J. L. Petersen, *Organometallics*, 1984, 3, 825–830.

49 P. B. Mackenzie, R. J. Coots, and R. H. Grubbs, *Organometallics*, 1989, 8, 8–14.

50 J. W. Park, P. B. Mackenzie, W. P. Schaefer, and R. H. Grubbs, *Journal of the American Chemical Society*, 1986, 108, 6402–6404.

51 S. Zhang and W. E. Piers, *Organometallics*, 2001, 20, 2088–2092.

52 M. L. H. Green, *Journal of Organometallic Chemistry*, 1995, 500, 127–148.

53 B. E. Bursten and R. H. Cayton, *Organometallics*, 1986, 5, 1051–1053.

54 J. H. Brownie, M. C. Baird, L. N. Zakharov, and A. L. Rheingold, *Organometallics*, 2003, 22, 33–41.

55 J. R. Hagadorn and M. J. McNevin, *Organometallics*, 2003, 22, 609–611.

56 E. G. Ijpeij, B. Coussens, M. A. Zuideveld, G. H. J. van Doremaele, P. Mountford, M. Lutz, and A. L. Spek, *Chemical Communications (Cambridge, England)*, 2010, 46, 3339–41.

57 T. Greiser, J. Kopf, D. Thoennes, and E. Weiss, *Chemische Berichte*, 1981, 114, 209–213.

58 E. Weiss, *Journal of Organometallic Chemistry*, 1964, 2, 314–321.

59 R. Gyepes, K. Mach, I. Císařová, J. Loub, J. Hiller, and P. Šindelář, *Journal of Organometallic Chemistry*, 1995, 497, 33–41.

60 E. Kurras and J. Otto, *Journal of Organometallic Chemistry*, 1965, 4, 114–118.

61 J. Krausse and G. Marx, *Journal of Organometallic Chemistry*, 1974, 65, 215–222.

62 J. Müller, H. Rau, P. Zdunneck, and K.-H. Thiele, *Zeitschrift für anorganische und allgemeine Chemie*, 1973, 401, 113–120.

63 K.-H. Thiele, K. Milowski, P. Zdunneck, J. Müller, and H. Rau, *Zeitschrift für Chemie*, 1972, 12, 186–187.

64 P. M. Morse and G. S. Girolami, *Journal of the American Chemical Society*, 1989, 111, 4114–4116.

65 F. Hein and K. Schmiedeknecht, *Journal of Organometallic Chemistry*, 1967, 8, 503–509.

66 T. Wöhrle and U. Thewalt, *Journal of Organometallic Chemistry*, 1993, 456, C21–C23.

67 J. L. Atwood, W. E. Hunter, D. C. Hrncir, E. Samuel, H. Alt, and M. D. Rausch, *Inorganic Chemistry*, 1975, 14, 1757–1762.

68 I. E. Nifant'ev, A. V. Churakov, I. F. Urazowski, S. G. Mkoyan, and L. O. Atovmyan, *Journal of Organometallic Chemistry*, 1992, 435, 37–42.

69 K. Mach, V. Varga, and V. Hanuš, *Journal of Organometallic Chemistry*, 1991, 415, 87–95.

70 M. Brookhart and M. L. H. Green, *Journal of Organometallic Chemistry*, 1983, 250, 395–408.

71 C. McDade, J. C. Green, and J. E. Bercaw, *Organometallics*, 1982, 1, 1629–1634.

Chapter Three

Synthesis of Permethylpentalene Titanium Complexes

3.1 Introduction

During the infancy of transition metal organometallic chemistry, it was initially thought that, due to the thermal instability of the compounds and difficulty in isolating them, the M-C bond in σ-alkyl complexes was inherently weak; this was in marked contrast to their main group analogues. The key to dispelling this fallacy came with the understanding that transition metal alkyls can decompose *via* β-hydrogen elimination, which is uncommon among main group alkyls under similar experimental conditions.[1] Further investigations revealed that transition metal M-C bonds are, broadly speaking, as thermodynamically stable as their main group analogues and the "inherent instability" of transition metal alkyl compounds comes from the presence of low energy valence *nd* orbitals, which make decomposition routes such as β-hydrogen elimination kinetically accessible.[2–6] This is exemplified by $PbEt_4$ and $TiEt_4$; the former is stable up to 100 °C with eventual decomposition by Pb-C homolysis and the latter's existence, is as yet unconfirmed (Table 3.1).

Table 3.1: Decomposition temperatures for some Group IV and XIV alkyls.

Group IV	T_{dec} / °C	Group XIV	T_{dec} / °C
$TiMe_4$	> −50	$PbMe_4$	> 200
$TiEt_4$	Existence doubtful	$PbEt_4$	> 100

In this knowledge, ligands were employed that circumnavigated these pitfalls by having large steric bulk to protect coordinatively unsaturated metal centres *via* suppression of intermolecular decomposition pathways and/or a lack of β-hydrogen atoms to prevent common intramolecular decomposition pathways. The use of ligands such as benzyl ($-CH_2Ph$), neopentyl ($-CH_2{}^tBu$) and neosilyl ($-CH_2SiMe_3$) marked the beginning of a

rapid development in the area, especially that of "stable" homoleptic transition metal-alkyl complexes.[1]

Another advance that was instrumental to the rapid development of modern organometallic chemistry was the introduction of the now ubiquitous, cyclopentadienyl ligand (Cp) and its permethylated analogue Cp*. The large steric bulk of the ligand when bound in its most common η^5 coordination mode, is thought to impart stability on M-alkyl bonds by blocking coordination sites that would otherwise be utilised for decomposition pathways.[1, 6] The extent to which Cp and its analogues have influenced modern organometallic chemistry may be witnessed on examination of any modern organometallic text book[7] or undergraduate course. There is a colossal disparity in frequency of Cp and Pn derivatives in the literature, emphasised by the number of complexes found in the CSD relating to each; there are 3,305 compounds alone for Ti-Cp derivatives compared to a total of 48 complexes containing any Pn derivative in combination with any metal.

Due to the incipient nature of pentalene titanium chemistry, the only carbon based ligand to be incorporated alongside any PnTi fragment is the cyclopentadienyl moiety.[8] Owing to the successful reactivity shown in Chapter Two, this chapter describes the reactions of **2.1** with RM (M = Li and Na) and RMgX reagents, *via* parallel metathesis routes, with classical organometallic ligands.

3.2 Synthesis and characterisation of Pn*Ti(CH$_2$Ph)$_2$ (3.1)

Combination of 4.2 equivalents of PhCH$_2$MgCl solution with **2.1** in Et$_2$O (Figure 3.1), afforded a dark brown solution upon warming to room temperature. Subsequent work up and cooling of a pentane solution produced a bronze microcrystalline solid in good yield (77%), which was identified as Pn*Ti(CH$_2$Ph)$_2$ (**3.1**) by elemental analysis and X-ray crystallography. Single crystals suitable for X-ray diffraction were grown by slow cooling of a hexane solution to −35 °C, and two views of the structure are shown in Figure 3.2 and 3.3.

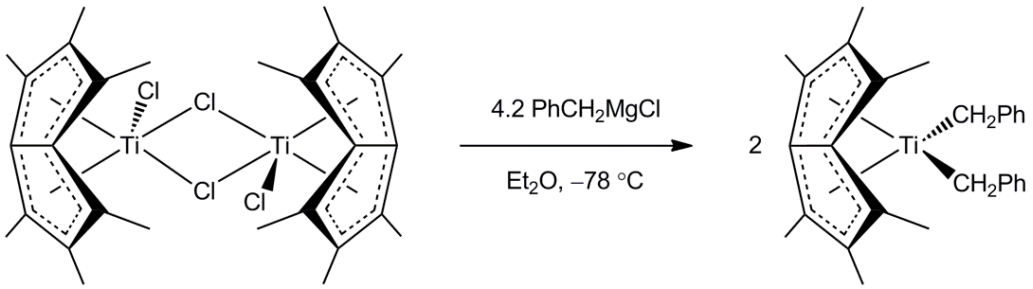

2.1 **3.1**

Figure 3.1: Synthesis of Pn*Ti(CH_2Ph)$_2$ (**3.1**).

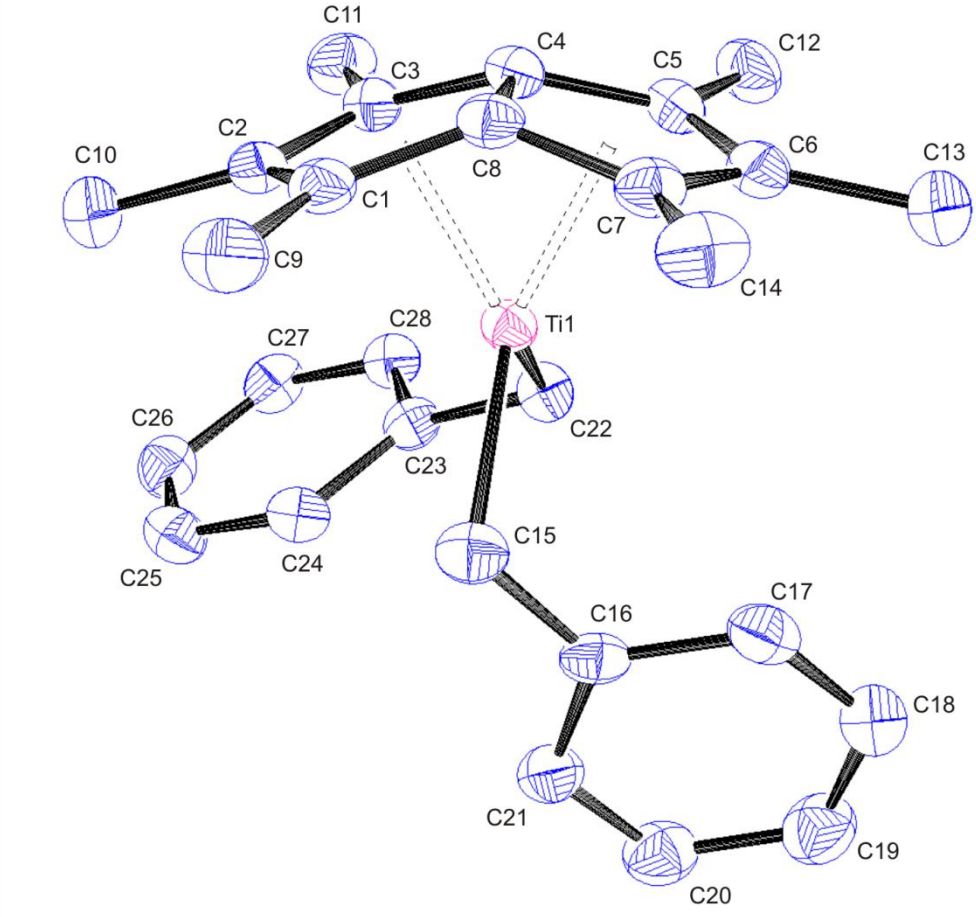

Figure 3.2: Side-on view of **3.1** with thermal ellipsoids at 50%. Hydrogen atoms omitted for clarity.

3.1 crystallises in the $P\bar{1}$ space group with one independent molecule in the asymmetric unit. The ligands are coordinated in a pseudo tetrahedral arrangement around Ti as exemplified by the C(15)-Ti(1)-C(22) angle [107.49(9)°], a feature paralleled in **2.7** and all compounds contained within this chapter {excluding dimeric [Pn*TiPh(μ-Cl)]$_2$ (**3.5**)}. This angle is considerably larger than seen for the analogous

bis Cp species $Cp_2Ti(CH_2Ph)_2$ [91.0(2)°],[9] which indicates the η^8-Pn* moiety is less sterically demanding than two Cp units, allowing the R-M-R angle to widen and approach the idealised tetrahedral angle (109.47°). **3.1** is monomeric and having 14 electrons, is isoelectronic with **2.7**. The fold angle (33.1°) is comparable with other monomeric 14 electron complexes; $Pn^*Ti(CH_2SiMe_3)_2$ (**3.2**), $Pn^*Ti(CH_2{}^tBu)_2$ (**3.3**) and $Pn^*TiCl(CH_2{}^tBu)$ (**3.4**) (32.9, 33.1 and 34.1° respectively, *vide infra* Table 3.9) but smaller than **2.7** (35.7°), as expected by exchange of two methyl groups for the more sterically demanding benzyl ligands. This again demonstrates the fold angle to be a sensitive function of electronic and steric factors at the metal centre.[10]

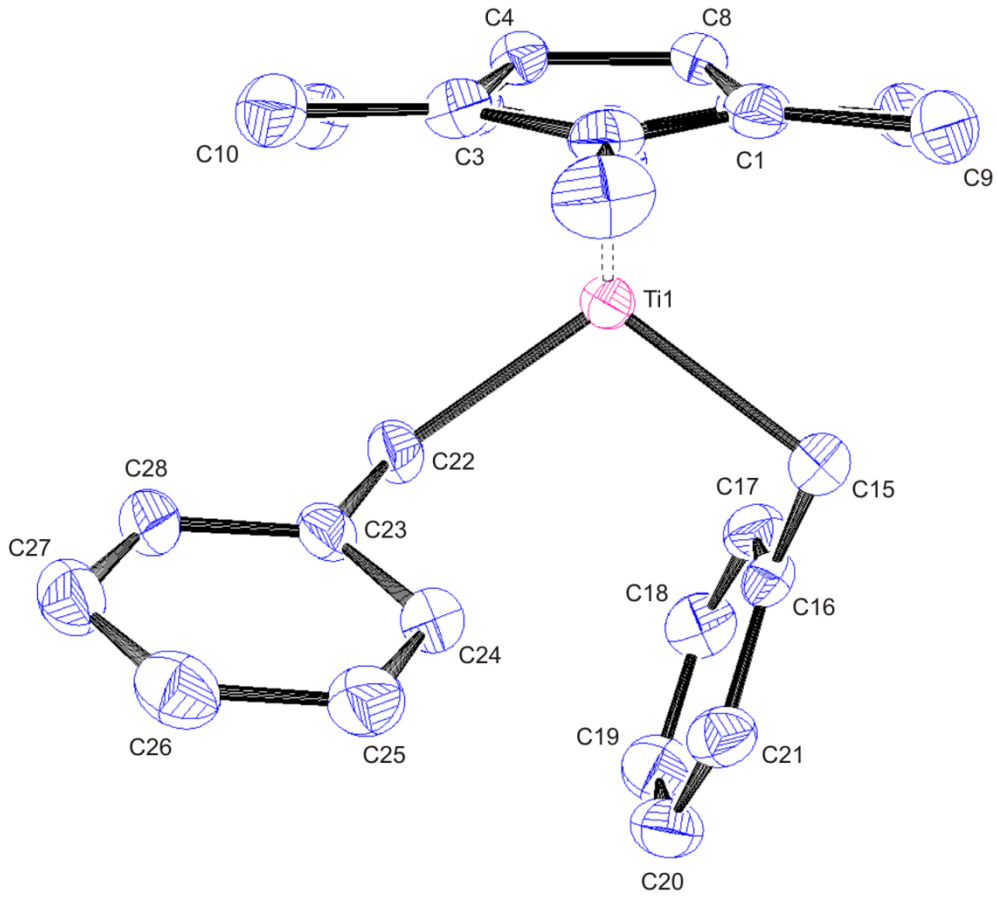

Figure 3.3: End-on view of **3.1** with thermal ellipsoids at 50%. Hydrogen atoms omitted for clarity.

The average Ti-CH_2 distance (2.172 Å) is shorter than that for the closely related $Cp_2Ti(CH_2Ph)_2$ (2.225 Å),[9] reasoned as the Ti centre being relatively electron deficient in **3.1** compared to $Cp_2Ti(CH_2Ph)_2$ (14 *vs.* 16 electron respectively). It also fits a near linear trend of lengthening average Ti-CH_2 distance on increasing electron density at the

titanium centre in the related 12, 14 and 16 electron complexes; Cp*Ti(CH_2Ph)$_3$,[11] **3.1** and $Cp_2Ti(CH_2Ph)_2$ (2.126, 2.172 and 2.225 Å respectively) with the average bond length increasing by approximately 0.05 Å increments on sequential increases of two valence electrons.

It is well documented that electron deficient benzyl complexes of the early transition metals may distort in order to relieve electronic unsaturation *via* methylene C-H agostic interactions and interaction of the C_6H_5 π-system (η^2- or η^n-benzyl) with the metal centre.[12–14] On inspection, the two benzyl ligands of **3.1** are bound in an asymmetric manner in the solid state and are inequivalent. The Ti(1)-C(15)-C(16) and Ti(1)-C(22)-C(23) angles are markedly different [101.94(15) and 115.23(15)° respectively], as are the Ti(1)-C_{ipso}(C16/C23) distances [2.886(2) and 3.085(2) Å respectively]. The angle and distance to the *ipso*-carbon, C(16) are in the range of that seen in (C_5Me_4ArO)Ti(CH_2Ph)$_2$ [106.7(7)° and 2.92(1) Å respectively], which has a proposed partial η^2-bonding interaction.[15] Formal η^2-bonding is observed in the bistitanium fulvalene {*anti*-[Ti(CH_2Ph)$_3$]$_2$(μ-η^5:η^5-$C_{10}H_8$)},[14] which has a much smaller Ti-CH_2-C_{ipso} angle [90.9(3)°] and Ti-C_{ipso} distance [2.611(4) Å] therefore this bonding mode is ruled out for **3.1**. These data and NMR analysis (*vide infra*), results in assignment of two η^1-benzyl ligands with their solid state inequivalence attributed to crystal packing forces or a very weak Ti-π interaction.

Table 3.2: Selected bond lengths, angles and structural parameters for **3.1**. ESDs are given in parentheses.

Lengths (Å)			
Ti(1) - C(1)	2.353(2)	C(1) - C(2)	1.419(3)
Ti(1) - C(2)	2.483(2)	C(2) - C(3)	1.421(3)
Ti(1) - C(3)	2.357(2)	C(3) - C(4)	1.441(3)
Ti(1) - C(4)	2.129(2)	C(4) - C(5)	1.439(3)
Ti(1) - C(5)	2.373(2)	C(5) - C(6)	1.417(3)
Ti(1) - C(6)	2.518(2)	C(6) - C(7)	1.418(3)
Ti(1) - C(7)	2.376(2)	C(7) - C(8)	1.438(3)
Ti(1) - C(8)	2.131(2)	C(8) - C(1)	1.442(3)
Ti(1) - C(15)	2.191(2)	C(4) - C(8)	1.466(2)
Ti(1) - C(16)	2.886(2)	Av. C_{ring} - Me	1.501
Ti(1) - C(22)	2.152(2)	Ti(1) - Pn^*_{cent}	1.961
Ti(1) - C(23)	3.085(2)	Ti(1) - Pn^*_{cent}	1.942
Angles (°)			
C(15) - Ti(1) - C(22)	107.49(9)		
Ti(1) - C(15) - C(16)	101.94(15)		
Ti(1) - C(22) - C(23)	115.23(15)		
Fold Angle	33.14		

Aside from characterisation in the solid state *via* X-ray crystallographic structural determinations, η^n-benzyl complexes ($n \neq 1$) have also been characterised in solution by NMR spectroscopy and show the following characteristic features; (i) high-field shifts for the *ortho*-Ph protons ($\delta < 6.8$ ppm) and methylene carbon ($\delta < 75$ ppm) resonances and (ii) large $^1J_{C\text{-}H}$ coupling constants for the methylene group ($^1J_{C\text{-}H} > 130$ Hz).[12, 16] **3.1** has an *ortho*-Ph ^{1}H NMR chemical shift ($\delta = 6.83$ ppm) and a CH_2 group $^1J_{C\text{-}H}$ coupling constants ($^1J_{C\text{-}H} = 120.9$ Hz) that is in the range observed for normal η^1-benzyl bonding. The Ti*C*H_2 ^{13}C NMR resonance ($\delta = 68.1$ ppm), differs slightly but is comparable to $Cp_2Ti(CH_2Ph)_2$ ($\delta = 74.1$ ppm, $^1J_{C\text{-}H} = 124.3$ Hz), which has confirmed η^1-bonding.[9, 17] The methylene group's $^1J_{C\text{-}H}$ coupling constant ($^1J_{C\text{-}H} = 120.9$ Hz) is also consistent with the absence of an agostic interaction, with it being close to the ideal value observed for sp^3 hybridised carbons (125 Hz) and much larger than the 75-100 Hz range reported as an indication of such a phenomenon.[18] The room temperature ^{1}H NMR spectrum of **3.1** consists of six resonances, with two singlets

corresponding to the Pn* moiety and three resonances relating to the Ph group, all within their usual range. The methylene proton resonance is a singlet in good agreement with that seen for $Cp_2Ti(CH_2Ph)_2$ (δ = 1.82 and 1.87 ppm respectively; C_6D_6)[19] and one may conclude that the solution phase structure of the molecule is of pseudo C_{2v} symmetry with equivalent benzyl ligands and NWT-Me groups, unlike the solid state where they are inequivalent. The ^{13}C NMR spectrum shows five resonances corresponding to the Pn* carbons and five for the benzyl ligands, all at unexceptional values.

The reactivity of **3.1** with small molecules (CO_2, CO, H_2 and C_2H_4) is discussed in detail in chapters four and five.

3.3 Synthesis and characterisation of Pn*Ti(CH_2SiMe_3)$_2$ (3.2)

It was found that combination of 4.4 equivalents of $NaCH_2SiMe_3$ with **2.1** in pentane, at room temperature were the optimum conditions for formation of Pn*Ti(CH_2SiMe_3)$_2$ (**3.2**) (Figure 3.4).

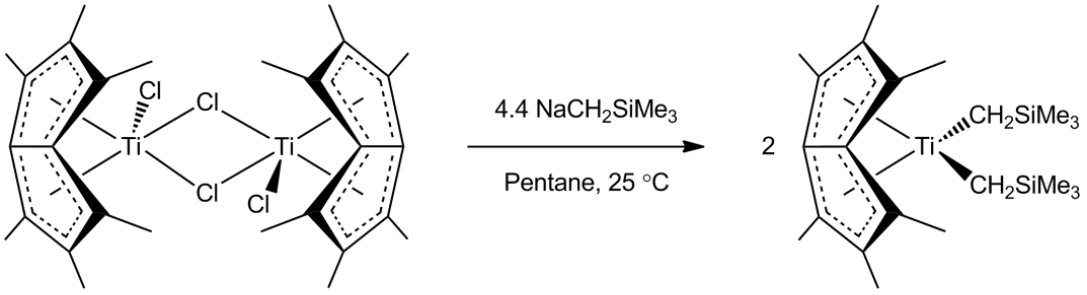

2.1 **3.2**

Figure 3.4: Synthesis of Pn*Ti(CH_2SiMe_3)$_2$ (**3.2**).

Attempts using MCH_2SiMe_3 (M = Li and K) analogues led to difficulties in product separation and evidence of over alkylation respectively (cf. **2.6**). Filtration and cooling of the pentane solution produced a deep purple microcrystalline solid in good yield (72%), which was identified as **3.2** by elemental analysis and X-ray crystallography. Single crystals suitable for X-ray diffraction were grown from slow diffusion of a pentane-toluene mix and two views of the structure are shown (Figure 3.5 and 3.6).

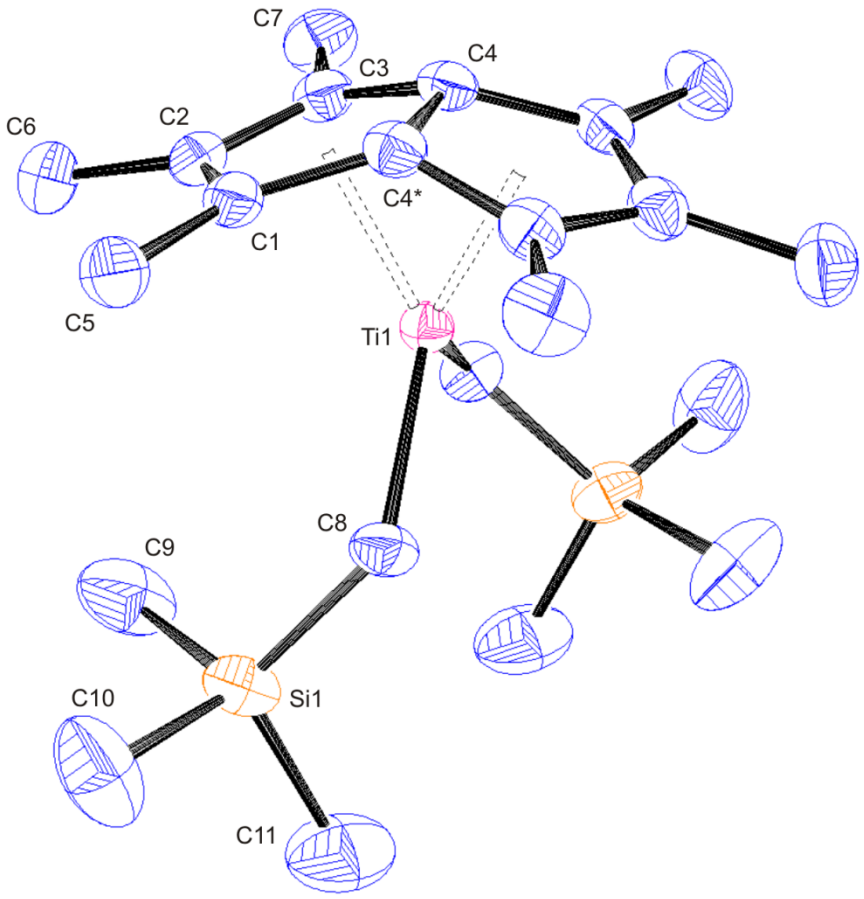

Figure 3.5: Side-on view of **3.2** with thermal ellipsoids at 50%. Hydrogen atoms omitted for clarity, * denotes atoms generated by (C_2) symmetry.

3.2 crystallises in the *C*2/*c* space group with one half molecule in the asymmetric unit, related by a crystallographic C_2 axis running through the mid-point of the Pn* bridgehead bond and the titanium atom, best visualised in Figure 3.6. **3.2** is monomeric and isoelectronic with **3.1**, being a 14 electron complex and is extremely air-sensitive, with instant decomposition on exposure to traces of O_2 or H_2O. The fold angle (32.9°) is comparable with other monomeric 14 electron complexes; **3.1**, **3.3** and **3.4** (33.1, 33.1 and 34.1° respectively, *vide infra* Table 3.9). The ligands are coordinated in a pseudo tetrahedral manner about Ti as exemplified by the C(8)-Ti(1)-C(8*) angle of 106.55(12)°, a feature paralleled in all compounds enclosed in this chapter (excluding dimeric **3.5**).

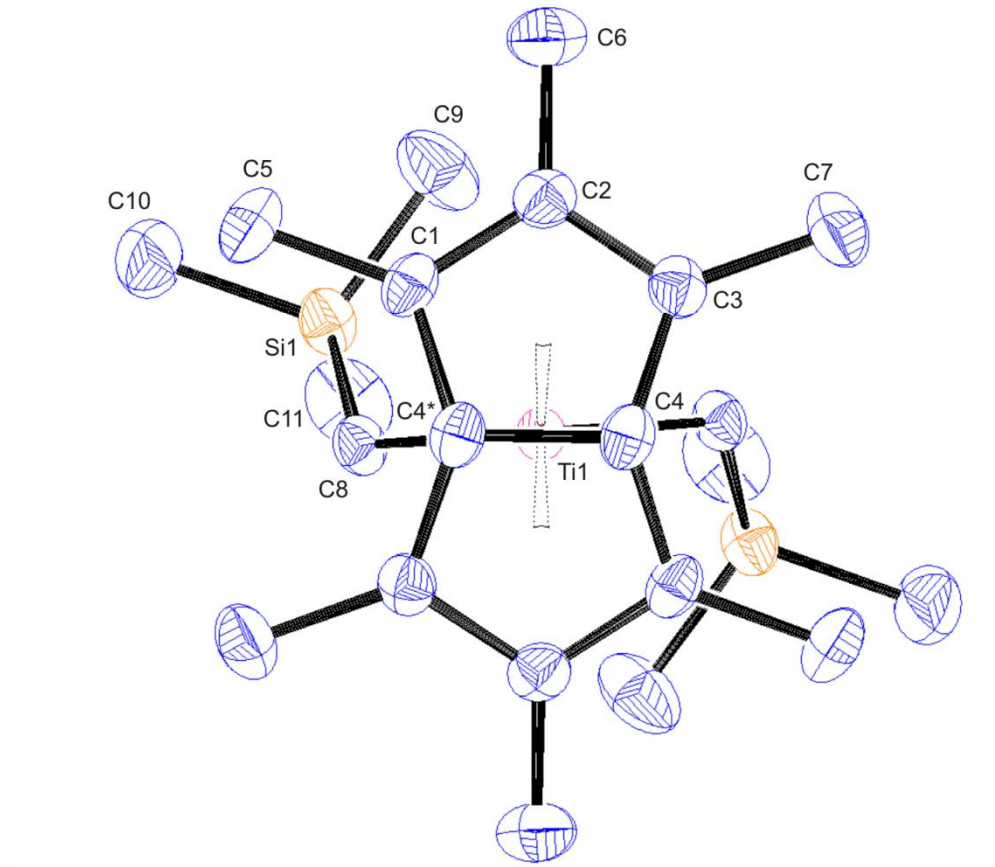

Figure 3.6: Top view of **3.2** with thermal ellipsoids at 50%. Hydrogen atoms omitted for clarity, * denotes atoms generated by (C_2) symmetry.

Due to the lack of structurally characterised carbocyclic titanium-CH_2SiMe_3 complexes, the most relevant structural comparisons are with the related [Me_2Si] *ansa*-bridged titanocenes, {[$Me_2Si(C_5R_4)_2$]$Ti(CH_2SiMe_3)_2$} (R = H, Me),[20, 21] which in the case of R = Me is thermally unstable towards $SiMe_4$ elimination, yielding the fulvene derivative {[$Me_2Si(C_5Me_4)(C_5Me_3CH_2)$]$Ti(CH_2SiMe_3)$}, analogous to CH_4 elimination in $Cp^*_2TiMe_2$.[22] The Ti-methylene distance is shorter for **3.2** [2.154(2) Å vs. 2.178 and 2.176 Å respectively], which is rationalised by the relatively electron deficient nature of the 14 electron Ti centre in **3.2** forming a stronger Ti(1)-C(8) interaction, thus alleviating its deficiency in comparison to the 16 electron {[$Me_2Si(C_5R_4)_2$]$Ti(CH_2SiMe_3)_2$} (R = H, Me) complexes. The Ti(1)-C(8)-Si(1) angle [124.19(11)°] is similar to that seen for [$Cp_2Ti(CH_2SiMe_3)(C{\equiv}CSiMe_3)$] [129.2(2)°][23] and deviates from an idealised tetrahedral angle due to the steric requirement of the bulky $SiMe_3$ group. In fact the angle can range up to 154.2(2)°, as seen for

{[$Me_2Si(C_5Me_4)_2$]Ti($CH_2SiMe_3)_2$}.[21] All other bond lengths and angles for the CH_2SiMe_3 group are unremarkable and similar to data reported in the literature.

Table 3.3: Selected bond lengths, angles and structural parameters for **3.2**. * denotes atoms generated by (C_2) symmetry and ESDs are given in parentheses.

Lengths (Å)			
Ti(1) - C(1)	2.360(2)	C(1) - C(2)	1.422(3)
Ti(1) - C(2)	2.505(2)	C(2) - C(3)	1.417(3)
Ti(1) - C(3)	2.380(2)	C(3) - C(4)	1.442(3)
Ti(1) - C(4)	2.131(2)	C(4*) - C(1)	1.438(3)
Ti(1) - C(8)	2.154(2)	C(4*) - C(4)	1.464(4)
Ti(1) - Pn^*_{cent}	1.956	Av. C_{ring} - Me	1.497
Angles (°)			
C(8) - Ti(1) - C(8*)		106.55(12)	
Ti(1) - C(8) - Si(1)		124.19(11)	
Fold Angle		32.94	

The room temperature ^{1}H NMR spectrum of **3.2** reveals four sharp singlet resonances in a 12:6:18:4 ratio, inferring the solution phase structure of the molecule to be of pseudo C_{2v} symmetry, which differs from that observed in the solid state (C_2). The singlet of lowest relative intensity, corresponds to the four methylene protons ($\delta = -0.15$ ppm; C_6D_6), which are shifted slightly upfield compared to that of {[$Me_2Si(C_5Me_4)_2$]Ti($CH_2SiMe_3)_2$} ($\delta = 0.01$ ppm; C_6D_6).[21] The trend is also paralleled in the ^{13}C NMR chemical shift (δ = 56.4 and 63.8 ppm respectively) and both have almost identical $^1J_{C\text{-}H}$ coupling constants ($^1J_{C\text{-}H}$ = 105.3 and 106.0 Hz). The $SiMe_3$ group's ^{1}H and ^{13}C NMR chemical shifts, and $^1J_{C\text{-}H}$ coupling constants are almost identical (δ = 0.25, 4.0 ppm; 116.1 Hz and δ = 0.18, 4.7 ppm; 118.0 Hz respectively)[21] and the remaining two proton and five carbon resonances correspond to the Pn* moiety and fall within the range of their usual values.

The reactivity of **3.2** with small molecules (CO_2, CO, H_2 and C_2H_4) is discussed in detail in chapters four and five.

3.4 Synthesis and characterisation of Pn*Ti($CH_2{}^tBu$)$_2$ (3.3)

The synthesis of Pn*Ti($CH_2{}^tBu$)$_2$ (**3.3**) is detailed in Figure 3.7; reaction of **2.1** with four equivalents of $LiCH_2{}^tBu$ in benzene afforded a dark red-purple solution. Subsequent work up and cooling of a hexane solution produced a red microcrystalline solid in good yield (73%), which was identified as **3.3** by X-ray crystallography. Single crystals suitable for X-ray diffraction were grown by slow cooling of a pentane solution to −80 °C and the structure is shown below (Figure 3.8).

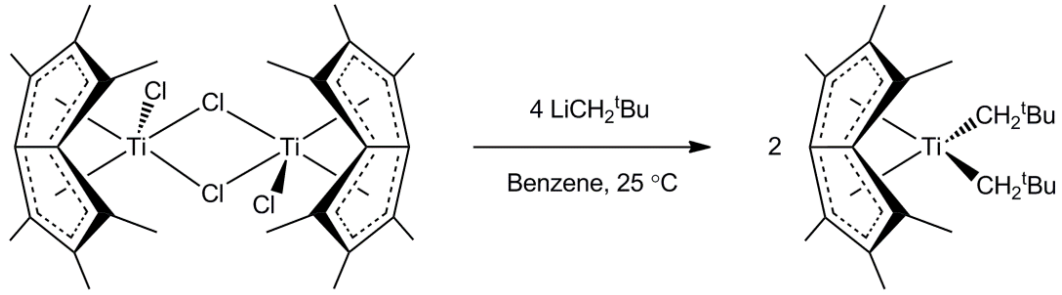

2.1 **3.3**

Figure 3.7: Synthesis of Pn*Ti($CH_2{}^tBu$)$_2$ (**3.3**).

3.3 crystallises in the $P2_1/n$ space group with one independent molecule in the asymmetric unit. The ligands are coordinated in a pseudo tetrahedral arrangement around Ti, a feature observed for all monomeric Pn*TiR_2 compounds reported here with a C(15)-Ti(1)-C(20) angle of [106.18(8)°]. **3.3** is isostructural and isoelectronic with **3.2** as might be expected on exchange of the isoleptic ligands; it similarly possesses C_2 symmetry (although not as a crystallographic axis) and a comparable fold angle (33.1°) to other monomeric 14 electron complexes (Table 3.9). The bond lengths and angles around the titanium atom are almost identical for **3.3** and **3.2**; average Ti-Pn*$_{cent}$, Ti-CH_2 distance and CH_2-Ti-CH_2 angle (1.962, 2.155 Å; 106.2° and 1.956, 2.154(2) Å; 106.6° respectively), but there is an increase in the Ti-CH_2-EMe_3 (E = C, Si) angle from 124.19° in **3.2**, to 129.99° in **3.3**. This is reasoned as being due to the shorter CH_2-E contact for **3.3** (1.545 Å) compared to **3.2** [1.844(2) Å], bringing the bulky EMe_3 groups into closer proximity and so the angle opens to reduce steric repulsion, as seen for the analogous angle in the compounds $(Me_3ECH_2)_3TiSi(SiMe_3)_3$ {E = C [141.7(12)°] and Si [130.4(4)°]}.[24] It is also the first π-hydrocarbon bound titanium species bearing two neopentyl groups to be crystallographically characterised.

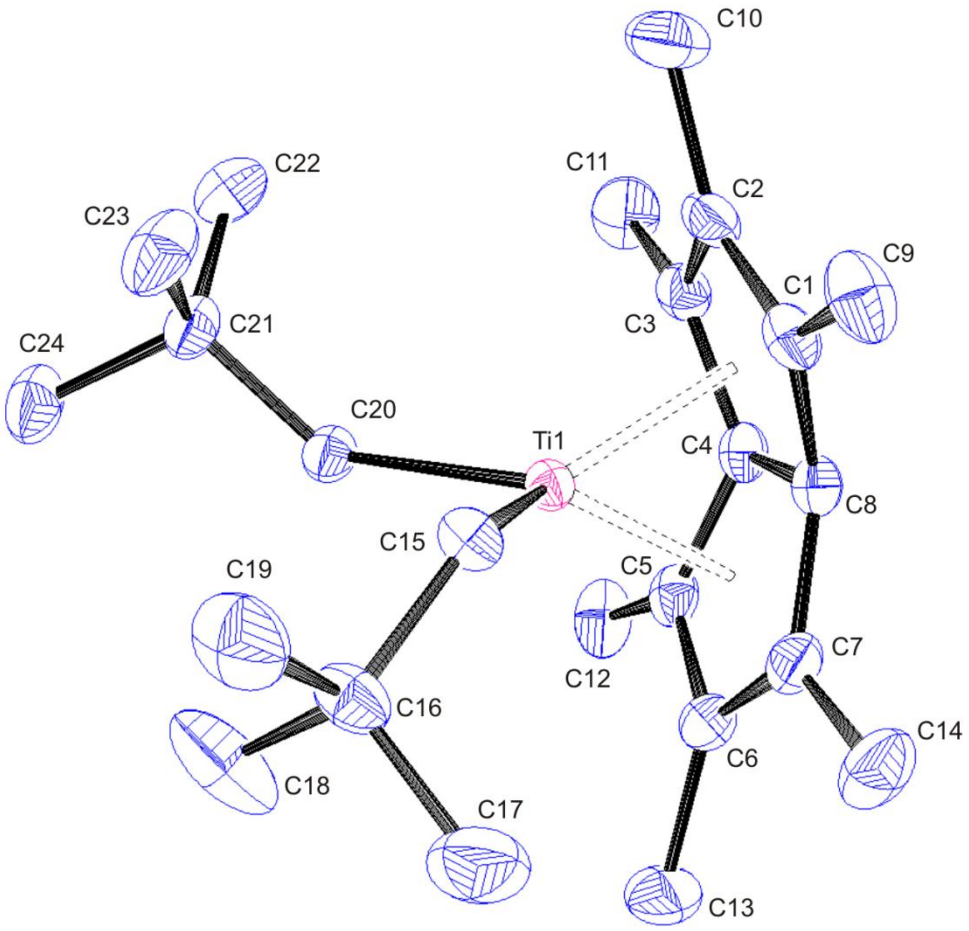

Figure 3.8: Side-on view of **3.3** with thermal ellipsoids at 50%. Hydrogen atoms omitted for clarity.

The room temperature ^{1}H NMR spectrum of **3.3** reveals four sharp singlets in a 12:6:18:4 intensity ratio and similar to **3.2**; one may conclude that the solution phase structure of the molecule differs from that observed in the solid state (pseudo C_{2v} *vs.* C_2 respectively). Although $(\eta^5\text{-}C_5R_5)_2Ti(CH_2{}^tBu)_2$ (R = H, Me) have been synthesised,[25, 26] no characterising data were reported for comparison, but the values for the methylene and ^{t}Bu group agree very well with its group IV congener, $Cp_2Zr(CH_2{}^tBu)_2$, with chemical shifts of δ = 0.77, 1.21 and 0.72, 1.12 ppm respectively; C_6D_6.[27] The ^{13}C NMR (C_6D_6) spectrum displays eight resonances, five of which correspond to Pn* carbons and two for the ^{t}Bu group at their expected values, with the resonance at δ = 90.7 ppm that of the methylene carbon.

Table 3.4: Selected bond lengths, angles and structural parameters for **3.3**. ESDs are given in parentheses.

Lengths (Å)			
Ti(1) - C(1)	2.3434(19)	C(1) - C(2)	1.419(3)
Ti(1) - C(2)	2.490(2)	C(2) - C(3)	1.412(3)
Ti(1) - C(3)	2.3936(19)	C(3) - C(4)	1.434(3)
Ti(1) - C(4)	2.1347(19)	C(4) - C(5)	1.439(3)
Ti(1) - C(5)	2.3561(19)	C(5) - C(6)	1.428(3)
Ti(1) - C(6)	2.518(2)	C(6) - C(7)	1.414(3)
Ti(1) - C(7)	2.410(2)	C(7) - C(8)	1.441(3)
Ti(1) - C(8)	2.1370(19)	C(8) - C(1)	1.436(3)
Ti(1) - C(15)	2.1570(19)	C(4) - C(8)	1.460(2)
Ti(1) - C(20)	2.1537(19)		
Ti(1) - Pn^*_{cent}	1.968	Av. C_{ring} - Me	1.499
Ti(1) - Pn^*_{cent}	1.956		
Angles (°)			
C(15) - Ti(1) - C(20)	106.18(8)		
Ti(1) - C(15) - C(16)	130.03(14)		
Ti(1) - C(20) - C(21)	129.94(13)		
Fold Angle	33.11		

There is a distinct lack of structurally characterised titanium neopentyl complexes in the literature, with the sole example of a pure organometallic species that of the 15 electron Ti^{III} complex, $Cp^*_2Ti(CH_2{}^tBu)$. The average Ti-CH_2 distance is longer [2.231(5) Å][28] compared to **3.3** (2.155 Å) as expected with the lower oxidation state, exerting a weaker electrostatic interaction with the formally anionic neopentyl ligand and subsequently, the contact is lengthened compared to **3.3**. The average Ti-CH_2-^{t}Bu angle for **3.3** (129.99°) is similar to its Ti^{III} analogues value [131.1(3)°], deviating from an ideal 109.5° due to steric requirements of the bulky ^{t}Bu group. All other lengths and angles within the neopentyl moiety are very similar.

Titanium neopentyl complexes are known to be thermally sensitive and prone to decomposition *via* a number of pathways.[25, 26, 28–30] As no β-hydrogens are present, the main heterolytic intramolecular decomposition routes for **3.3** are α- and γ-hydrogen abstraction from a neopentyl group, forming an alkylidene and metallocycle respectively, with concomitant liberation of neopentane (CMe_4, Figure 3.9). Another

possibility is homolytic cleavage of the Ti-C bond to give a Ti^{III} species and a neopentyl radical. The latter is known to scavenge hydrogen efficiently to form neopentane, couple to form dineopentyl, eliminate a hydrogen atom to yield 1,1-dimethylcyclopropane, or eliminate a methyl group to form isobutylene (Figure 3.10).[31]

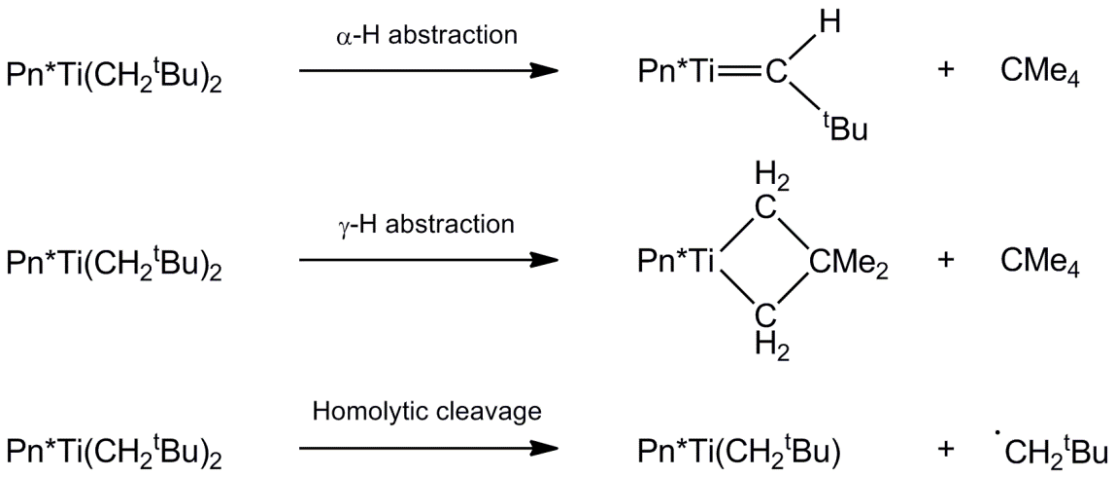

Figure 3.9: Possible unimolecular decomposition pathways of **3.3**.

It has been documented for the related complexes $Cp^*_2Ti(CH_2{}^tBu)_2$ and $Ti(CH_2{}^tBu)_4$ that both α- and γ-hydrogen activation occur,[25, 30] with the former assigned as the major decomposition pathway on steric grounds, proceeding 25 times faster for $Ti(CH_2{}^tBu)_4$; no homolytic cleavage is observed.[30]

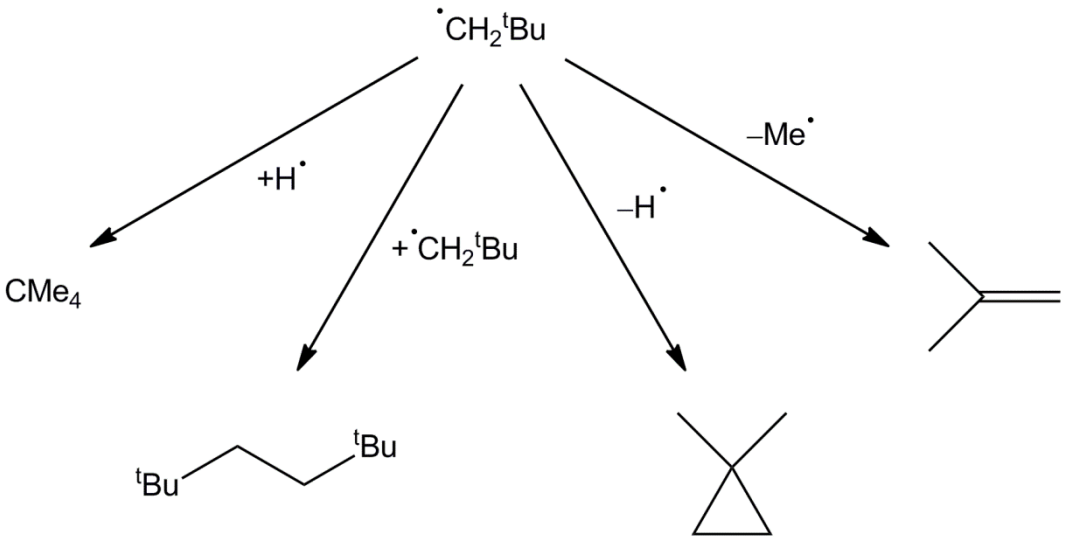

Figure 3.10: Possible organic products formed from neopentyl radical termination.

It was found that solutions of **3.3** decomposed slowly over a number of weeks to give an orange-brown solution and under certain conditions, a black precipitate, depending on the solvent employed. Samples were monitored by ^{1}H NMR spectroscopy at room temperature in C_6D_6 and cyclohexane-d_{12} (C_6D_{12}), with the latter producing the black precipitate. An approximate half-life ($t_{½}$) of 4.5 days was calculated using the integration of the residual protio-solvent peak in comparison to the known resonances of **3.3**. This is significantly slower than observed in solution at 20 °C for (η^5-$C_5H_4R)_2Ti(CH_2{}^tBu)_2$ (R = H, Me), which have $t_{½}$ = 56 and 20 minutes respectively, indicating that alkyl substitution on the Cp ligand facilitates the α-abstraction process.[26] This is further supported by the non-isolable nature of (η^5-C_5H_4Me)(η^5-$C_5H_4{}^tBu$)$Ti(CH_2{}^tBu)_2$, which spontaneously decomposes *via* α-hydrogen elimination followed by rapid intramolecular addition of a C-H bond of the cyclopentadienyl ^{t}Bu substituent to yield the cyclometallated complex (η^5-C_5H_4Me)(η^5,η^1-$C_5H_4CMe_2CH_2$)$Ti(CH_2{}^tBu)$ (Figure 3.11).[29] There is no precedent in the literature for any η^8-Pn species to form tuck-in complexes, which could be envisaged to lead to a large deformation of the ring system, and be highly unfavourable. There is no evidence of a parallel pathway operating for **3.3**, and the enhanced stability of Pn*$TiCl(CH_2{}^tBu)$ (**3.4**, *vide infra*) in comparison suggests that the abstracted hydrogen atom originates from the second $CH_2{}^tBu$ group and not the Pn* ligand.

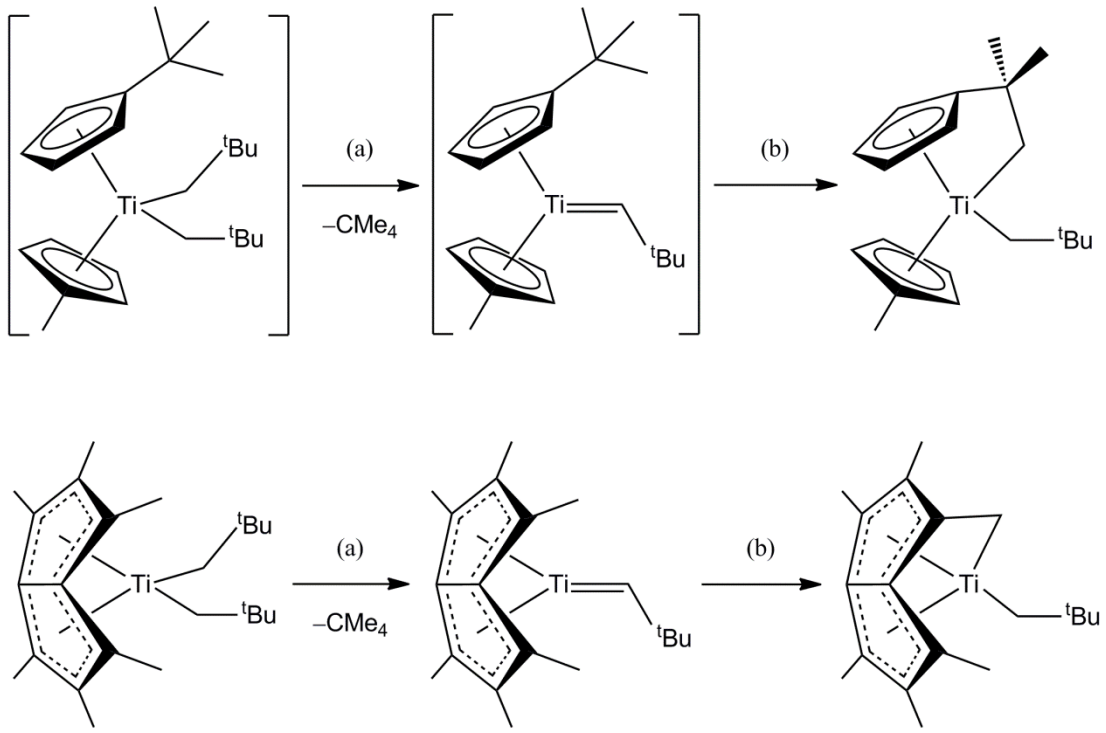

Figure 3.11: Proposed decomposition of (η^5-C_5H_4Me)(η^5-$C_5H_4{}^tBu$)$Ti(CH_2{}^tBu)_2$ and possible analogous pathway for **3.3**. (a) intramolecular α-H abstraction, (b) H-migration.

The sole organic product detected by NMR methods in both C_6D_6 and C_6D_{12} solvents was CMe_4, which is a by-product in two of the intramolecular decomposition modes (α- and γ-hydrogen abstraction, Figure 3.9). Importantly no other organic compounds were identified, which precludes homolytic cleavage of the Ti-$CH_2{}^tBu$ bond as other side products would be expected[31] including $DCH_2{}^tBu$ by deuterium scavenging from the solvent of the free radical produced, which was not observed. There is no evidence for the formation of a highly symmetric metallocycle akin to that observed from the thermal decomposition of $Cp^*_2Th(CH_2{}^tBu)_2$ to $Cp^*_2Th[(CH_2)_2CMe_2]$,[32] and isobutylene is also absent, which would be expected as a decomposition product from the subsequent degradation of such a species as seen for $Cp^*_2Ti(CH_2{}^tBu)_2$.[25] These observations indicate α-hydrogen abstraction may be the dominant pathway which would produce an alkylidene that possesses a very diagnostic downfield shift in both ^1H and ^{13}C NMR spectroscopy;[33, 34] unfortunately no obvious chemical shifts were discerned. This may be due to the expected reactivity of the species being too great to isolate as is the case for $Ti(CH_2{}^tBu)_4$;[30] such functionalities are known to activate sp^2 - C-D bonds[26, 29, 30] in C_6D_6, benzylic sp^3 - C-H bonds,[26] and have even been shown to activate aliphatic C-D bonds in C_6D_{12}.[30] Attempts were made

to trap out any coordinatively unsaturated intermediates with PMe_3, which has previously shown to be successful with such species,[26, 29, 30] but this proved ineffective with no isolable product identified. The nature of the black precipitate produced through decomposition in a C_6D_{12} medium is unknown but is thought to contain the Ti organometallic fragment. The reason for its absence in the C_6D_6 solution may be a result of the differing solubility in aliphatic and aromatic solvents for the by-product, or that a different mechanism is operating in each solvent. This is suggested for $Ti(CH_2{}^tBu)_4$, where an α-hydrogen elimination/solvent assisted pathway is described for benzene but a more complex mechanism involving competing pathways is operating in C_6D_{12}.[30]

Unfortunately these experiments have proven unsuccessful in determining the decomposition mechanism for **3.3** and further investigations are required to elucidate its pathway. **3.3** is however, significantly more thermally robust in the solid state, with crystalline samples displaying minimal decomposition over a number of weeks when stored in the glovebox, although low temperatures (−35° C) are preferable for prolonged storage.

The extremely high sensitivity of **3.3** has precluded the acquisition of an accurate elemental analysis. The reactivity of **3.3** with small molecules (CO_2, CO, H_2 and C_2H_4) is discussed in detail in chapters four and five.

3.5 Synthesis and characterisation of Pn*TiCl($CH_2{}^tBu$) (3.4)

Two equivalents of $LiCH_2{}^tBu$ were quickly added to **2.1** in benzene at room temperature (Figure 3.12), which afforded a dark red-purple solution. Subsequent work up and cooling of a pentane solution produced a red microcrystalline solid in moderate yield (57%), which was identified as Pn*TiCl($CH_2{}^tBu$) (**3.4**) by elemental analysis and X-ray crystallography. Single crystals suitable for X-ray diffraction were grown by slow cooling of a solution in the same solvent to −35 °C and the structure is shown in Figure **3.13**.

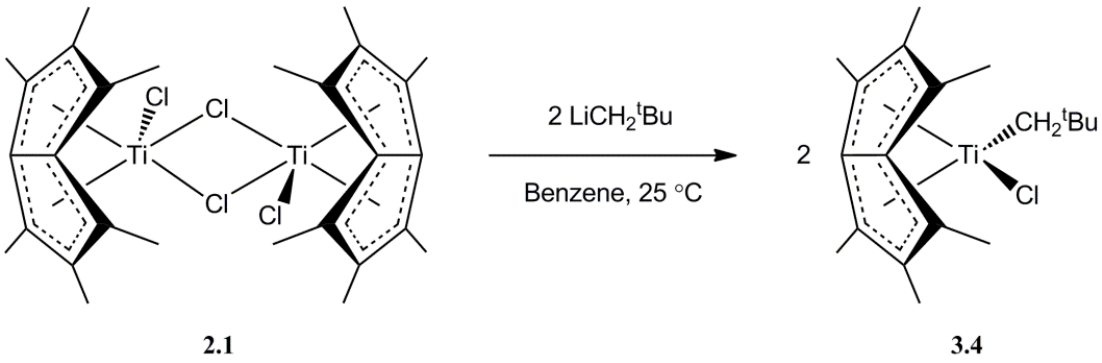

2.1 **3.4**

Figure 3.12: Synthesis of Pn*TiCl($CH_2{}^tBu$) (**3.4**).

3.4 crystallises in the $P2_1/c$ space group, with one independent molecule in the asymmetric unit and four in the unit cell. Again, the ligands are coordinated in a pseudo tetrahedral arrangement about Ti, as exemplified by the C(15)-Ti(1)-Cl(1) angle [106.12(5)°].

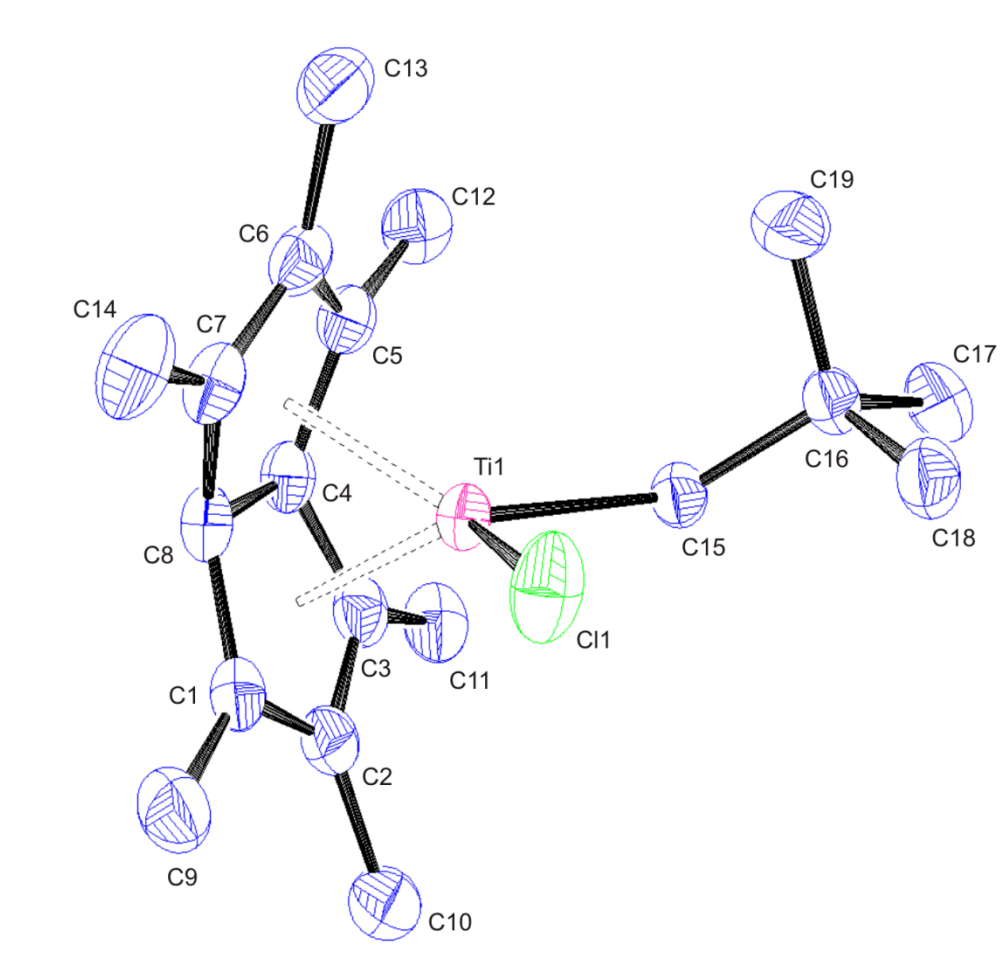

Figure 3.13: Side-on view of **3.4** with thermal ellipsoids at 50%. Hydrogen atoms omitted for clarity.

3.4 is a 14 electron monomeric species unlike other reported 'Pn*TiClR' complexes, [Pn*TiMe(μ-Cl)]$_2$ (**2.2**) and [Pn*TiPh(μ-Cl)]$_2$ (**3.5**, *vide infra*), which both contain μ-Cl ligands, resulting in 16 electron counts for each titanium centre. It is proposed that an interplay between electronic stabilisation at the metal centre and steric repulsion between ligands is key to determining the monomer/dimer formation of a 'Pn*TiClR' species. This hypothesis is supported for the dimeric structures **2.2** and **3.5**, which contain Me (small) and Ph (planar) ligands. A consequence of the monomeric formulation is the larger fold angle for **3.4** (34.1°), compared to **2.2** and **3.5** (30.6 and 31.6° respectively), which is predicted on steric grounds, since the former has two additional ligands and the latter three bound to each Pn*Ti fragment. This results in less steric congestion around titanium and enabling the pentalene framework to fold more and maximise Ti-C(Pn*) contacts. This, in conjunction with its relatively deficient 14 electron configuration, results in a larger fold angle. It also possesses a greater fold angle than **3.3** (33.1°), as expected on replacing a $CH_2{}^tBu$ group with an electron withdrawing Cl.[10]

The Ti(1)-Cl(1) bond length [2.2989(6) Å], is shorter than the corresponding terminal Ti-Cl distance in **2.1** [2.3595(9) Å],[35] which may be rationalised by the electron deficiency compared to the 16 electron **2.1**, resulting in a stronger Ti-Cl attraction. It is also shorter than the analogous bond in the related isoelectronic Cp*TiCl($CH_2{}^tBu$)[N(^{i}Pr)C(Me)N(^{i}Pr)] [2.3412(4) Å], as is the corresponding Ti(1)-C(15) bond length [2.1548(19) and 2.1794(13) Å respectively].[36] The Ti-CH_2 distances of **3.4**, **3.3** and **3.2** are almost identical but the former has a shorter Ti-Pn*$_{cent}$ distance (1.943 compared to 1.962 and 1.956 Å respectively); a stronger Ti-C(Pn*) interaction on inclusion of the electronegative Cl group, is a trend paralleled by decreasing fold angles (34.1, 33.1 and 32.9° respectively, Table 3.9).[10]

The Ti(1)-C(15)-C(16) angle [124.44(14)°] is smaller than the analogous average parameter for **3.3** (129.99°), which results from reduction in crowding around Ti on replacement of the sterically cumbersome neopentyl group with the smaller Cl, permitting the angle to approach its idealised tetrahedral value more closely.

Table 3.5: Selected bond lengths, angles and structural parameters for **3.4**. ESDs are given in parentheses.

Lengths (Å)			
Ti(1) - C(1)	2.345(2)	C(1) - C(2)	1.420(3)
Ti(1) - C(2)	2.481(2)	C(2) - C(3)	1.421(3)
Ti(1) - C(3)	2.3692(19)	C(3) - C(4)	1.437(3)
Ti(1) - C(4)	2.1288(18)	C(4) - C(5)	1.447(3)
Ti(1) - C(5)	2.350(2)	C(5) - C(6)	1.419(3)
Ti(1) - C(6)	2.491(2)	C(6) - C(7)	1.417(3)
Ti(1) - C(7)	2.370(2)	C(7) - C(8)	1.444(3)
Ti(1) - C(8)	2.1230(19)	C(8) - C(1)	1.436(3)
Ti(1) - Cl(1)	2.2989(6)	C(4) - C(8)	1.465(2)
Ti(1) - C(15)	2.1548(19)		
Ti(1) - Pn^*_{cent}	1.944	Av. C_{ring} - Me	1.498
Ti(1) - Pn^*_{cent}	1.942		
Angles (°)			
Cl(1) - Ti(1) - C(15)	106.12(5)		
Ti(1) - C(15) - C(16)	124.44(14)		
Fold Angle	34.08		

The room temperature ^{1}H NMR spectrum of **3.4** reveals five sharp resonances in a 6:6:6:9:2 intensity ratio and one may conclude that the solution phase structure of the molecule is of C_s symmetry, as observed in the solid state. The Pn* resonances are split into three sets of equal intensity, due to the reduced symmetry of the molecule, which results in two pairs of independent NWT-Me protons (Figure 3.14). This is in contrast to other observed 'Pn*TiClR' complexes, **2.2** and **3.5**, which in solution contain equivalent NWT-Me groups but are both of C_{2h} symmetry in the solid state, indicating a fluxional process is operating. The origins of this fluxional process are unclear but could arise from Pn* ring-whizzing, a phenomenon readily observed in Cp and Cp* complexes. It is proposed that an interplay between fold angle and steric bulk of the ancillary ligands bound to the metal centre effect the rate of such a process; large fold angles in tandem with large 'R' groups make the process energetically unfavourable at room temperature, which results in non-equivalent NWT-Me groups (e.g. **3.4**). However, smaller fold angles in conjunction with smaller R groups (e.g. **2.2**), allow the process to operate, rendering all NWT-Me groups equivalent on the NMR timescale. It

is thought to be a delicate balance as demonstrated by the intermediate example **3.5**, which has equivalent NWT-Me groups at room temperature but whose resonance broadens on cooling (*vide infra*), indicating a retardation of the process.

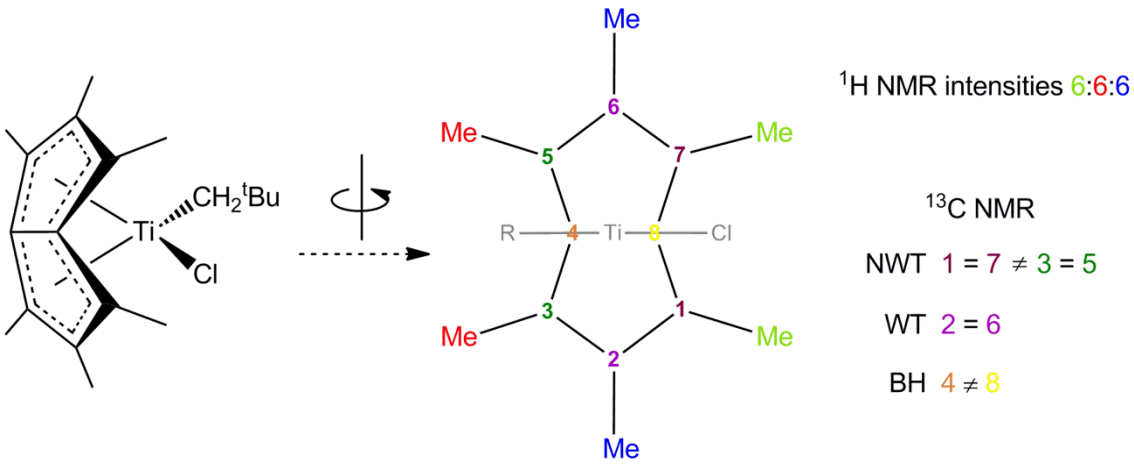

Figure 3.14: $^{1}H/^{13}C$ NMR splitings for Pn*TiRR' (R ≠ R'), C_s symmetric complexes.

The WT-Me resonance was found to occur at higher field to the remaining two Pn* resonances, which have the absolute configuration shown, as determined by 2D-NOESY NMR. It might be expected that replacement of a $CH_2{}^tBu$ group with Cl (**3.3**/**3.4**), would result in a downfield shift of the remaining methylene resonance in its ^{1}H NMR spectrum on the basis of Cl's greater electronegativity, as demonstrated by **2.2**/**2.7** and the series $Ta(\eta^8\text{-}Pn^{1,4\text{-}Si^iPr_3})Me_yX_{3-y}$ (y = 1-3, X = Cl).[10] This was found not to be the case as the chemical shift corresponding to the resonance of relative intensity two (δ = 0.58 ppm; C_6D_6), is upfield to that of **3.3** (δ = 0.77 ppm; C_6D_6). Coincidentally the methylene ^{13}C NMR chemical shift is also to higher field than that of **3.3** (83.5 and 90.7 ppm respectively), which is paralleled in **2.2**/**2.7** and the series $Ta(\eta^8\text{-}Pn^{1,4\text{-}Si^iPr_3})Me_yX_{3-y}$ (y = 1-3, X = Cl). The remainder of the ^{13}C NMR (C_6D_6) spectrum displays ten resonances, two for the ^{t}Bu group at their expected values and eight corresponding to Pn* carbons as the result of reduced symmetry in the molecule; the bridgehead carbons are non-equivalent and differ by 5 ppm (Figure 3.14).

In contrast to **3.3**, **3.4** is stable indefinitely in both solution and the solid state (298 K), contrasting with $Cp^*_2TiCl(CH_2{}^tBu)$,[37] [which instantly decomposes on formation yielding Cp^*_2TiCl and $(CH_2{}^tBu)^{\bullet}$] and the related amidinate $Cp^*TiCl(CH_2{}^tBu)[N(^iPr)C(Me)N(^iPr)]$,[36] {which decomposes by means of an

α-hydrogen activation of the Cp* ring, with release of CMe_4, forming the tuck-in product, $[\eta^5{:}\eta^1\text{-}C_5Me_4(CH_2)]TiCl[N(^iPr)C(Me)N(^iPr)]\}$. As mentioned previously, the latter de-activation pathway has yet to be observed with any pentalene derivative and is thought to be unfavourable due to the large deformation enforced on the resultant tucked-in ring system.

The enhanced thermal stability of **3.4** stands in marked contrast to the related dimeric 'Pn*TiClR' species **2.2** and **3.5**, which decompose when stored in solution at room temperature and rapidly upon heating, with concomitant liberation of RH (R = Me, Ph), and the clean formation of novel Pn* species (Section 2.5). It is postulated the dimeric structure of these complexes is crucial for the decomposition pathway involved and that it is intramolecular in nature with the complexes prearranged to eliminate RH *via* hydrogen abstraction. **3.4**'s persistent stability suggests that neither solvent participation nor an intermolecular pathway is operating in the decomposition of these complexes. It is also thought the nature of the resulting bridging group is not a critical factor as, although there are no structurally characterised examples of bridging CH^tBu moieties between two Ti centres, there is precedent in the literature with other transition metals.[38, 39]

3.6 Synthesis and characterisation of [Pn*TiPh(μ-Cl)]$_2$ (3.5)

The synthesis of $[Pn^*TiPh(\mu\text{-}Cl)]_2$ (**3.5**) is detailed in Figure 3.15; rapid combination of two equivalents of PhMgCl solution with **2.1** (C_6H_6, 298 K), instantly afforded a vivid green solution. Subsequent work up and cooling of a toluene solution produced an emerald green microcrystalline solid in good yield (68%), which was identified as **3.5** by elemental analysis and X-ray crystallography. Single crystals suitable for X-ray diffraction were grown by slow cooling of a solution in the same solvent to −35 °C and two views of the structure are shown (Figures 3.16 and 3.17).

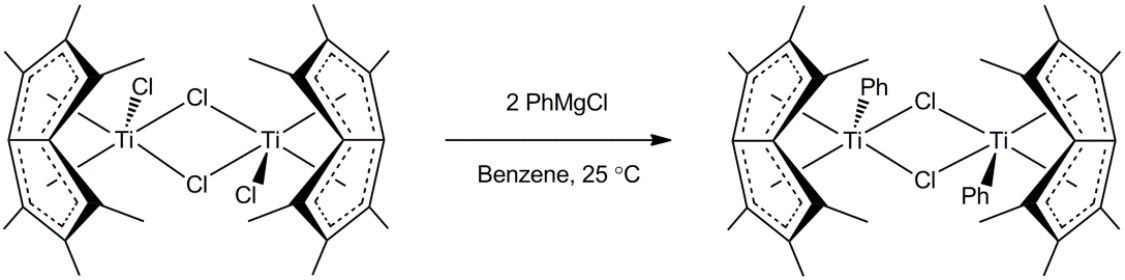

2.1 **3.5**

Figure 3.15: Synthesis of $[Pn^*TiPh(\mu\text{-}Cl)]_2$ (**3.5**).

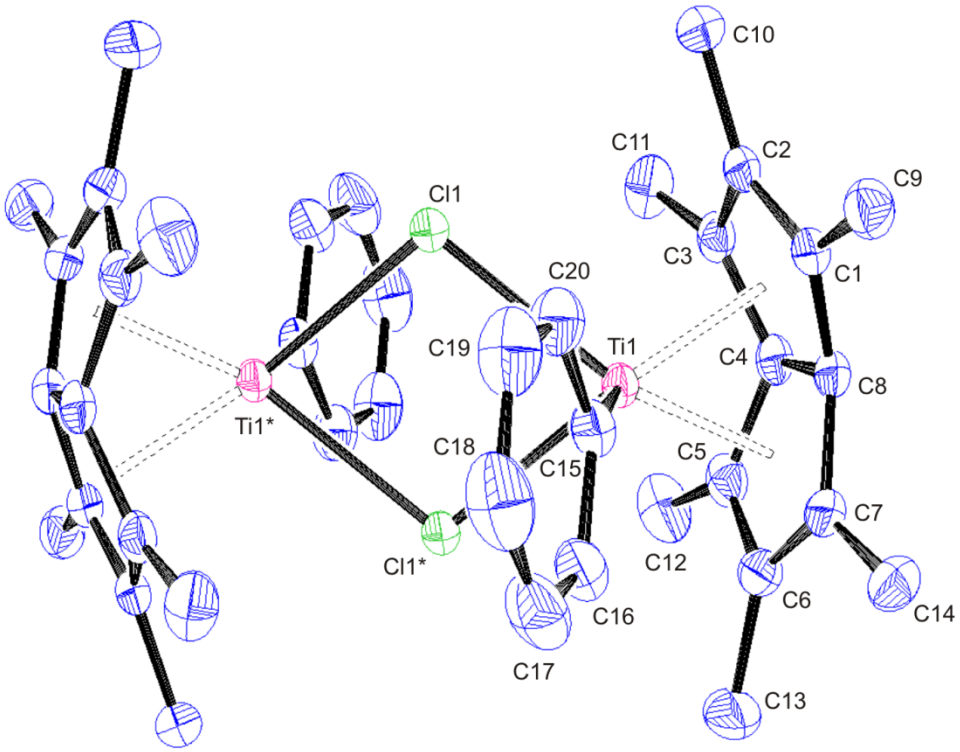

Figure 3.16: Side-on view of **3.5** with thermal ellipsoids at 50%. Hydrogen atoms and toluene molecule omitted for clarity, * denotes atoms generated by inversion symmetry.

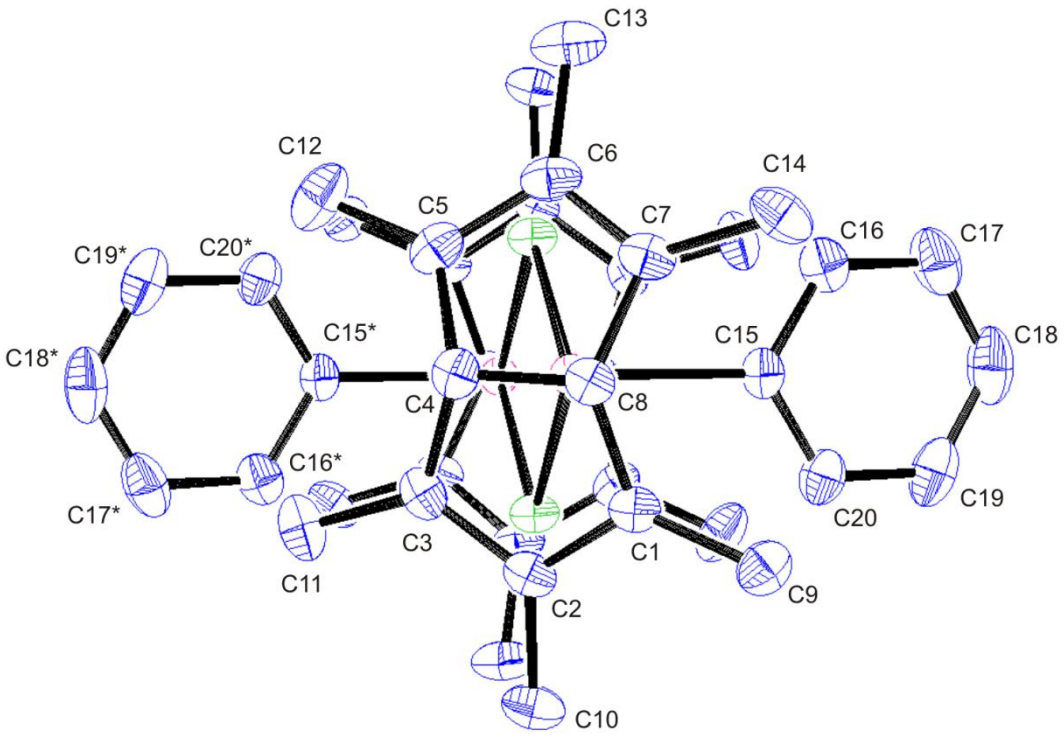

Figure 3.17: End-on view of **3.5** with thermal ellipsoids at 50%. Hydrogen atoms and toluene molecule omitted for clarity, * denotes atoms generated by inversion symmetry.

3.5 crystallises in the *C*2/*c* space group with one half-molecule in the asymmetric unit possessing inversion symmetry to form the constituent dimer, and a co-crystallised solvent molecule. The titanium centre has alleviated electron deficiency through dimerisation from a 14 electron monomer, akin to **3.4**, to the 16 electron dimer, analogous to **2.1**[35] and **2.2**. The Ti atoms are bridged by two chloride ligands and **3.5** possesses C_{2h} symmetry in the solid state with the principle axis dissecting the two chloride ligands [Cl(1) and Cl(1*)], isostructural with **2.1** and **2.2**.

The Pn* ligands are almost eclipsed around the $Ti_2(\mu\text{-}Cl)_2$ core (Figure 3.17), paralleling the structures of **2.1** and **2.2** and the average value for the Ti-(μ-Cl) bond (2.488 Å) is in good agreement (2.485 and 2.508 Å respectively). Also comparable are the fold angles of **3.5** and **2.2** (31.6 and 30.6° respectively), which are considerably smaller than the associated monomeric **3.4** (34.1°), predicted on steric grounds, as the former have three additional ligands and the latter two bound to each Pn*Ti fragment, resulting in greater steric congestion around titanium. The Ti(1)-C(15) bond length [2.1762(19) Å] is almost identical to the related isoelectronic [Me_2Si] *ansa*-bridged

titanocene $[Me_2Si(C_5Me_4)_2]TiClPh$, [2.172(3) Å][40] but appreciably shorter than seen for Cp_2TiPh_2, [2.272(12) Å].[41]

With a Ti···Ti distance of 3.8335(5) Å, which is similar to **2.2** [3.8401(11) Å] and slightly larger than seen in **2.1** (3.806 Å), there is no evidence of a titanium-titanium bond present (sum of covalent radii = 2.64 Å).

Table 3.6: Selected bond lengths, angles and structural parameters for **3.5**. * denotes atoms generated by inversion symmetry and ESDs are given in parentheses.

Lengths (Å)			
Ti(1) - C(1)	2.4234(19)	C(1) - C(2)	1.412(3)
Ti(1) - C(2)	2.5321(19)	C(2) - C(3)	1.420(3)
Ti(1) - C(3)	2.3385(19)	C(3) - C(4)	1.439(3)
Ti(1) - C(4)	2.1240(18)	C(4) - C(5)	1.434(3)
Ti(1) - C(5)	2.3230(19)	C(5) - C(6)	1.426(3)
Ti(1) - C(6)	2.526(2)	C(6) - C(7)	1.406(3)
Ti(1) - C(7)	2.4466(19)	C(7) - C(8)	1.439(3)
Ti(1) - C(8)	2.1510(18)	C(8) - C(1)	1.439(3)
Ti(1) - Ti(1*)	3.8335(5)	C(4) - C(8)	1.453(3)
Ti(1) - C(15)	2.1762(19)	Av. C_{ring} – Me	1.499
Ti(1) - Cl(1)	2.4720(5)	Ti(1) - Pn^*_{cent}	1.974
Ti(1) - Cl(1*)	2.5046(5)	Ti(1) - Pn^*_{cent}	1.973

Angles (°)	
C(15) - Ti(1) - Cl(1)	90.72(5)
C(15) - Ti(1) - Cl(1*)	90.47(5)
Ti(1) - Cl(1) - Ti(1*)	100.763(17)
Cl(1) - Ti(1) - Cl(1*)	79.237(17)
Fold Angle	31.55

The room temperature ^1H NMR spectrum of **3.5** reveals five resonances in a 4:4:2:12:24 intensity ratio and one may conclude that the solution phase structure of the molecule is in contrast to that observed in the solid state (C_{2h}) from which a reduction in symmetry would be expected resulting in two sets of non equivalent NWT-Me groups. The resonances corresponding to the Ph group occur within their usual range (6.87-7.11 ppm; CD_2Cl_2) and are symmetric, as illustrated by the 4:4:2 intensity ratio. This contrasts with $Cp^*_2TiClPh$, which has hindered rotation about the Ti-Ph bond due to

steric crowding, resulting in five unique resonances in the ^{1}H NMR and six in the ^{13}C NMR spectrum,[42] a phenomenon also seen in $[Me_2Si(C_5Me_4)_2]TiClPh$.[40] Interestingly the WT-Me resonance lies at lower field relative to the NWT-Me as observed for **2.2**, which also contains μ-Cl ligands and terminal R groups and is different to that adopted for all Pn*TiR_2 complexes, which have WT-Me resonances at higher field. The NWT-Me resonance is broad ($\nu_{½}$ = 3.7 Hz) at room temperature, indicating that a fluxional process is occurring. VT ^{1}H NMR measurements were acquired in an attempt to 'freeze-out' any fluxional process and upon cooling, the resonance broadens to $\nu_{½}$ = 55.5 Hz at −30 °C but further measurements at lower temperature were hampered due to the compound's inherently poor solubility. This indicates that the fluxional process operating to equate all NWT-Me groups in solution is much faster for the isostructural **2.2**, which displayed no line broadening on cooling to −60 °C. This is reasoned on steric grounds; since Me is much smaller than Ph in conjunction with the larger fold angle in **3.5** (31.6 *vs.* 30.6°), the process is more facile (Section 3.5). The ^{13}C NMR (CD_2Cl_2) spectrum displays nine resonances, five of which correspond to Pn* carbons at their expected values and the remaining four to that of the Ph group. The resonance at δ = 187.6 ppm belongs to the *ipso*-carbon, which corresponds well with Cp_2TiPh_2 (δ = 192.9 ppm; CD_2Cl_2).[43]

Due to the isomorphic nature of **3.5** and **2.2**, the thermal stability of **3.5** was investigated to see if it resembled that of the latter, which cleanly decomposes in solution to give the interesting methylene bridged **2.3** and CH_4. Similarly to **2.2**, **3.5** was found to be indefinitely stable in the solid state under an inert atmosphere and also decomposed in solution, albeit at a much slower rate (months *vs.* days) at room temperature. An NMR sample of **3.5** in CD_2Cl_2 was heated to 50 °C over a period of 60 hours, which lead to the complete consumption of **3.5** and formation of a highly symmetric novel Pn* species and C_6H_6 (7.35 ppm) as the sole diamagnetic products. The room temperature ^{1}H NMR spectrum (Figure 3.18) consists of four resonances in an intensity ratio 2:2:24:12, with two resonances corresponding to the Pn* moiety falling within their normal range. The two resonances furthest downfield in the region associated with aryl chemical shifts possess a highly symmetrical line shape that is consistent with an AA'BB' splitting pattern, containing complex 2nd order coupling.

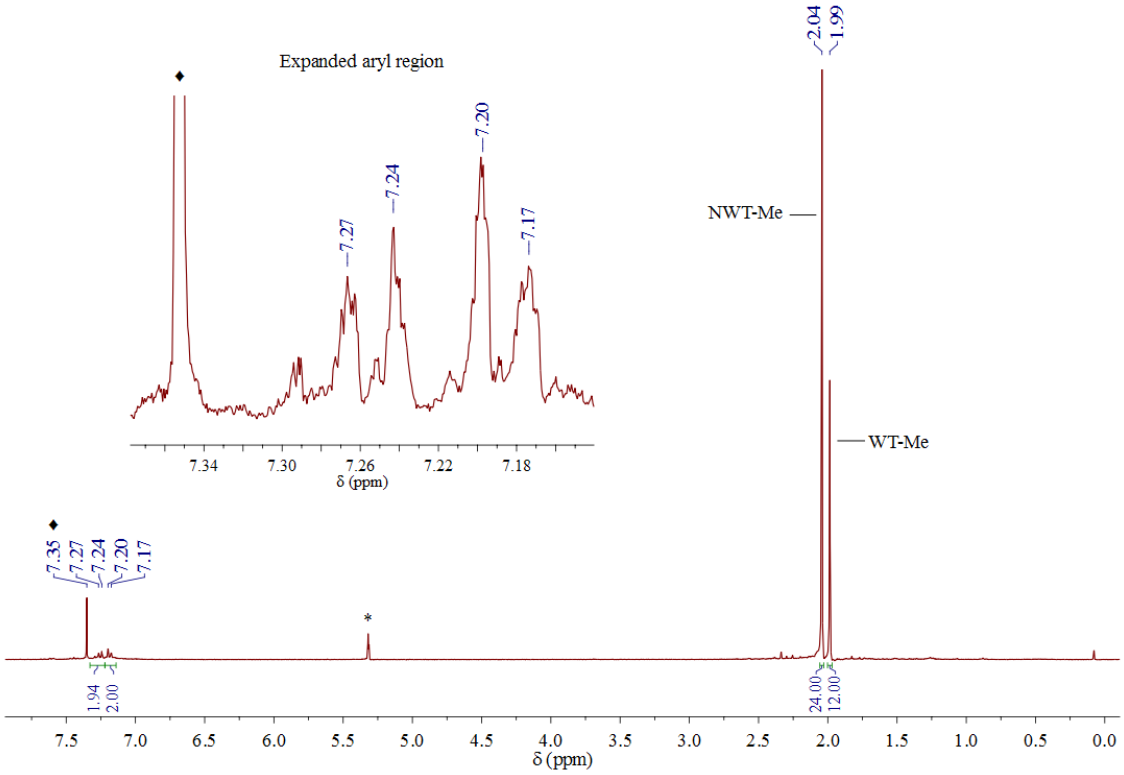

Figure 3.18: ^{1}H NMR spectra of **3.5**'s decomposition product in CD_2Cl_2. * denotes residual protio-solvent, ♦ denotes C_6H_6.

Due to the structural similarities of **2.2** and **3.5**, and the correlation in spectroscopic data of their respective decomposition products, it seems reasonable to suggest the same mode of decomposition is operating in both cases, with the dimeric structure again proving pivotal at facilitating such a mechanistic pathway (Figure 2.12). This, in conjunction with the intensity ratio and highly symmetric nature of the decomposition product's ^{1}H NMR spectra, indicates the species' structure may consist of two μ-Cls and a "C_6H_4" unit bridging two equivalent Pn*Ti fragments, analogous to **2.3**. The "C_6H_4" bridging moiety has been reported in the literature between two metal centres for the late transition elements in an *o*-phenylene[44] and benzyne[45] bonding mode but has yet to be observed for titanium or any of the early transition metals; both proposed structures (Figure 3.19) are consistent with the experimental data obtained, and monomeric group IV transition metal benzyne complexes are known;[46] the most pertinent example is that of the transient species formed from the thermal decomposition of Cp_2TiPh_2. Extensive labelling and trapping experiments[47, 48] have conclusively shown its thermal decomposition pathway to proceed *via ortho*-hydrogen activation by the neighbouring Ph group, with formation of a "$Cp_2Ti(C_6H_4)$" benzyne

complex and liberation of C_6H_6. The mechanism proposed for the decomposition of **3.5** is analogous, but involving two metal centres as opposed to one.

m- and *p*-phenylene structures have been ruled out due to the symmetric nature of the ^{1}H NMR spectrum not being consistent with a *m*-substituted aryl and on steric grounds for the *p*-phenylene, as it would be too large to fit into the cavity, which is constricted in size by the Ti(μ-Cl)$_2$Ti arrangement.

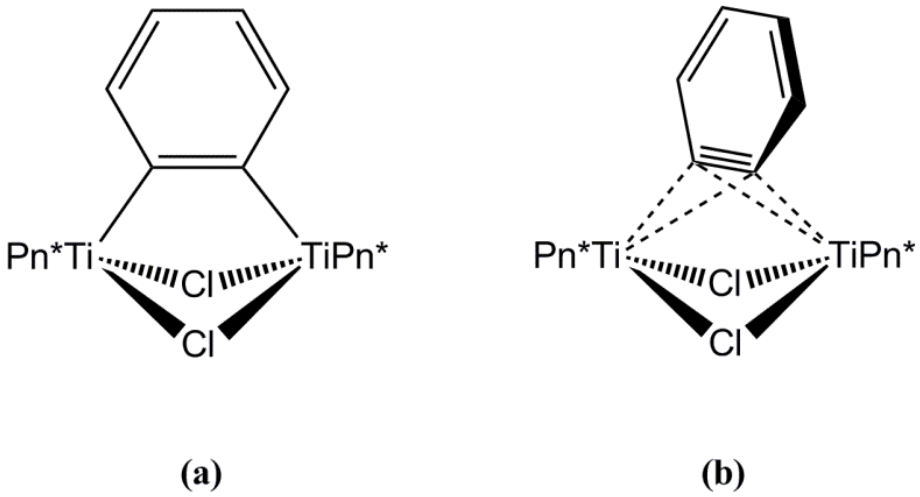

Figure 3.19: Possible structures for the thermal decomposition product of **3.5**.

Unfortunately time constraints prevented the complete characterisation of this novel species but with the data obtained and the prominence of bridging *o*-phenylene moieties in the literature, it seems reasonable to tentatively assign [Pn*Ti(μ-Cl)]$_2$(μ-C$_6$H$_4$) [Figure 3.19 (a)], as the most likely structure, which is analogous to the Pt containing dianion $[Pt_4(C_6H_4)_2Cl_{14}]^{2-}$ (Figure 3.20).[49]

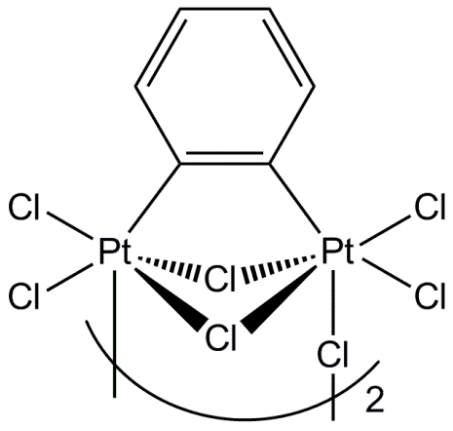

Figure 3.20: Solid state structure of $[Pt_4(C_6H_4)_2Cl_{14}]^{2-}$.

3.7 Synthesis and characterisation of Pn*TiClCp (3.6)

Jonas *et al.* were the first to establish the η^8-bonding mode for pentalene complexes of the group IV metals in 1997.[8] Treatment of $CpTiCl_2$ with the pentalene dianion furnished the paramagnetic PnTiCp; reaction of this species with half an equivalent of 1,2-dichloroethane resulted in the facile oxidation of the Ti^{III} centre, affording the 18 electron species PnTiClCp. This report details the only two structurally characterised η^8-Pn complexes of Ti before investigations in the area by O'Hare *et al.* and a permethylated analogue was targeted for comparison.

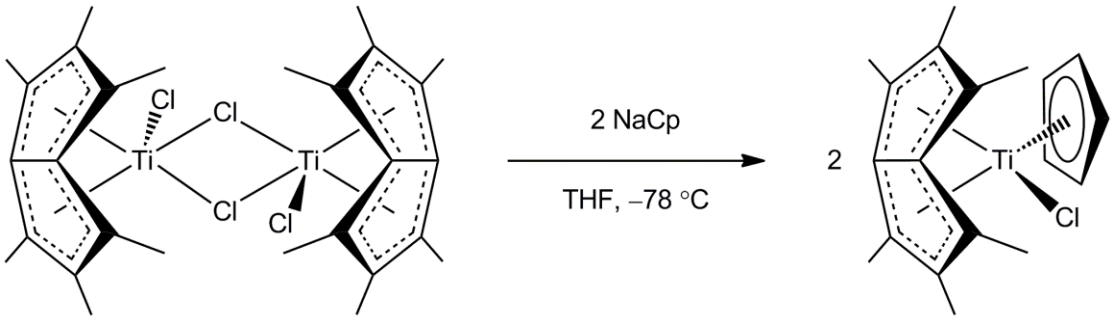

2.1 **3.6**

Figure 3.21: Synthesis of Pn*TiClCp (**3.6**).

The reaction of **2.1** with two equivalents of NaCp in THF, shown in Figure 3.21, afforded a red solution upon warming to room temperature. Subsequent work up and cooling of a hexane solution produced a red microcrystalline solid in excellent yield (83%), which was identified as Pn*TiClCp (**3.6**) by elemental analysis, X-ray crystallography and mass spectrometry (EI), the latter showing the molecular ion at accurate mass, followed by a peak ascribed to the loss of Cl and Cp. Single crystals suitable for X-ray diffraction were grown by slow cooling of a hexane solution to −35 °C and two views of the structure are shown (Figure 3.22 and 3.23).

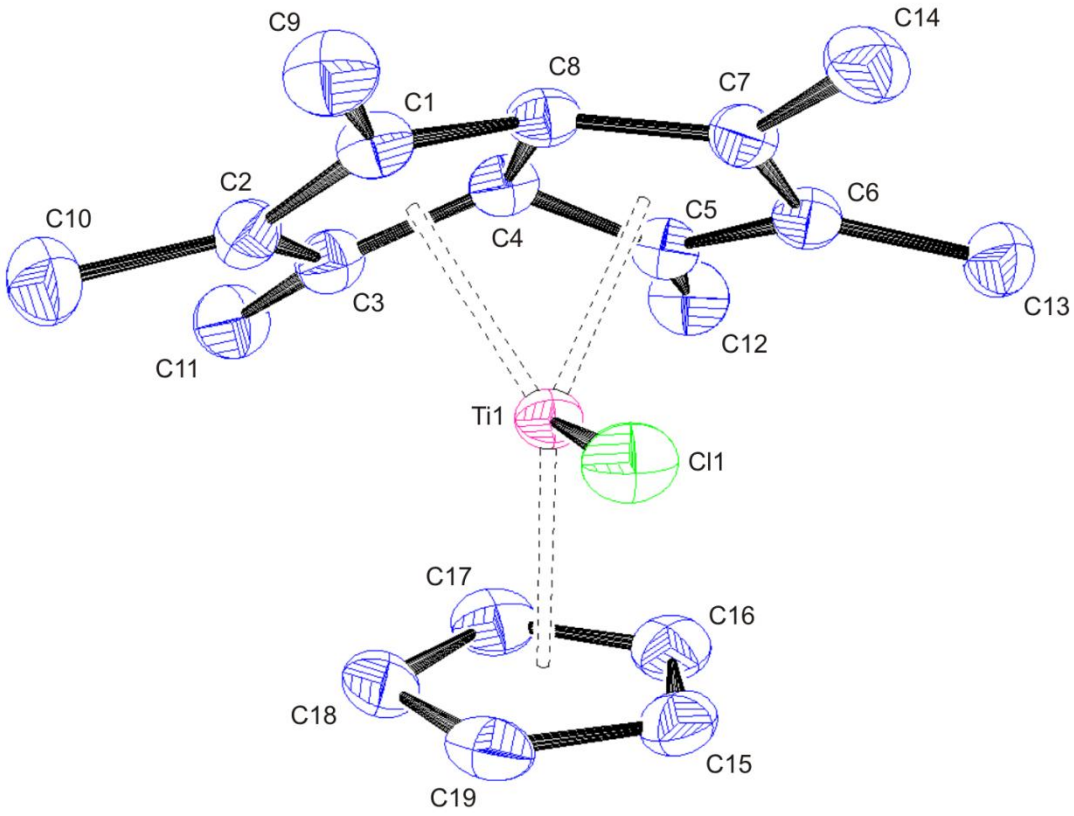

Figure 3.22: Side-on view of **3.6** with thermal ellipsoids at 50%. Hydrogen atoms omitted for clarity.

The room temperature ^{1}H NMR spectrum of **3.6** reveals four sharp singlets in a 5:6:6:6 intensity ratio and one may conclude that the solution phase structure of the molecule is of C_s symmetry, as observed in the solid state. The Pn* resonances are split into three sets of equal intensity, due to the reduced symmetry of the molecule. A mirror plane is present, which bisects the molecule through the Pn* and Cp ligands, and runs along the Ti(1)-Cl(1) bond, resulting in two sets of independent NWT-Me protons, as seen for **3.4** (Figure 3.14). As with **3.4**, the WT-Me resonance occurs at higher field to the remaining two Pn* resonances, which have the absolute configuration shown (Chapter 7) as determined by 2D-NOESY NMR. The resonance corresponding to the Cp moiety (δ = 5.38 ppm; C_6D_6), is similar to PnTiClCp (δ = 5.76 ppm; THF-d_8)[8] as is the ^{13}C NMR chemical shift (δ = 110.6 and 109.1 ppm respectively). The remainder of the ^{13}C NMR (C_6D_6) spectrum displays eight resonances corresponding to Pn* carbons as the result of reduced symmetry in the molecule; the bridgehead carbons are non-

equivalent and differ by 11.5 ppm compared to Jonas' unsubstituted analogue PnTiClCp, where they differ by 8.2 ppm.

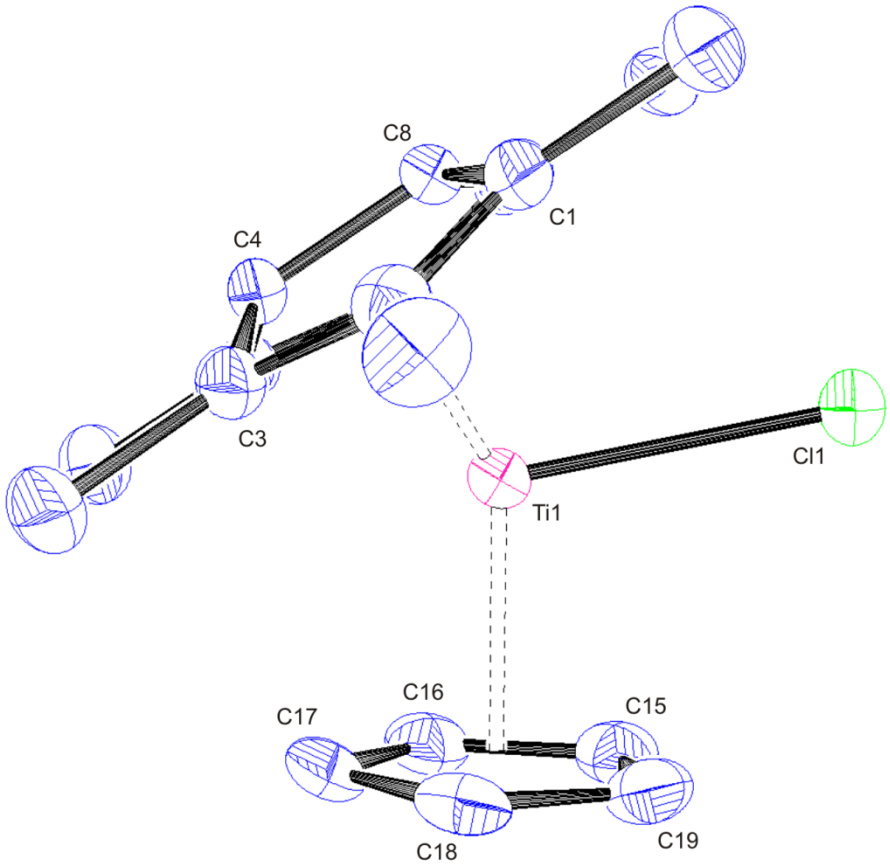

Figure 3.23: End-on view of **3.6** with thermal ellipsoids at 50%. Hydrogen atoms omitted for clarity.

3.6 crystallises in the $P2_1/c$ space group, with one independent molecule in the asymmetric unit and four in the unit cell. It is isoelectronic and isostructural with its nonmethylated counterpart PnTiClCp, being a an 18 electron complex and possessing a distorted pseudo tetrahedral arrangement of ligands about Ti, as exemplified by the Cp_{cent}-Ti(1)-Cl(1) and average Pn^*_{cent}-Ti(1)-Cl(1) angles (102.0 and 107.8° respectively), which are almost identical to PnTiClCp (103.7 and 107.5° respectively).[8]

Table 3.7: Selected bond lengths, angles and structural parameters for **3.6**. ESDs are given in parentheses.

Lengths (Å)			
Ti(1) - C(1)	2.338(2)	C(1) - C(2)	1.425(4)
Ti(1) - C(2)	2.541(3)	C(2) - C(3)	1.405(4)
Ti(1) - C(3)	2.470(2)	C(3) - C(4)	1.439(3)
Ti(1) - C(4)	2.169(2)	C(4) - C(5)	1.441(3)
Ti(1) - C(5)	2.473(2)	C(5) - C(6)	1.402(3)
Ti(1) - C(6)	2.544(3)	C(6) - C(7)	1.434(4)
Ti(1) - C(7)	2.355(2)	C(7) - C(8)	1.434(4)
Ti(1) - C(8)	2.130(2)	C(8) - C(1)	1.430(3)
		C(4) - C(8)	1.458(3)
Ti(1) - Cl(1)	2.5068(8)	Av. C_{ring} - Me	1.501
Ti(1) - Pn^*_{cent}	1.997	Av. Ti(1) - Cp	2.386
Ti(1) - Pn^*_{cent}	1.992	Ti(1) - Cp_{cent}	2.063
Angles (°)			
Cp_{cent} - Ti(1) - Cl(1)		101.97	
Pn^*_{cent} - Ti(1) - Cl(1)		108.24	
Pn^*_{cent} - Ti(1) - Cl(1)		107.39	
Fold Angle		30.98	

The fold angle (31.0°) is 2° less than reported for PnTiClCp (33.0°) and this smaller value may be attributed to the increased donor capability of the Pn* ligand relative to Pn; it can be posited that a less extreme fold is required for Pn* to balance any electron deficiency at Ti. The average Ti(1)-Pn^*_{cent} distance (1.995 Å), is shorter than the Ti(1)-Cp_{cent} distance (2.063 Å), which is possibly a reflectance of the higher electron count on the ligand available for donation to the metal (eight compared to five), the same ordering is observed for PnTiClCp (1.970 and 2.057 Å respectively).[8] The Ti(1)-Cl(1) bond [2.5068(8) Å], is unusually long compared with Cp_2TiCl_2 (2.364 Å)[50] and $Cp^*_2TiCl_2$ (2.349 Å)[51] but is comparable to Jonas' mixed sandwich analogue PnTiClCp [2.512(1) Å] and is thought to be the result of steric congestion around the Ti centre.

There is significant deviation between the average Ti(1)-C(1/7) (2.347 Å) and Ti(1)-C(3/5) (2.472 Å) distances, resulting in a tilting of the Pn* moiety towards the Cl atom and away from symmetric η^8-binding to the metal centre. This is also seen in

PnTiClCp (2.433 and 2.321 Å respectively) but interestingly is reversed with the ligand canting away from the Cl atom, which presumably is a result of the inclusion of the Me groups and a negative steric interaction with the Cp fragment in **3.6**.

3.8 Synthesis and characterisation of Pn*Ti(η^5-Cp)(η^1-Cp) (3.7)

Jonas also reported the zirconium analogue of **3.6**, PnZrClCp, which was synthesised by the direct combination of Cp_2ZrCl_2 and $PnLi_2$, whereby a cyclopentadienyl ligand is substituted in preference to a chloride.[8] The alternative product, $PnZrCp_2$ produced by substitution of both chloride ligands was later postulated as being too sterically saturated to form under the conditions.[52] Preliminary NMR scale investigations involved sonication of **2.1** with excess NaCp, which produced a novel Pn* species containing two Cp resonances that significantly differed from that observed for **3.6**. Attempts at scaling up the reaction with simple stirring over a range of different temperatures, prolonged reaction times and in a variety of ethereal, aromatic and aliphatic hydrocarbon solvents, failed to replicate the reactivity exhibited on the NMR scale; the only product identified was **3.6** and an intractable pyrophoric solid, presumed to be unreacted NaCp. It was subsequently noted that the preliminary NMR scale reactions required sonication, in order to solubilise the ionic NaCp, in the non-polar C_6D_6 medium.

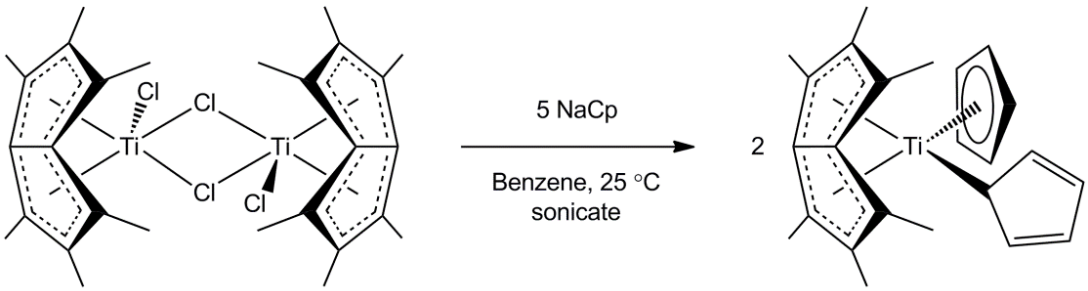

2.1 **3.7**

Figure 3.24: Synthesis of Pn*Ti(η^5-Cp)(η^1-Cp) (**3.7**).

The synthesis of Pn*Ti(η^5-Cp)(η^1-Cp) (**3.7**) is detailed in Figure 3.24; reaction of **2.1** with five equivalents of NaCp was found to form the target compound only upon prolonged sonication in benzene, which afforded a red solution. Subsequent work up and cooling of a hexane solution produced a red microcrystalline solid in good yield (62%), which was identified as **3.7** by elemental analysis and X-ray crystallography.

Single crystals suitable for X-ray diffraction were grown by slow cooling of a solution in the same solvent to 0 °C and two views of the structure are shown (Figure 3.25 and 3.26).

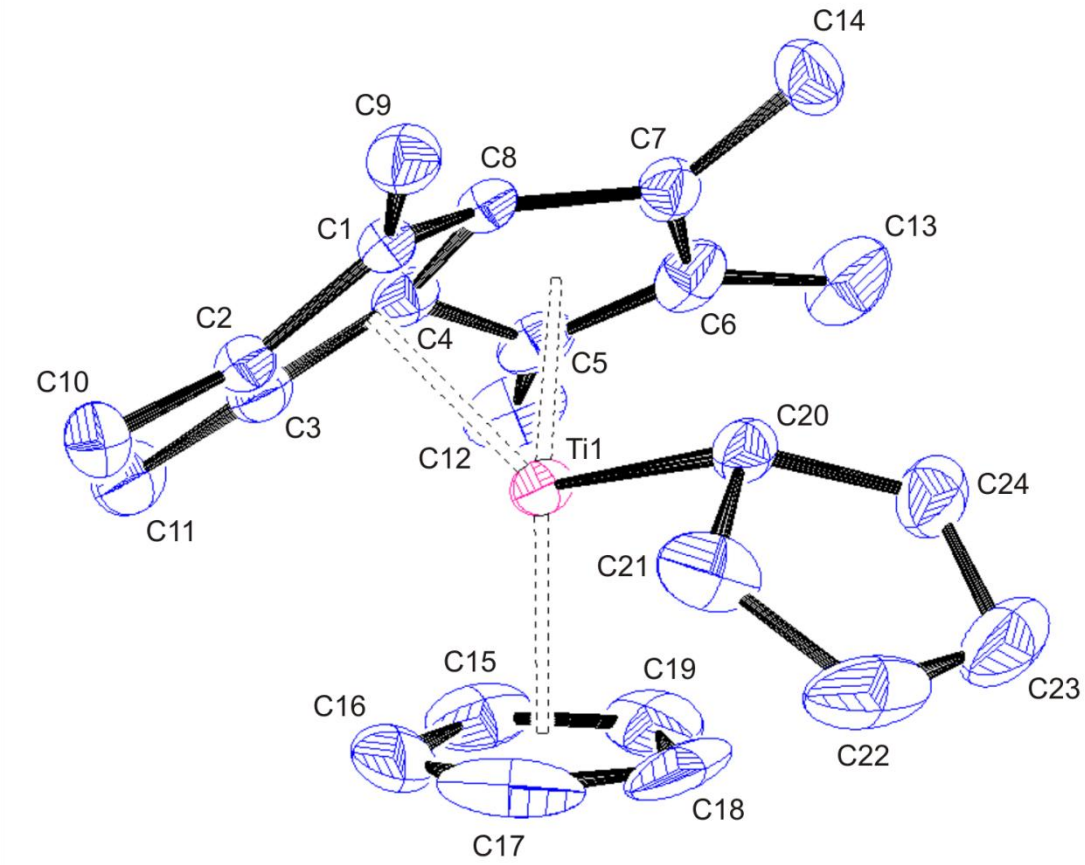

Figure 3.25: Side-on view of **3.7** with thermal ellipsoids at 50%. Hydrogen atoms omitted for clarity.

3.7 crystallises in the $P\bar{1}$ space group, with one independent molecule in the asymmetric unit. It possesses two distinctly different Cp coordination modes, η^1 and η^5 and is only the fourth complex containing a Ti(η^1-Cp) fragment to be structurally characterised by single crystal X-ray crystallography.[53–55] The geometry around Ti is distorted pseudo tetrahedral analogous to **3.6**. The average Ti-C(Pn*), Ti-Pn*$_{cent}$ and Ti-Cp$_{cent}$ distances (2.380, 1.998, 2.054 Å) and fold angle (31.7°) are almost identical with **3.6** (2.378, 1.995, 2.063 Å and 31.0° respectively), which would be expected for the structurally similar isoelectronic 18 electron complex. The Ti(1)-C(20) bond length [2.439(3) Å], is substantially longer than the 16 electron complex Ti(η^5-Cp)$_2$(η^1-Cp)$_2$ [2.332(2) Å][53] and even more so than CpTi(NH^{t}Bu)(μ-η^1:η^1-NNMe$_2$)(μ-η^2:η^1-NNMe$_2$)TiCp(η^1-Cp) [2.293(3) Å].[55] This parallels the unusually long Ti(1)-Cl(1) bond in **3.6** and PnTiClCp,[8] which may be due to the extreme steric crowding at the Ti centre, preventing a closer

approach of the (η^1-Cp) moiety. The monohapto-cyclopentadienyl moiety is planar; no carbon atom deviates from the mean plane by more than 0.023 Å and the C-C bond lengths vary systematically around the ring in a manner consistent with a bond-alternant diene structure [starting at the carbon atom bound to Ti: 1.445(5), 1.374(6), 1.422(8), 1.365(6) and 1.456(5) Å]. This bonding pattern and the bond lengths are consistent with those seen for other structurally characterised Ti-(η^1-Cp) complexes.[53–55]

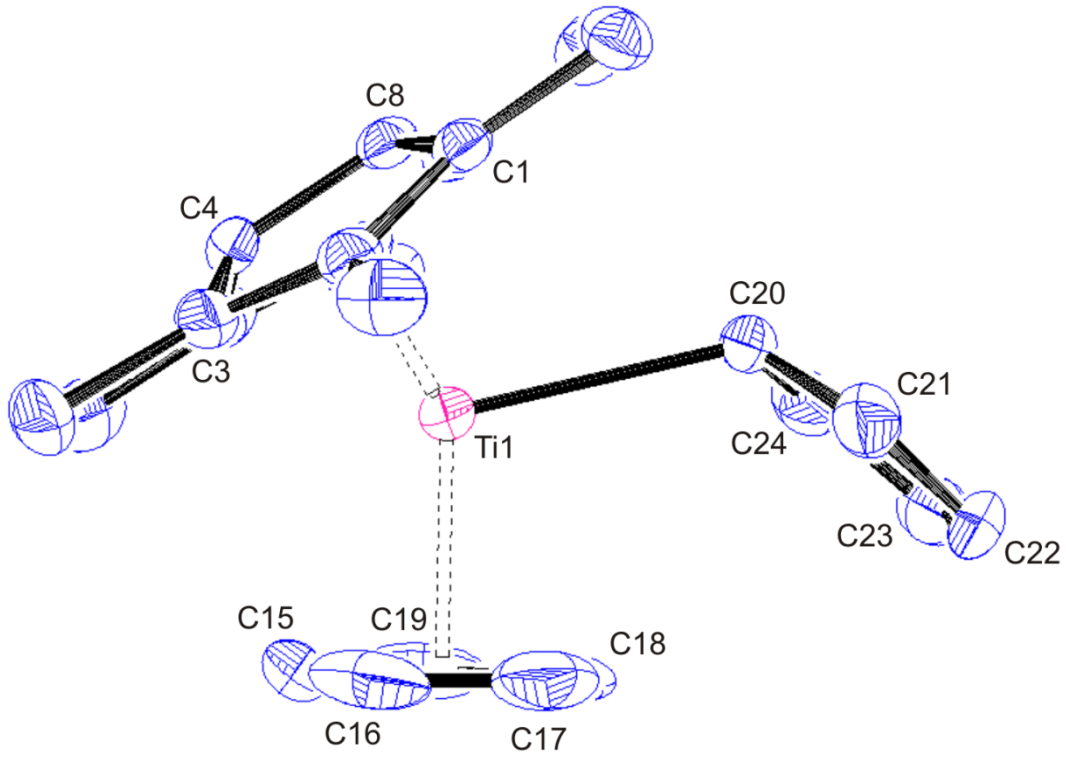

Figure 3.26: End-on view of **3.7** with thermal ellipsoids at 50%. Hydrogen atoms omitted for clarity.

In a similar manner to **3.6**, there are two distinct sets of Ti-C(NWT) distances. Here the average Ti(1)-C(1/7) (2.466 Å) is longer than Ti(1)-C(3/5) (2.361 Å) meaning the Pn* moiety is canting in the opposite direction to **3.6**, which is reasoned by the replacement of Cl with the sterically cumbersome η^1-Cp ligand. This canting seen for **3.6** and **3.7** is not observed for the other C_s symmetric complex in the chapter, **3.4**, whose average difference in the two sets of distances is only 0.002 Å, demonstrating symmetric η^8-Pn* bonding is present.

Table 3.8: Selected bond lengths, angles and structural parameters for **3.7**. ESDs are given in parentheses.

Lengths (Å)			
Ti(1) - C(1)	2.438(3)	C(1) - C(2)	1.423(4)
Ti(1) - C(2)	2.518(3)	C(2) - C(3)	1.416(5)
Ti(1) - C(3)	2.369(3)	C(3) - C(4)	1.438(5)
Ti(1) - C(4)	2.135(3)	C(4) - C(5)	1.436(5)
Ti(1) - C(5)	2.352(4)	C(5) - C(6)	1.427(6)
Ti(1) - C(6)	2.560(4)	C(6) - C(7)	1.408(5)
Ti(1) - C(7)	2.493(3)	C(7) - C(8)	1.429(5)
Ti(1) - C(8)	2.174(3)	C(8) - C(1)	1.438(5)
Ti(1) - C(20)	2.439(3)	C(4) - C(8)	1.455(4)
Ti(1) - Pn^*_{cent}	1.987	C(20) - C(21)	1.445(5)
Ti(1) - Pn^*_{cent}	2.009	C(21) - C(22)	1.374(6)
Ti(1) - Cp_{cent}	2.054	C(22) - C(23)	1.442(8)
Av. Ti(1) – Cp	2.363	C(23) - C(24)	1.365(6)
Av. C_{ring} – Me	1.502	C(24) - C(20)	1.456(5)
Angles (°)			
Cp_{cent} - Ti(1) - C(20)		104.30	
Pn^*_{cent} - Ti(1) - C(20)		107.94	
Pn^*_{cent} - Ti(1) - C(20)		104.88	
Fold Angle		31.66	

The room temperature ^{1}H NMR spectrum of **3.7** reveals five resonances, four sharp and one broad in an intensity ratio 5:5:6:6:6. Similar to **3.6**, the molecule is of C_s symmetry both in the solution and solid state, with an identical mirror plane bisecting both the Pn* and Cp ligands, running along the Ti-C(20) bond. The result is two sets of independent NWT-Me protons, as seen for **3.4** and **3.6** (Figure 3.14), with the WT-Me resonance again occurring at higher field to the remaining two. The other sharp resonance (δ = 4.61 ppm; C_6D_6) is assigned to the η^5-Cp moiety, which is shifted considerably to higher field compared to **3.6** (δ = 5.38 ppm; C_6D_6), postulated as the result of replacing the highly electron withdrawing Cl group, with the inductively donating η^1-Cp fragment. The remaining broad resonance (δ = 6.02 ppm, $\nu_{½}$ = 36.1 Hz; C_6D_6), is attributed to the η^1-Cp and indicates the presence of fluxional behaviour; VT ^{1}H NMR measurements were conducted to investigate its origin. The occurrence of η^1-Cp fluxional behaviour is known for a number of metal complexes;[56–58] it was Cotton

and co-workers that first produced a qualitative argument to suggest that line shape analysis of the ^{1}H NMR spectra could be instrumental in determining the mechanism operating.[57] He proposed that if 1,2-shifts of the metal atom round the ring were predominant, the line corresponding to H_A should broaden more rapidly with increasing temperature than that corresponding to H_B; 1,3-shifts would produce the opposite effect. On cooling **3.7**, it was possible to freeze-out the η^1-Cp rotation into three separate resonances, characteristic of allylic and vinylic proton environments. Upon warming, the resonance at δ = 5.38 ppm (toluene-d_8), was found to collapse more rapidly and implementing a multitude of NMR techniques, the chemical shift was assigned as H_A, indicating that a 1,2-sigmatropic shift was operating. The data was modelled and a regression analysis (R^2 = 0.9934) between the temperatures 215-300 K permitted the extraction of thermodynamic parameters for the exchange mechanism, these were as follows, $\Delta G^{\ddagger}$ = 47±4 kJ mol^{-1}, $\Delta H^{\ddagger}$ = 29±2 kJ mol^{-1} and $\Delta S^{\ddagger}$ = −65±8 kJ mol^{-1}.

Upon heating **3.7**, the initially broad resonance at room temperature sharpened to a line width comparable to that of the η^5-Cp but no coalescence and hence interconversion (η^1-Cp ↔ η^5-Cp') was observed. This is in stark contrast to the highly fluxional $TiCp_4$,[58] which is observed to interconvert, even at low temperatures. The reasoning for this observation was attributed to $TiCp_4$ being a 16 electron species and thus possessing an empty valence-shell orbital, which could stabilise a transition state for the interconversion. This is not available to **3.7**, being an 18 electron complex and therefore is unable to facilitate a low energy pathway for the transition, making interconversion of the Cp's energetically unviable.

3.9 Highly thermally unstable complexes

Although the compounds documented so far in this chapter have had varying thermal stabilities, all are persistent at room temperature over a matter of days, which has facilitated their complete characterisation. The compounds described in the following section display an extremely finite stability and decompose in a matter of hours at room temperature, limiting prospects for their comprehensive characterisation.

3.9.1 Synthesis and characterisation of Pn*Ti(C_3H_5)$_2$ (3.8)

The allyl moiety (C_3H_5), displays a number of fascinating features in organometallic chemistry from varied hapticity (η^1 and η^3), to fluxional behaviour

($\eta^1 \leftrightarrow \eta^3$) and rearrangements that have interested chemists for a number of years.[59] Initial attempts at synthesising $Cp_2Ti(C_3H_5)_2$ from Cp_2TiCl_2 and $(C_3H_5)MgCl$ led to reduction of the metal, with formation of the Ti^{III} π-allyl complex $Cp_2Ti(\eta^3\text{-}C_3H_5)$.[60] Greater success was achieved in preparing the Zr^{IV} analogue *via* a parallel route due to the greater resistance to reduction for the 2nd row congener.[61, 62] The allyl ligands are fluxional and in rapid equilibrium at room temperature, as ascertained from ^{1}H NMR spectroscopy, with no line broadening observed even at temperatures as low as −90 °C. Infrared spectroscopy, however, indicates a structure containing mixed hapticity C_3H_5 groups, with one ($\eta^3\text{-}C_3H_5$) and one ($\eta^1\text{-}C_3H_5$) ligand, and a formal representation $Cp_2Zr(\eta^3\text{-}C_3H_5)(\eta^1\text{-}C_3H_5)$. The conflicting conclusions of the two techniques are ascribed to the difference in frequencies, and hence different timescales, of the two procedures.[61]

Reaction of **2.1** with 4.4 equivalents of $(C_3H_5)MgCl$ solution in Et_2O, shown in Figure 3.27, afforded a dark brown solution upon warming to 0 °C. Subsequent work up and cooling of a saturated hexane solution deposited yellow-orange needle-shaped crystals, albeit in poor yield (12.4%). The product was assigned the formula $Pn^*Ti(C_3H_5)_2$ (**3.8**), on the basis of ^{1}H and ^{13}C NMR spectroscopy and mass spectrometry (EI), the latter showing the molecular ion at accurate mass followed by a peak ascribed to the loss of both (C_3H_5) groups.

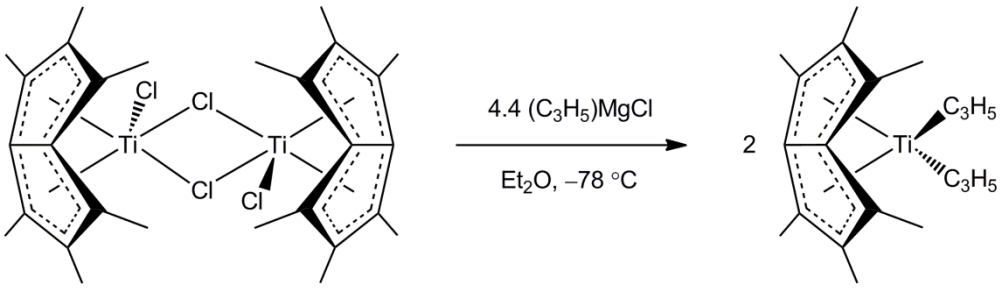

2.1 **3.8**

Figure 3.27: Synthesis of $Pn^*Ti(C_3H_5)_2$ (**3.8**).

In the absence of solid state structures, the ^{1}H NMR spectra of allyl complexes can be very informative at revealing the bonding mode of the ligand.[63, 64] The two static coordination modes of allyl ligands are well established; $\eta^1\text{-}C_3H_5$ and $\eta^3\text{-}C_3H_5$, with the latter containing a distinct AM_2X_2 splitting pattern, due to the inequivalence of protons on the CH_2 groups, resulting in two sets of doublets for the protons H_{anti} and H_{syn} to a

complex multiplet for the central methine H_{meso} proton (Figure 3.28). Another distinctive splitting pattern results from fluxional behaviour associated with allyl rotation and/or η^1-C_3H_5 ↔ η^3-C_3H_5 interconversion; this spectrum consists of a well defined quintet and doublet in a 1:4 intensity ratio, a result of the indistinguishable CH_2 group protons observed in an AX_4 system.

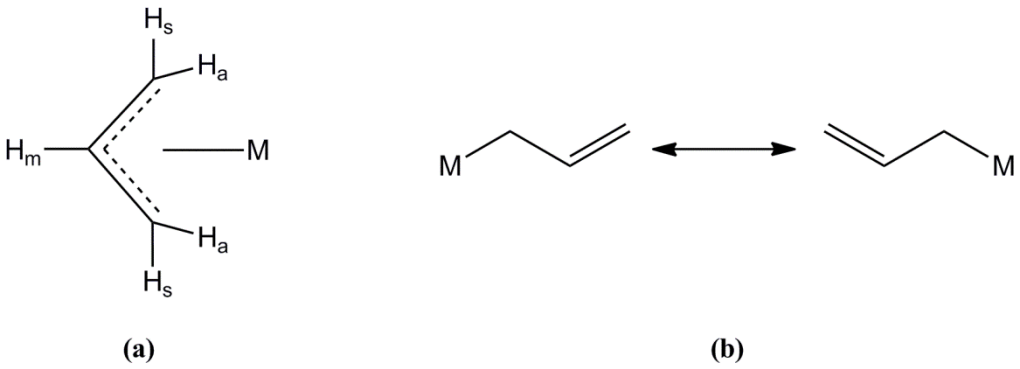

Figure 3.28: Possible binding modes of the allyl ligand; (a) η^3-C_3H_5, (b) η^1-C_3H_5.

The room temperature ^{1}H NMR spectrum of **3.8** (Figure 3.29) reveals four sharp resonances, two corresponding to the Pn* moiety in a 12:6 ratio and two resonances in a distinct AX_4 splitting pattern for the equivalent C_3H_5 ligands; the quintet (δ = 4.81 ppm, $^3J_{H\text{-}H}$ = 12.3 Hz; C_6D_6) and doublet (δ = 2.44 ppm, $^3J_{H\text{-}H}$ = 12.3 Hz; C_6D_6) are in reasonable agreement to that seen for the related $Cp_2Zr(C_3H_5)_2$ (δ = 5.63 and 2.89 ppm respectively, $^3J_{H\text{-}H}$ = 11.5 Hz; C_6D_6).[61] This demonstrates that both allyl groups are highly fluxional in solution at room temperature on the NMR timescale. Unfortunately time constraints prevented further investigation into the mode of fluxionality in the system.

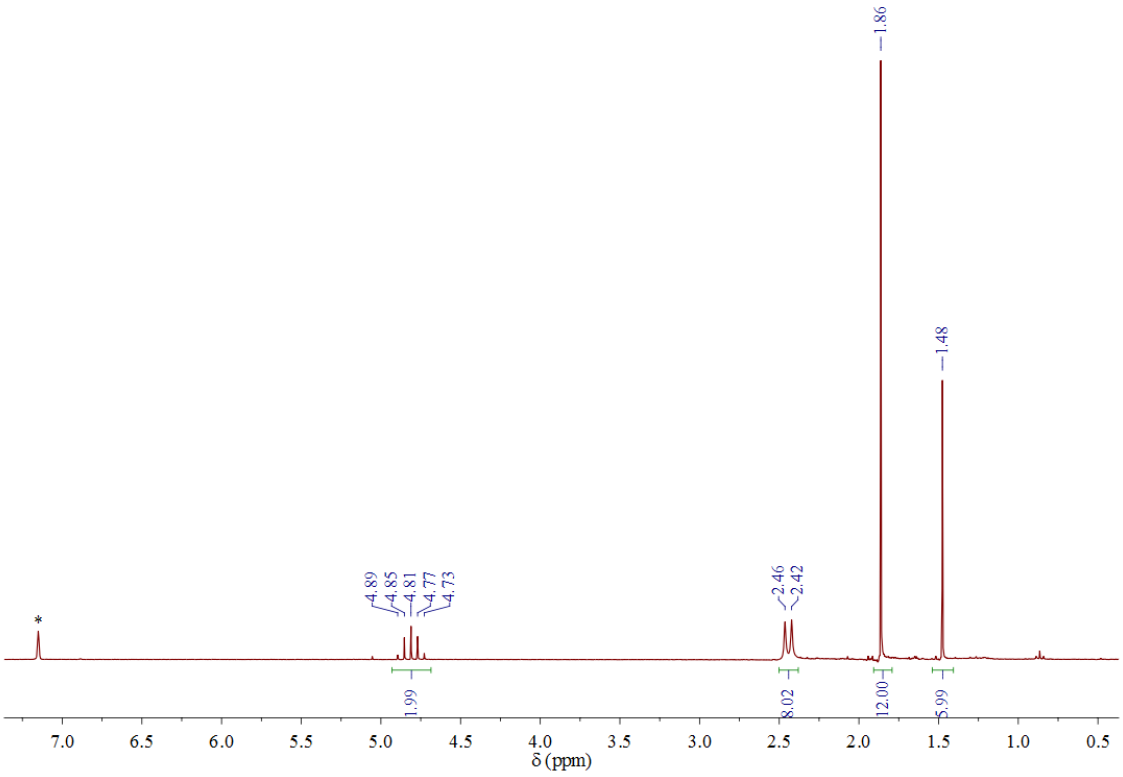

Figure 3.29: ^{1}H NMR spectra of **3.8** in C_6D_6. * denotes residual protio-solvent.

Unlike previous compounds reported in this chapter, **3.8** does not possess a prolonged lifespan at ambient temperature, whether stored as a solution or in the solid state. Complete decomposition was found to occur over a period of 12 hours; initial yellow-orange solutions gradually darken to grey-black over time and eventually deposit a yellow oil after a number of days when stored at room temperature. Similarly, when stored in the glovebox, crystalline **3.8** changed from yellow-orange to black-brown in colour albeit over a marginally longer time frame. It is known that some allyl complexes undergo a thermal rearrangement, as in the case of $Cp^*_2Zr(C_3H_5)_2$. When heated to 60-80 °C for 12 hours, a hydrocarbyl ligand migration to the β-carbon of the η^3-allyl results in an allyl substituted zirconacyclobutane (Figure 3.30).[65] No evidence of this was found and the precise nature of the black solid/solution and yellow oil are unknown; attempts at assigning these products from ^{1}H NMR spectra were hampered due to their very complex nature.

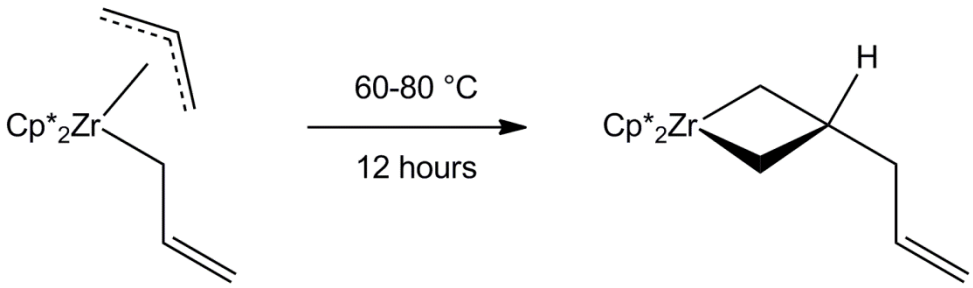

Figure 3.30: Allyl rearrangement for $Cp^*_2Zr(C_3H_5)_2$.

3.9.2 Synthesis and characterisation of Pn*TiPh$_2$ (3.9)

The synthesis of Pn*TiPh$_2$ (**3.9**) is detailed in Figure 3.31; combination of 4.2 equivalents of PhMgCl solution with **2.1** in Et_2O at −78 °C, instantly afforded a green solution. The reaction was monitored by ^{1}H NMR spectroscopy; after 30 minutes all of **2.1** had been consumed and a novel Pn* species, **3.9**, had formed. **3.9** is extremely thermally sensitive and rigorous efforts ensured that the compound was kept as cold as possible during all work up procedures. The use of a jacketed frit cooled to −78 °C was paramount to yielding product from the reaction, with initial attempts utilising standard work up procedures at room temperature furnishing no identifiable product. Cooling of an Et_2O solution to −78 °C produced purple needle-shaped crystals in poor yield (8.4%), which were identified as **3.9** on the basis of ^{1}H NMR spectroscopy.

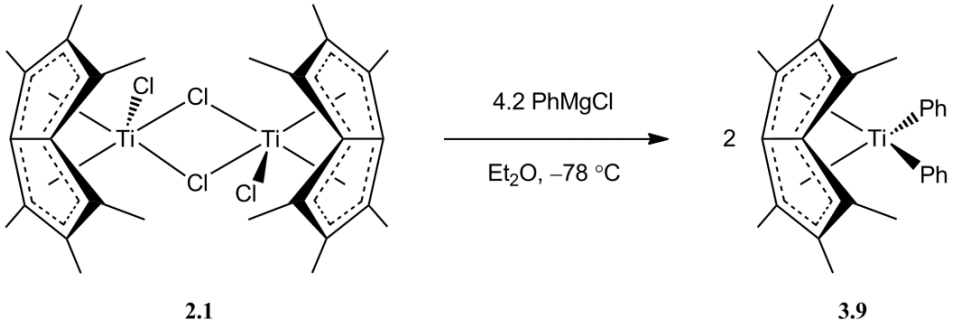

Figure 3.31: Synthesis of Pn*TiPh$_2$ (**3.9**).

The room temperature ^{1}H NMR spectrum of **3.9** (Figure 3.32) reveals five sharp resonances in a 4:4:2:12:6 intensity ratio, implying the solution phase structure of the molecule is of the same symmetry observed for other Pn*TiR$_2$ compounds (**2.7**, **3.1**, **3.2** and **3.3**). The symmetric nature of the Ph groups suggests that there is free rotation about the Ti-Ph bond, resulting in the chemical equivalence of *ortho*- and *meta*-hydrogens. The chemical shifts for the Pn* and Ph moieties are within the range of their

normal values. Unfortunately, due to the compound's thermal instability, ^{13}C NMR data could not be obtained.

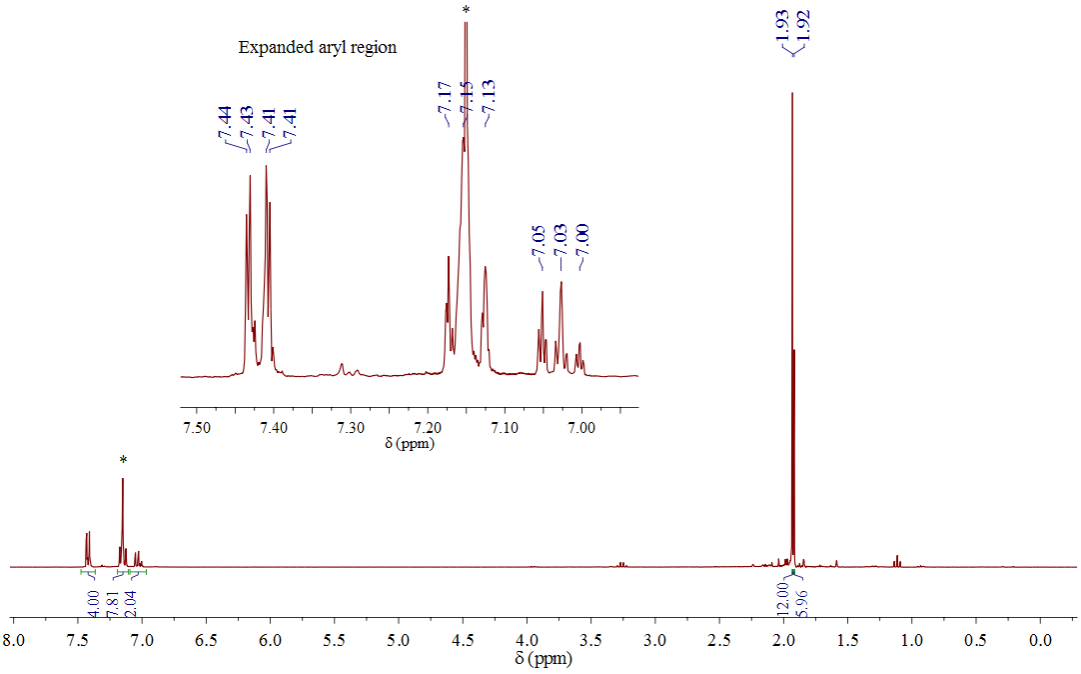

Figure 3.32: ^{1}H NMR spectra of **3.9** in C_6D_6. * denotes residual protio-solvent.

NMR samples (C_6D_6) of **3.9** were found to decompose within a matter of hours at room temperature with rapid decolouration of the vivid purple solution to a red-brown and formation of a precipitate. Although marginally more robust in the solid state, full decomposition was found to occur within 24 hours with decolouration to a black solid. The exact mode of deactivation is unclear, as no decomposition products could be identified or isolated. It seems reasonable to compare **3.9** to Cp_2TiPh_2, which is known to decompose *via* thermal[47] and photochemical[66] routes to form benzene and biphenyl respectively. Extensive labelling and trapping experiments[47, 48] have conclusively shown its thermal decomposition pathway to proceed *via ortho*-hydrogen abstraction by the neighbouring Ph, with formation of a "$Cp_2Ti(C_6H_4)$" benzyne complex and liberation of benzene. Unfortunately time constraints prevented further investigation into decomposition pathways using labelling and trapping experiments and the identity of the precipitate formed is unknown, but could comprise of oligomeric $[Pn^*Ti]_n$ units.

3.10 Conclusion

A number of complexes have been synthesised and characterised, incorporating classical organometallic ligands into the Pn*Ti moiety. They include the first examples of benzyl, alkyl, aryl, allyl or η^1-cyclopentadienyl ligands bound to a PnTi fragment. Seven compounds have been characterised in the solid state including Pn*Ti($CH_2{}^tBu)_2$, the first example of a π-hydrocarbon bound titanium species bearing two neopentyl groups to be crystallographically characterised. An interplay between steric and electronic unsaturation at the Ti centre has been postulated to determine the monomeric and dimeric formulations of Pn*TiCl($CH_2{}^tBu$) and [Pn*TiPh(μ-Cl)]$_2$, with the latter's dimeric nature proving crucial to its decomposition pathway, paralleling the reactivity shown by [Pn*TiMe(μ-Cl)]$_2$ (**2.2**). The varying thermal stabilities are emphasised by the highly unstable nature of Pn*Ti($C_3H_5)_2$ and Pn*TiPh$_2$; the former is shown to possess highly fluxional allyl groups on the NMR timescale. Pn*TiClCp is isostructural with its unmethylated analogue, however the smaller fold angle of the Pn* unit supports current bonding theory which suggests that the ligand distortion correlates with electron deficiency at the metal centre. Reaction with a second equivalent of NaCp yields the sterically congested mixed hapticity Pn*Ti(η^5-Cp)(η^1-Cp), whose η^1-Cp moiety is fluxional and rearranges *via* a 1,2-sigmatropic shift. A comparison of the solid state structural properties of all crystallographically characterised complexes throughout this chapter has been performed.

Table 3.9: Collection of solid state parameters and valence electron counts for Chapter Three.

Compound	Av. Fold Angle (°)	Av. Ti-C Distance (Å)	Av. Ti-Pn*$_{cent}$ Distance (Å)	Av. C-C Distance (Pn*) (Å)	Ti Valence Electron Count
3.1	33.14	2.340	1.952	1.433	14
3.2	32.94	2.344	1.956	1.437	14
3.3	33.11	2.348	1.962	1.431	14
3.4	34.08	2.332	1.943	1.434	14
3.5	31.55	2.358	1.974	1.430	16
3.6	30.98	2.378	1.995	1.430	18
3.7	31.66	2.380	1.998	1.430	18

3.11 References for Chapter Three

1 R. R. Schrock and G. W. Parshall, *Chemical Reviews*, 1976, 76, 243–268.

2 M. R. Collier, M. F. Lappert, and M. M. Truelock, *Journal of Organometallic Chemistry*, 1970, 25, C36–C38.

3 G. Yagupsky, W. Mowat, A. Shortland, and G. Wilkinson, *Journal of the Chemical Society D: Chemical Communications*, 1970, 1369.

4 M. R. Collier, M. F. Lappert, and R. Pearce, *Journal of the Chemical Society, Dalton Transactions*, 1973, 445.

5 W. Mowat, A. Shortland, G. Yagupsky, N. J. Hill, M. Yagupsky, and G. Wilkinson, *Journal of the Chemical Society, Dalton Transactions*, 1972, 533.

6 P. J. Davidson, M. F. Lappert, and R. Pearce, *Chemical Reviews*, 1976, 76, 219–242.

7 C. Elschenbroich and A. Salzer, *Organometallics - A concise introduction*, VCH, Second Ed., 1991.

8 K. Jonas, P. Kolb, G. Kollbach, B. Gabor, R. Mynott, K. Angermund, O. Heinemann, and C. Krüger, *Angewandte Chemie International Edition in English*, 1997, 36, 1714–1718.

9 J. Scholz, F. Rehbaum, K.-H. Thiele, R. Goddard, P. Betz, and C. Krüger, *Journal of Organometallic Chemistry*, 1993, 443, 93–99.

10 F. G. N. Cloke, P. B. Hitchcock, M. C. Kuchta, and N. A. Morley-Smith, *Polyhedron*, 2004, 23, 2625–2630.

11 M. Mena, M. A. Pellinghelli, P. Royo, R. Serrano, and A. Tiripicchio, *Journal of the Chemical Society, Chemical Communications*, 1986, 3, 1118.

12 A. K. Hughes, A. Meetsma, and J. H. Teuben, *Organometallics*, 1993, 12, 1936–1945.

13 D. J. Crowther, R. F. Jordan, N. C. Baenziger, and A. Verma, *Organometallics*, 1990, 9, 2574–2580.

14 L. M. Alvaro, T. Cuenca, J. C. Flores, M. A. Pellinghelli, A. Tiripicchio, and P. Royo, *Organometallics*, 1992, 11, 3301–3306.

15 Y.-X. Chen, P.-F. Fu, C. L. Stern, and T. J. Marks, *Organometallics*, 1997, 16, 5958–5963.

16 S. L. Latesky, A. K. McMullen, G. P. Niccolai, I. P. Rothwell, and J. C. Huffman, *Organometallics*, 1985, 4, 902–908.

17 J. Scholz, M. Schlegel, and K. Thiele, *Chemische Berichte*, 1987, 120, 1369–1374.

18 M. Brookhart and M. L. H. Green, *Journal of Organometallic Chemistry*, 1983, 250, 395–408.

19 S. L. Borkowsky, N. C. Baenziger, and R. F. Jordan, *Organometallics*, 1993, 12, 486–495.

20 R. Gómez, T. Cuenca, P. Royo, W. A. Herrmann, and E. Herdtweck, *Journal of Organometallic Chemistry*, 1990, 382, 103–108.

21 H. Lee, J. B. Bonanno, T. Hascall, J. Cordaro, J. M. Hahn, and G. Parkin, *Journal of the Chemical Society, Dalton Transactions*, 1999, 1365–1368.

22 C. McDade, J. C. Green, and J. E. Bercaw, *Organometallics*, 1982, 1, 1629–1634.

23 S. Back, R. A. Gossage, G. Rheinwald, I. del Río, H. Lang, and G. van Koten, *Journal of Organometallic Chemistry*, 1999, 582, 126–138.

24 L. H. McAlexander, M. Hung, L. Li, J. B. Diminnie, Z. Xue, G. P. A. Yap, and A. L. Rheingold, *Organometallics*, 1996, 15, 5231–5235.

25 B.-H. Chang, H.-S. Tung, and C. H. Brubaker, *Inorganica Chimica Acta*, 1981, 51, 143–148.

26 H. van der Heijden and B. Hessen, *Journal of the Chemical Society, Chemical Communications*, 1995, 145.

27 J. Jeffery, M. F. Lappert, N. T. Luong-Thi, M. Webb, J. L. Atwood, and W. E. Hunter, *Journal of the Chemical Society, Dalton Transactions*, 1981, 1593.

28 G. A. Luinstra, L. C. Ten Cate, H. J. Heeres, J. W. Pattiasina, A. Meetsma, and J. H. Teuben, *Organometallics*, 1991, 10, 3227–3237.

29 H. van der Heijden and B. Hessen, *Inorganica Chimica Acta*, 2003, 345, 27–36.

30 J. Cheon, D. M. Rogers, and G. S. Girolami, *Journal of the American Chemical Society*, 1997, 119, 6804–6813.

31 A. H. Popkin, H. I. Bernstein, F. Whitmore, and J. P. Wilkins, *Journal of the American Chemical Society*, 1941, 63, 124–127.

32 J. W. Bruno, T. J. Marks, and V. W. Day, *Journal of the American Chemical Society*, 1982, 104, 7357–7360.

33 L. R. Gilliom and R. H. Grubbs, *Organometallics*, 1986, 5, 721–724.

34 J. D. Meinhart, E. V. Anslyn, and R. H. Grubbs, *Organometallics*, 1989, 8, 583–589.

35 A. E. Ashley, Permethylpentalene Chemistry, Thesis, University of Oxford, 2006.

36 E. F. Trunkely, A. Epshteyn, P. Y. Zavalij, and L. R. Sita, *Organometallics*, 2010, 29, 6587–6593.

37 G. A. Luinstra and J. H. Teuben, *Organometallics*, 1992, 11, 1793–1801.

38 J. A. Bandy, F. G. N. Cloke, M. L. H. Green, D. O'Hare, and K. Prout, *Journal of the Chemical Society, Chemical Communications*, 1984, 240.

39 P. Legzdins, S. J. Rettig, and J. E. Veltheer, *Journal of the American Chemical Society*, 1992, 114, 6922–6923.

40 H. Lee, J. B. Bonanno, B. M. Bridgewater, D. G. Churchill, and G. Parkin, *Polyhedron*, 2005, 24, 1356–1365.

41 V. Kocman, J. C. Rucklidge, R. J. O'Brien, and W. Santo, *Journal of the Chemical Society D: Chemical Communications*, 1971, 1340a.

42 G. A. Luinstra and J. H. Teuben, *Organometallics*, 1992, 11, 1793–1801.

43 L. F. Farnell, E. W. Randall, and E. Rosenberg, *Journal of the Chemical Society D: Chemical Communications*, 1971, 1078.

44 M. A. Bennett and H. P. Schwemlein, *Angewandte Chemie International Edition in English*, 1989, 28, 1296–1320.

45 M. A. Bennett, *Australian Journal of Chemistry*, 2010, 63, 1066.

46 S. L. Buchwald and R. B. Nielsen, *Chemical Reviews*, 1988, 88, 1047–1058.

47 J. Dvorak, R. J. O'Brien, and W. Santo, *Journal of the Chemical Society D: Chemical Communications*, 1970, 67, 411.

48 I. S. Kolomnikov, T. S. Loveeva, V. V. Gorbachevskaya, G. G. Aleksandrov, Y. T. Struckhov, and M. E. Vol'pin, *Journal of the Chemical Society D: Chemical Communications*, 1971, 972.

49 P. M. Cook, L. F. Dahl, and D. W. Dickerhoof, *Journal of the American Chemical Society*, 1972, 94, 5511–5513.

50 A. Clearfield, D. K. Warner, C. H. Saldarriaga-Molina, R. Ropal, and I. Bernal, *Canadian Journal of Chemistry*, 1975, 53, 1622–1629.

51 T. C. McKenzie, R. D. Sanner, and J. E. Bercaw, *Journal of Organometallic Chemistry*, 1975, 102, 457–466.

52 O. T. Summerscales and F. G. N. Cloke, *Coordination Chemistry Reviews*, 2006, 250, 1122–1140.

53 F. A. Cotton, J. L. Calderon, B. G. DeBoer, and J. Takats, *Journal of the American Chemical Society*, 1971, 93, 3592–3597.

54 F. Guérin, C. L. Beddie, D. W. Stephan, R. E. v. H. Spence, and R. Wurz, *Organometallics*, 2001, 20, 3466–3471.

55 J. D. Selby, M. Feliz, A. D. Schwarz, E. Clot, and P. Mountford, *Organometallics*, 2011, 30, 2295–2307.

56 F. A. Cotton and P. Legzdins, *Journal of the American Chemical Society*, 1968, 90, 6232–6233.

57 F. A. Cotton, A. Davison, and W. Faller, *Journal of the American Chemical Society*, 1966, 4371–4376.

58 F. A. Cotton, J. L. Calderon, and J. Takats, *Journal of the American Chemical Society*, 1971, 93, 3587–3591.

59 G. Wilke, B. Bogdanović, P. Hardt, P. Heimbach, W. Keim, M. Kröner, W. Oberkirch, K. Tanaka, E. Steinrücke, D. Walter, and H. Zimmermann, *Angewandte Chemie International Edition in English*, 1966, 5, 151–164.

60 H. A. Martin and F. Jellinek, *Journal of Organometallic Chemistry*, 1967, 8, 115–128.

61 H. A. Martin, P. J. Lemaire, and F. Jellinek, *Journal of Organometallic Chemistry*, 1968, 14, 149–156.

62 J. Emsley, *The Elements*, Oxford University Press, 2000.

63 J. K. Becconsall and S. O'Brien, *Chemical Communications (London)*, 1966, 302.

64 M. B. Abrams, J. C. Yoder, C. Loeber, M. W. Day, and J. E. Bercaw, *Organometallics*, 1999, 18, 1389–1401.

65 E. B. Tjaden and J. M. Stryker, *Journal of the American Chemical Society*, 1993, 115, 2083–2085.

66 M. D. Rausch, W. H. Boon, and E. A. Mintz, *Journal of Organometallic Chemistry*, 1978, 160, 81–92.

Chapter Four

Reactivity Studies of Novel Permethylpentalene Titanium Dialkyls with Small Molecules

4.1 Introduction

It is known that simple small molecules such as H_2 are ubiquitous reservoirs of chemical energy and potentially hold the key to the development of green energy sources and new, more efficient chemical processes.[1] Transformation of simple abundant chemical feedstocks, such as carbon dioxide, carbon monoxide and dihydrogen to more industrially relevant compounds is arguably one of the most paramount objectives of modern times.[1–3] Such small molecules are generally quite thermodynamically stable and their successful utilisation depends on surmounting often quite significant kinetic barriers. It has long been recognised that metal centres play an important role in providing low energy reaction pathways through binding and activation of these small molecules.[1]

Literature examples documenting the reaction of pentalene complexes with small molecules are scarce.[4–6] This chapter describes the reactivity of Pn*$TiMe_2$ (**2.7**), Pn*$Ti(CH_2Ph)_2$ (**3.1**), Pn*$Ti(CH_2SiMe_3)_2$ (**3.2**) and Pn*$Ti(CH_2{}^tBu)_2$ (**3.3**) with CO_2, CO and H_2 and the serendipitous reaction of Pn*$TiCl(CH_2{}^tBu)$ (**3.4**) with H_2O.

4.2 Reactions with CO_2

Currently, there is significant interest in the use of industrially produced CO_2 as a chemical feedstock. This growing attention is driven by environmental,[7] legal[8] and social factors.[9] Atmospheric CO_2 is a major contributor to the greenhouse effect and the development of various strategies and practical methodologies of CO_2 fixation is imperative in the management of this greenhouse gas and has been the subject of much discussion and research in recent times.[10] The activation and derivatisation of CO_2 *via* a transition metal centre is well established and of significant interest due to the possibility of utilising CO_2 as an inexpensive C_1 fragment in synthesis.[3, 11–15] It is currently used industrially to produce a range of different products including formic and

salicyclic acid, urea and methanol.[3, 10, 11, 15, 16] Although the use of CO_2 in chemical synthesis contributes relatively little to mitigation of the CO_2 concentration in the atmosphere,[3] several other factors render CO_2 an attractive alternative chemical C_1 feedstock to the currently used carbon monoxide (CO) and phosgene ($COCl_2$), such as its high abundance and relative low toxicity, cost, and critical temperature.

An important step in the functionalisation of small molecules, such as CO_2, is their interaction with metal centres and their insertion into metal-element bonds; among these reactions, insertion into a M-C bond is probably the most fascinating, since it can lead to C-C bond formation. This in turn may lead to further chain lengthening processes and functionalisation. This is especially pertinent for CO_2, due to it being highly thermodynamically stable and kinetically inert as an organic entity.[17] Examples of CO_2 insertion into Ti-C bonds are relatively rare[18–26] (especially Ti-C σ-bonds),[24–27] even though it was first observed over 40 years ago, with the first examples documented by Vol'pin, trapping the thermal decomposition product of Cp_2TiPh_2 (Figure 4.1),[28, 29] and Zucchini's work with $Ti(CH_2Ph)_4$.[27]

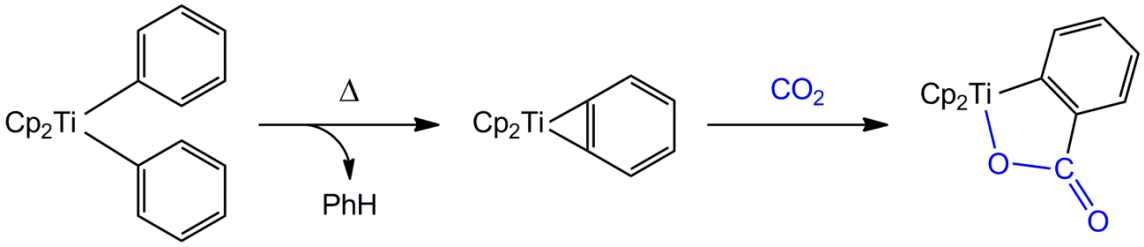

Figure 4.1: CO_2 insertion into the thermal decomposition product of Cp_2TiPh_2.

There are two possible modes of CO_2 insertion into the M-C bond of a complex; "normal" insertion leads to the formation of a carboxylate complex and is observed much more frequently than, "abnormal" insertion, which leads to the formation of a metalated formate ester, [Figure 4.2 (a) and (b) respectively].[21]

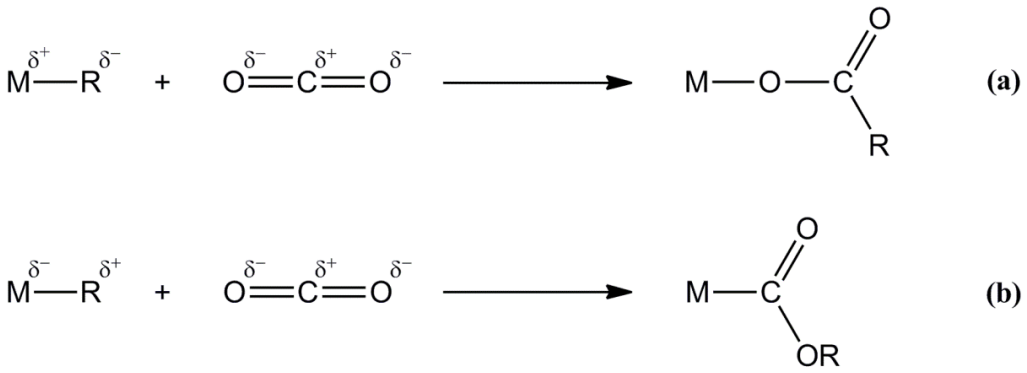

Figure 4.2: (a) "normal" and **(b)** "abnormal" insertion of CO_2 into a M-C bond.

4.2.1 Synthesis and characterisation of Pn*Ti(κ^2-O_2CMe)$_2$ (4.1)

A benzene solution of **2.7** was degassed *via* a freeze-pump-thaw method as follows: the solution was frozen into a glass then subjected to a dynamic vacuum (10^{-3} mbar) for 20 minutes followed by thawing under a static vacuum. The cycle was repeated twice more before CO_2 was admitted to the stirred solution (Figure 4.3), resulting in an instant colour change through murky orange-brown to a bright orange. Work up was completed in a glovebox and the slow cooling of a hexane solution furnished a yellow microcrystalline solid in excellent yield (82%), which was identified as Pn*Ti(κ^2-O_2CMe)$_2$ (**4.1**) by elemental analysis, X-ray crystallography and mass spectrometry (EI). The latter showed the molecular ion at accurate mass followed by a peak ascribed to the loss of acetate ($MeCO_2$).

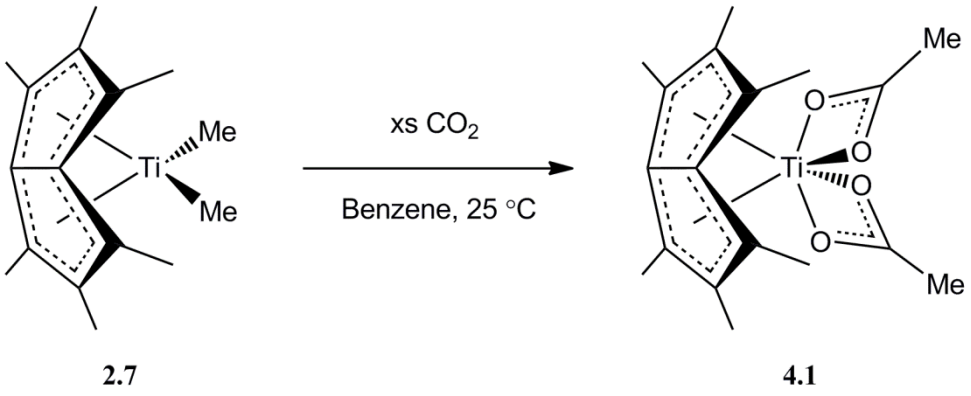

2.7 **4.1**

Figure 4.3: Synthesis of Pn*Ti(κ^2-O_2CMe)$_2$ (**4.1**).

This Pn* complex gave yellow X-ray quality crystals upon slow evaporation of a C_6D_6 solution and two views of the solid state structure of Pn*Ti(κ^2-O_2CMe)$_2$ (**4.1**) are shown in Figure 4.4 and 4.5.

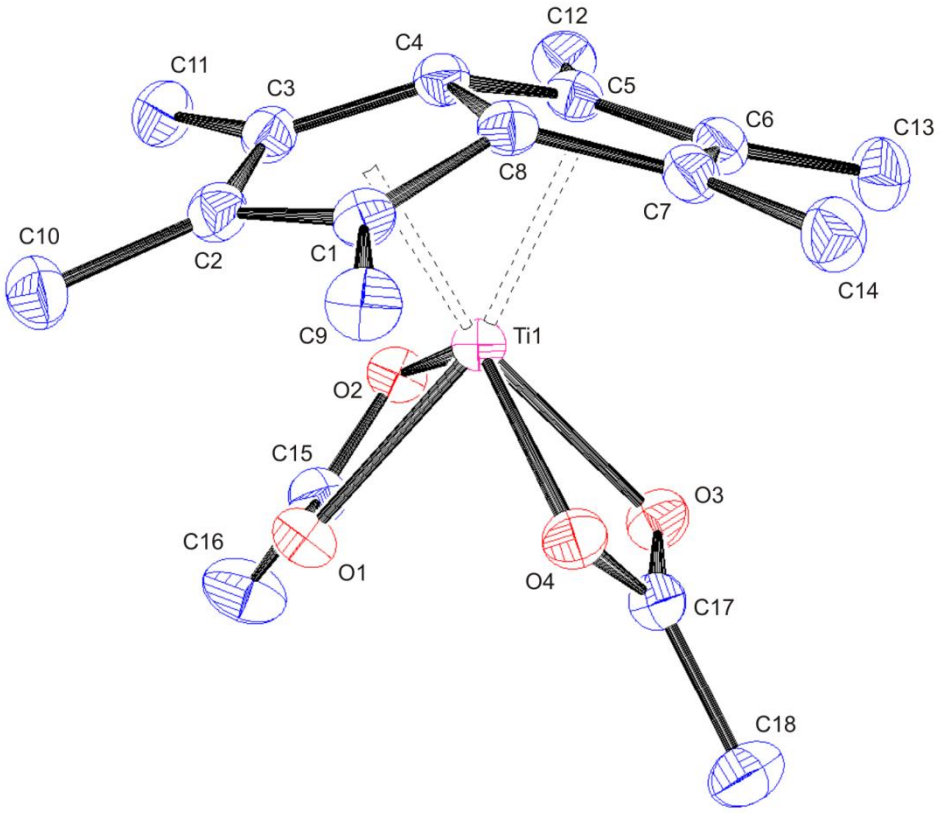

Figure 4.4: Side-on view of **4.1** with thermal ellipsoids at 50%. Hydrogen atoms omitted for clarity.

Crystallographic analysis demonstrates **4.1** to crystallise in the $P\bar{1}$ space group with one independent molecule in the asymmetric unit, which possesses C_2 symmetry. The principal axis intersects the mid-point of the Pn* bridgehead bond and the titanium atom, best visualised in Figure 4.5, as with **3.2**. The CO_2 moiety has inserted into both Ti-Me bonds in a normal fashion[21] and is coordinated in a bidentate manner, resulting in a distorted octahedral arrangement of ligands around titanium. This is in contrast to reactivity observed for the related Cp_2TiMe_2, which only inserts CO_2 into one Ti-Me bond at elevated temperatures (80 °C).[30] Similarly, photochemically activated insertion leads to $Cp_2Ti(O_2CMe)Me$ formation, albeit at a lower temperature.[26] This may be attributed to the resulting electronic configuration at each metal centre with both **4.1** and the isoelectronic $Cp_2Ti(O_2CMe)Me$, possessing a stable electron count of 18. In contrast however, analogous reactivity to form the hypothetical "$Cp_2Ti(O_2CMe)_2$", would result in an unfavourable 20 electron configuration. This highlights a distinct disparity between the structurally similar bis-Cp and Pn* moieties, with Pn* formally possessing two fewer electrons. The fold angle (32.4°) is comparable to other 18 electron Pn*Ti complexes contained within this work, **3.6** and **3.7** (31.0 and 31.7° respectively) but as

expected is much smaller than the pseudo tetrahedral, less sterically congested 14 electron starting material, **2.7** (35.7°).

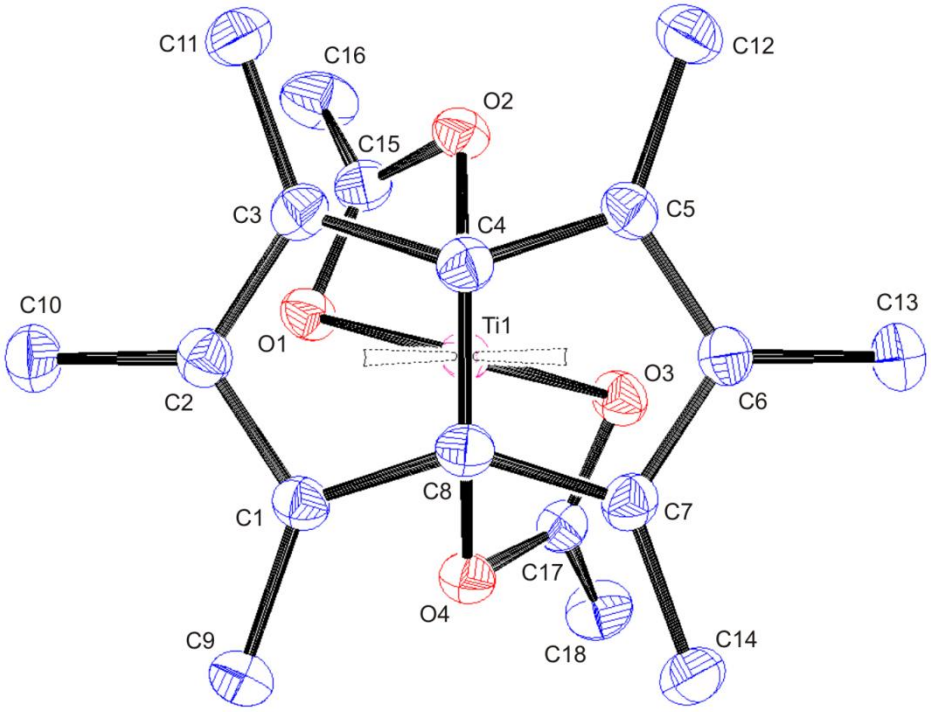

Figure 4.5: Top view of **4.1** with thermal ellipsoids at 50%. Hydrogen atoms omitted for clarity.

The two four membered metallocycles of **4.1** are bound in a highly symmetrical fashion, with a Ti-O bond length range of 2.1393(14)-2.1489(14) Å and an average of 2.143 Å, which is slightly shorter than the analogous isoelectronic, $CpTi(O_2CMe)_3$ (2.154 Å).[31] This does not portray an accurate bonding representation within the molecule as there are two distinct Ti-O distances contained in each acetate moiety with an average of 2.202 and 2.105 Å, indicating an asymmetrical bonding motif in each. A symmetrical fragment is however, observed for the structurally similar Ti^{III} $\{[Cp_2Ti]_2[\mu\text{-}(O_2C)_2CMe_2]\}$,[32] which possesses indistinguishable Ti-O distances (2.159 Å) within experimental error, with the slight elongation compared to **4.1** reasoned as the lower oxidation state on Ti exerting less of an electrostatic attraction to the formally anionic $\mu\text{-}(O_2C)_2CMe_2$ ligand. The average C-O bond distances for **4.1**, $CpTi(O_2CMe)_3$ and $\{[Cp_2Ti]_2[\mu\text{-}(O_2C)_2CMe_2]\}$ are very similar (1.268, 1.270 and 1.266 Å respectively), as are the average O-Ti-O angles (61.7, 60.4 and 60.7°), which results in comparable bidentate binding, as is expected when reasoned on electronic and steric grounds due to the highly oxophilic nature of Ti.

IR spectroscopy has proven an insightful technique in characterising coordination modes of metal-carboxylate species. The key parameter is the separation in asymmetric and symmetric CO absorptions [ν_{as}(CO) and ν_s(CO), respectively] and its comparison to the free carboxyate ion value.[33] Separations between ν(CO) frequencies substantially greater than that of the free ion are characteristic of unidentate carboxylate coordination whereas, separations significantly less than ionic values are indicative of bidentate coordination. The ν_{as}(CO) and ν_s(CO) values of **4.1** (1541 and 1473 cm^{-1}, respectively) result in a difference of 68 cm^{-1}, which is considerably smaller than the free ion (164 cm^{-1}),[34] further supporting crystallographic data of a highly symmetric, κ^2-O-O'- bonding mode. The values are also in good agreement with the aforementioned {[$Cp_2Ti]_2$[μ-$(O_2C)_2CMe_2$]} (1528 and 1467 cm^{-1}).[32]

Table 4.1: Selected bond lengths, angles and structural parameters for **4.1**. ESDs are given in parentheses.

Lengths (Å)			
Ti(1) - C(1)	2.3645(18)	C(1) - C(2)	1.417(3)
Ti(1) - C(2)	2.5140(19)	C(2) - C(3)	1.415(3)
Ti(1) - C(3)	2.3669(19)	C(3) - C(4)	1.447(3)
Ti(1) - C(4)	2.1279(18)	C(4) - C(5)	1.441(3)
Ti(1) - C(5)	2.3750(19)	C(5) - C(6)	1.417(3)
Ti(1) - C(6)	2.5165(19)	C(6) - C(7)	1.416(3)
Ti(1) - C(7)	2.3656(19)	C(7) - C(8)	1.444(3)
Ti(1) - C(8)	2.1249(18)	C(8) - C(1)	1.440(3)
Ti(1) - Pn^*_{cent}	1.958	C(4) - C(8)	1.456(2)
Ti(1) - Pn^*_{cent}	1.955	Av. C_{ring} – Me	1.501
Ti(1) - O(1)	2.1393(14)	Ti(1) - O(3)	2.1426(14)
Ti(1) - O(2)	2.1489(14)	Ti(1) - O(4)	2.1406(14)
C(15) - O(1)	1.267(2)	C(17) - O(3)	1.270(2)
C(15) - O(2)	1.271(2)	C(17) - O(4)	1.263(2)
C(15) - C(16)	1.500(3)	C(17) - C(18)	1.495(3)
Angles (°)			
O(1) - Ti(1) - O(2)	62.20(5)	O(3) - Ti(1) - O(4)	61.22(5)
Ti(1) - O(1) - C(15)	90.14(12)	Ti(1) - O(3) - C(17)	89.51(11)
Ti(1) - O(2) - C(15)	89.61(11)	Ti(1) - O(4) - C(17)	89.82(11)
O(1) - C(15) - O(2)	118.64(18)	O(3) - C(17) - O(4)	118.87(17)
O(1) - C(15) - C(16)	120.23(19)	O(3) - C(17) - C(18)	120.30(18)
O(2) - C(15) - C(16)	121.12(19)	O(4) - C(17) - C(18)	120.81(18)
Fold Angle	32.37		

The room temperature ^{1}H NMR spectrum of **4.1** reveals four resonances in a 6:6:6:6 intensity ratio and one may conclude that the solution phase structure of the molecule is of C_2 symmetry, as observed in the solid state (Figure 4.5). Due to the reduced symmetry of the molecule, the Pn* resonances are split into three sets of equal intensity, which results in two pairs of independent NWT-Me protons (Figure 4.6). These two pairs of NWT-Me resonances are broad ($\nu_{½}$ = 80.7 and 108.0 Hz), indicating the presence of fluxionality within the molecule. Variable temperature ^{1}H NMR studies were undertaken to probe this in order to gain further understanding and upon cooling to −10 °C, the non-equivalent NWT-Me resonances sharpened to freeze out a static C_2 symmetric system. Conversely, upon heating the independent resonances broadened, then shifted and coalesced at 30 °C and continued to sharpen up to 70 °C, resulting in a C_{2v} symmetric system with equivalent NWT-Me groups, possessing an integral of 12.

The difference between solid state and solution phase symmetries observed for complexes contained within this work, have been postulated to be the result of equivalent NWT-Me environments, induced *via* the rotation of the Pn* fragment around the titanium centre, analogous to the phenomenon of ring-whizzing, regularly observed in complexes incorporating Cp and Cp* fragments. It has been proposed that an interplay between the steric bulk of the ancillary ligands and the extent to which the Pn* ligand is wrapped around the metal centre (fold angle), determines how energetically viable this process is (Section 3.5). When the process is operating within a NMR solvent's temperature range, it is possible to monitor and model this change in symmetry as a function of temperature, as in the case of **4.1** ($C_2 \rightarrow C_{2v}$), resulting in a Gibbs free energy of activation for the fluxionality of $\Delta G^{\ddagger} \approx 61.26$ kJ mol^{-1}.[35, 36]

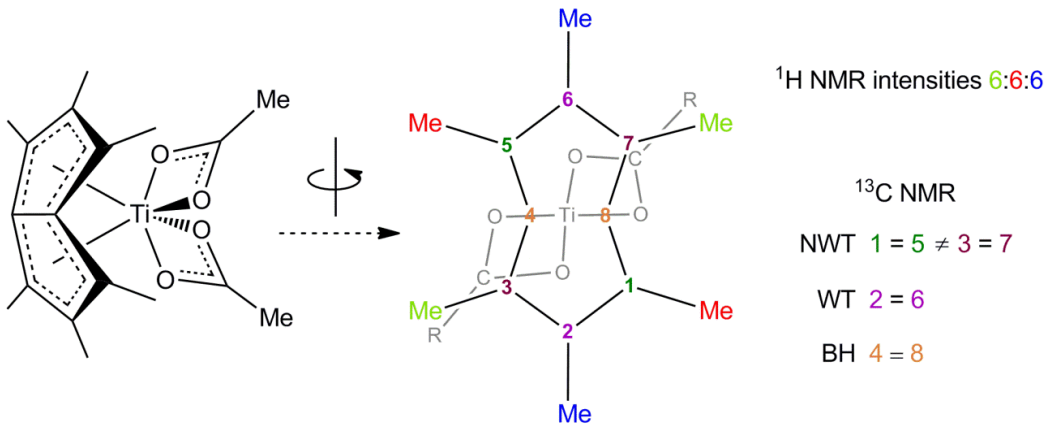

Figure 4.6: ^{1}H/^{13}C NMR splitings for Pn*Ti(κ^2-$O_2CR)_2$, C_2 symmetric complexes.

The WT-Me resonance was found to occur at higher field to the remaining two Pn* resonances, which have the absolute configuration shown, as determined by 2D-NOESY NMR. The remaining resonance of relative intensity six corresponds to the acetate Me protons (δ = 1.78 ppm; toluene-d_8), which is in good agreement with that observed for $Cp_2Ti(O_2CMe)Me$[26] and $Cp^*Ti(O_2CMe)_3$[37] (δ = 1.66 and 1.83 ppm respectively), as is the corresponding ^{13}C resonance for **4.1** and the former (δ = 22.8 and 23.0 ppm respectively). The remainder of the ^{13}C NMR (toluene-d_8) spectrum displays eight resonances, seven corresponding to Pn* carbons as the result of reduced symmetry in the molecule; the bridgehead carbons are equivalent, which is contrary to that observed in C_s symmetric compounds **3.4**, **3.6** and **3.7**, where they differ (Figure 3.12). The resonance furthest downfield is that of the carboxylate carbon and is in excellent agreement with that observed in $CpTi(O_2CMe)_3$ (δ = 188.5 and 189.2 ppm, respectively).[31]

4.2.2 Synthesis and characterisation of Pn*Ti(κ^2-$O_2CCH_2Ph)_2$ (4.2)

To date, there has only been one reported example of CO_2 insertion into a Ti-CH_2Ph bond, and that involved the Ti^{III} species, $Cp^*_2Ti(CH_2Ph)$ in 1991.[25] The complex was reported to react smoothly in solution at room temperature, with gaseous CO_2, resulting in metal carboxylate formation but no evidence or characterising data were presented. In an attempt to reproduce this reactivity with a Pn*Ti fragment and document the findings in greater detail, an identical synthesis to the one stated in Section 4.2.1 was employed on the $Pn^*Ti(CH_2Ph)_2$ (**3.1**) starting material (Figure 4.7). The reaction proceeded considerably slower than in the formation of **4.1**, taking 40 hours to run to completion as judged by ^1H NMR spectroscopy and resulted in a yellow solution. This prolonged reaction time is thought to be the consequence of steric bulk around the Ti centre, with two CH_2Ph ligands being much more demanding compared to two smaller Me ligands, retarding CO_2 binding and insertion. Similarly, work up was completed in a glovebox and the slow cooling of a hexane solution furnished a yellow microcrystalline solid in very good yield (73%), which was identified as $Pn^*Ti(\kappa^2\text{-}O_2CCH_2Ph)_2$ (**4.2**) by elemental analysis, X-ray crystallography and mass spectrometry (EI). The latter showed the molecular ion at accurate mass followed by a peak ascribed to the loss of $PhCH_2CO_2$.

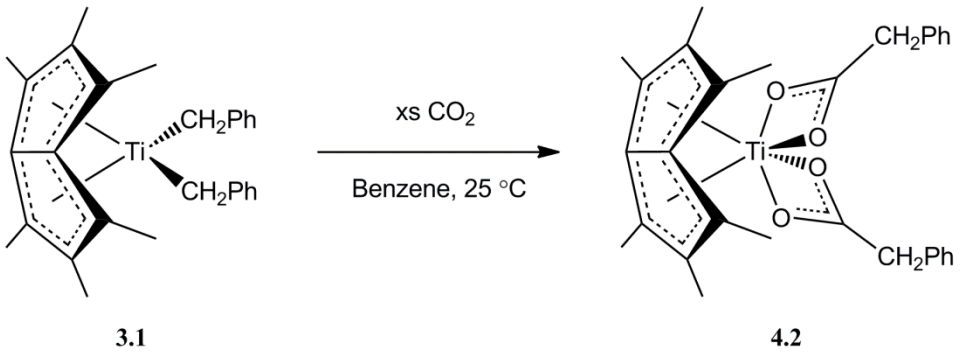

3.1 **4.2**

Figure 4.7: Synthesis of Pn*Ti(κ^2-$O_2CCH_2Ph)_2$ (**4.2**).

The room temperature ^{1}H NMR spectrum of **4.2** revealed seven resonances in a 4:4:2:4:6:6:6 intensity ratio. The spectrum is comparable to that of **4.1** with the Pn* resonances split into three sets of equal intensity and the two independent sets of NWT-Me protons are broad ($\nu_{½}$ = 148.7 and 153.7 Hz), indicating that the solution phase structure of the molecule is similar and of C_2 symmetry (Figure 4.6). NOESY, HMBC and HMQC 2D-NMR techniques were used to assign the complex's spectra and similar to **4.1**, the WT-Me resonance was found to occur at higher field compared to the remaining two Pn* resonances. The three resonances corresponding to the Ph group fall within their normal range and are shifted slightly downfield to that of the starting material, **3.1** (δ = 7.04-7.18 and 6.83-7.13 ppm respectively). The methylene proton resonance is a broad singlet ($\nu_{½}$ = 6.7 Hz), which is shifted downfield to that of its analogous value in **3.1** (δ = 3.37 and 1.82 ppm respectively). This is as expected due to its close proximity to the highly electron withdrawing carboxylate group, but is in good agreement with that seen for phenylacetic acid ($PhCH_2CO_2H$, 3.53 ppm) as is the corresponding ^{13}C resonance (δ = 43.9 and 47.1 ppm respectively). The remainder of the ^{13}C NMR (toluene-d_8) spectrum displays 12 resonances, seven corresponding to Pn* carbons and four to the Ph group, all at unsurprising values. Similar to **4.1**, the bridgehead carbons are equivalent (Figure 4.6), differing from C_s symmetric compounds and the remaining carboxylate carbon chemical shift is almost identical (δ = 188.6 and 188.5 ppm respectively).

As with **4.1**, VT ^{1}H NMR measurements (Figure 4.8) were conducted in an attempt to monitor and model the fluxionality present within the molecule. Upon cooling to −10 °C, the non-equivalent NWT-Me resonances sharpened to freeze-out a static C_2 symmetric system, analogous to **4.1**. Associated with this deceleration and the

suspension of Pn* ring-whizzing about titanium, is a concurrent broadening of the methylene resonance and the formation of an AB quartet, which displays a large 'roofing effect' and a germinal coupling constant, $^{2}J_{H\text{-}H} = -14.1$ Hz. This is due to the static C_2 symmetric system possessing diastereotopic CH_2 groups, which creates two sets of doublets as observed in the ^{1}H NMR spectrum. Upon heating, the exact trend witnessed for **4.1** was detected with the independent NWT-Me resonances broadening, shifting and then converging, but this time at a higher temperature compared to **4.1** (35 *vs.* 30 °C). The line width at half height continued to contract with increasing temperature down to $\nu_{½} = 4.2$ Hz at 70 °C, resulting in an analogous C_{2v} symmetric system, with equivalent NWT-Me groups. Accompanying this was the coalescence of the methylene AB quartet to a sharp singlet resonance. Modelling this rotation and change in symmetry ($C_2 \rightarrow C_{2v}$), gives a Gibbs free energy of activation for the process of $\Delta G^{\ddagger} \approx 60.94$ kJ mol^{-1},[35, 36] which is marginally smaller than **4.1** ($\Delta G^{\ddagger} \approx 61.26$ kJ mol^{-1}).

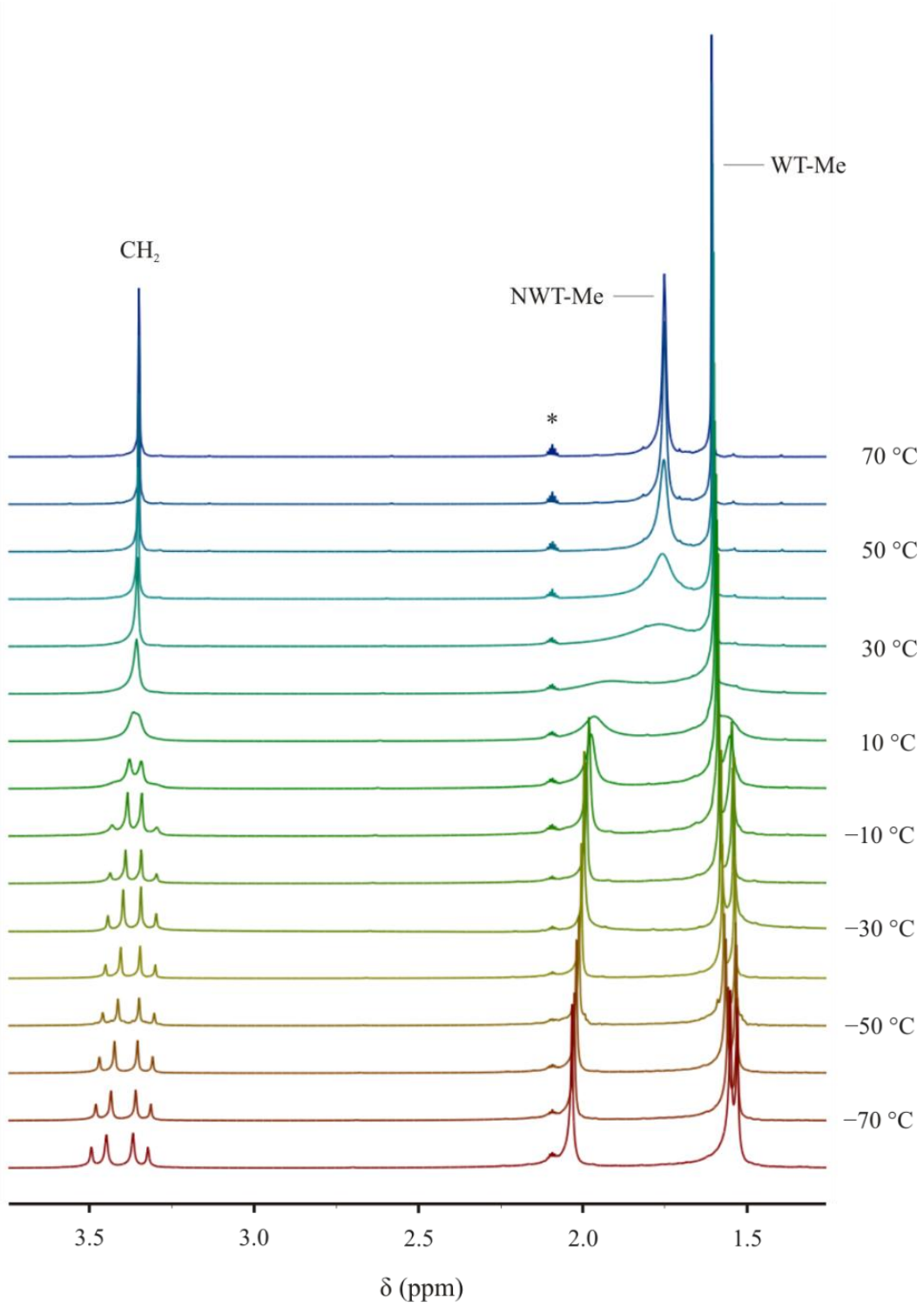

Figure 4.8: Variable temperature ^{1}H NMR study of **4.2** in toluene-d_8, displaying the permethylpentalene and methylene region of the spectrum between 1.5 and 3.5 ppm. * denotes residual protio-solvent.

Single crystals suitable for X-ray diffraction were grown by the slow cooling of a hexane solution to −35 °C and two views of the structure are shown (Figure 4.9 and 4.10).

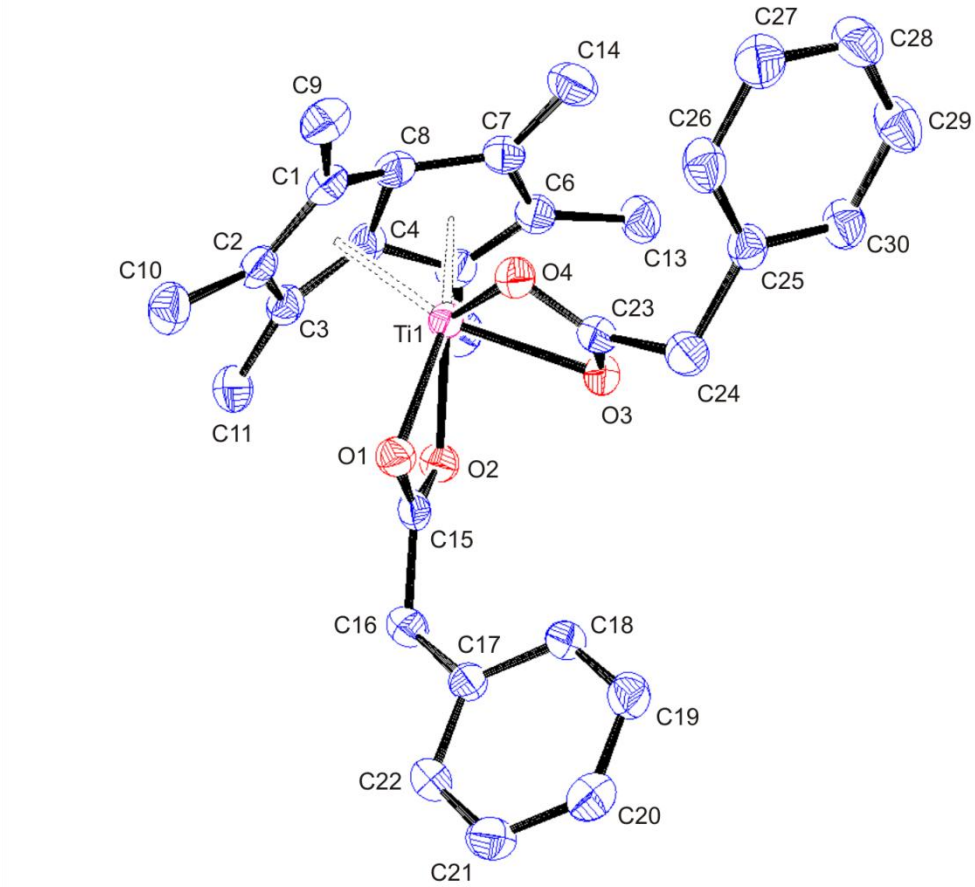

Figure 4.9: Tilted view of **4.2** with thermal ellipsoids at 50%. Hydrogen atoms omitted for clarity.

4.2 crystallises in the *C*2/*c* space group with one independent molecule in the asymmetric unit, which possesses C_2 symmetry; the principal axis intersects the mid-point of the Pn* bridgehead bond and the titanium atom, analogous to **3.2** and **4.1**. The CO_2 moiety has inserted into both Ti-CH_2Ph bonds in a normal fashion[21] and is coordinated in a symmetrical bidentate manner, resulting in the same distorted octahedral disposition of ligands around titanium as **4.1**. Similarly, it possesses a valence electron count of 18 but exhibits a marginally smaller fold angle (31.9° *vs.* 32.4°), which is postulated to be a factor in the difference in calculated Gibbs free energy of activation for the Pn* ring-whizzing observed within the molecules. As expected, and parallel to **4.1**, **4.2** has a smaller fold angle than its 14 electron precursor (**3.1**, 33.1°).

4.2 is the first example of CO_2 insertion into any M-CH_2Ph bond (M = transition metal), to be fully characterised in both solution and the solid state. Indeed, the double

insertion observed is very rare and there are only two documented examples where the M-(κ^2-$O_2CCH_2Ph)_2$ motif has been structurally characterised and they are both for 1D coordination polymers incorporating Cd. These are synthesised by hydrothermal methods with 2-phenylmalonic acid[38] and standard methods using phenylacetic acid.[39]

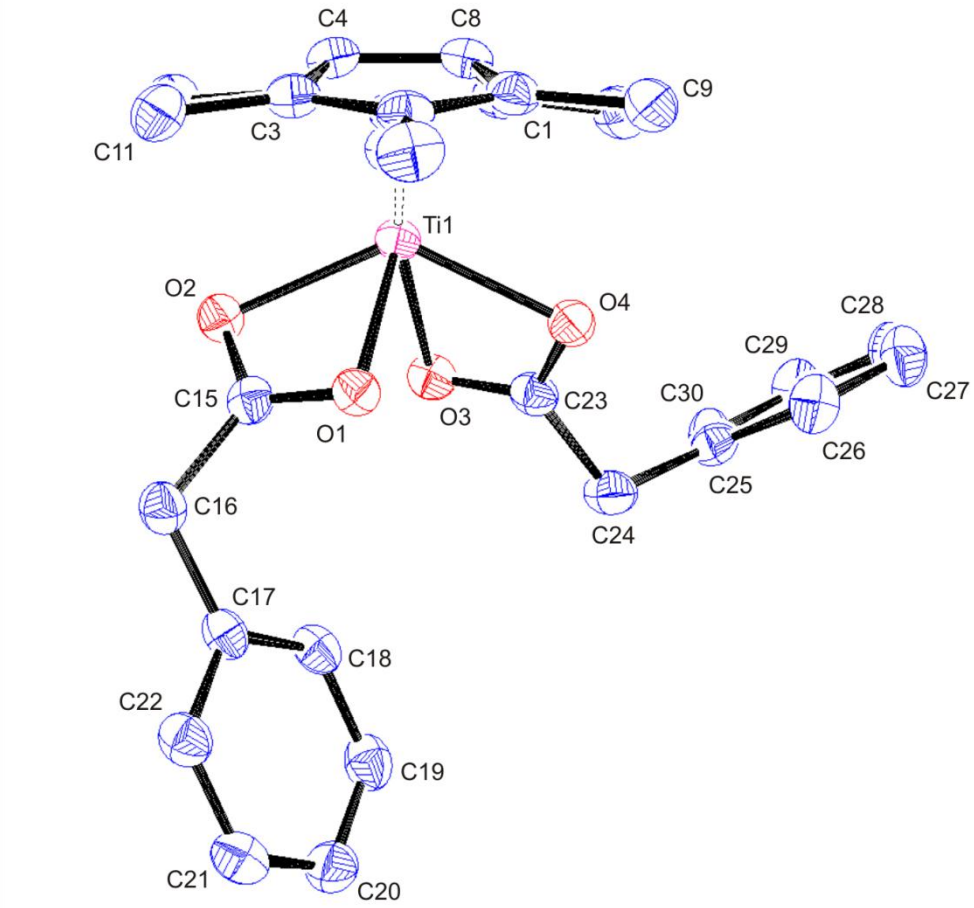

Figure 4.10: End-on view of **4.2** with thermal ellipsoids at 50%. Hydrogen atoms omitted for clarity.

The average Ti-O bond length is smaller than **4.1** (2.1386 vs. 2.1429 Å) but the corresponding range is larger (2.1196-2.1610 and 2.1393-2.1489 Å respectively). The average length is also comparable with the 18 electron species Cp*Ti($O_2CCH_2SMes)_3$ (2.1498 Å),[40] which has been demonstrated to show cytotoxic activity towards tumour cells – a major breakthrough as monocyclopentadienyl Ti^{IV} complexes have previously been discarded as possible anticancer drugs due to potential hydrolysis problems.[40] Again, the four membered metallocycle is coordinated in a highly symmetric fashion with nearly identical C-O distances (average = 1.27 Å) and is essentially planar with no atom deviating from the mean Ti-O-C-O plane by more than 0.046 Å. As previously mentioned, there are no other structurally characterised examples of Ti-(κ^2-O_2CCH_2Ph)

fragments in the literature but there are for other first row transition metals; [(TIM)Fe(O_2CCH_2Ph)][ClO_4][41] {TIM = bis[(imidazol-4-methyl) 4'-imidazol-2'-yl]methane} and for the group 12 metals [η^3-HB(3-Phpz)$_3$]ZnO_2CCH_2Ph[42] [HB(3-Phpz)$_3$ = tris(3-phenylpyrazolyl)hydroborate] and [Cd(O_2CCH_2Ph)$_2$(H_2O)(μ_2-hmt)]$_n$[39] (hmt = hexamethylenetetramine). The average angle at the methylene carbon in **4.2** is comparable to those reported for the above [112.2, 114.0(0), 113.0(8) and 109.7° respectively]. IR spectroscopy reveals a separation of 80 cm^{-1} for ν_{as}(CO) and ν_s(CO) (1538 and 1458 cm^{-1}, respectively), which is significantly smaller than the ionic form (190 cm^{-1}),[41] substantiating bidentate coordination in the solid state.

Table 4.2: Selected bond lengths, angles and structural parameters for **4.2**. ESDs are given in parentheses.

Lengths (Å)			
Ti(1) - C(1)	2.391(2)	C(1) - C(2)	1.418(3)
Ti(1) - C(2)	2.5229(19)	C(2) - C(3)	1.418(3)
Ti(1) - C(3)	2.3496(19)	C(3) - C(4)	1.450(3)
Ti(1) - C(4)	2.1202(19)	C(4) - C(5)	1.448(3)
Ti(1) - C(5)	2.376(2)	C(5) - C(6)	1.413(3)
Ti(1) - C(6)	2.5144(19)	C(6) - C(7)	1.411(30)
Ti(1) - C(7)	2.369(2)	C(7) - C(8)	1.443(3)
Ti(1) - C(8)	2.1324(19)	C(8) - C(1)	1.433(3)
Ti(1) - Pn*$_{cent}$	1.959	C(4) - C(8)	1.459(3)
Ti(1) - Pn*$_{cent}$	1.958	Av. C_{ring} – Me	1.501
Ti(1) - O(1)	2.1421(13)	Ti(1) - O(3)	2.1610(14)
Ti(1) - O(2)	2.1318(14)	Ti(1) - O(4)	2.1196(14)
C(15) - O(1)	1.265(2)	C(23) - O(3)	1.271(2)
C(15) - O(2)	1.272(2)	C(23) - O(4)	1.272(2)
C(15) - C(16)	1.506(3)	C(23) - C(24)	1.510(3)
Angles (°)			
O(1) - Ti(1) - O(2)	61.31(5)	O(3) - Ti(1) - O(4)	61.20(5)
Ti(1) - O(1) - C(15)	89.79(11)	Ti(1) - O(3) - C(23)	89.24(11)
Ti(1) - O(2) - C(15)	90.05(11)	Ti(1) - O(4) - C(23)	91.06(11)
O(1) - C(15) - O(2)	118.42(17)	O(3) - C(23) - O(4)	117.97(18)
O(1) - C(15) - C(16)	121.25(17)	O(3) - C(23) - C(24)	121.53(18)
O(2) - C(15) - C(16)	120.32(17)	O(4) - C(23) - C(24)	120.49(18)
C(15) - C(16) - C(17)	113.54(16)	C(23) - C(24) - C(25)	110.83(16)
Fold Angle	31.92		

4.2.3 Synthesis and characterisation of Pn*Ti(κ^2-$O_2CCH_2SiMe_3$)$_2$ (4.3)

CO_2 was admitted to **3.2** in an analogous manner to Section 4.2.1 (Figure 4.11) and the purple solution steadily changed to orange in colour over a period of three hours, which was slower than for the formation of **4.1** (instantaneous) but considerably faster than **4.2** (40 hours). The solutions were evaporated to dryness and Pn*Ti(κ^2-$O_2CCH_2SiMe_3$)$_2$ (**4.3**) was obtained as a highly viscous, dark orange oil, which was initially identified by mass spectrometry (EI), revealing the molecular ion at accurate mass followed by a peak ascribed to the loss of $O_2CCH_2SiMe_3$.

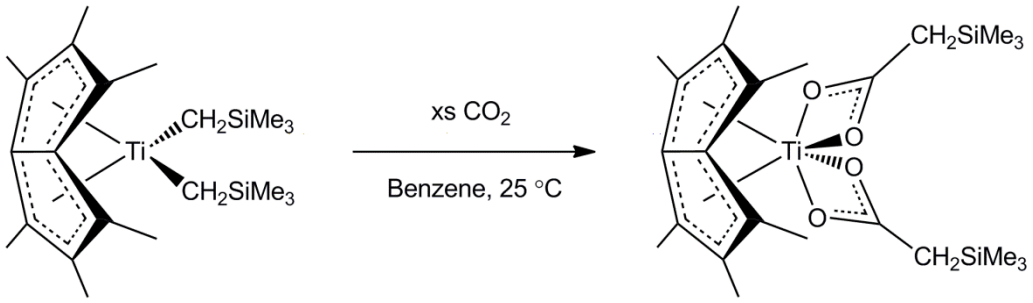

3.2 **4.3**

Figure 4.11: Synthesis of Pn*Ti(κ^2-$O_2CCH_2SiMe_3$)$_2$ (**4.3**).

Due to difficulties associated with removing the highly viscous oil from its receptacle, it was stored in an ampoule at room temperature under a N_2 atmosphere and left for a number of months after which small orange, plate-shaped crystals began to form from the viscous oil. The crystals were single and suitable for X-ray diffraction and two views of the structure are shown in Figures 4.12 and 4.14.

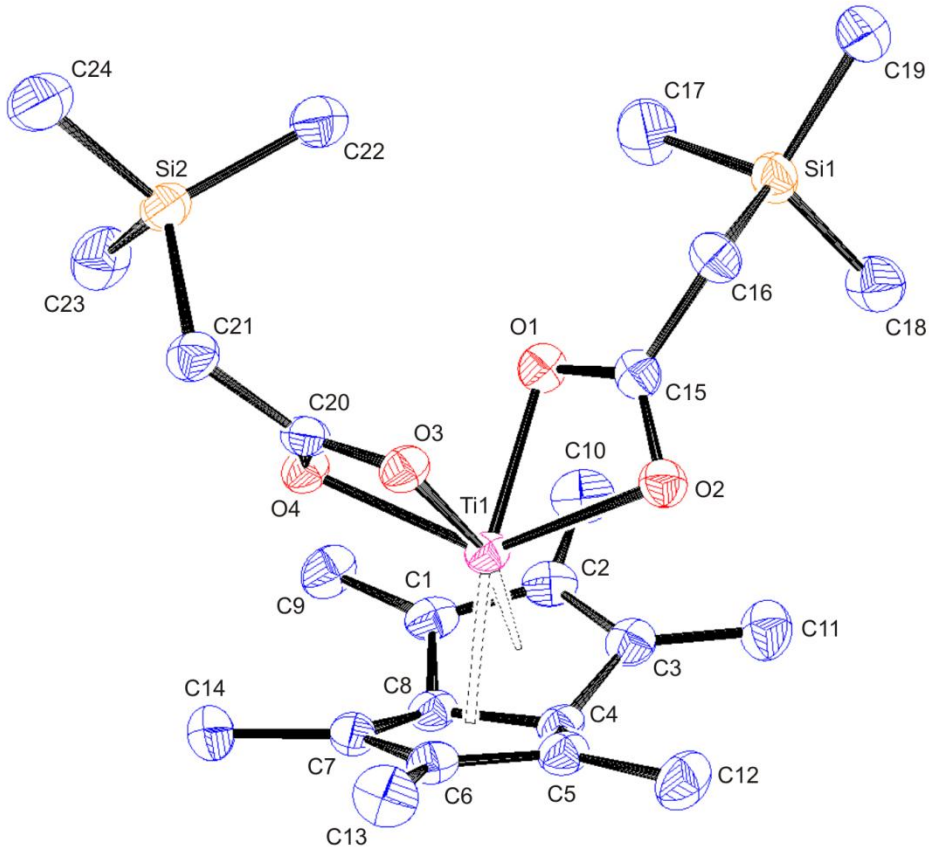

Figure 4.12: Side-on view of **4.3** with thermal ellipsoids at 50%. Hydrogen atoms omitted for clarity.

Crystallographic analysis reveals **4.3** to crystallise in the $P2_1/c$ space group with one independent molecule in the asymmetric unit possessing the same C_2 symmetry and principal axis (best visualised in Figure 4.14) as **4.1** and **4.2**. The CO_2 moiety has inserted in an identical "normal" fashion[21] into both Ti-CH_2SiMe_3 bonds, as observed for **4.1** and **4.2**, and is bound to the Ti centre in a bidentate mode. **4.3** is the first crystallographically characterised example for any metallic element of [κ^2-O,O'-($O_2CCH_2SiMe_3$)] binding to a single metal centre. The most common bonding mode in the CSD is bridging two metal centres in a μ-η^1:η^1-$O_2CCH_2SiMe_3$ fashion (Figure 4.13), which is displayed for the dimeric complexes, [$Cp^*_2Sm(O_2CCH_2SiMe_3)]_2$,[43] [$Cu(O_2CCH_2SiMe_3)_2R]_2$ (R = C_5H_5N, *o*-Me-C_5H_4N, *m*-Me-C_5H_4N and C_9H_7N)[44] and [$(C_5Me_4SiMe_3)Ln(O_2CCH_2SiMe_3)_2]_2$ (Ln = Y , Lu and Sc).[45] Also present in the literature is the more closely related [(μ-η^1:η^1-$O_2CCH_2SiMe_3$)(μ-η^1:η^2-$O_2CCH_2SiMe_3$)]$_2$ mode, exhibited for the dimeric yttrium complexes, {[$(C_5Me_4)SiMe_2(CH_2CH{=}CH_2)$]$Y(O_2CCH_2SiMe_3)_2$}$_2$[46] and [$Y(O_2CCH_2SiMe_3)_2(THF)_3]_2[BPh_4]_2$.[47]

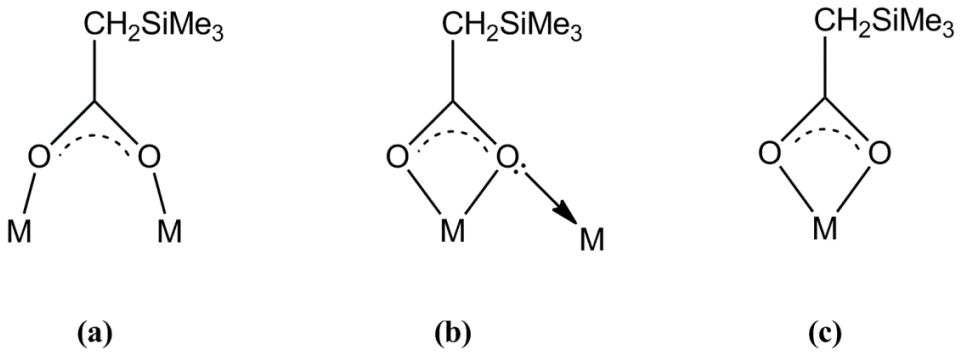

Figure 4.13: Coordination modes of $O_2CCH_2SiMe_3$; (a) μ-η^1:η^1-, (b) μ-η^1:η^2-, (c) κ^2-O-O'-.

Similar to **4.1** and **4.2**, the ligands in **4.3** are positioned in a distorted octahedral arrangement and the complex also possesses an 18 valence electron count. The fold angle (32.3°) is between those observed for **4.1** and **4.2** (31.9 and 32.4° respectively), and is only marginally smaller than found for its 14 electron starting material **3.2** (32.9°).

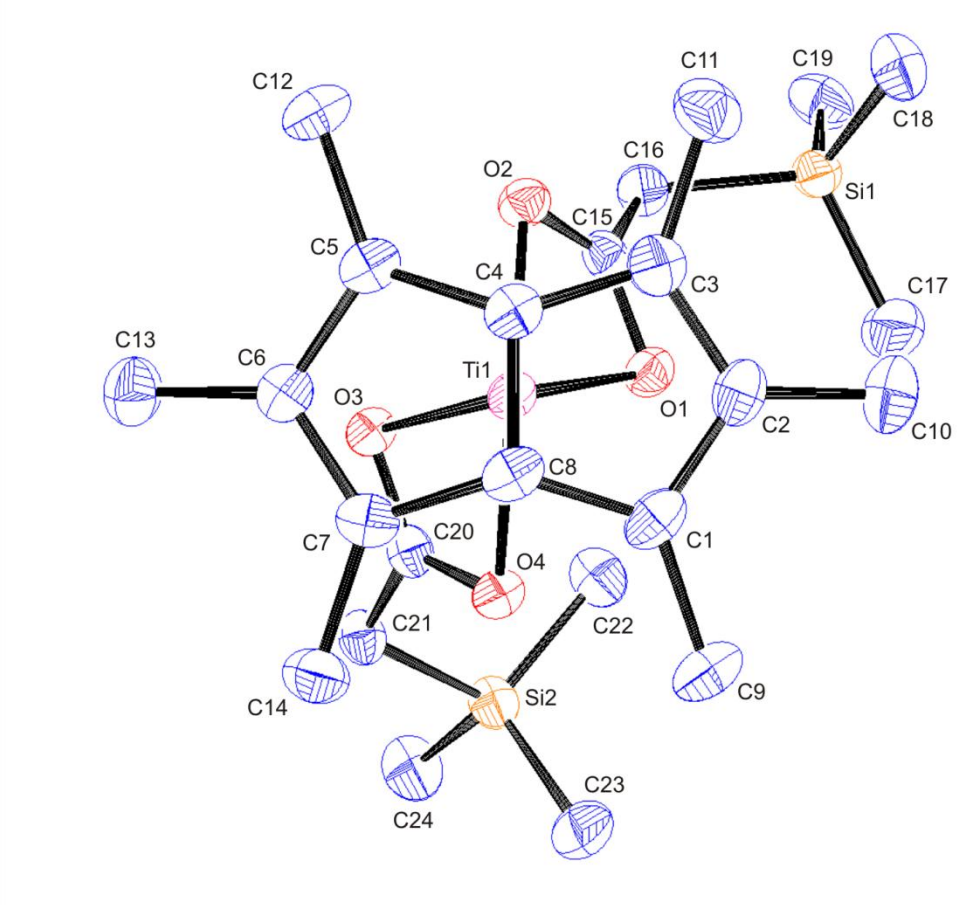

Figure 4.14: Top view of **4.3** with thermal ellipsoids at 50%. Hydrogen atoms omitted for clarity.

The average Ti-Pn*$_{cent}$ distances are almost identical for **4.3**, **4.2** and **4.1** (1.958, 1.959 and 1.957 Å respectively) as are the average Ti-C(Pn*) distances (2.344, 2.347 and 2.344 Å respectively, Table 4.9) indicating equivalent Ti-Pn* bonding in each case. The parameters associated with the essentially planar, four membered metallocycle fragments are also very similar for the three compounds as illustrated in Table 4.3, with **4.3** marginally possessing the shortest average Ti-O distance of the set and bears no atom which deviates from the mean Ti-O-C-O plane by more than 0.054 Å.

Table 4.3: Collection of solid state parameters for the four membered metallocycles of structurally characterised CO_2 insertion products.

Compound	Av. Ti-O Distance (Å)	Ti-O range (Å)	Av. C-O Distance (Å)	Av. O-Ti-O Angle (°)
4.1	2.1429	2.1393-2.1489	1.268	61.7
4.2	2.1386	2.1196-2.1610	1.270	61.3
4.3	2.1348	2.1180-2.1520	1.277	61.3

This highly symmetrical bonding motif is in contrast to the $[(\mu\text{-}\eta^1\text{:}\eta^1\text{-}O_2CCH_2SiMe_3)(\mu\text{-}\eta^1\text{:}\eta^2\text{-}O_2CCH_2SiMe_3)]$ coordination mode present in $[Y(O_2CCH_2SiMe_3)_2(THF)_3]_2[BPh_4]_2$, which is bound in a highly unsymmetrical fashion with clearly distinct Y-O distances [2.333(2) and 2.532(2) Å],[47] although it is essentially planar. It also possesses a smaller corresponding methylene angle than **4.3** [111.1(2) and 114.6° respectively], which is postulated to be the result of reduced steric crowding around the larger second row metallic centre, permitting the angle to approach its idealised tetrahedral value more closely.

Table 4.4: Selected bond lengths, angles and structural parameters for **4.3**. ESDs are given in parentheses.

Lengths (Å)			
Ti(1) - C(1)	2.339(3)	C(1) - C(2)	1.408(5)
Ti(1) - C(2)	2.509(4)	C(2) - C(3)	1.410(5)
Ti(1) - C(3)	2.389(4)	C(3) - C(4)	1.435(5)
Ti(1) - C(4)	2.129(3)	C(4) - C(5)	1.442(5)
Ti(1) - C(5)	2.353(3)	C(5) - C(6)	1.412(5)
Ti(1) - C(6)	2.513(3)	C(6) - C(7)	1.413(5)
Ti(1) - C(7)	2.393(3)	C(7) - C(8)	1.438(5)
Ti(1) - C(8)	2.127(3)	C(8) - C(1)	1.435(5)
Ti(1) - Pn^*_{cent}	1.960	C(4) - C(8)	1.460(5)
Ti(1) - Pn^*_{cent}	1.956	Av. C_{ring} - Me	1.503
Ti(1) - O(1)	2.118(2)	Ti(1) - O(3)	2.152(2)
Ti(1) - O(2)	2.139(2)	Ti(1) - O(4)	2.130(2)
C(15) - O(1)	1.283(4)	C(20) - O(3)	1.276(4)
C(15) - O(2)	1.276(4)	C(20) - O(4)	1.274(4)
C(15) - C(16)	1.487(5)	C(20) - C(21)	1.489(5)
Angles (°)			
O(1) - Ti(1) - O(2)	61.31(5)	O(3) - Ti(1) - O(4)	61.20(5)
Ti(1) - O(1) - C(15)	90.4(2)	Ti(1) - O(3) - C(20)	89.82(19)
Ti(1) - O(2) - C(15)	89.6(2)	Ti(1) - O(4) - C(20)	90.9(2)
O(1) - C(15) - O(2)	117.4(3)	O(3) - C(20) - O(4)	117.9(3)
O(1) - C(15) - C(16)	120.2(3)	O(3) - C(20) - C(21)	122.2(3)
O(2) - C(15) - C(16)	122.3(3)	O(4) - C(20) - C(21)	119.9(3)
C(15) - C(16) - Si(1)	116.2(3)	C(20) - C(21) - Si(2)	113.0(3)
Fold Angle	32.27		

The room temperature ^{1}H and ^{13}C NMR spectra corresponding to the Pn* moiety of **4.3** are parallel to those observed for **4.2** and **4.1**, indicating C_2 symmetry in solution (Figure 4.6). The resonances in the former are similarly split into three sets of equal intensity, with two independent NWT-Me groups indicating the presence of fluxionality due to their large line widths ($\nu_{½}$ = 104.3 and 77.7 Hz) and the WT-Me resonance is also found furthest upfield. The latter spectra likewise displays seven Pn* resonances and the bridgehead carbons are again equivalent representing a diagnostic feature for differentiating between C_2 symmetric Pn* systems, present here and C_s symmetric systems, which on initial inspection of ^{1}H NMR spectra are indistinguishable

and can easily be mistaken on account of the distinctive 6:6:6 intensity ratio. As expected with being α- to the highly electron withdrawing carboxylate group, the singlet corresponding to the methylene protons (δ = 1.79 ppm; toluene-d_8) is shifted considerably downfield to that of the starting material, **3.2** (δ = −0.15 ppm; C_6D_6). It is, however, in good agreement with the chemical shifts observed in the most closely structurally related complexes $\{[(C_5Me_4)SiMe_2(CH_2CH{=}CH_2)]Y(O_2CCH_2SiMe_3)_2\}_2$ and $[Y(O_2CCH_2SiMe_3)_2(THF)_3]_2[BPh_4]_2$ (δ = 1.91 and 2.18 ppm; C_6D_6 and pyridine-d_5 respectively), as are the corresponding ^{13}C resonances [δ = 29.1 (**4.3**) and, 30.5 and 30.3 ppm respectively].[46, 47] Almost identical ^{1}H and ^{13}C NMR chemical shift values are witnessed for the $SiMe_3$ group in the related three complexes [δ = 0.11, 0.17 and 0.13; −1.0, −1.0 and −0.7 ppm respectively]. In addition, the carboxylate carbon chemical shifts are similar (δ = 189.8, 184.7 and 191.3 ppm respectively).

VT ^{1}H NMR studies were conducted to monitor the Pn* ring-whizzing – postulated as the same dynamic process operating in solution for **4.1** and **4.2** – and similarly a static C_2 symmetric system bearing non-equivalent NWT-Me groups is observed at −10 °C, which transforms into a C_{2v} symmetric system with equivalent NWT-Me groups, possessing an integral of 12 upon heating to 70 °C. The coalescence temperature is midway between that observed for **4.1** and **4.2** (32 *vs.* 30 and 35 °C respectively) and modelling this rotation and change in symmetry ($C_2 \rightarrow C_{2v}$), gives a Gibbs free energy of activation for the Pn* ring-whizzing in **4.3** of $\Delta G^{\ddagger} \approx 62.46$ kJ mol^{-1}.[35, 36]

4.2.4 Synthesis and characterisation of Pn*Ti(κ^2-$O_2CCH_2{}^tBu)_2$ (4.4)

The only report of CO_2 insertion into a Ti-$CH_2{}^tBu$ bond was for the Ti^{III} complex $Cp^*_2Ti(CH_2{}^tBu)$, which was documented in the same publication that described the synthesis of $Cp^*_2Ti(CH_2Ph)$; a similar lack of characterising data was presented (Section 4.2.2).[25] The complex was deemed to form a metal carboxylate species after reacting in solution smoothly, at room temperature, with gaseous CO_2. Attempts were pursued in order to replicate the reactivity utilising the Pn*Ti moiety and CO_2 was admitted to **3.3** (Figure 4.15); the dark red solution gradually lightened, over a 15 hour period, to orange. The reaction proceeded considerably slower than in the formation of **4.1** and **4.3** (instantaneous and three hours, respectively) but faster than **4.2** (40 hours), which is thought to be the consequence of steric bulk around the Ti centre.

Analogous to **4.3**, Pn*Ti(κ^2-$O_2CCH_2{}^tBu)_2$ (**4.4**) was isolated as a highly viscous dark orange oil upon evaporation of all solvents and identified by mass spectrometry (EI), which revealed the molecular ion at accurate mass, followed by a peak designated to the loss of $O_2CCH_2{}^tBu$. Unfortunately, prolonged storage of the compound under the same conditions as **4.3** failed to produce a crystalline material suitable for X-ray diffraction.

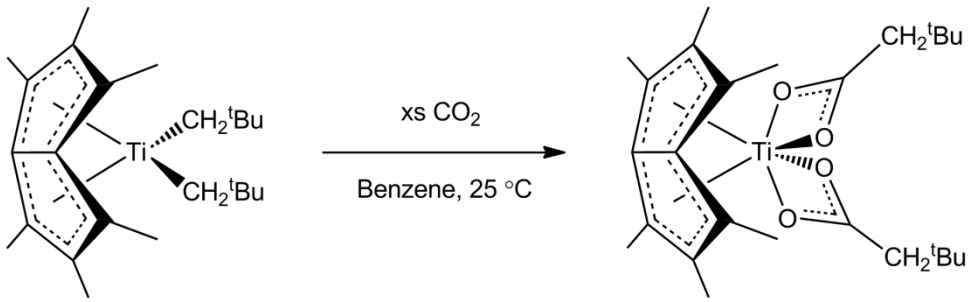

3.3 **4.4**

Figure 4.15: Synthesis of Pn*Ti(κ^2-$O_2CCH_2{}^tBu)_2$ (**4.4**).

The room temperature ^{1}H NMR spectrum of **4.4** reveals five resonances, three sharp and two broad in a 4:6:6:6:18 intensity ratio and one may conclude that the solution phase structure of the molecule is of C_2 symmetry, analogous to that observed for **4.1**, **4.2** and **4.3**. Due to the C_2 symmetry within the molecule, the Pn* resonances are similarly split into three sets of equal intensity, resulting in two pairs of independent NWT-Me protons (Figure 4.6), which are broad ($\nu_{½}$ = 130.0 and 130.4 Hz), indicating the same dynamic process is in operation. VT ^{1}H NMR measurements were conducted to analyse this dynamic process and an analogous transformation to the complexes reported thus far in this chapter was recorded. At high temperatures (70 °C), a C_{2v} symmetric system with equivalent NWT-Me groups was observed and upon cooling a decoalescense of this resonance occurred, this time at 27 °C, which resulted in a static C_2 symmetric system bearing non-equivalent NWT-Me groups at −10 °C. Modelling the change in symmetry ($C_2 \rightarrow C_{2v}$), gives a Gibbs free energy of activation for the Pn* ring-whizzing in **4.4** of $\Delta G^{\ddagger} \approx 61.26$ kJ mol^{-1},[35, 36] which is identical to **4.1**.

A number of 2D-NMR techniques (NOESY, HMBC and HMQC) were employed to assign the complex's spectra and similar to **4.1**, **4.2** and **4.3**, the WT-Me resonance was found to occur at higher field than the remaining two Pn* resonances. The methylene proton resonance is shifted downfield to that of **3.3** (δ = 2.11 and 0.77 ppm; toluene-d_8 and C_6D_6 respectively), as expected with its close proximity to the

highly electron withdrawing carboxylate group, but is in good agreement with that seen for the multinuclear Ti^{IV} bridging oxo carboxylate species $[Ti_8O_8(O_2CCH_2{}^tBu)_{16}]$ (δ = 2.30 ppm; toluene-d_8), as is the corresponding ^{13}C resonance (δ = 50.3 and 50.1 ppm respectively).[48] This species contains the μ-η^1:η^1-$O_2CCH_2{}^tBu$ bonding motif and is a rare example of a compound containing a Ti-$O_2CCH_2{}^tBu$ fragment. The ^tBu, ^1H and ^{13}C NMR chemical shifts are almost identical to another rare example, the hexanuclear Ti^{IV} siloxo carboxylate complex $[Ti_6O_6(OSiMe_3)_6(O_2CCH_2{}^tBu)_6]$ [δ = 1.04 (29.9 and 30.4) and 1.05 (30.1 and 30.3) ppm].[49] The remainder of the ^{13}C NMR (toluene-d_8) spectrum displays eight resonances, seven corresponding to Pn* carbons as the result of reduced symmetry in the molecule; the bridgehead carbons are again equivalent, similar to **4.1**, **4.2** and **4.3** differentiating C_2 and C_s symmetric Pn* systems, and the remaining carboxylate carbon chemical shift is almost identical to the compounds within this chapter thus far and the multinuclear Ti^{IV} oxo carboxylate species (δ = 189.9; 188.5, 188.6, 189.8 and 183.6 ppm respectively).[48]

Due to a lack of suitable single crystals for X-ray diffraction, the solid state structure of **4.4** can only be hypothesised but due to the similarity in reactivity and the MS, IR, ^1H and ^{13}C NMR data obtained it seems highly likely that it would be isostructural with **4.3**, possessing C_2 symmetry.

4.3 Reactions with CO

The migratory insertion of CO (generically referred to as carbonylation) into M-C bonds is an extremely important organometallic reaction due to the scope it offers for functionalising hydrocarbons and other substrates to yield organic compounds of greater value.[1] Carbonylation is well known among transition, lanthanide and actinide elements with the archetypal example that of $Mn(CO)_5(COMe)$, on which much early mechanistic work was conducted.[50–53] $Mn(CO)_5(COMe)$ was synthesised by the reversible reaction of $Mn(CO)_5Me$ with CO and demonstrates η^1-bonding of the resulting acyl fragment [Figure 4.16 (a)], due to orbital occupation and interaction effects.[54–56]

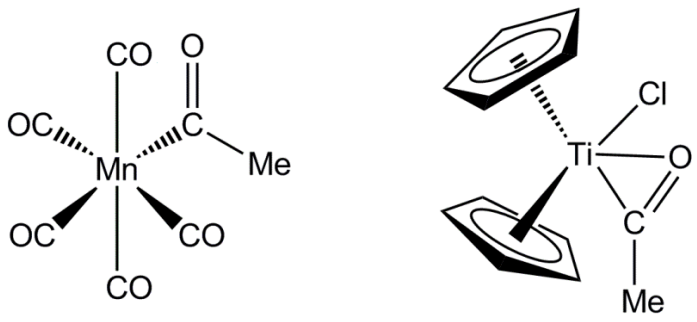

Figure 4.16: Common coordination modes of COR fragments in (a) late; $Mn(CO)_5(\eta^1\text{-COMe})$ and (b) early; $Cp_2Ti(\eta^2\text{-COMe})Cl$ transition metals.

The reactivity of the resulting metal acyl determines the types of organic products that can be obtained using CO as a C_1 feedstock. A characteristic of acyl groups is their ability, in certain cases, to bind to a metal through both the carbon and oxygen atoms. This η^2-bonding typically occurs at electron deficient metal centres, in particular for high-valent, early d-block, lanthanide and actinide metal centres, which was demonstrated by the pioneering work of Floriani with the reaction of Cp_2TiRCl (R = Me and CH_2Ph) with CO to form $Cp_2Ti(\eta^2\text{-COR})Cl$ [Figure 4.16 (b)].[57, 58] Subsequent studies including the carbonylation of Cp_2ZrMe_2,[59, 60] demonstrated that 16 electron group IV metallocenes of the type Cp_2MRX (X = alkyl, halide, alkoxide etc.), reversibly absorb one equivalent of CO to generate the corresponding 18 electron mono acyls, $Cp_2M(\eta^2\text{-COR})X$. There are two isomers observed, which have the oxygen atom directed away from, "O-outside" or directed towards, "O-inside" the non-inserted X group. A mechanistic study by Erker[61] on the carbonylaton of the aforementioned Cp_2ZrMe_2, demonstrated the initially formed O-outside product to isomerise above −60 °C to the thermodynamically more stable O-inside isomer, which has been observed for such acyl complexes in the solid state *via* X-ray analysis.[58, 60, 62–64] These results were interpreted as an indication of the approach of CO from a lateral position, as opposed to centrally, between the two groups, a fact corroborated by subsequent computational studies.[56, 65, 66] η^2-acyl complexes are extremely reactive and undergo a number of fascinating transformations.[67, 68] Common reactions among mixed alkyl-acyl complexes are; 1,2-migratory insertion of the alkyl group into the acyl moiety to generate an η^2-ketone and insertion of a second CO molecule with subsequent rearrangement to form an enediolate fragment. The latter has been observed for both

group IV and actinide bis-Cp complexes but are reported to proceed *via* drastically different mechanistic pathways (Figure 4.20).[67, 69]

4.3.1 Synthesis and characterisation of Pn*Ti[κ^2-O-C(CH$_2$^{t}Bu)=C(CH$_2$ ^{t}Bu)-O] (4.5)

The identical freeze-pump-thaw method as stated in Section 4.2.1 was replicated for a benzene solution of **3.3**, after which CO was admitted (Figure 4.17), resulting in a subtle colour change of the initially red solution. Work up was completed in a glovebox and the slow cooling of a hexane solution furnished an orange microcrystalline solid in 28% yield, which was identified as Pn*Ti[κ^2-O-C(CH$_2$^{t}Bu)=C(CH$_2$^{t}Bu)-O] (**4.5**) by X-ray crystallography and mass spectrometry (EI). The latter showed the molecular ion at accurate mass followed by peaks ascribed to the sequential loss of one and two ^{t}Bu groups. Diminished yields are thought to arise from an inherent solubility of **4.5** in hydrocarbon, aromatic and chlorinated solvents, as the reaction was demonstrated to proceed in a quantitative manner by ^{1}H NMR spectroscopy.

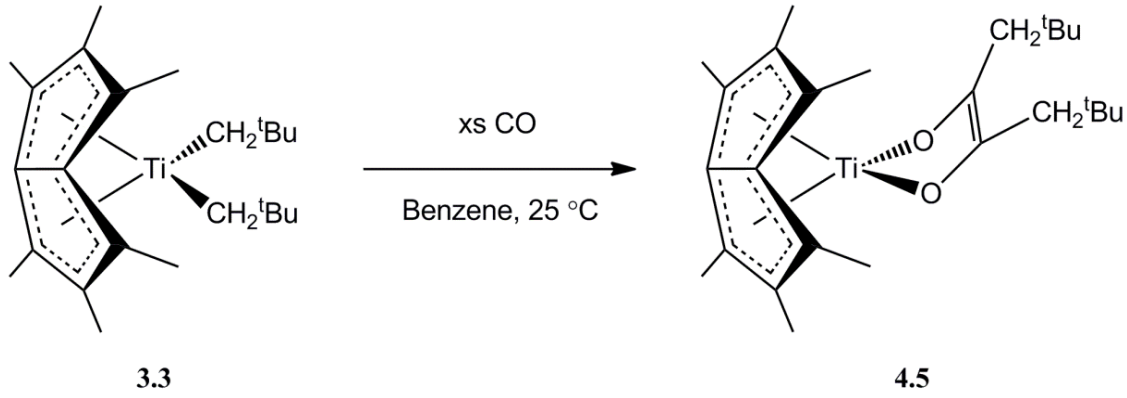

3.3 **4.5**

Figure 4.17: Synthesis of Pn*Ti[κ^2-O-C(CH$_2$^{t}Bu)=C(CH$_2$^{t}Bu)-O] (**4.5**).

Single crystals suitable for X-ray diffraction were grown by the slow cooling of a hexane solution to −35 °C and two views of the structure are shown (Figure 4.18 and 4.19).

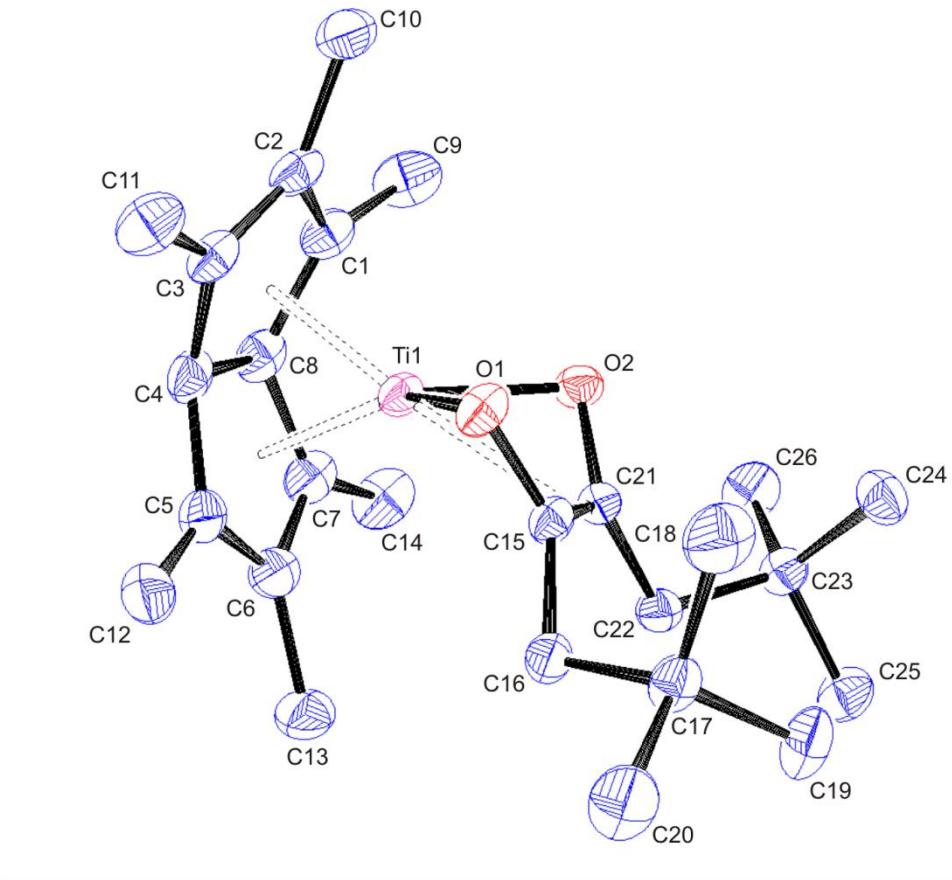

Figure 4.18: Side-on view of **4.5** with thermal ellipsoids at 50%. Hydrogen atoms omitted for clarity.

Crystallographic analysis demonstrates **4.5** to crystallise in the $P2_12_12_1$ space group with one independent molecule in the asymmetric unit, which possesses C_s symmetry; the solitary mirror plane runs through Ti(1) and the WT-Pn* atoms [C(2) and C(6)], best visualised in Figure 4.19. The carbonylation of **3.3** has resulted in the direct reductive coupling of two CO molecules to yield a mononuclear *cis*-enediolate complex, which possesses a large fold about the O-O vector, resulting in a σ^2, π-bonding mode, analogous to the related Ti^{IV} *cis*-diene complexes, $CpTi(NP^tBu_3)[CH_2\text{-}C(Me)=C(Me)\text{-}CH_2]$ and $(Ar'O)_2Ti[CH_2\text{-}C(Me)=C(Me)\text{-}CH_2]$ (Ar'O = 2,6-diphenylphenoxide).[70, 71] **4.5** exhibits the largest fold angle contained within this work (36.7°), nearly equalling the largest reported for any Ti pentalene derivative, that of the Ti^{III} species, PnTiCp (37.0°).[72]

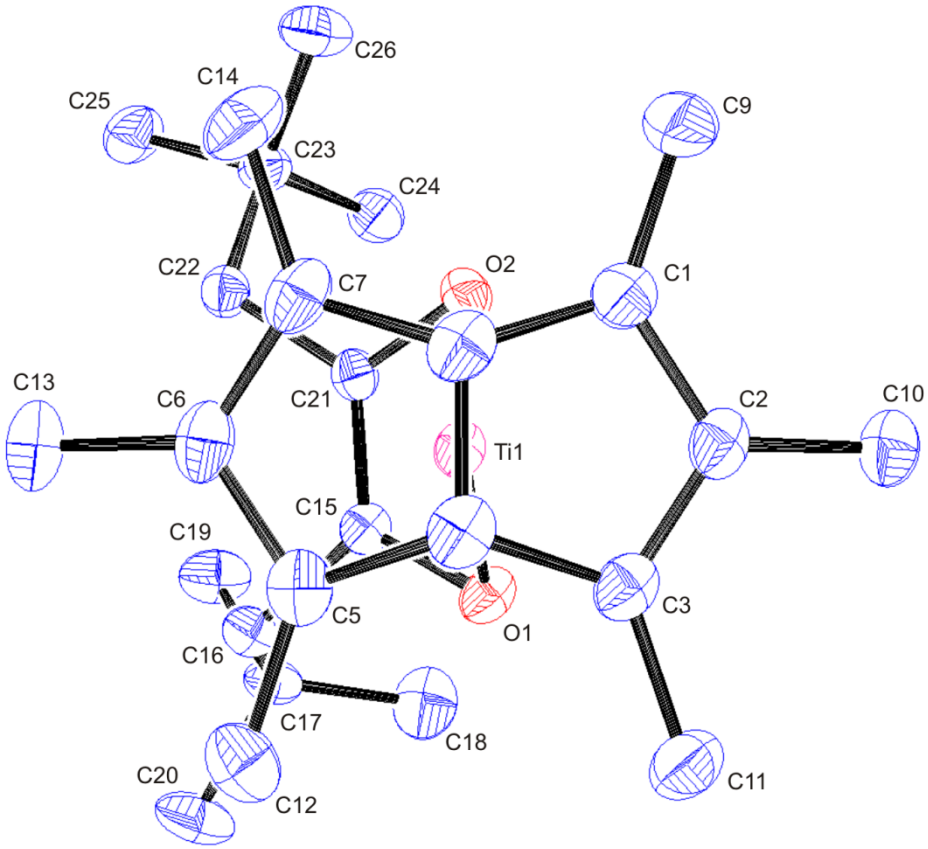

Figure 4.19: Top view of **4.5** with thermal ellipsoids at 50%. Hydrogen atoms omitted for clarity.

4.5 is only the fourth structurally characterised monomeric group IV enediolate complex to be reported in the literature and the first of any metal bearing $CH_2{}^tBu$ groups on the enediolate moiety. Comparisons are limited to the only structurally characterised Ti enediolate to date, Cp_2Ti[O-C(Ph)=C(Ph)-O] prepared *via* a one pot[73] or two step[74] synthesis using Cp_2TiCl_2. The average Ti-O bond length for **4.5** (1.938 Å) is shorter than the distance seen in Cp_2Ti[O-C(Ph)=C(Ph)-O] (1.963 Å), reasoned as the consequence of Pn* formally containing two electrons fewer than the bis-Cp fragment, which results in a stronger Ti-O interaction. The average C-O distances are very similar (1.359 and 1.349 Å respectively) but the C=C bond length in **4.5** is notably elongated [1.398(2) *vs.* 1.371(6) Å], especially when compared to a typical C=C bond distance (1.340 Å), which may be a consequence of delocalisation of electron density away from the bond into the five membered ring.[73]

As stated previously, the five membered titanoheterocycle [Ti(1)O(1)O(2)C(15)C(21)] is non-planar and puckered about the O-O vector. The

dihedral angle between the two planes Ti(1)O(1)O(2) and O(1)O(2)C(15)C(21) is considerably smaller than for Cp_2Ti[O-C(Ph)=C(Ph)-O] (112.0 and 145.1°, respectively),[73] indicating a much greater degree of folding and a closer approach of the olefin moiety towards the Ti atom and a σ^2, π-bonding mode. This is highlighted by the substantially shorter average Ti-C(olefinic) distance (2.268 compared to 2.657 Å) and represents an interaction that is only marginally longer than Ti-(σ-C) bond lengths seen for complexes in Chapter Two and Three. Indeed, the bonding motif is much closer related to the Ti^{IV} *cis*-diene complexes $CpTi(NP^tBu_3)[CH_2\text{-}C(Me)=C(Me)\text{-}CH_2]$ and $(Ar'O)_2Ti[CH_2\text{-}C(Me)=C(Me)\text{-}CH_2]$ (Ar'O = 2,6-diphenylphenoxide), which possess a σ^2, π-bonding mode and contain comparable Ti-C(olefinic) distances and dihedral angle (2.413 Å; 110.6° and 2.295 Å; 104.9° respectively).[70, 71] Conversely the remaining structurally characterised monomeric group IV enediolate complexes, Cp^*_2Zr[O-C(R)=C(R)-O] (R = Me, ^{t}Bu),[75] display a much smaller fold about the O-O axis (163.2 and 179.6° respectively), resulting in a nearly planar five membered ring, indicating a simplified σ^2-bonding mode.

The room temperature ^{1}H NMR spectrum of **4.5** reveals four sharp singlets in a 4:12:6:18 intensity ratio and one may conclude the solution phase structure of the molecule to be of pseudo C_{2v} symmetry, which differs from that observed in the solid state (C_s). This is reasoned as the consequence of the Pn* ring-whizzing phenomenon discussed earlier (Section 3.5). The two resonances corresponding to the Pn* moiety fall within their expected range while the resonance of relative intensity four (δ = 2.16 ppm; C_6D_6), attributed to that of the methylene protons, is shifted downfield from its **3.3** starting material (δ = 0.77 ppm; C_6D_6). The ^{13}C NMR (C_6D_6) spectrum displays nine resonances, five of which correspond to Pn* carbons and two for the ^{t}Bu group at their expected values, with the resonance at δ = 44.1 ppm that of the methylene carbons, and δ = 135.6 ppm corresponding to the olefinic carbons.

Table 4.5: Selected bond lengths, angles and structural parameters for **4.5**. ESDs are given in parentheses.

Lengths (Å)			
Ti(1) - C(1)	2.3310(16)	C(1) - C(2)	1.427(2)
Ti(1) - C(2)	2.4655(15)	C(2) - C(3)	1.410(2)
Ti(1) - C(3)	2.3573(15)	C(3) - C(4)	1.450(2)
Ti(1) - C(4)	2.1306(15)	C(4) - C(5)	1.445(2)
Ti(1) - C(5)	2.3131(17)	C(5) - C(6)	1.430(2)
Ti(1) - C(6)	2.4477(16)	C(6) - C(7)	1.416(3)
Ti(1) - C(7)	2.3428(15)	C(7) - C(8)	1.447(2)
Ti(1) - C(8)	2.1297(15)	C(8) - C(1)	1.449(2)
Ti(1) - O(1)	1.9310(11)	C(4) - C(8)	1.461(2)
Ti(1) - O(2)	1.9448(11)		
Ti(1) - C(15)	2.2679(14)	C(15) - O(1)	1.3634(18)
Ti(1) - C(21)	2.2688(14)	C(21) - O(2)	1.3540(18)
Ti(1) - Pn^*_{cent}	1.931	C(15) - C(21)	1.398(2)
Ti(1) - Pn^*_{cent}	1.919	Av. C_{ring} – Me	1.502
Angles (°)			
Ti(1) - O(1) - C(15)	85.17(8)	Ti(1) - O(2) - C(21)	84.90(8)
O(1) - C(15) - C(21)	117.98(13)	O(2) - C(21) - C(15)	118.23(13)
O(1) - C(15) - C(16)	115.24(13)	O(2) - C(21) - C(22)	117.11(13)
C(22) - C(21) - C(15)	124.43(13)	C(16) - C(15) - C(21)	126.28(13)
C(15) - C(16) - C(17)	115.73(13)	C(21) - C(22) - C(23)	115.09(12)
O(1) - Ti(1) - O(2)	87.41(5)	Fold Angle	36.66

There are two proposed mechanisms in the literature for enediolate formation by carbonylation of $Cp^*_2MR_2$ species; when M = Zr, R = Me, $Cp^*_2Zr(\eta^2\text{-COMe})Me$ initially forms,[76] verified by its similar spectroscopic data to the isolated $Cp_2Zr(\eta^2\text{-COMe})Me$,[60] and this intermediate can react further at elevated temperatures with a second equivalent of CO to induce a 1,2-migratory insertion of the alkyl group into the acyl moiety, generating an η^2-ketone species.[67] Coordination of a second CO molecule is thought to be the driving force for this step and subsequent migratory insertion of the second CO molecule and rearrangement gives the enediolate product (Figure 4.20).[67, 75, 76] Conversely, when M = Th and U, and R = $CH_2{}^tBu$ and CH_2SiMe_3, $Cp^*_2M(\eta^2\text{-COR})_2$ forms, which is then able to rearrange *via* a coupling of the two acyl groups to give the enediolate connectivity (Figure 4.20).[69, 77]

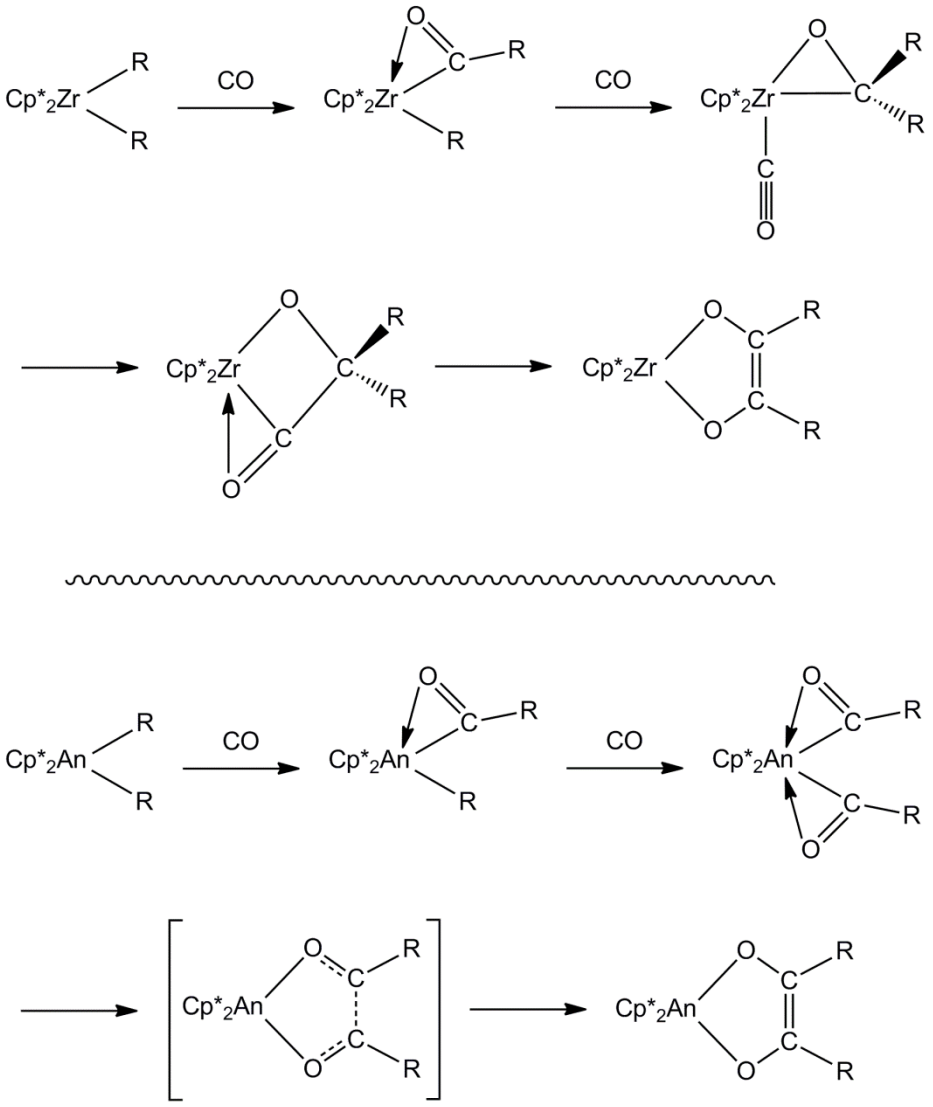

Figure 4.20: Proposed mechanisms for enediolate formation of group IV and actinide $Cp^*_2MR_2$ species.

The principal reason behind the difference in proposed mechanisms lies with the instability of the hypothetical intermediate, "$Cp^*_2Zr(\eta^2\text{-}COR)_2$", which would be highly unstable due to its unfavourable 20 electron configuration, contravening the 18 electron rule for transition metal complexes.[78] The relaxation of such electronic and steric constraints for actinide complexes results in the analogous $Cp^*_2M(\eta^2\text{-}COR)_2$ (M = Th and U) being a stable, viable intermediate as seen in the structurally characterised bis carbamoyl $Cp^*_2U[\eta^2\text{-}CO(NMe_2)]_2$.[79] The Zr analogue circumnavigates this limitation by pursuing an alternative mechanism, which includes intermediates that obey this requirement and rearrangements that have previously been observed in the literature.[67] Cross over experiments using 1:1 stoichiometric mixtures of $Cp^*_2Zr(CH_3)_2$ and $Cp^*_2Zr(CD_3)_2$, and, $Cp^*_2Th(CH_3)_2$ and $Cp^*_2Th(^{13}CH_3)_2$, have conclusively deduced

both mechanisms to proceed *via* an intramolecular pathway, as no scrambling is observed in the resulting enediolate moiety.[67, 69]

The transformation of **3.3** into **4.5** on exposure to CO is proposed to occur *via* a mechanism more closely resembling that of the actinide species stated previously, than that of the Zr complex. This is reasoned by the viable existence of the Pn*Ti(η^2-COR)$_2$ intermediate, which would contain a stable electron count of 18, due to the electronic difference between Pn* and the bis-Cp fragment, formally containing two electrons fewer. The proposed mechanism will be discussed further in Section 4.3.3.1, with the support of computational studies.

4.3.2 Synthesis and characterisation of Pn*Ti[κ^2-O-C(CH_2SiMe_3)=C(CH_2SiMe_3)-O] (4.6)

CO was admitted to a benzene solution of **3.2** in a manner identical to Section 4.3.1 (Figure 4.21) and the initial purple solution changed through red, to orange in colour. Work up was similarly completed in a glovebox and the slow cooling of a hexane solution furnished fine, needle-shaped, orange crystals in 21% yield after two crops. This was identified as Pn*Ti[κ^2-O-C(CH_2SiMe_3)=C(CH_2SiMe_3)-O] (**4.6**) by mass spectrometry (EI), revealing the molecular ion at accurate mass, followed by a peak ascribed to the loss of $SiMe_3$, and its correlation of spectroscopic data with **4.5**.

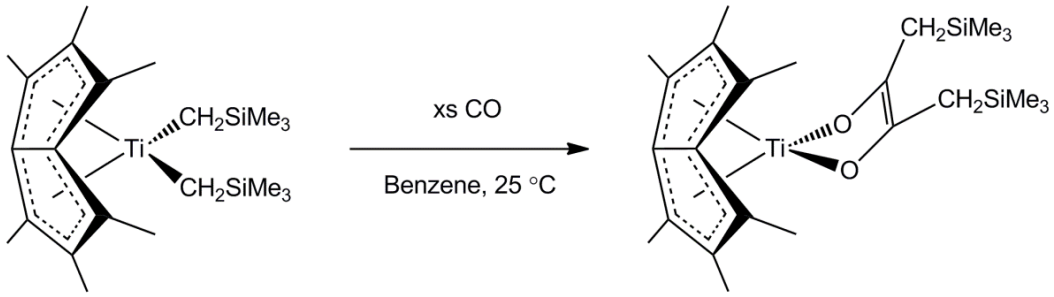

3.2 **4.6**

Figure 4.21: Synthesis of Pn*Ti[κ^2-O-C(CH_2SiMe_3)=C(CH_2SiMe_3)-O] (**4.6**).

The room temperature ^{1}H NMR spectrum of **4.6** reveals four sharp singlets in a 12:4:6:18 intensity ratio and one may conclude the solution phase structure of the molecule to be of C_{2v} symmetry, analogous to that observed for **4.5**. The singlet of lowest relative intensity corresponds to the four methylene protons (δ = 1.64 ppm; C_6D_6), which is comparatively shifted downfield from its **3.2** starting material

($\delta = -0.15$ ppm; C_6D_6) but slightly upfield to that of $Cp^*_2Th[O\text{-}C(CH_2SiMe_3)=C(CH_2SiMe_3)\text{-}O]$ (δ = 1.77 ppm; C_6D_6), one of only two $Cp^*_2MR_2$ (R = CH_2SiMe_3) species to react with CO and form an enediolate motif.[77] The two resonances corresponding to the Pn* moiety fall within their expected range and are almost coincidental with those found for **4.5** (δ = 1.96, 1.58 and 1.92, 1.55 ppm respectively; C_6D_6). The ^{13}C NMR (C_6D_6) spectrum displays eight resonances, consisting of five Pn* carbons and two for the CH_2SiMe_3 group at their expected values, with the remaining resonance at δ = 132.9 ppm, that of the olefinic carbons, which corresponds very well with the analogous chemical shift for **4.5** (δ = 135.6 ppm).

As with **4.5**, although the reaction proceeded quantitatively (as demonstrated by ^1H NMR spectroscopy), the extreme solubility of **4.6** precluded isolation in higher yields, which hampered crystallisation attempts and production of crystals suitable for single crystal X-ray diffraction. This prevented the elucidation of the solid state structure of **4.6** but due to the similarities in reactivity, colour, accurate MS of the molecular ion and ^1H and ^{13}C NMR data obtained, that it would be isostructural with **4.5**, possessing C_s symmetry and formed *via* an identical mechanism.

4.3.3 Synthesis and characterisation of $\{Pn^*Ti[\mu\text{-}\eta^1(O):\eta^2\text{-}OC(Me)_2]\}_2$ (4.7)

An identical methodology was implemented on a benzene solution of **2.7** as was undertaken in Section 4.3.1, with the aim of replicating enediolate formation from the **2.7** starting material and parallel reactivity seen for the analogous bent metallocene, $Cp^*_2ZrMe_2$.[75, 76] On interaction with CO, the initial pink solution transformed to orange in colour, akin to the formation of **4.5** and **4.6**. However, analysis of the crude products *via* ^1H NMR spectroscopy revealed a drastically different outcome, with formation of a complex mixture of species, contrasting the single product obtained with **4.5** and **4.6**. Interestingly, upon exposure to further CO, no subsequent reactivity was noted, nor any alteration in the ratio of products. This, in combination with a similar thermal stability of the mixture's components, and the unsuccessful attempts at fractional crystallisation *via* a number of methods, meant isolation of the pure individual components was not viable by this route. Hindered by a lack of specialised equipment for stoichiometric addition of gases, this problem was partially circumnavigated *via* the fine tuning of CO addition; induction of a partial vacuum into a C_6D_6 solution of **2.7** on the NMR scale, followed by vigorous shaking after CO admission, led to the predominant species

formed that of {Pn*Ti[μ-η^1(O):η^2-OC(Me)$_2$]}$_2$ (**4.7**), as indicated by ^{1}H NMR analysis (Figure 4.22). **4.7** was identified by X-ray crystallography and mass spectrometry (EI), with the latter revealing the monomer unit, Pn*TiOC(Me)$_2$, at accurate mass.

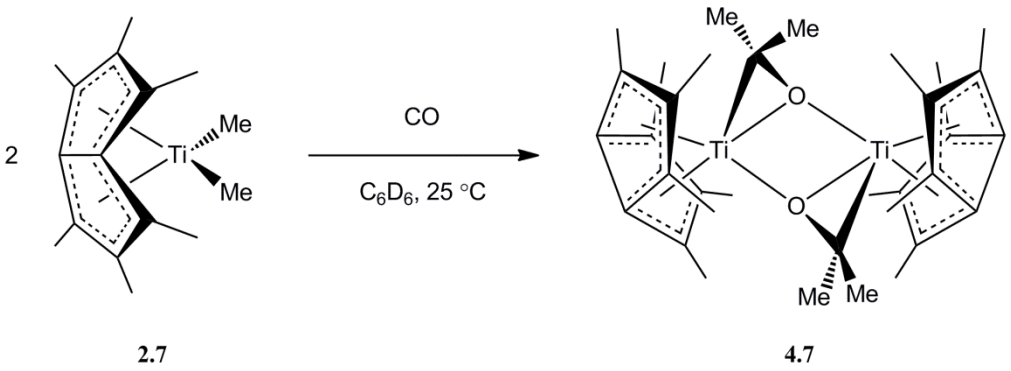

2.7 **4.7**

Figure 4.22: Synthesis of {Pn*Ti[μ-η^1(O):η^2-OC(Me)$_2$]}$_2$ (**4.7**).

This Pn* complex gave large, red crystals upon slow evaporation of a C_6D_6 solution; the resulting X-ray data was not of sufficient quality (R-factor = 10.18%), and thus can not be used to provide a comprehensive structural analysis, with detailed comparisons to pertinent literature material but may still function as a useful insight into connectivity and tentative literature comparisons. Multiple crystallisations were attempted with the aim of producing higher quality data but this was unsuccessful and is thought to be a result of the problems encountered with purifying the compound and the scale on which the reaction was conducted. A view of the solid state structure is shown in Figure 4.23.

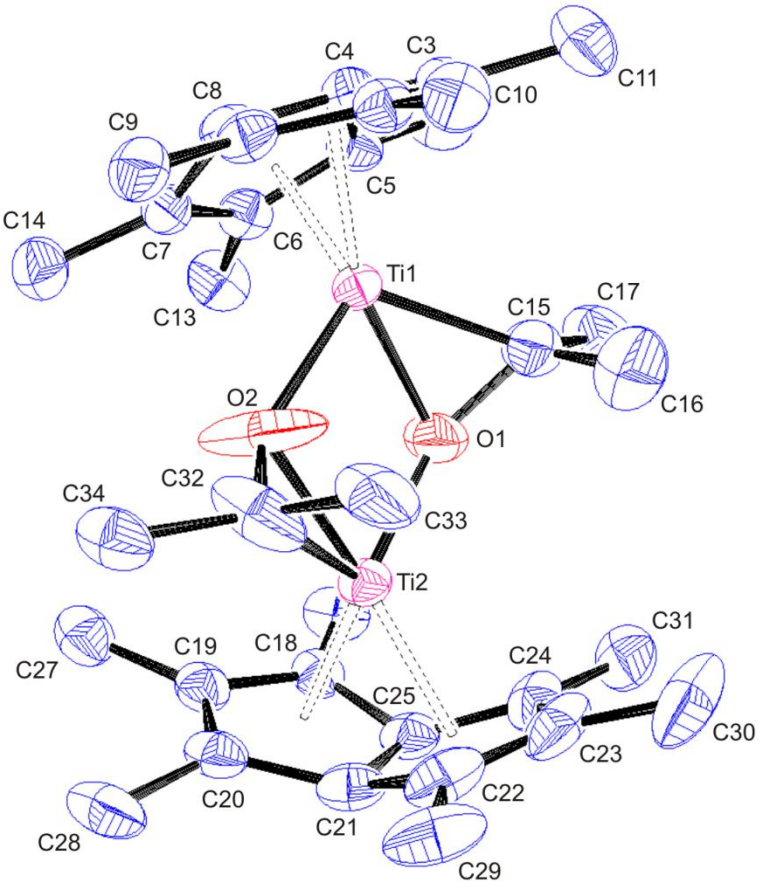

Figure 4.23: Side-on view of **4.7** with thermal ellipsoids at 50%. Hydrogen atoms omitted for clarity.

Crystallographic analysis reveals **4.7** to crystallise in the $P\bar{1}$ space group with three independent dimeric molecules in the asymmetric unit. The three molecules are almost identical geometrically, with a slight twist (34.6°) of the Pn* units towards a staggered conformation, encapsulating an alternating Ti_2O_2 core (Figure 4.24). In the solid state, **4.7** is of pseudo C_2 symmetry with the principal axis running through the centre of the Ti_2O_2 core and *via* dimerisation, the titanium centre has alleviated electron deficiency from a 14 electron monomer to the 16 electron dimer, a feature also observed in **2.1**,[80] **2.2** and **3.5**.

4.7 is only the third dimeric titanaoxirane complex to be structurally characterised with $[Cp_2Ti(\mu\text{-}OC{=}CPh_2)]_2$[81] and $\{Cp^*Ti[\mu\text{-}O\overline{CCH_2C(Me)=C(Me)CH_2}]Cl\}_2$[82] reported prior, both of which are centred around a planar Ti_2O_2 core. Due to the data quality, there is a small deviation from this but **4.7**'s core is within error for planar. The difference in average Ti-O(titanaoxirane)

and Ti-(μ-O) distances for **4.7** (2.002 and 2.047 Å), lies between the highly symmetrical {Cp*Ti[μ-OCCH$_2$C(Me)=C(Me)CH$_2$]Cl}$_2$ [2.012(2) and 1.996(2) Å][82] and the asymmetrical [Cp$_2$Ti(μ-OC=CPh$_2$)]$_2$ [2.037(2) and 2.250(3) Å],[81] although close to that of the former. Another similarity of **4.7** to {Cp*Ti[μ-OCCH$_2$C(Me)=C(Me)CH$_2$]Cl}$_2$ is the average C-O distance [1.401 and 1.408 (4) Å respectively],[82] which is comparable to those in Ti-alkoxides such as that seen in Cp$_2$Ti(OEt)Cl [1.415(4) Å],[83] demonstrating a reduction to a single bond, which is also observed for the dimeric zirconaoxiranes [Cp$_2$Zr(μ-OCPh$_2$)]$_2$ and {(η^8-COT)Zr[μ-OC(mes)$_2$]}$_2$ [1.422(4) and 1.446(22) Å respectively).[84, 85] The corresponding distance in [Cp$_2$Ti(μ-OC=CPh$_2$)]$_2$ [1.311(4) Å],[81] is considerably shorter and thus possesses double bond character, which is emphasised when compared to the parameter in the parent ketone, acetone (1.210 Å).[86] The average Ti-C(titanaoxirane) distance (2.149 Å) is slightly elongated but comparable to the corresponding lengths in {Cp*Ti[μ-OCCH$_2$C(Me)=C(Me)CH$_2$]Cl}$_2$ and [Cp$_2$Ti(μ-OC=CPh$_2$)]$_2$ [2.094(3) and 2.099(3) Å respectively],[82, 81] and in all three examples the Ti-O bonds are shorter than the Ti-C distances, consistent with the high oxophilicity of titanium. The carbon atoms C(15) and C(32) are positioned in a *syn* arrangement relative to the Ti$_2$O$_2$ core (Figure 4.24), this is opposite to that found for {Cp*Ti[μ-OCCH$_2$C(Me)=C(Me)CH$_2$]Cl}$_2$, which possesses an *anti* arrangement, although the corresponding distances from the plane of best fit and dihedral angle compare well (0.843, 0.629 and 0.889 Å; 138.6, 148.7 and 138.7° respectively).[82]

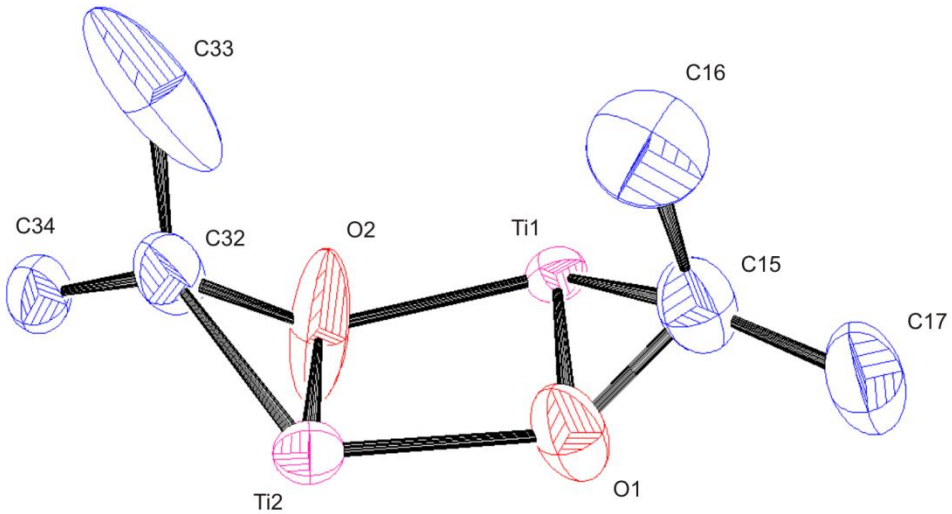

Figure 4.24: Central core of **4.7** with thermal ellipsoids at 50%. Hydrogen atoms and Pn* omitted for clarity.

Table 4.6: Selected bond lengths, angles and structural parameters for one of the molecules in the asymmetric unit of **4.7**. ESDs are given in parentheses.

Lengths (Å)			
Ti(1) - C(1)	2.407(6)	Ti(2) - C(18)	2.376(6)
Ti(1) - C(2)	2.515(6)	Ti(2) - C(19)	2.507(6)
Ti(1) - C(3)	2.356(6)	Ti(2) - C(20)	2.375(7)
Ti(1) - C(4)	2.143(6)	Ti(2) - C(21)	2.134(6)
Ti(1) - C(5)	2.410(6)	Ti(2) - C(22)	2.340(7)
Ti(1) - C(6)	2.496(6)	Ti(2) - C(23)	2.500(7)
Ti(1) - C(7)	2.362(6)	Ti(2) - C(24)	2.419(6)
Ti(1) - C(8)	2.146(6)	Ti(2) - C(25)	2.153(6)
Ti(1) - O(1)	2.017(5)	Ti(2) - O(1)	2.070(5)
Ti(1) - O(2)	2.023(6)	Ti(2) - O(2)	1.987(6)
Ti(1) - C(15)	2.112(8)	Ti(2) - C(32)	2.185(7)
C(15) - O(1)	1.418(9)	C(32) - O(2)	1.384(12)
C(1) - C(2)	1.409(9)	C(18) - C(19)	1.433(9)
C(2) - C(3)	1.397(9)	C(19) - C(20)	1.415(9)
C(3) - C(4)	1.461(9)	C(20) - C(21)	1.447(10)
C(4) - C(5)	1.415(9)	C(21) - C(22)	1.429(11)
C(5) - C(6)	1.429(9)	C(22) - C(23)	1.385(13)
C(6) - C(7)	1.425(9)	C(23) - C(24)	1.416(11)
C(7) - C(8)	1.445(9)	C(24) - C(25)	1.429(10)
C(8) - C(1)	1.430(9)	C(25) - C(18)	1.435(9)
C(4) - C(8)	1.463(9)	C(21) - C(25)	1.450(9)
Ti(1) - Pn^*_{cent}	1.972	Ti(2) - Pn^*_{cent}	1.973
Ti(1) - Pn^*_{cent}	1.968	Ti(2) - Pn^*_{cent}	1.965
Ti(1) - Ti(2)	3.1033(14)		
Angles (°)			
Ti(1) - O(1) - Ti(2)	98.8(2)	Ti(2) - O(2) - Ti(1)	101.4(3)
O(1) - Ti(2) - O(2)	78.8(2)	O(2) - Ti(1) - O(1)	79.3(2)
Ti(1) - O(1) - C(15)	73.5(4)	Ti(2) - O(2) - C(32)	78.5(5)
Ti(1) - C(15) - O(1)	66.4(4)	Ti(2) - C(32) - O(2)	63.1(3)
O(1) - Ti(1) - C(15)	40.1(3)	O(2) - Ti(2) - C(32)	38.4(3)
Fold Angle	32.87	Fold Angle	33.45

The room temperature ^{1}H NMR spectrum of **4.7** reveals four sharp singlets in a 12:12:12:12 intensity ratio and one may conclude that the solution phase structure shares the same C_2 symmetry observed in the solid state. As a result of the reduced symmetry in the molecule, the Pn* resonances are split into three sets of equal intensity,

resulting in two pairs of independent NWT-Me protons. The WT-Me resonance was found to occur at higher field to the remaining two Pn* resonances, as observed for other C_2 symmetric complexes reported in this chapter, **4.1**, **4.2**, **4.3** and **4.4**. The remaining resonance is found furthest upfield and corresponds to the η^2-OC(*Me*)$_2$ group (δ = 1.13 ppm; C_6D_6). This is in reasonable agreement with those observed for Cp*TaMe$_2$[η^2-OC(Me)$_2$] and Cp*TaCl$_2$[η^2-OC(Me)$_2$] (δ = 1.83 ppm; toluene-d_8 and 1.85 ppm; C_6D_6, respectively).[87, 88] The corresponding ^{13}C NMR chemical shift is in very good agreement (δ = 29.6 and 28.1 ppm respectively) and the titanaoxirane carbon compares very well with that seen for the dimeric group IV metallaoxirane {Cp$_2$Zr[μ-OC(Ph)$_2$]}$_2$ (δ = 90.1 and 92.6 ppm respectively; C_6D_6).[85] The remainder of the ^{13}C NMR (C_6D_6) spectrum displays eight resonances, all of which correspond to Pn* carbons as the result of reduced symmetry in the molecule; the bridgehead carbons are non-equivalent, which is contrary to that observed for other C_2 symmetric compounds **4.1**, **4.2**, **4.3** and **4.4**, postulated to be a result of the principal axis not bisecting the Pn* ligand.

As previously mentioned, initial attempts to follow a parallel synthesis to the formation of **4.5** and **4.6** led to the generation of a complex mixture of products. Although the complete elucidation of this mixture could not be accomplished, partial assignment was achieved through comparisons of ^{1}H and ^{13}C NMR data to previously synthesised complexes and literature material, along with assistance from other analytical tools such as mass spectrometry and single crystal X-ray diffraction. Using a range of 2D-NMR techniques (NOESY, HMBC and HMQC), it was found that a carbon atom (δ = 135.3 ppm; C_6D_6) bearing no protons was connected to a methyl group; this chemical shift correlated extremely well with those seen for olefinic carbons in **4.5** and **4.6** (δ = 135.6 and 132.9 ppm respectively; C_6D_6), suggesting the possible presence of an enediolate moiety, which was further supported by the discovery of Pn*Ti($O_2C_2Me_2$) at accurate mass [found (calculated): 320.1258 (320.1256)]. Final confirmation of the simultaneous production of Pn*Ti[κ^2-O-C(Me)=C(Me)-O] was revealed by single crystal X-ray diffraction, which affirmed its formation as part of a co-crystallised enediolate-titanaoxirane dimer (Figure 4.25). As with **4.7**, the resulting X-ray data was not of sufficient quality, but may still provide an insight into the gross features of the molecule's connectivity. The enediolate moiety is bound in an asymmetrical fashion to the two Pn*Ti fragments; primarily it binds through both oxygen atoms to each Ti but it

is also heavily puckered about its O-O vector, resulting in a close approach of the olefin moiety towards Ti(2) in a similar σ^2, π-bonding mode to **4.5**, and formally acting as a four electron donor. The titanaoxirane moiety is coordinated in an identical manner to **4.7**, binding η^2- to one Ti and bridging the other through its oxygen atom in a μ-η^1(O):η^2-OC(Me)$_2$ fashion. Overall there is a central Ti_2O_3 core positioned in a trigonal bipyramidal arrangement, with Ti occupying both the apical positions, encapsulated by two Pn* ligands, with each metal centre formally possessing a stable electron count of 18.

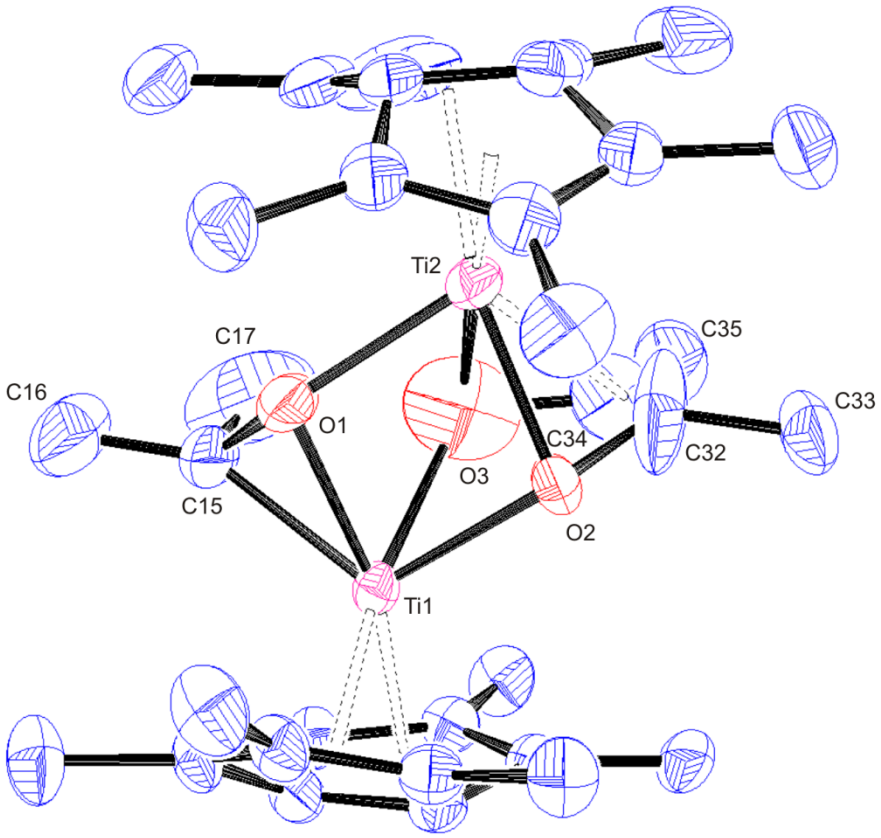

Figure 4.25: Side-on view of {(Pn*Ti)$_2$[μ-η^1(O):η^2-OC(Me)$_2$][μ-κ^2-O-C(Me)=C(Me)-O]} with thermal ellipsoids at 40%. Hydrogen atoms omitted for clarity.

This is not the first structurally characterised example of a mixed enediolate-metallaoxirane dimer in the literature; it was found that the reactive hafnacyclobutane $Cp_2Hf(CH_2)_3$, rapidly absorbed 1.5 equivalents of CO under ambient conditions, to form a 1:1 adduct of enediolate-metallaoxirane as the sole product in good yield (Figure 4.26).[89] The pronounced difference between the two structures is the coordination mode of the enediolate moiety; in the Hf example, only one oxygen atom

bridges the adjacent metal centre and the five membered metallaheterocycle is near planar, whereas for the Ti complex, both oxygens bridge and there is a large fold about the O-O vector. This is postulated to be another example of differing coordination modes in similar systems as a result of substitution of Pn* into a bis-Cp species, due to it formally containing two fewer electrons; in both examples the formal electron count on all metal centres is 18.

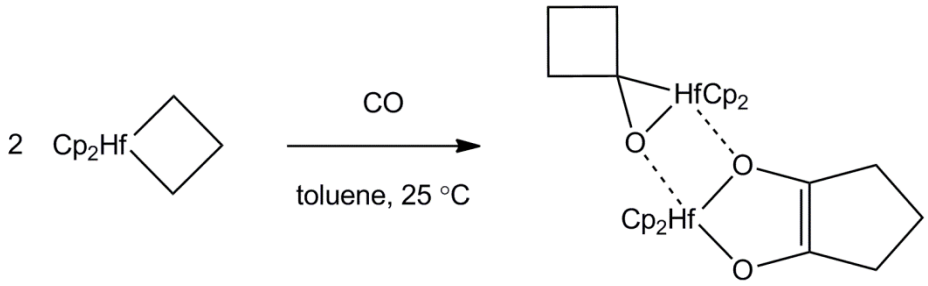

Figure 4.26: Reaction scheme of $Cp_2Hf(CH_2)_3$ with CO.

Also present in the ^{1}H NMR spectrum of the initial complex mixture of products were two distinctive resonances of equal intensity downfield in the vinylic region at δ = 4.11 and 5.09 ppm (C_6D_6), which are in reasonable agreement with those seen for the non-equivalent methylene protons in the metal ketene complex $Cp_2Ti(\eta^2\text{-}OC{=}CH_2)$ (δ = 3.88 and 4.85 ppm; C_6D_6).[90] Further investigation utilising 2D-NMR techniques (HMBC and HMQC), concluded the methylene group to be connected to a carbon bearing no protons at very highfield (δ = 218.8 ppm; C_6D_6), which agrees excellently with that found for enriched $Cp_2Ti(\eta^2\text{-}O^{13}C{=}CH_2)$ (δ = 220.4 ppm; C_6D_6). On occasion during the numerous attempts at processing X-ray data in the quest to elucidate the solid state structures of this mixture, the processing software employed struggled to decipher between a methylene group or two methyls attached to the titanaoxirane moiety. This may just be the trivial result of poor quality X-ray data but with the additional ^{1}H and ^{13}C data and its similarity to $Cp_2Ti(\eta^2\text{-}OC{=}CH_2)$, the tentative assignment of a $Pn^*Ti(\eta^2\text{-}OC{=}CH_2)$ ketene species has been made, although the mechanism of its formation remains unclear.

4.3.3.1 DFT analysis of Pn^*TiR_2 reaction mechanism with CO

In order to gain a greater understanding of the mechanism involved for the formation of **4.7** and the competing pathway for enediolate (c.f. **4.5** and **4.6**) formation,

DFT calculations were performed by Dr. Muhsen Al-Ibadi. Geometry optimisations were conducted on the simplified unsubstituted **2.7** analogue, $PnTiMe_2$ without any symmetry constraints, for all intermediates and transition states for its reactivity with CO. A schematic representation of the potential energy surface for the migratory CO insertion and subsequent reactivity is depicted in Figure 4.27.

The initial step of all mechanisms operating to produce the types of products seen (**4.7** and **4.5**/**4.6**) is migratory insertion and coordination of the of the electrophillic CO molecule to the electron deficient metal centre (**Ti1**→**Ti2**). Detailed mechanistic and computational studies have been conducted for the related Cp_2ZrMe_2,[61, 65–67] which concluded that the most kinetically and thermodynamically favourable approach of CO was in the Me-Zr-Me plane from a lateral direction, lying 1.3 kcal mol^{-1} below the sum of the reactants.[66] The lateral/central argument of CO approach to **Ti1** is not applicable as its lowest energy approach is perpendicular to the Me-Ti-Me plane. Coordination is however, significantly more energetically favourable with **Ti2** lying 11.4 kcal mol^{-1} below **Ti1**, presumably a result of **Ti1** possessing a greater electron deficiency, being a 14 electron complex compared to Cp_2ZrMe_2, hence greater stabilisation is achieved upon CO coordination.

The migratory insertion step (**Ti2**→**Ti3**) is marginally uphill in energy but this outlay is then recouped and further stabilisation occurs upon η^2-COMe coordination (**Ti4**), which is significantly more stable than η^1-COMe by 23.9 kcal mol^{-1}, a trend paralleled in Cp_2MMe_2 (M = Ti, Zr and U) species, although to a lesser extent.[66, 67, 69] As with the lateral/central argument of CO approach to Cp_2ZrMe_2 not being relevant to this Pn* system, nor is the observed rearrangement put forward for η^2, O-outside → O-inside conversion, postulated to proceed *via* an η^1 intermediate. There is minimal rearrangement involved for **Ti4**→**Ti5**, as seen by its extremely small energy barrier (1.9 kcal mol^{-1}) and it is at this point where the mechanisms for the two different products diverge.

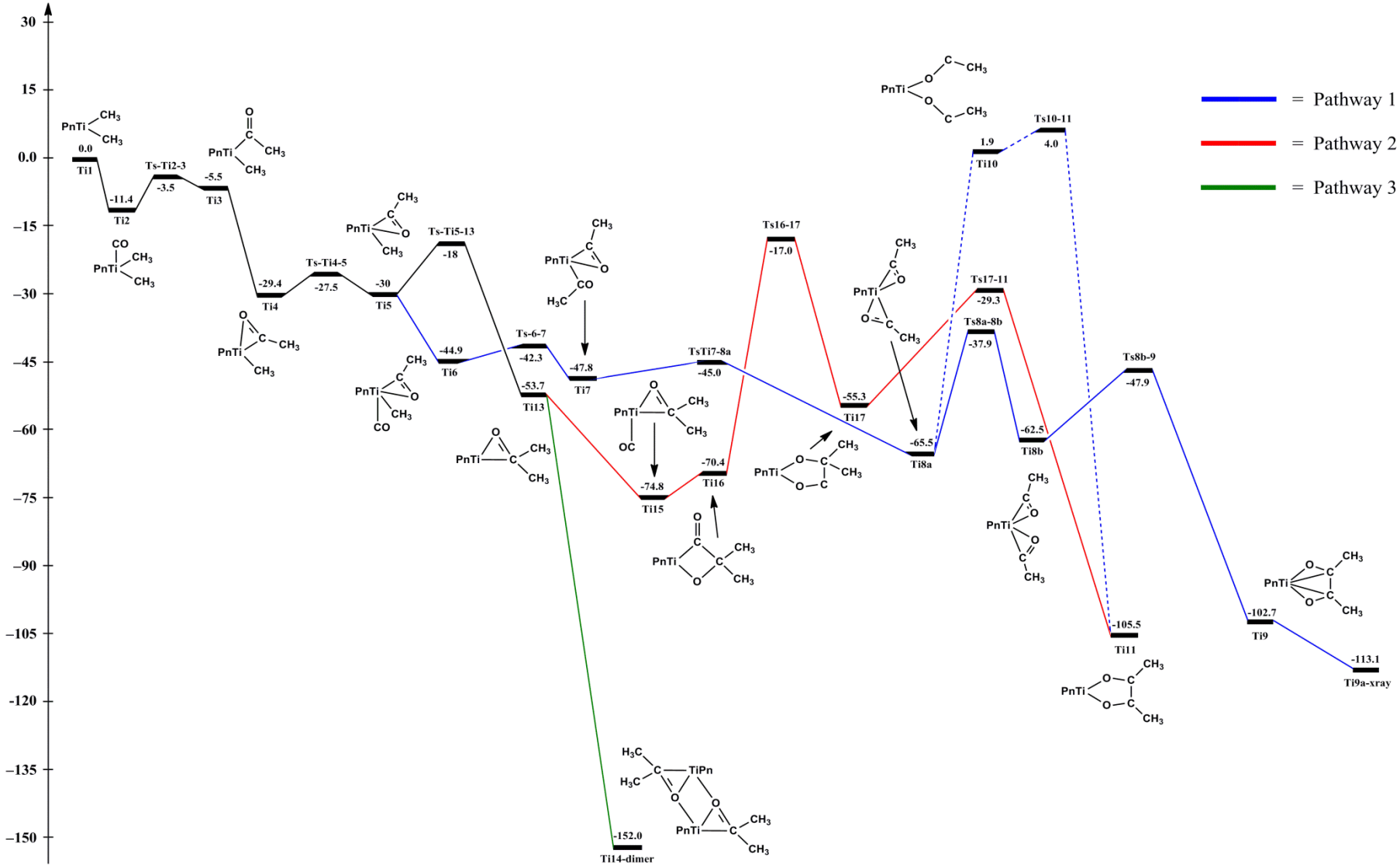

Figure 4.27: Schematic representation of the potential energy surface for the reaction of $PnTiMe_2$ with CO.

If an excess of CO is present, coordination of a second equivalent to the Ti centre and subsequent migratory insertion is a very facile process and energetically favourable, forming **Ti7**. Enediolate formation *via* this route (**pathway 1**, Figure 4.27) more closely resembles that of the postulated pathway for Cp_2AnR_2 (An = U, Th) species, as formation of $PnTi(\eta^2\text{-COMe})_2$ (**Ti8a**) is more stable than $PnTi(\eta^2\text{-COMe})(\eta^1\text{-COMe})$ (**Ti7**) by 17.7 kcal mol^{-1}. The reason this coordination mode is accessible is due to Pn formally containing two fewer electrons than a bis-Cp unit, making the resulting **Ti8a**, an 18 electron species, which does not contravene the 18 electron rule, as would the hypothetical 20 electron species, $Cp_2Zr(\eta^2\text{-COMe})_2$ (this rule is relaxed for actinide f-elements). Rearrangement of **Ti8a** and formation of the enediolate moiety possesses an energy barrier of 27.6 kcal mol^{-1} but overall is exothermic, with **Ti9a-xray** 47.6 kcal mol^{-1} lower in energy. An alternative pathway *via* the coupling of an oxycarbene species (**Ti10**), previously postulated as a possible intermediate for enediolate formation,[67, 69] was found to be extremely unfavourable and very high in energy with a barrier of activation significantly higher (67.4 *vs* 27.6 kcal mol^{-1}).

Two alternative pathways initially involve migratory insertion of the second Me group into the acyl moiety to generate an η^2-ketone structure (**Ti13**), the second mechanistic crossroad of the scheme, with an energy barrier of 12.0 kcal mol^{-1} but overall 23.7 kcal mol^{-1} more stable than **Ti5**. **Pathway 2** (Figure 4.27) parallels the mechanism[67] postulated for $Cp^*_2Zr[O\text{-}C(Me)=C(Me)\text{-}O]$ formation from $Cp^*_2ZrMe_2$ and is energetically viable, overall being 51.8 kcal mol^{-1} more favourable but also possessing an energy barrier of 53.4 kcal mol^{-1}. In direct competition with this is dimerisation of **Ti13** to form **Ti14-dimer** (**pathway 3**), the postulated mechanism of **4.7** formation, which is significantly (98.3 kcal mol^{-1}) more exothermic and hugely energetically more favourable. This is one of the reasons why enediolate formation is predicted to proceed *via* **pathway 1**, as opposed to **pathway 2** for the latter is in direct competition with the significantly more energetically favourable **pathway 3** and concomitantly possesses a higher energy of activation (53.4 compared with 27.6 kcal mol^{-1}), making it less likely to occur.

The proportion of molecules entering each pathway is postulated to be determined by the concentration of CO, with the fate of **Ti5** the crucial factor; if one or fewer equivalents of CO are present **pathway 3** will be favoured but with an excess

pathway 1 will compete and the relative rates of each will determine the distribution of products. The fine tuning required for the synthesis of **4.7**, resulted in only a partial vacuum being induced in the reaction vessel hence, fewer equivalents of CO were added compared to the methods implemented in the formation of **4.5**, **4.6** and the initial complex mixture. This resulted in a greater proportion of **2.7** following **pathway 3** and led to the predominant species formed that of the dimeric titanaoxirane **4.7**, as observed by ^{1}H NMR spectroscopy.

The reason why **4.5** and **4.6** were produced as the sole product in their respective reactions is thought to occur due to the potentially unfavourable steric interactions on formation of the **Ti13** intermediate, with the sterically demanding $CH_2{}^{t}Bu$ and CH_2SiMe_3 groups. The lack of observed titanaoxirane in **4.5** and **4.6** production, further supports enediolate formation proceeding *via* **pathway 1** because if formation was *via* **pathway 2** it would be expected that **pathway 3** would operate simultaneously as they share the same intermediate, **Ti13**.

To unequivocally verify these claims, further investigations utilising specialised equipment (e.g. Toepler pump) capable of adding precise equivalents of CO are needed but unfortunately time constraints and resources prevented this.

4.3.4 Reaction of Pn*Ti(CH$_2$Ph)$_2$ (3.1) with CO

Reaction of a benzene solution of **3.1** with CO, was conducted in an identical manner to that described in Section 4.3.1. On addition of CO the initial dark brown solution lightened to red-orange in colour and a bright red solid was precipitated. Analysis of the solution failed to yield any identifiable products using mass spectrometry or NMR techniques with the latter's ^{1}H NMR spectrum proving complex. The red solid was found to be extremely insoluble in all hydrocarbon, aromatic and ethereal solvents tested, which prevented its identification. Interestingly, exposure of this heterogeneous mixture to further CO *via* an additional freeze-pump-thaw cycle, led to dissolution of the red precipitate and formation of a red-yellow solution, which possessed an equally ambiguous, complex ^{1}H NMR spectrum.

The lack of isolable products is not fully understood but it is thought the Pn* containing fragment may well be present in the initially formed red precipitate but subsequently decomposes on exposure to excess CO. There is precedent in the literature

for Ti-CH_2Ph complexes to cleanly react with CO, with the carbonylation of the related $Cp_2Ti(CH_2Ph)_2$ in heptane, producing dibenzyl ketone and $Cp_2Ti(CO)_2$[91] (Figure 4.28).

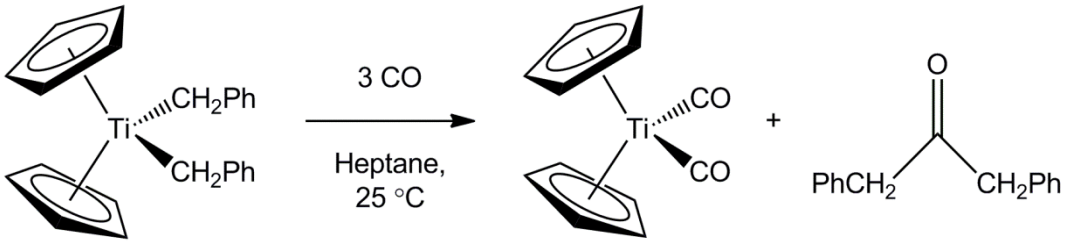

Figure 4.28: Reaction of $Cp_2Ti(CH_2Ph)_2$ with CO.

The reaction may be regarded as a reductive elimination assisted by CO and had provided an alternative, high yielding route to $Cp_2Ti(CO)_2$,[91] which precluded the need for high pressure and temperature previously required.[92] The mechanism involves initial formation of a mixed benzyl, acyl complex prior to a second benzyl transfer to generate the ketonic fragment.[68]

It is uncertain if the red solid was the Pn* equivalent of $Cp_2Ti(CO)_2$, $Pn^*Ti(CO)_2$, which was unstable under the reaction conditions or another Pn*Ti containing species altogether. Importantly no dibenzyl ketone [$(CH_2Ph)_2CO$] was observed, so it is unclear if a parallel mechanism to that of $Cp_2Ti(CH_2Ph)_2$ with CO was operating.

4.4 Reactions with H_2

Metal hydride complexes of the d-block play an important role in synthetic, structural and catalytic inorganic and organometallic chemistry.[93–95] Indeed, the vast majority of all the significant industrial processes in the petrochemical industry depend on the involvement of an M–H moiety in one or more key steps.[95] One of the simplest methods to form M-H bonds is to expose highly reactive M-alkyl species to a H_2 atmosphere (hydrogenolysis).[96] It is recognised that there are two, fundamentally different mechanisms for cleaving dihydrogen with metal-alkyl species; the first, oxidative addition, occurs at electron rich, coordinatively unsaturated metal centres, usually found for the later transition elements [Figure 4.29 (a)] and the second, σ-bond metathesis by coordinatively unsaturated electron deficient metal centres. The latter process, whereby ligand exchange is mediated at the metal centre, without formal

oxidative addition taking place, typically utilises d^0 metals and involves a four centre transition state [Figure 4.29 (b)].[97]

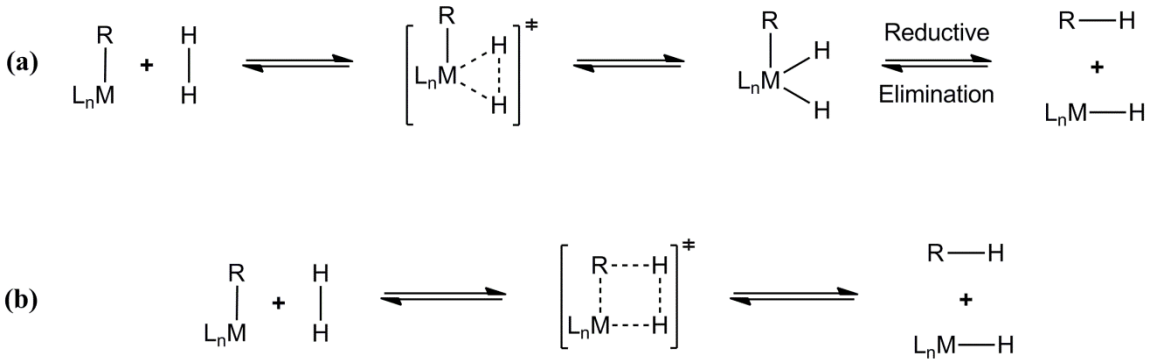

Figure 4.29: Reaction pathway for (a) oxidative addition and (b) σ-bond metathesis of a H_2 moiety.

A limitation of this method is the sometimes unpredictable and complex nature of the reactivity and subsequent products produced. For example, in solution Cp_2TiMe_2 is reduced to form the Ti^{III} dimeric fulvalene $[Cp(C_5H_4)Ti(\mu\text{-}H)]_2$,[98] whose solid state structure was confirmed some 36 years after its initial synthesis.[99] Comparatively, the action of H_2 on solid Cp_2TiMe_2 is postulated to yield $[Cp_2Ti(\mu\text{-}H)]_2$[100] and the analogous $Cp^*_2TiMe_2$ does not react, even at elevated temperatures.[101]

NMR and IR spectroscopy have proved keystone techniques in the study of M-H systems, especially as many hydride complexes are fluxional on the NMR timescale and posses characteristic signatures. The elucidation of solid state structures by standard diffraction techniques encounters substantial problems; the low scattering ability of hydrogen in the proximity of heavier elements makes accurate location of hydrides particularly difficult by X-ray diffraction. Although developments in modern instrumentation and software have improved this situation, the superlative technique for full and accurate structural characterisation remains neutron diffraction. This can be prohibitive as the high cost and low availability connected with the technique renders it applicable only to a limited number of systems.

4.4.1 Synthesis and characterisation of $[Pn^*Ti(\mu_2\text{-}H)]_3(\mu_3\text{-}H)$ (4.8)

A benzene solution of **3.2** was degassed as described in Section 4.2.1, after which H_2 gas was introduced (Figure 4.30), and the initial purple solution gradually turned blue-grey in colour. Work up was completed in a glovebox and slow cooling of a

hexane solution furnished a very dark purple crystalline solid in poor yield (24%), which was consistent with [Pn*Ti(μ_2-H)]$_3$(μ_3-H) (**4.8**) using X-ray crystallography in combination with NMR spectroscopy.

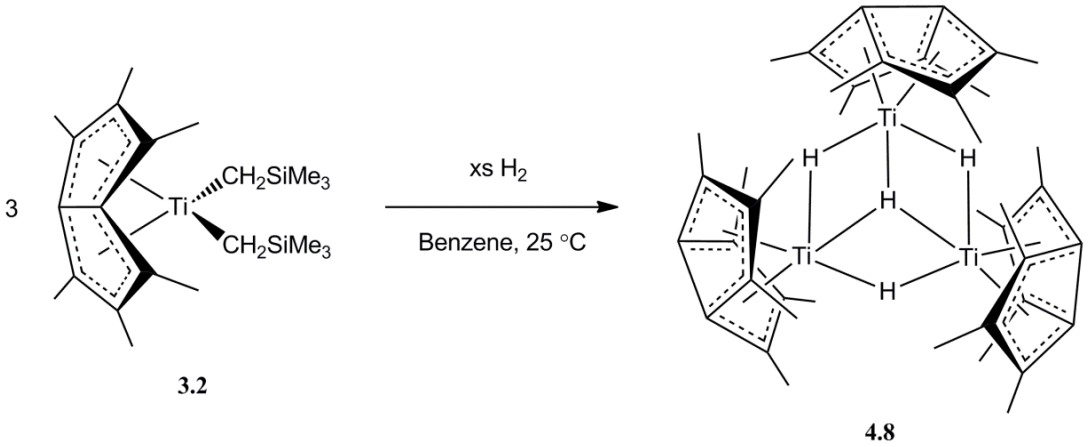

3.2 **4.8**

Figure 4.30: Synthesis of [Pn*Ti(μ_2-H)]$_3$(μ_3-H) (**4.8**).

Single crystals suitable for X-ray diffraction were grown by slow cooling of a solution in the same solvent to −35 °C, and two views of the structure are shown (Figure 4.31 and 4.32).

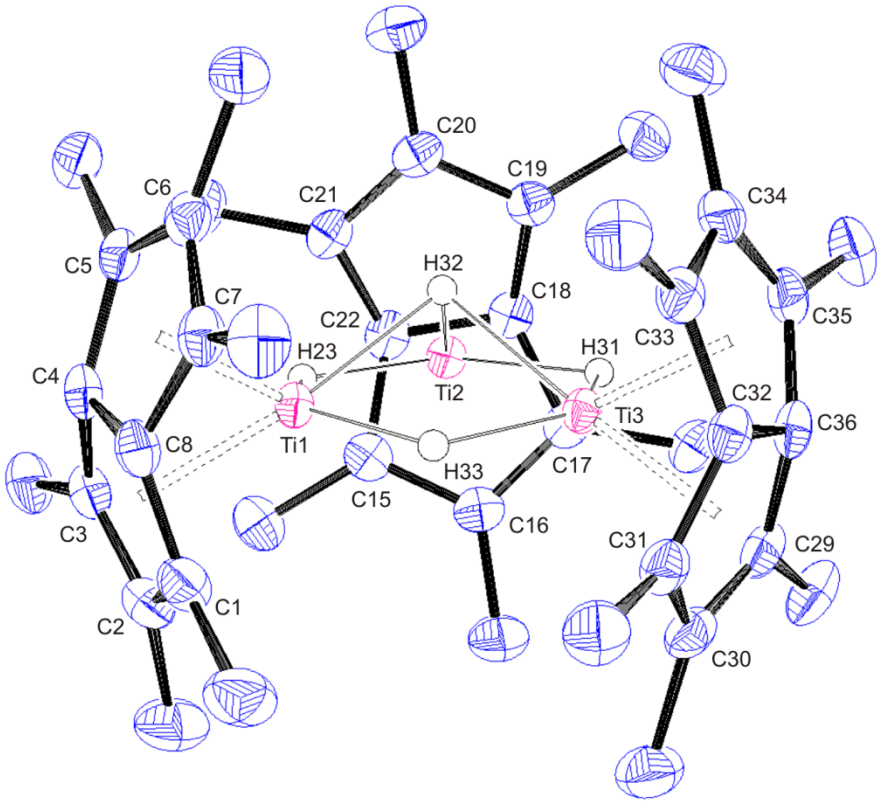

Figure 4.31: Side-on view of **4.8** with thermal ellipsoids at 50%. Hydrogen atoms and hexane molecule omitted for clarity.

4.8 crystallises in the $P2_1/n$ space group with one independent molecule in the asymmetric unit, which possesses C_3 symmetry, and a co-crystallised solvent molecule. The structure reveals an unusual trimeric $(Pn^*Ti)_3$ cluster, with three Ti atoms at the apices of a hypothetical equilateral triangle, capped by a (μ_3-H) moiety and symmetrically bridged by three (μ_2-H), to form a six membered Ti_3H_3 ring. Although the hydrogens could not be located on a Fourier difference map, a common problem with hydrides in X-ray diffraction,[95] the structure is in excellent agreement with data extracted from the ^{1}H NMR spectrum by careful integration over the hydridic protons (*vide infra*). The principal axis intersects H(32) and the centre point of the hypothetical Ti triangle and is the first structurally characterised example of a trimeric titanium hydride species as well as the first to incorporate a Ti-(μ_3-H) moiety in the literature.

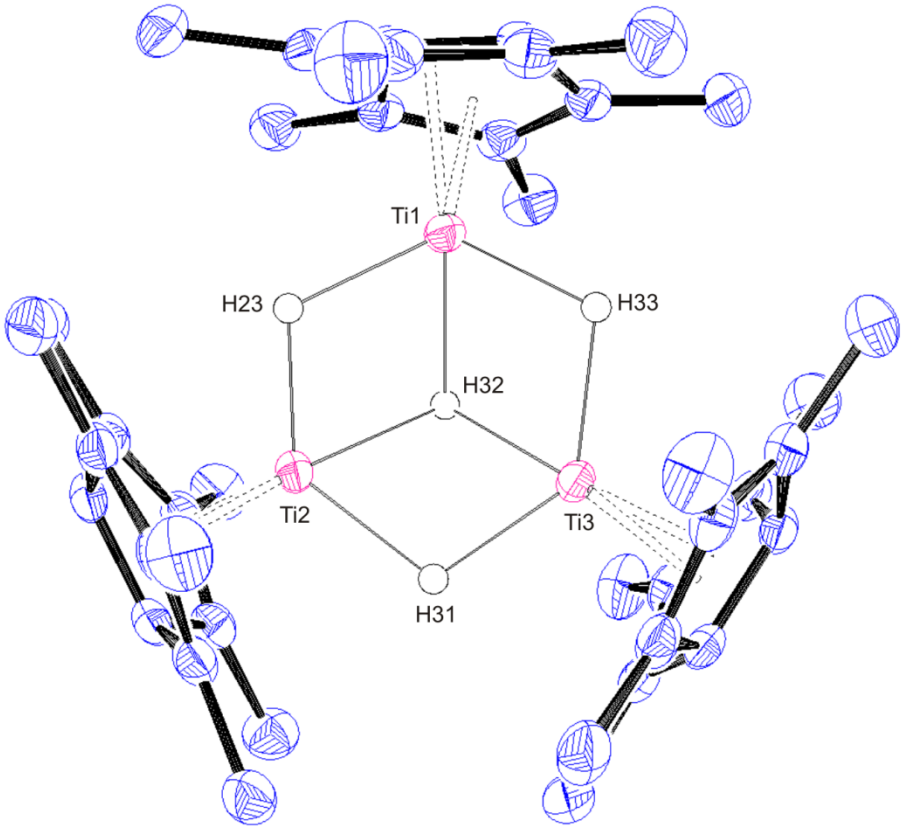

Figure 4.32: Bottom view of **4.8** with thermal ellipsoids at 50%. Hydrogen atoms and hexane molecule omitted for clarity.

The six membered Ti_3H_3 ring is approximately planar, with no atom deviating by more than 0.055 Å from a plane of its best fit. It is structurally very similar to its group IV congener $\{[(Me_2Si)_2(\eta^5\text{-}C_5H_3)_2]Zr\}_3(\mu_3\text{-}H)_2(\mu_2\text{-}H)_3$, synthesised *via* a parallel method of H_2 addition to the alkyl, $[(Me_2Si)_2(\eta^5\text{-}C_5H_3)_2]ZrMe_2$, although elevated temperatures (100 °C) were required.[102] The Zr_3H_3 ring is also nearly co-planar but is capped by two (μ_3-H), as opposed to one in **4.8**, resulting in a formal $Zr^{IV}/Zr^{IV}/Zr^{III}$ mixed valence, paramagnetic species, that is postulated to possess some Zr-Zr interaction.[102] The compound is completely insoluble in common organic solvents and the only characterising data reported was the solid state structure. This contrasts that observed for diamagnetic **4.8**, which is postulated to formally be a $Ti^{III}/Ti^{III}/Ti^{IV}$ mixed valence species, on account of charge balancing and its diamagnetism. Supporting this postulation are two similar and one distinct fold angle on the Pn* ligands (33.2, 33.0 and 31.9°), indicating the possible presence of a separate oxidation state on one of the titanium centres. There is also a slight elongation of average Ti-Pn*$_{cent}$ distance at this

unique Ti(2) (1.989 *vs.* 1.982 and 1.978 Å), which is thought to be the Ti^{IV} centre. As mentioned previously, the angles between the Ti atoms (59.9, 60.3 and 59.8°) essentially form an equilateral triangle, with an average Ti-Ti distance of 2.937 Å, which is between the values observed for the similar trimeric Ti species $[Cp^*Ti(\mu_2\text{-}O)]_3(\mu_3\text{-}CMe)$ and $\{[CpTi(\mu_2\text{-}OMe)(OMe)]_3(\mu_3\text{-}O)\}\{BPh_4\}$ (2.820 and 3.176 Å respectively).[103, 104]

Table 4.7: Selected bond lengths, angles and structural parameters for **4.8**. ESDs are given in parentheses.

Lengths (Å)					
Ti(1) - C(1)	2.3665(17)	Ti(2) - C(15)	2.3520(16)	Ti(3) - C(29)	2.3738(15)
Ti(1) - C(2)	2.5265(17)	Ti(2) - C(16)	2.5260(16)	Ti(3) - C(30)	2.5269(16)
Ti(1) - C(3)	2.4255(16)	Ti(2) - C(17)	2.4276(16)	Ti(3) - C(31)	2.4081(16)
Ti(1) - C(4)	2.1501(15)	Ti(2) - C(18)	2.1546(15)	Ti(3) - C(32)	2.1490(15)
Ti(1) - C(5)	2.3454(16)	Ti(2) - C(19)	2.3788(16)	Ti(3) - C(33)	2.3584(16)
Ti(1) - C(6)	2.5141(16)	Ti(2) - C(20)	2.5421(16)	Ti(3) - C(34)	2.5040(16)
Ti(1) - C(7)	2.4302(16)	Ti(2) - C(21)	2.4337(15)	Ti(3) - C(35)	2.4092(16)
Ti(1) - C(8)	2.1561(15)	Ti(2) - C(22)	2.1510(15)	Ti(3) - C(36)	2.1506(15)
Ti(1) - Ti(2)	2.9456(4)	Ti(2) - Ti(3)	2.9304(4)	Ti(3) - Ti(1)	2.9356(4)
C(1) - C(2)	1.423(3)	C(15) - C(16)	1.419(2)	C(29) - C(30)	1.410(3)
C(2) - C(3)	1.409(2)	C(16) - C(17)	1.412(2)	C(30) - C(31)	1.412(2)
C(3) - C(4)	1.442(2)	C(17) - C(18)	1.437(2)	C(31) - C(32)	1.439(2)
C(4) - C(5)	1.438(2)	C(18) - C(19)	1.437(2)	C(32) - C(33)	1.444(2)
C(5) - C(6)	1.428(2)	C(19) - C(20)	1.420(2)	C(33) - C(34)	1.425(2)
C(6) - C(7)	1.409(2)	C(20) - C(21)	1.411(2)	C(34) - C(35)	1.411(2)
C(7) - C(8)	1.438(2)	C(21) - C(22)	1.440(2)	C(35) - C(36)	1.436(2)
C(8) - C(1)	1.444(2)	C(22) - C(15)	1.441(2)	C(36) - C(29)	1.442(2)
C(4) - C(8)	1.453(2)	C(18) - C(22)	1.451(2)	C(32) - C(36)	1.449(2)
Ti(1) - Pn^*_{cent}	1.985	Ti(2) - Pn^*_{cent}	1.995	Ti(3) - Pn^*_{cent}	1.983
Ti(1) - Pn^*_{cent}	1.978	Ti(2) - Pn^*_{cent}	1.983	Ti(3) - Pn^*_{cent}	1.972
Av. C_{ring} - Me	1.499	Av. C_{ring} - Me	1.499	Av. C_{ring} - Me	1.500

Angles (°)	
Ti(1) - Ti(2) - Ti(3)	59.947(9)
Ti(1) - Ti(3) - Ti(2)	60.284(9)
Ti(2) - Ti(1) - Ti(3)	59.770(9)
Fold Angle	33.01 & 31.86 & 33.15

Unlike the insoluble, paramagnetic $\{[(Me_2Si)_2(\eta^5\text{-}C_5H_3)_2]Zr\}_3(\mu_3\text{-}H)_2(\mu_2\text{-}H)_3$,[102] **4.8** demonstrates moderate solubility in aromatic and hydrocarbon solvents and solution

phase characterising data could be obtained. The room temperature ^{1}H NMR spectrum of **4.8** reveals three resonances, two sharp and one broad in a 36:18:4 intensity ratio and one may conclude that the solution phase structure differs from that observed in the solid state. The two sharp resonances correspond to the Pn* moiety and their chemical shifts are within the range of their normal values. Interestingly, the equivalence of all NWT-Me groups indicates Pn* ring-whizzing is operating and energetically favourable at room temperature and indeed, does so down to temperatures as low as −90 °C (*vide infra*). The resonance attributed to the hydridic protons is broad (δ = −2.91 ppm, $\nu_{½}$ = 6.5 Hz; C_6D_6), indicating the (μ_3-H) and (μ_2-H) moieties are fluxional on the NMR timescale, which is a well known phenomenon for bridging hydride species.[95] The ^{13}C NMR spectrum consists of four resonances, all of which correspond to the Pn* ligand and are within their normal range but due to the compound's moderate solubility, the quaternary bridgehead carbons could not be detected. VT ^{1}H NMR measurements were conducted in an attempt to freeze-out the fluxional process involving (μ_3-H) and (μ_2-H) but unfortunately this was unsuccessful, even at temperatures as low as −90 °C. Interestingly upon cooling, the hydridic resonance sharpened to $\nu_{½}$ = 3.6 Hz at −50 °C and conversely upon heating the resonance broadened to $\nu_{½}$ = 81.4 Hz at 100 °C, which is contrary to the anticipated trend. There was also no temperature dependence on the resonance, with the chemical shift changing by no more than 0.2 ppm over the −90 to 100 °C temperature range. Another phenomenon that was not observed was the retardation of Pn* ring-whizzing, which was freely operating at −90 °C, with no sign of line broadening or decoalescence of the NWT-Me groups.

The synthesis of **4.8** was repeated on a NMR scale, with the aim of monitoring the reaction closely to observe any possible intermediates, which may aid with assignment of the mechanism operating in its formation. Upon H_2 admission, the relative intensity of **3.2** decreased and the sample gradually became swamped by a resonance attributed to Me_4Si (δ = 0.00 ppm; C_6D_6). During this transition two novel species were formed, one of which was identified as **4.8** and the second, an intermediate species that possessed distinct Pn* symmetry, with three resonances in a 6:6:6 intensity ratio. This can equate to C_s or C_2 symmetry of the Pn* moiety as observed for **3.4**, **3.6**, **3.7**, **4.1**, **4.2**, **4.3**, **4.4** and **4.7**. A generalised formula for C_s symmetric complexes can take the form, Pn*TiRR' (R ≠ R'), which could hypothetically belong to a species such as, Pn*Ti(CH_2SiMe_3)H, the product of initial σ-bond metathesis or a variation thereof.

Accompanying these resonances in the Pn* region were three complex multiplets between δ = −1.35 and −4.44 ppm, which are thought to relate to hydridic resonances for any intermediates. Unfortunately this diamagnetic species could neither be isolated nor identified and was consumed with the remaining **3.2**, as **4.8** and Me_4Si were simultaneously produced. The exact mechanism for the formation of **4.8** remains unclear but is likely to involve an initial σ-bond metathesis step of H_2 with **3.2**, resulting in liberation of Me_4Si and formation of a highly reactive intermediate Pn*Ti-hydride species, which can subsequently react with either more H_2 or a further equivalent of **3.2**, to form **4.8**.

Investigations into the reactivity of **4.8** were conducted in order to probe its stability; it was exposed to a D_2 atmosphere, in an attempt to initiate H/D exchange and potentially form **4.8-*d*$_4$**. The action of D_2 on a C_6D_6 solution of **4.8**, initially led to the formation of a small resonance at δ = 4.47 ppm (C_6D_6), attributed to H_2 and the simultaneous disappearance of the hydridic resonance. The resulting species was unstable and decomposed to unidentifiable products in a very short period of time. It is not known whether the D_2 had exchanged and the proposed **4.8-*d*$_4$** species formed was inherently unstable or if there was partial decomposition on the freeze-pump-thaw cycles, which catalysed the remaining decomposition. However, a bright red solid precipitated from the C_6D_6 solution, which exhibited very similar properties to that formed from the reaction of **3.1** with CO (Section 4.3.4), possessing an inherent insolubility in common organic solvents, which hindered characterisation. The bright red solid, which is also seen in the reaction of **3.1** with H_2 (*vide infra*), may be some form of oligomeric Pn*Ti species, which would explain its lack of solubility and further discussions as to its nature are conducted in Section 4.4.2. Unfortunately, time constraints and availability of **4.8** prevented further experimentation.

4.4.2 Reaction of Pn*Ti(CH_2Ph)$_2$ (3.1) with H_2

The same method described in Section 4.4.1 was performed initially, on a C_6D_6 solution of **3.1** and monitored by ^{1}H NMR spectroscopy. As in the formation of **4.8**, following admission of H_2, RH (R = CH_2Ph) gradually began to form and the relative intensity of **3.1** started to regress. Accompanying this, was the formation of four novel resonances, which continued to grow in intensity with time. Overnight the sample precipitated a bright red solid, akin to Sections 4.3.4 and 4.4.1, and the ^{1}H NMR

spectrum had marginally decreased in intensity, relative to the residual solvent peak. However, the spectra remained essentially constant, with the exception of the appearance of a novel resonance at δ = 4.47 ppm, attributed to H_2. It is thought the H_2 in solution either originated from its initial addition, which gradually dissolved in the C_6D_6 medium, or that an intermediate species was formed, which subsequently reacted to eliminate H_2 and, potentially, to form the insoluble red precipitate.

A sample of the solution was sent to mass spectrometry for analysis, which revealed Pn*Ti(CH_2Ph)H at accurate mass [found (calculated): 326.1515 (326.1514)] and the Pn*Ti fragment. Although this species does not correlate to the relative intensities observed in the ^{1}H NMR spectrum, it could be envisaged that the hypothetical intermediate [Pn*Ti(CH_2Ph)H], reacts further forming a novel Pn*Ti species, under the reaction conditions. Again, the bright red precipitate was insoluble in common organic solvents, although a nominal amount was taken up in THF-d_8. The resulting ^{1}H NMR spectrum was extremely weak but did display three novel resonances in a 6:6:6 intensity ratio, in the chemical shift region associated with Pn*. The three resonances (δ = 1.58, 1.88 and 2.05 ppm), could correspond to a Pn*Ti species, which contains no other protio groups. Possibilities include: the monomeric Ti^{IV} sandwich compound Pn*$_2$Ti, the permethylated analogue of Jonas' Pn_2Ti,[72] or perhaps, following reduction of the Ti^{IV} centre, potentially the formation of Pn*$_2Ti_2$. It is postulated that Pn*$_2$Ti would be extremely sterically congested, leading to hindered rotation of the Pn* ligands and thus a reduction of symmetry from the isomorphic Pn*$_2$U[105] and Pn*$_2$Ce,[106] which were highly fluxional on the NMR timescale and found to exist as three stereoisomers in the solid state. Pn*$_2Ti_2$ could form two possible isomers, as either the missing double metallocene from the series, Pn*$_2M_2$ (M = V, Cr, Mn, Co and Ni)[107] or the 'dumb bell' isomer, with two η^8-Pn*Ti fragments connected by a Ti-Ti bond, analogous to the postulated coproduced species in the formation of the double metallocene, $(\eta^8\text{-Pn}^{1,4\text{-Si}^i\text{Pr}_3})_2Mo_2$.[4]

The attempt to use a similar scale to the one which was used for the synthesis of **4.8** failed to clarify any of the potential products seen on the NMR scale. Comparatively, only a very small amount of bright red precipitate formed and the bulk solution resembled that of a very complex organic mixture, containing none of the species witnessed previously. This may possibly be an example of what Turner

describes as a 'point' reaction,[108] where product yields are extremely sensitive to conditions such as stirring, particle size and temperature.

4.4.3 Reaction of Pn*TiMe$_2$ (2.7) & Pn*Ti(CH$_2$^{t}Bu)$_2$ (3.3) with H$_2$

The addition of H_2 to benzene solutions of **2.7** and **3.3**, was administered in an identical fashion to that described in Section 4.4.1. Both solutions instantly followed a parallel sequence, turning orange in colour, and then deepening overnight to a very dark brown, with formation of a grey-black precipitate. The reactions were simultaneously monitored by ^{1}H NMR spectroscopy, which revealed the formation of RH (R = Me and $CH_2{}^tBu$, respectively) in synchrony with the reduction in intensity of the **2.7** and **3.3** starting materials, paralleling the observations for the action of H_2 on **3.1** and **3.2**. Following consumption of all the starting material, the only identifiable products present in the ^{1}H NMR spectra, were the aforementioned RH (R = Me and $CH_2{}^tBu$). This indicates that the Pn*Ti fragment was either still in solution, in which case it had been reduced to a paramagnetic, NMR silent species (a common spectroscopic NMR feature for d^1, Ti^{III} complexes), or it was present in the solid deposited. Unfortunately, the nature of the grey-black precipitate was not elucidated, leaving the fate of the Pn*Ti fragment unknown.

4.5 Reaction with H$_2$O

It is known that the M-alkyl moiety can be extremely susceptible towards a number of outside influences such as light, temperature, O_2, small molecules, Lewis acids and bases, and especially towards protic sources, such as H_2O.[109] This can be a major obstacle to their synthesis, manipulation and storage but can also be exploited in synthetic terms and the interesting reactivity they display (i.e. α-olefin polymerisation catalysts).[110] This is in part due to the polarity of the M-C bond; the carbon atom possesses considerable carbanionic character and so interaction with protic sources can cleave the M-R bond, with evolution of RH and formation of reactive, useful species, such as cationic centres, alkoxides and following hydrolysis, formation of M-O bonds as in the case of $(Cp_2TiCl)_2O$ (Figure 4.33).[111] It is for this very reason why M-alkyl complexes have fascinated organometallic chemists for over 250 years and continues to do so.[112]

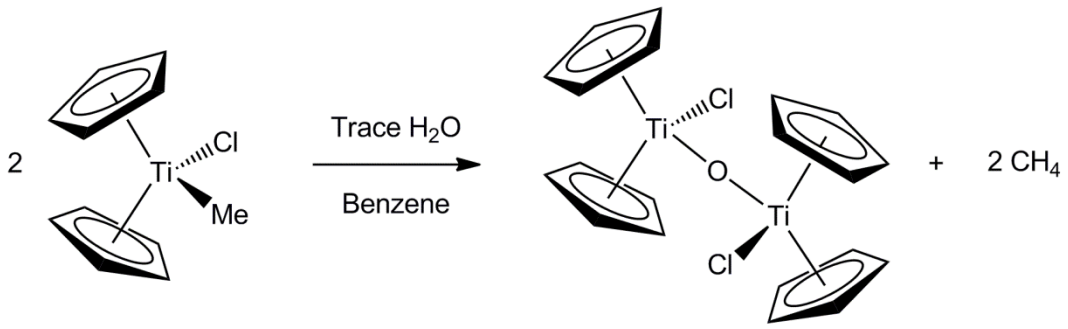

Figure 4.33: Formation of $(Cp_2TiCl)_2O$

4.5.1 Synthesis and characterisation of $(Pn^*TiCl)_2(\mu\text{-}O)$ (4.9)

An identical method used for the production of **3.4** (Section 3.5), was implemented; two equivalents of $LiCH_2{}^tBu$ were quickly added to **2.1** in benzene at room temperature and following standard work up procedures, crude **3.4** was extracted into hexane, containing adventitious H_2O. Cooling of this solution furnished a crimson microcrystalline solid in poor yield (Figure 4.34; 28%), which was identified as **4.9** by X-ray crystallography and mass spectrometry (EI). The latter showed the molecular ion at accurate mass, followed by peaks ascribed to the loss of chloride (Cl) and the Pn*TiCl fragment. Single crystals suitable for X-ray diffraction were grown by slow cooling of a solution in the same solvent to −35 °C and the structure is shown in Figure 4.35.

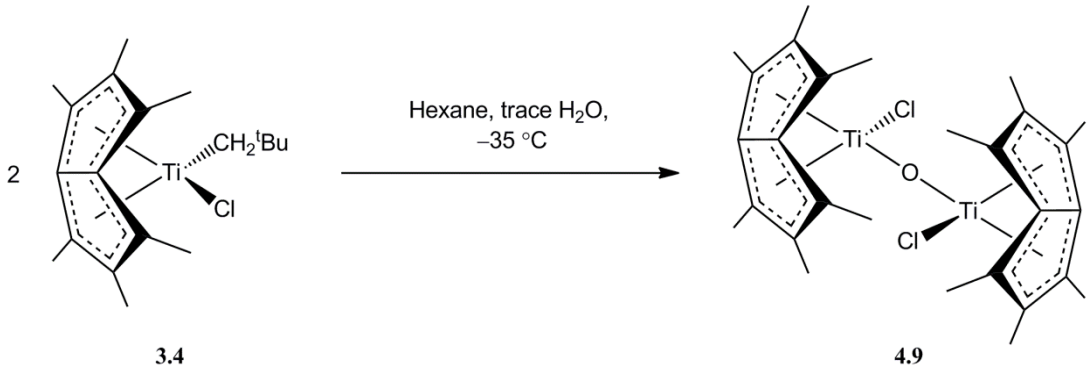

Figure 4.34: Synthesis of $(Pn^*TiCl)_2(\mu\text{-}O)$ (**4.9**).

4.9 crystallises in the *Pbca* space group, with one half-molecule in the asymmetric unit possessing inversion symmetry to form the constituent dimer. The ligands are coordinated in a pseudo tetrahedral arrangement around Ti, as exemplified by the Cl(1)-Ti(1)-O(1) angle [104.832(18)°] and the two Pn*TiCl fragments are bridged by an

essentially linear Ti-O-Ti bond. The resulting solid state symmetry is C_{2h}, with the principal axis bisecting O(1) perpendicular to the sole mirror plane, which consists of the atoms, C(4)/C(8)/Cl(1)/Ti(1)/O(1)/Ti(1*)/Cl(1*)/C(8*)/C(4*). The formal electron count on each Ti centre [in the absence of (p-d)π bonding] is 14 but it is known for some linear oxo bridged species of this type to possess partial double bond character (*vide infra*).

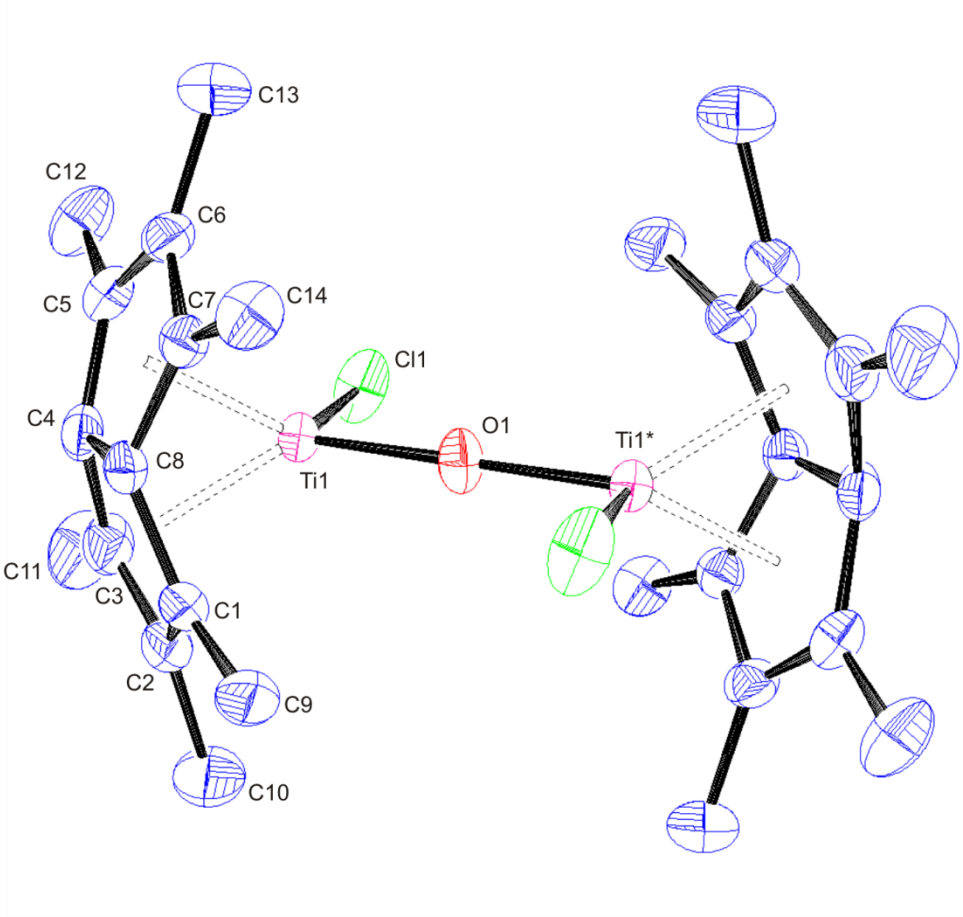

Figure 4.35: Side-on view of **4.9** with thermal ellipsoids at 50%. Hydrogen atoms omitted for clarity.

The Ti-Cl distance [2.3437(6) Å], falls between the corresponding distances in the 12 and 16 electron oxo-bridged species, $(CpTiCl_2)_2O$ and $(Cp_2TiCl)_2O$ [2.239(2) and 2.409(1) Å, respectively].[113, 111] This is expected on electronic grounds as the Pn* fragment formally contains two electrons fewer than the bis-Cp unit, resulting in a stronger Ti-Cl interaction for **4.9** and a shorter Ti-Cl distance compared to the 16 electron $(Cp_2TiCl)_2O$, which was formed in a parallel manner *via* interaction of trace amounts of H_2O, with an alkyl/chloride, $Cp_2TiClMe$ (Figure 4.33).[111] The Ti-Cl bond length also compares well to other compounds reported in this work possessing a

terminal Ti-Cl bond, **3.4**, **2.1** and **3.6** [2.2929(6), 2.35959(6) and 2.5068(8) Å, respectively), which fit a linear trend of increasing Ti-Cl bond length with increasing electron count on the Ti centres (Figure 4.36).

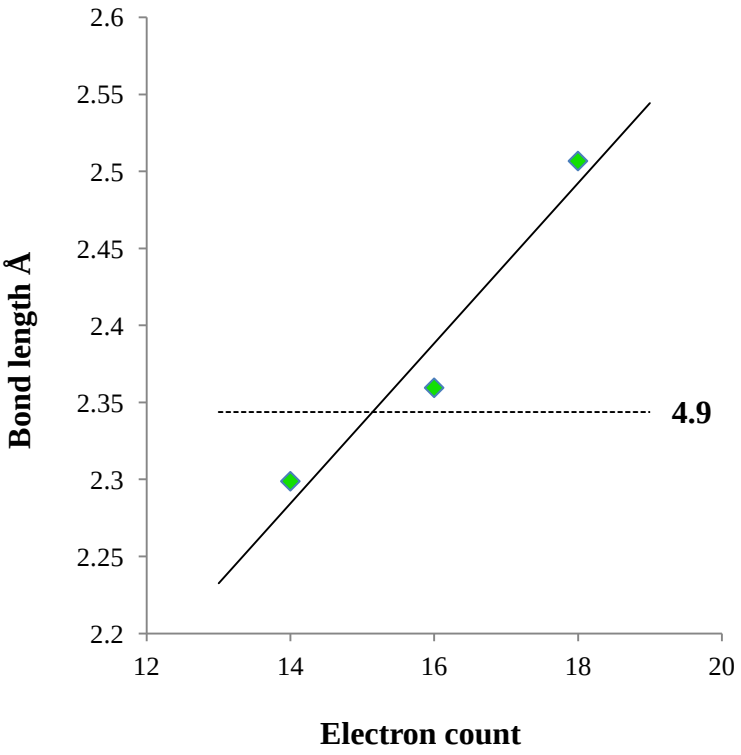

Figure 4.36: Plot of Ti-Cl bond length against electron count for Pn*Ti species.

Interestingly, the corresponding bond length for **4.9** falls in-between that of the 14 and 16 electron species, which may be an indication of extra electron density on the Ti centre as a result of $2p_{O\pi}$-$3d_{Ti\pi}$ interaction from the oxo bridge.

The Ti-O bond length and linear Ti-O-Ti angle [1.8369(3) Å and 180.0°], are also in excellent agreement with the related $(Cp_2TiCl)_2O$ and $(CpTiCl_2)_2O$ [1.837(2), 1.777(1) Å and 173.8, 180.0° respectively],[111, 113] with the slightly shorter distance for $(CpTiCl_2)_2O$, attributed to the relatively deficient 12 electron metal centre maximising Ti-O interaction. These distances and angles are very similar to other titanium oxo bridged species, which are reported to possess partial and significant Ti-O double bond character.[114–116] This possibility is corroborated by the average Ti-O distance for **4.5** (1.938 Å), which is known to be a single bond, being considerably longer than in **4.9**.

Table 4.8: Selected bond lengths, angles and structural parameters for **4.9**. ESDs are given in parentheses.

Lengths (Å)			
Ti(1) - C(1)	2.2907(19)	C(1) - C(2)	1.425(3)
Ti(1) - C(2)	2.469(2)	C(2) - C(3)	1.410(3)
Ti(1) - C(3)	2.416(2)	C(3) - C(4)	1.440(3)
Ti(1) - C(4)	2.1554(17)	C(4) - C(5)	1.429(3)
Ti(1) - C(5)	2.4085(19)	C(5) - C(6)	1.412(3)
Ti(1) - C(6)	2.4638(19)	C(6) - C(7)	1.423(3)
Ti(1) - C(7)	2.2905(18)	C(7) - C(8)	1.434(3)
Ti(1) - C(8)	2.1010(17)	C(8) - C(1)	1.445(3)
Ti(1) - Cl(1)	2.3437(6)	C(4) - C(8)	1.467(3)
Ti(1) - O(1)	1.8369(3)	Av. C_{ring} - Me	1.497
Ti(1) - Pn^*_{cent}	1.937	Ti(1) - Pn^*_{cent}	1.936

Angles (°)	
Cl(1) - Ti(1) - O(1)	104.832(18)
Ti(1) - O(1) - Ti(1*)	179.994
Fold Angle	35.39

Preliminary DFT calculations were conducted by Prof. John McGrady in order to examine the bonding in **4.9**. The optimised Ti-O bond length (1.84 Å), is in excellent agreement with the crystallographic distance and the O 2p orbitals were computed to be buried deep in energy and lie below several of the Ti-Pn* bonding orbitals. Representations of these MOs are shown (Figure 4.37) and it is quite clear that they possess substantial multiple Ti-O bonding character.

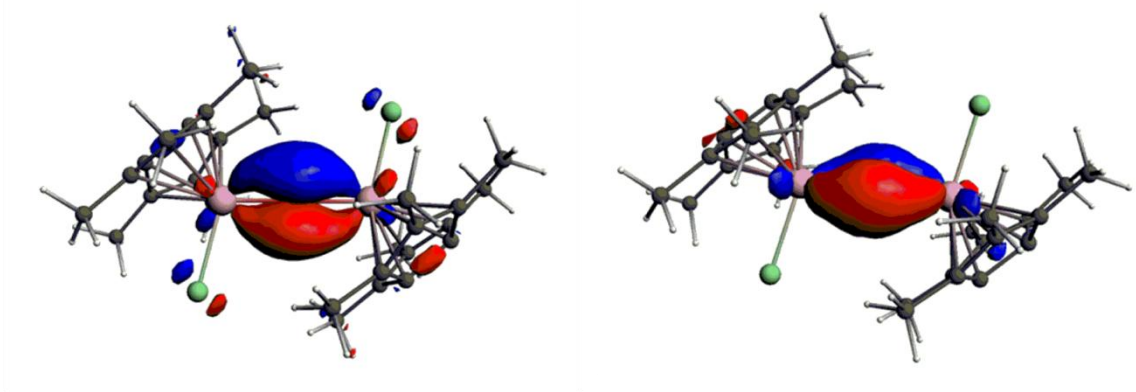

Figure 4.37: Oxygen's 2p orbitals in **4.9**.

The room temperature ^{1}H NMR spectrum of **4.9** reveals two sharp resonances in a 24:12 ratio and one may conclude that the solution phase structure of the molecule is in contrast to that observed in the solid state (C_{2h}), from which a reduction of symmetry would be expected, resulting in two sets of non equivalent NWT-Me groups. The equivalence of all NWT-Me groups is indicative of two orthogonal mirror planes bisecting the Pn* ligand and demonstrates that Pn* ring-whizzing is highly favourable and operational at room temperature. This is further supported by the ^{13}C NMR spectrum displaying five resonances, all of which correspond to the Pn* carbons.

4.6 Conclusion

The reactivity of the novel compounds **2.7**, **3.1**, **3.2** and **3.3** with CO_2, CO and H_2 has been investigated. Upon interaction with CO_2, all four compounds demonstrate "normal" insertion of the CO_2 moiety into both Ti-R (R = Me, CH_2Ph, CH_2SiMe_3 and $CH_2{}^tBu$ respectively) bonds. Of these, three were characterised in the solid state revealing C_2 symmetry and the symmetrical bidentate coordination of the RCO_2 units. Pn*Ti(κ^2-$O_2CCH_2Ph)_2$ (**4.2**) is the first example of CO_2 insertion into a Ti-CH_2Ph bond to be fully characterised in both the solid and solution state and Pn*Ti(κ^2-$O_2CCH_2SiMe_3)_2$ (**4.3**) contains the first crystallographically characterised κ^2-O,O'-($O_2CCH_2SiMe_3$) entity, for any transition metal. All four transform from $C_2 \rightarrow C_{2v}$ symmetric upon heating in solution, as Pn* ring-whizzing becomes operational and their Gibbs free energies of activation have been calculated. The action of CO on **3.2** and **3.3**, results in the direct reductive coupling of two CO molecules to yield mononuclear *cis*-enediolate complexes. The latter forms the first enediolate moiety for any metal bearing two $CH_2{}^tBu$ groups and the fourth group IV monomeric enediolate complex to be structurally characterised {Pn*Ti[κ^2-O-C($CH_2{}^tBu$)=C($CH_2{}^tBu$)-O] (**4.5**)}. It possesses a large fold about the O-O vector, resulting in a σ^2, π-bonding mode, analogous to Ti^{IV} *cis*-diene complexes and displays the second largest Ti-Pn fold angle to date (36.7°), eclipsed only by the Ti^{III} compound, PnTiCp (37.0°). **2.7** was found to form a complex mixture of products on reaction with CO, two of which were structurally elucidated; the Me analogue of enediolates, **4.5** and **4.6**, and the dimeric titanaoxirane, {Pn*Ti[μ-η^1(O):η^2-$OC(Me)_2$]}$_2$ (**4.7**). Computational studies highlighted two competing pathways, which are dependent on the concentration of CO; low levels promote formation of the titanaoxirane as seen with isolation of **4.7** and conversely

excess results in enediolate formation. The latter route is postulated to be progress *via* the key intermediate, Pn*Ti(η^2-COR)$_2$, which is not accessible for Cp*$_2$MMe$_2$ (M = group IV metal), as the intermediate would contravene the 18 electron rule. However, due to the Pn* fragment formally containing two fewer electrons than the bis-Cp unit, it is viable and hence enediolate formation proceeds in an analogous manner to that seen for Cp*$_2$AnR$_2$ (An = U, Th; R = CH_2SiMe_3 and $CH_2{}^tBu$). Titanaoxirane formation is not observed for the bulky derivatives (R = CH_2SiMe_3 and $CH_2{}^tBu$), postulated as a result of the steric encumbrance of the resulting Pn*Ti[η^2-OC(R)$_2$] species and its dimerisation product {Pn*Ti[μ-η^1(O):η^2-OC(R)$_2$]}$_2$, hence the only product seen are the enediolates, **4.5** and **4.6**. Although the reactions with H_2 yielded more complex results, they did produce the trimeric complex, thought to be the mixed valence [Pn*Ti(μ_2-H)]$_3$(μ_3-H) (**4.8**), which contains a near planar six-membered Ti_3H_3 ring. It is also the first structurally characterised example of a trimeric titanium-hydride species and the first to include a Ti-(μ_3-H) moiety. The adventitious action of H_2O on **3.4**, yields (Pn*TiCl)$_2$(μ-O) (**4.9**), which possesses a linear Ti-O-Ti bridge and a degree of Ti-O double bond character, supported by the crystallographic data and DFT calculations. A comparison of the solid state structural properties of all crystallographically characterised complexes through out this chapter has been performed

Table 4.9: Collection of solid state parameters and valence electron counts for Chapter Four.

Compound	Av. Fold Angle (°)	Av. Ti-C Distance (Å)	Av. Ti-Pn*$_{cent}$ Distance (Å)	Av. C-C Distance (Pn*) (Å)	Ti Valence Electron Count
4.1	32.37	2.344	1.957	1.433	18
4.2	31.92	2.347	1.959	1.433	18
4.3	32.27	2.344	1.958	1.429	18
4.5	36.66	2.315	1.925	1.437	16
4.7	33.16	2.352	1.970	1.429	16
4.8	32.67	2.365	1.983	1.430	16
4.9	35.39	2.324	1.937	1.432	14

4.7 References for Chapter Four

1 W. B. Tolman, *Activation of Small Molecules*, Wiley-VCH Verlag GmbH & Co. KGaA, Weinheim, Germany, 2006.

2 G. A. Olah, A. Goeppert, and G. K. S. Prakash, *Beyond Oil and Gas; The methanol Economy*, Wiley-VCH Verlag GmbH & Co. KGaA, Weinheim, Germany, 2006.

3 M. Aresta and A. Dibenedetto, *Dalton transactions (Cambridge, England : 2003)*, 2007, 2975–92.

4 M. C. Kuchta, F. G. N. Cloke, and P. B. Hitchcock, *Organometallics*, 1998, 17, 1934–1936.

5 F. Burgos, I. Chávez, J. M. Manriquez, M. Valderrama, E. Lago, E. Molins, F. Delpech, A. Castel, and P. Rivière, *Organometallics*, 2001, 20, 1287–1291.

6 F. G. N. Cloke and P. B. Hitchcock, *Journal of the American Chemical Society*, 2002, 124, 9352–9353.

7 *Climate Change 2001: The Scientific Basis*, Cambridge University Press, 2001.

8 *In Kyoto Protocol to the United Nations Framework Convention on Climate Change*, Kyoto, 1998.

9 B. Clark and R. York, *Theory and Society*, 2005, 34, 391–428.

10 H. Arakawa, M. Aresta, J. N. Armor, M. A. Barteau, E. J. Beckman, A. T. Bell, J. E. Bercaw, C. Creutz, E. Dinjus, D. A. Dixon, K. Domen, D. L. DuBois, J. Eckert, E. Fujita, D. H. Gibson, W. A. Goddard, D. W. Goodman, J. Keller, G. J. Kubas, H. H. Kung, J. E. Lyons, L. E. Manzer, T. J. Marks, K. Morokuma, K. M. Nicholas, R. Periana, L. Que, J. Rostrup-Nielson, W. M. H. Sachtler, L. D. Schmidt, A. Sen, G. A. Somorjai, P. C. Stair, B. R. Stults, and W. Tumas, *Chemical Reviews*, 2001, 101, 953–996.

11 I. Omae, *Catalysis Today*, 2006, 115, 33–52.

12 D. J. Darensbourg, *Chemical Reviews*, 2007, 107, 2388–410.

13 D. H. Gibson, *Chemical Reviews*, 1996, 96, 2063–2096.

14 W. Leitner, *Coordination Chemistry Reviews*, 1996, 153, 257–284.

15 M. Aresta and A. Dibenedetto, *Catalysis Today*, 2004, 98, 455–462.

16 A. Baiker, *Applied Organometallic Chemistry*, 2000, 14, 751–762.

17 X. Yin and J. R. Moss, *Coordination Chemistry Reviews*, 1999, 181, 27–59.

18 B. Demerseman, R. Mahé, and P. H. Dixneuf, *Journal of the Chemical Society, Chemical Communications*, 1984, 1394.

19 H. G. Alt, G. S. Herrmann, M. D. Rausch, and D. T. Mallin, *Journal of Organometallic Chemistry*, 1988, 356, C53–C56.

20 H. G. Alt and G. S. Herrmann, *Journal of Organometallic Chemistry*, 1990, 390, 159–169.

21 P. Braunstein, D. Matt, and D. Nobel, *Chemical Reviews*, 1988, 88, 747–764.

22 Y. Gao, S. Iijima, H. Urabe, and F. Sato, *Inorganica Chimica Acta*, 1994, 222, 145–153.

23 V. V. Burlakov, A. I. Yanovsky, Y. T. Struchkov, U. Rosenthal, A. Spannenberg, R. Kempe, O. G. Ellert, and V. B. Shur, *Journal of Organometallic Chemistry*, 1997, 542, 105–112.

24 F. G. Kirchbauer, P. Pellny, H. Sun, V. V. Burlakov, P. Arndt, W. Baumann, A. Spannenberg, and U. Rosenthal, *Organometallics*, 2001, 20, 5289–5296.

25 G. A. Luinstra, L. C. Ten Cate, H. J. Heeres, J. W. Pattiasina, A. Meetsma, and J. H. Teuben, *Organometallics*, 1991, 10, 3227–3237.

26 R. F. Johnston and J. C. Cooper, *Organometallics*, 1987, 6, 2448–2449.

27 U. Zucchini, E. Albizzati, and U. Giannini, *Journal of Organometallic Chemistry*, 1971, 26, 357–372.

28 J. Dvorak, R. J. O'Brien, and W. Santo, *Journal of the Chemical Society D: Chemical Communications*, 1970, 67, 411.

29 I. S. Kolomnikov, T. S. Loveeva, V. V. Gorbachevskaya, G. G. Aleksandrov, Y. T. Struckhov, and M. E. Vol'pin, *Journal of the Chemical Society D: Chemical Communications*, 1971, 972.

30 I. S. Kolomnikov, T. S. Lobeeva, and M. E. Vol'pin, *Zh. Obschch. Khim.*, 1972, 42, 2232.

31 Y. Huang, N. Etkin, R. R. Heyn, T. T. Nadasdi, and D. W. Stephan, *Organometallics*, 1996, 15, 2320–2330.

32 T. Krüger, C. Albrecht, T. Rüffer, H. Lang, J. Griebel, R. Kirmse, and D. Steinborn, *Zeitschrift für Anorganische und Allgemeine Chemie*, 2008, 634, 1030–1034.

33 G. Deacon, *Coordination Chemistry Reviews*, 1980, 33, 227–250.

34 K. Ito and H. J. Bernstein, *Canadian Journal of Chemistry*, 1956, 34, 170–178.

35 W. A. Thomas, *Annu. Rev. NMR Spectrosc.*, 1968, 1, 43.

36 P. Legzdins, E. C. Phillips, J. Trotter, V. C. Yee, F. W. B. Einstein, and R. H. Jones, *Organometallics*, 1991, 10, 986–1002.

37 P. Gómez-Sal, B. Royo, P. Royo, R. Serrano, I. Sáez, and S. Martinez-Carreras, *Journal of the Chemical Society, Dalton Transactions*, 1991, 1575.

38 İ. Kani and Y. Aksu, *Journal of Inorganic and Organometallic Polymers and Materials*, 2009, 20, 69–77.

39 S. Hazra, B. Sarkar, S. Naiya, M. G. B. Drew, A. Frontera, D. Escudero, and A. Ghosh, *Crystal Growth & Design*, 2010, 10, 1677–1687.

40 S. Gómez-Ruiz, B. Gallego, Ž. Žižak, E. Hey-Hawkins, Z. D. Juranić, and G. N. Kaluđerović, *Polyhedron*, 2010, 29, 354–360.

41 G. Lemercier, E. Mulliez, C. Brouca-Cabarrecq, F. Dahan, and J.-P. Tuchagues, *Inorganic Chemistry*, 2004, 43, 2105–13.

42 D. J. Darensbourg, M. W. Holtcamp, B. Khandelwal, K. K. Klausmeyer, and J. H. Reibenspies, *Inorganic Chemistry*, 1995, 34, 2389–2398.

43 W. J. Evans, J. M. Perotti, and J. W. Ziller, *Journal of the American Chemical Society*, 2005, 127, 3894–909.

44 H. Nakagawa, Y. Kani, M. Tsuchimoto, S. Ohba, H. Matsushima, and T. Tokii, *Acta Crystallographica Section C Crystal Structure Communications*, 2000, 56, 12–16.

45 D. Cui, M. Nishiura, and Z. Hou, *Macromolecules*, 2005, 38, 4089–4095.

46 W. J. Evans, J. C. Brady, and J. W. Ziller, *Journal of the American Chemical Society*, 2001, 123, 7711–7712.

47 Y. Nakajima and J. Okuda, *Organometallics*, 2007, 26, 1270–1278.

48 P. Piszczek, M. Richert, A. Grodzicki, T. Głowiak, and A. Wojtczak, *Polyhedron*, 2005, 24, 663–670.

49 P. Piszczek, M. Richert, and A. Wojtczak, *Polyhedron*, 2008, 27, 602–608.

50 R. Closson, J. Kozikowski, and T. Coffield, *Journal of Organic Chemistry*, 1957, 22, 598.

51 T. Coffield, J. Kozikowski, and R. Closson, *Journal of Organic Chemistry*, 1957, 22, 598.

52 F. Calderazzo and F. A. Cotton, *Inorganic Chemistry*, 1962, 1, 30–36.

53 K. Noack and F. Calderazzo, *Journal of Organometallic Chemistry*, 1967, 10, 101–104.

54 C. P. Casey, C. A. Bunnell, and J. C. Calabrese, *Journal of the American Chemical Society*, 1976, 98, 1166–1171.

55 C. P. Casey and C. A. Bunnell, *Journal of the American Chemical Society*, 1976, 98, 436–441.

56 K. Tatsumi, A. Nakamura, P. Hofmann, P. Stauffert, and R. Hoffmann, *Journal of the American Chemical Society*, 1985, 107, 4440–4451.

57 G. Fachinetti and C. Floriani, *Journal of Organometallic Chemistry*, 1974, 71, C5–C7.

58 G. Fachinetti, C. Floriani, and H. Stoeckli-Evans, *Journal of the Chemical Society, Dalton Transactions*, 1977, 2297.

59 G. Fachinetti, G. Fochi, and C. Floriani, *Journal of the Chemical Society, Dalton Transactions*, 1977, 1946.

60 G. Fachinetti, C. Floriani, F. Marchetti, and S. Merlino, *Journal of the Chemical Society, Chemical Communications*, 1976, 522.

61 G. Erker, *Accounts of Chemical Research*, 1984, 17, 103–109.

62 Z. Han, T. Fujioka, S.-I. Usugi, H. Yorimitsu, H. Shinokubo, and K. Oshima, *Organic & Biomolecular Chemistry*, 2005, 3, 1622–3.

63 G. Erker, R. Schlund, and C. Krueger, *Organometallics*, 1989, 8, 2349–2355.

64 M. Pankowski, *Journal of Organometallic Chemistry*, 1996, 516, 11–16.

65 P. Hofmann, P. Stauffert, K. Tatsumi, A. Nakamura, and R. Hoffmann, *Organometallics*, 1985, 4, 404–406.

66 F. De Angelis and A. Sgamellotti, *Organometallics*, 2000, 19, 4904–4911.

67 P. Hofmann, P. Stauffert, M. Frede, and K. Tatsumi, *Chemische Berichte*, 1989, 122, 1559–1577.

68 L. D. Durfee and I. P. Rothwell, *Chemical Reviews*, 1988, 88, 1059–1079.

69 K. Tatsumi, A. Nakamura, P. Hofmann, R. Hoffmann, K. G. Moloy, and T. J. Marks, *Journal of the American Chemical Society*, 1986, 108, 4467–4476.

70 T. W. Graham, J. Kickham, S. Courtenay, P. Wei, and D. W. Stephan, *Organometallics*, 2004, 23, 3309–3318.

71 G. J. Balaich, J. E. Hill, S. A. Waratuke, P. E. Fanwick, and I. P. Rothwell, *Organometallics*, 1995, 14, 656–665.

72 K. Jonas, P. Kolb, G. Kollbach, B. Gabor, R. Mynott, K. Angermund, O. Heinemann, and C. Krüger, *Angewandte Chemie International Edition in English*, 1997, 36, 1714–1718.

73 L.-C. Song, P.-C. Liu, C. Han, and Q.-M. Hu, *Journal of Organometallic Chemistry*, 2002, 648, 119–125.

74 S. Dürr, U. Höhlein, and R. Schobert, *Journal of Organometallic Chemistry*, 1993, 458, 89–96.

75 P. Hofmann, M. Frede, P. Stauffert, W. Lasser, and U. Thewalt, *Angewandte Chemie*, 1985, 97, 693–694.

76 J. M. Manriquez, D. R. McAlister, R. D. Sanner, and J. E. Bercaw, *Journal of the American Chemical Society*, 1978, 100, 2716–2724.

77 J. M. Manriquez, P. J. Fagan, T. J. Marks, C. S. Day, and V. W. Day, *Journal of the American Chemical Society*, 1978, 100, 7112–7114.

78 W. B. Jensen, *Journal of Chemical Education*, 2005, 82, 28.

79 P. J. Fagan, J. M. Manriquez, S. H. Vollmer, C. S. Day, V. W. Day, and T. J. Marks, *Journal of the American Chemical Society*, 1981, 103, 2206–2220.

80 A. E. Ashley, Permethylpentalene Chemistry, Thesis, University of Oxford, 2006.

81 G. Fachinetti, C. Biran, C. Floriani, A. Chiesi Villa, and C. Guastini, *Inorganic Chemistry*, 1978, 17, 2995–3002.

82 B. Hessen, J. Blenkers, J. H. Teuben, G. Helgesson, and S. Jagner, *Organometallics*, 1989, 8, 2809–2812.

83 J. C. Huffman, K. G. Moloy, J. A. Marsella, and K. G. Caulton, *Journal of the American Chemical Society*, 1980, 102, 3009–3014.

84 P. Berno, S. Stella, C. Floriani, A. Chiesi-Villa, and C. Guastini, *Journal of the Chemical Society, Dalton Transactions*, 1990, 2669.

85 G. Erker, U. Dorf, P. Czisch, and J. L. Peterson, *Organometallics*, 1986, 5, 668–676.

86 T. Iijima, *Bulletin of the Chemical Society of Japan*, 1972, 45, 3526–3530.

87 C. D. Wood and R. R. Schrock, *Journal of the American Chemical Society*, 1979, 101, 5421–5422.

88 M. Gómez, P. Gómez-Sal, G. Jiménez, A. Martín, P. Royo, and J. Sánchez-Nieves, *Organometallics*, 1996, 15, 3579–3587.

89 G. Erker, P. Czisch, R. Schlund, K. Angermund, and C. Krüger, *Angewandte Chemie International Edition in English*, 1986, 25, 364–365.

90 D. A. Straus and R. H. Grubbs, *Journal of the American Chemical Society*, 1982, 104, 5499–5500.

91 G. Fachinetti and C. Floriani, *Journal of the Chemical Society, Chemical Communications*, 1972, 654.

92 J. G. Murray, *Journal of the American Chemical Society*, 1961, 83, 1287.

93 M. A. Esteruelas and L. A. Oro, *Chemical Reviews*, 1998, 98, 577–588.

94 A. Hoskin and D. W. Stephan, *Coordination Chemistry Reviews*, 2002, 233-234, 107–129.

95 G. S. McGrady and G. Guilera, *Chemical Society Reviews*, 2003, 32, 383.

96 J. B. Love, H. C. S. Clark, F. G. N. Cloke, J. C. Green, and P. B. Hitchcock, *Journal of the American Chemical Society*, 1999, 121, 6843–6849.

97 M. E. Thompson, S. M. Baxter, A. R. Bulls, B. J. Burger, M. C. Nolan, B. D. Santarsiero, W. P. Schaefer, and J. E. Bercaw, *Journal of the American Chemical Society*, 1987, 109, 203–219.

98 K. Clauss and H. Bestian, *Justus Liebigs Annalen der Chemie*, 1962, 654, 8–19.

99 S. I. Troyanov, H. Antropiusová, and K. Mach, *Journal of Organometallic Chemistry*, 1992, 427, 49–55.

100 J. E. Bercaw and H. H. Brintzinger, *Journal of the American Chemical Society*, 1969, 91, 7301–7306.

101 J. E. Bercaw, R. H. Marvich, L. G. Bell, and H. H. Brintzinger, *Journal of the American Chemical Society*, 1972, 94, 1219–1238.

102 P. J. Chirik, L. M. Henling, and J. E. Bercaw, *Organometallics*, 2001, 20, 534–544.

103 R. Andres, M. V. Galakhov, A. Martin, M. Mena, and C. Santamaria, *Organometallics*, 1994, 13, 2159–2163.

104 H. Aslan, T. Sielisch, and R. Dieter Fischer, *Journal of Organometallic Chemistry*, 1986, 315, C69–C72.

105 F. M. Chadwick, A. Ashley, G. Wildgoose, J. M. Goicoechea, S. Randall, and D. O'Hare, *Dalton Transactions (Cambridge, England: 2003)*, 2010, 39, 6789–93.

106 A. Ashley, G. Balazs, A. Cowley, J. Green, C. H. Booth, and D. O'Hare, *Chemical communications (Cambridge, England)*, 2007, 1515–7.

107 A. E. Ashley, R. T. Cooper, G. G. Wildgoose, J. C. Green, and D. O'Hare, *Journal of the American Chemical Society*, 2008, 130, 15662–77.

108 S. Turner, *"The Design of Organic Syntheses,"* Elsevier: Amsterdam, 1976.

109 R. R. Schrock and G. W. Parshall, *Chemical Reviews*, 1976, 76, 243–268.

110 E. Y.-X. Chen and T. J. Marks, *Chemical Reviews*, 2000, 100, 1391–1434.

111 Y. Le Page, J. D. McCowan, B. K. Hunter, and R. D. Heyding, *Journal of Organometallic Chemistry*, 1980, 193, 201–207.

112 C. Elschenbroich and A. Salzer, *Organometallics - A concise introduction*, VCH, Second Ed., 1991.

113 U. Thewalt and D. Schomburg, *Journal of Organometallic Chemistry*, 1977, 127, 169–174.

114 T. Carofiglio, C. Floriani, A. Sgamellotti, M. Rosi, A. Chiesi-Villa, and C. Rizzoli, *Journal of the Chemical Society, Dalton Transactions*, 1992, 1081.

115 S. Ciruelos, T. Cuenca, J. C. Flores, R. Gomez, P. Gomez-Sal, and P. Royo, *Organometallics*, 1993, 12, 944–948.

116 T. Cuenca, J. C. Flores, R. Gomez, P. Gomez-Sal, M. Parra-Hake, and P. Royo, *Inorganic Chemistry*, 1993, 32, 3608–3612.

Chapter Five

Ethylene Polymerisation Studies of Monomeric Pn*TiR_2 Complexes

5.1 Introduction

5.1.1 Industrial overview

The synthetic polymer industry is dominated by polyolefins with approximately 65 million tons of polyethylene (PE) and 40 million tons of polypropylene (PP) being produced annually worldwide.[1] This is unsurprising considering the multitude of industrial uses for these polymers including films, packaging, machinery parts, electrical insulators, inks, petroleum additives, and hot melt adhesives to name but a few.[1]

5.1.2 Catalyst development

The 1950s saw the inception of polyolefin catalysis pioneered by Ziegler[2, 3] and Natta[4, 5] from which Ziegler-Natta catalysts came to be known. Ziegler-Natta catalysts are polymerising media and contain multiple catalytic sites and active species.[2, 3] They comprise a transition metal of group 4-8 and an aluminium derivative, for example $TiCl_3$ and $AlEt_2Cl$. This complex process has been continuously developed over the past 50 years and remains the predominant method of polyolefin production due to low costs and high performance. However, there are some key drawbacks of Ziegler-Natta catalysts; namely rational modification of the reactivity and stereospecificity of multiple catalytic sites is difficult, limiting control of the polymers' molecular weight distribution, chain tacticity and composition.

The first homogenous metallocene polymerisation catalyst, Cp_2TiCl_2-$AlEt_2Cl$, was discovered shortly after Ziegler's discovery. Homogenous catalysts are characterised by the presence of a singular catalytic site and species as well as being soluble in the polymerising medium. However, homogenous polymerisation conditions make it more difficult to control particle growth resulting in reactor fouling which

makes these catalysts more demanding to implement in industrial polyolefin production processes.

The introduction of methylaluminoxane (MAO) as a co-catalyst dramatically improves the activity of metallocene and post-metallocene catalysts.[6, 7] Furthermore, these single-site catalysts can be engineered by prudent substitution of the metallocene framework to positively influence activity, polymer molecular weight, co-monomer incorporation, and stereospecifity in α-olefin polymerisation.[8] Such polymer control is of obvious commercial interest but drawbacks include the prohibitive cost and requirement of a large excess of MAO relative to the catalyst ($[MAO]_0 / [Cat]_0 > 1000$), which have hampered their commercialisation.

5.1.3 Polymerisation mechanism

Cossee and Arlman proposed their mechanism for Ziegler-Natta polymerisation in the mid-1960s.[9, 10] In the Cossee-Arlman mechanism (Figure 5.1) the monomer first coordinates to a vacant site in the active species (generally a cationic alkyl complex) to form an olefin π-adduct. This is followed by a migratory insertion reaction into the metal-carbon bond of the alkyl group (or growing polymer chain) to regenerate the active species. Following the discovery of alkylidene complexes in the 1970s, Green and Rooney proposed a new mechanism consisting of a hydride shift to give a metal-alkylidene hydride intermediate, which reacts with an olefin to give a metallacyclobutane species, regenerating the active species following a reductive elimination.[11, 12] Deuterium labelling experiments have been used to distinguish between the direct insertion and hydride shift mechanisms.[13] Group 4 metallocene catalysts, having no d-electrons, are unable to undergo the formal oxidative addition required by the Green-Rooney mechanism.

Cossee-Arlman Mechanism

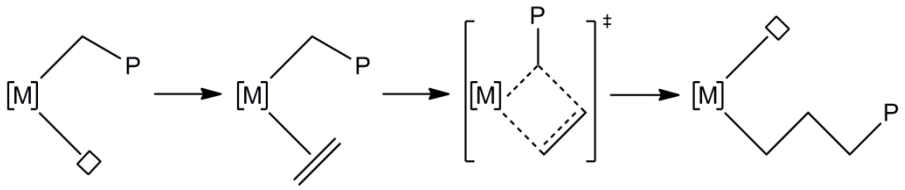

Green-Rooney Mechanism

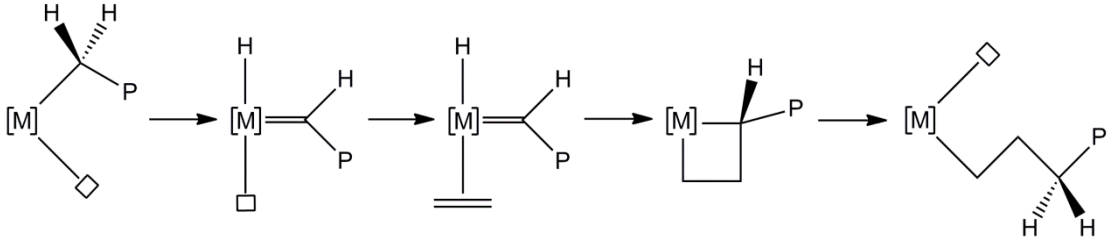

Modified Green-Rooney Mechanism

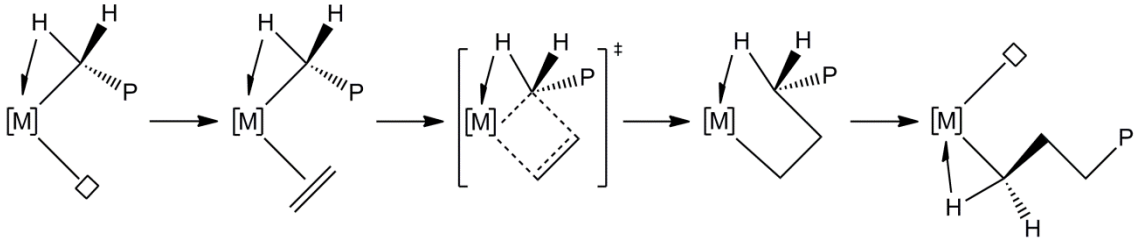

Transition State α-Agostic Mechanism

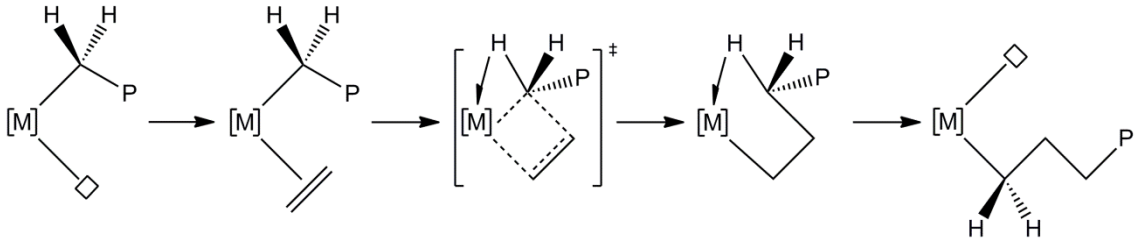

Figure 5.1: Proposed mechanisms for Ziegler-Natta catalysis.

Two further mechanisms that are intermediate between the Cossee-Arlman and Green-Rooney mechanisms have been proposed, both involving α-agostic interactions. Studies on the role of α-agostic interactions in Ziegler-Natta catalysis has been reviewed.[14]

5.1.4 Activators

The mechanism for homogenous Ziegler-Natta catalysis described above requires in the first instance an alkyl species having a vacant coordination site to accommodate an incoming ethylene molecule. In general an activator (or co-catalyst) is required to achieve this. The most widely used activator is MAO (methylaluminoxane), formed by the controlled hydrolysis of Al_2Me_6. MAO is believed to have the general

formula $[Al(Me)O]_n$, consisting of a mixture of cyclic and linear oligomeric methylaluminoxanes.[15]

MAO is usually used to activate dichloride systems, where it is thought to perform three roles: alkylation of the metal centre; abstraction of a halide or alkyl ligand to leave a vacant site; scavenging impurities (such as water) from the system. MAO is typically used in an excess of *ca.* 1000:1 in relation to the pre-catalyst. It is believed[16] that such a large excess is required to shift an equilibrium in favour of the cationic active species. Using such large excesses of MAO is expensive, and the ill-defined nature of MAO activated systems makes mechanistic studies difficult. Commercially available MAO solutions also contain significant amounts (up to 30 wt%) of "$AlMe_3$" which is involved in deactivation processes. Stoichiometric amounts of borane and borate activators, such as $B(C_6F_5)_3$, $[Ph_3C][B(C_6F_5)_4]$ and $[PhNMe_2H][B(C_6F_5)_4]$ can be used to activate dialkyl precursors. Activators for Ziegler-Natta catalysis have been reviewed.[17]

5.2 Polymerisation testing

The group of four monomeric dialkyl species, Pn*TiR_2 [R = Me (**2.7**), CH_2Ph (**3.1**), CH_2SiMe_3 (**3.2**) and $CH_2{}^tBu$ (**3.3**)], which demonstrated interesting reactivity with CO_2, CO and H_2 were tested as potential catalyst for the polymerisation of ethylene. They are all isoelectronic 14 electron species with the same geometry at Ti, therefore the effect of the metal-bound alkyl group in the initial active species could be investigated. It is hoped that these 14 electron metal alkyl complexes would exhibit interesting activity towards olefins. Activation should generate highly electron deficient and coordinatively unsaturated, 12 electron Pn*TiR^+ species.

5.2.1 Conditions

The polymerisation activity of Pn*TiR_2 [R = Me (**2.7**), CH_2Ph (**3.1**), CH_2SiMe_3 (**3.2**) and $CH_2{}^tBu$ (**3.3**)] were studied in toluene solution at 60 °C under an atmosphere of two bar ethylene. The full details of the experimental procedure are described in Section 6.9.1.

5.2.2 Ethene polymerisation using Pn*TiR_2 precursors

The polymerisation of ethylene using Pn*TiR_2 precursors were initially tested in the absence of an external activator as preliminary experimentation on the NMR scale revealed PE was produced upon their exposure to ethylene in toluene-d_8. The results are summarised below.

Table 5.1: Summary of ethylene polymerisation activity using Pn*TiR_2 pre-catalysts with no activator.

Compound	Catalyst loading (mg)	T (°C)	Time (min)	Activator loading (mg)	Pressure (bar)	PE (g)	Activity (kg_{PE} mol_{cat}^{-1} h^{-1} bar^{-1})
2.7	5	60	30	0	2	0	0
3.1	5	60	30	0	2	0.001	1.51×10^{-1}
3.2	5	60	30	0	2	0.016	1.31
3.3	5	60	30	0	2	0	0

It was found that the measured activities are extremely low and no PE was produced for the R = Me and $CH_2{}^tBu$ derivatives. However, this is somewhat expected as coordination of the monomer unit in the proposed mechanism is postulated to be to a cationic metal centre and so these neutral derivatives lack this electrostatic attraction.

The first activator to be tested was the alkyl abstracting agent $[Ph_3C][B(C_6F_5)_4]$, a common initiator for alkyl species.[17]

Table 5.2: Summary of ethylene polymerisation activity using Pn*TiR_2 pro-catalyst with $[Ph_3C][B(C_6F_5)_4]$.

Compound	Catalyst loading (mg)	T (°C)	Time (min)	Activator loading (mg)	Pressure (bar)	PE (g)	Activity (kg_{PE} mol_{cat}^{-1} h^{-1} bar^{-1})
2.7	5	60	30	17.5	2	0.2	10.6
3.1	5	60	30	12.3	2	0	0
3.2	5	60	30	11.3	2	0.267	21.8
3.3	5	60	30	12.3	2	0.012	9.04×10^{-1}

The introduction of $[Ph_3C][B(C_6F_5)_4]$ had a significant impact on the activities of the Pn* catalysts. The highest activity for the series is **3.2**, which interestingly had the

highest with no activator present as well. This however, is only at a moderate level on the Gibson scale of reactivity, falling along way short of other group IV catalysts.[18] No activity was noted for **3.1**, which is postulated to be the result of the active species precipitating from solution as a green microcrystalline solid.

The second activator to be tested was the protonation reagent $[PhNMe_2H][B(C_6F_5)_4]$ (Table 5.3), and this was found to produce lower activities for all compounds tested. Due to the same counter ion in both, it indicates abstracting agents are better suited to Pn^*TiR_2 species for higher activity in the polymerisation of ethylene. Interestingly **3.1** again failed to produce any PE and similarly precipitated out of solution as a green microcrystalline solid indicating the same insoluble species is formed in both cases, most probably $[Pn^*TiCH_2Ph][B(C_6F_5)_4]$.

Table 5.3: Results summary of Pn^*TiR_2 with $[PhNMe_2H][B(C_6F_5)_4]$ on ethylene polymerisation.

Compound	Catalyst loading (mg)	T (°C)	Time (min)	Activator loading (mg)	Pressure (bar)	PE (g)	Activity ($kg_{PE}\ mol_{cat}^{-1}\ h^{-1}\ bar^{-1}$)
2.7	5	60	30	15.2	2	0.041	2.17
3.1	5	60	30	9.6	2	0	0
3.2	5	60	30	9.8	2	0.174	14.2
3.3	5	60	30	10.6	2	0.002	1.51×10^{-1}

The activity of Pn^*TiR_2 [R = Me (**2.7**), CH_2Ph (**3.1**), CH_2SiMe_3 (**3.2**) and $CH_2{}^tBu$ (**3.3**)] were studied in toluene solution following the addition of 10 equivalents of $Al(^iBu_3)$.

Table 5.4: Results summary of Pn^*TiR_2 with $[Al^iBu_3]$ on ethylene polymerisation.

Compound	Catalyst loading (mg)	T (°C)	Time (min)	Activator loading (mg)	Pressure (bar)	PE (g)	Activity ($kg_{PE}\ mol_{cat}^{-1}\ h^{-1}\ bar^{-1}$)
2.7	5	60	30	37.5	2	0	0
3.1	5	60	30	23.8	2	0	0
3.2	5	60	30	24.3	2	0.005	4.09×10^{-1}
3.3	5	60	30	26.3	2	0.139	10.5
3.3(b)	5	60	30	26.3	2	0.068	5.12

Activation with hydrogen failed to produce any PE for any of the catalysts. This seems somewhat erroneous as even though the activities for the other systems are poor there is still some PE produced even in the absence of activator.

5.3 Conclusion

The activity of a series of monomeric Pn*TiR_2 complexes for the homogeneous polymerisation of ethylene have been investigate using three activators. In general, the observed activities were low, the highest activity was achieved for a combination of **3.2** and $[Ph_3C][B(C_6F_5)_4]$, yielding an activity of 21.8 kgPE molcat^{-1} h^{-1} bar^{-1}. Indeed, **3.2** was consistently more active than the others but deemed moderate on Gibsons scale. These findings are somewhat surprising giving the compounds electronic deficiency compared to other metallocene catalysts.

5.4 References for Chapter Five

1 B. Heurtefeu, C. Bouilhac, É. Cloutet, D. Taton, A. Deffieux, and H. Cramail, *Progress in Polymer Science*, 2011, 36, 89–126.

2 K. Ziegler, H. G. Gellert, K. Zosel, W. Lehmkuhl, and W. Pfohl, *Angewandte Chemie*, 1955, 67, 424–424.

3 K. Ziegler, E. Holzkamp, H. Breil, and H. Martin, *Chimica e l'Industria (Milan, Italy)*, 1955, 37, 881–882.

4 G. Natta, P. Pino, P. Corradini, F. Danusso, E. Mantica, G. Mazzanti, and G. Moraglio, *Journal of the American Chemical Society*, 1955, 77, 1708.

5 G. Natta, *Journal of Polymer Science*, 1955, XVI, 143–151.

6 A. Andresen, H.-G. Cordes, J. Herwig, W. Kaminsky, A. Merck, R. Mottweiler, J. Pein, H. Sinn, and H.-J. Vollmer, *Angewandte Chemie*, 1976, 88, 689–690.

7 H. Sinn, W. Kaminsky, H.-J. Vollmer, and R. Woldt, *Angewandte Chemie*, 1980, 92, 396–402.

8 J. A. Ewen, *Journal of the American Chemical Society*, 1984, 106, 6355–6364.

9 P. Cossee, *Journal of Catalysis*, 1964, 3, 80–88.

10 E. Arlman and P. Cossee, *Journal of Catalysis*, 1964, 3, 99–104.

11 M. L. H. Green, *Pure and Applied Chemistry*, 1978, 50, 27–35.

12 K. J. Ivin, J. J. Rooney, C. D. Stewart, M. L. H. Green, and R. Mahtab, *Journal of the Chemical Society, Chemical Communications*, 1978, 604.

13 P. L. Watson, *Journal of the American Chemical Society*, 1982, 104, 337–339.

14 R. H. Grubbs and G. W. Coates, *Accounts of Chemical Research*, 1996, 29, 85–93.

15 M. R. Mason, J. M. Smith, S. G. Bott, and A. R. Barron, *Journal of the American Chemical Society*, 1993, 115, 4971–4984.

16 D. Fischer and R. Mülhaupt, *Journal of Organometallic Chemistry*, 1991, 417, C7–C11.

17 E. Y.-X. Chen and T. J. Marks, *Chemical Reviews*, 2000, 100, 1391–1434.

18 P. Ransom, A. E. Ashley, N. D. Brown, A. L. Thompson, and D. O'Hare, *Organometallics*, 2011, 30, 800–814.

Chapter Six

Experimental Details

6.1 General procedures and physical measurements

6.1.1 General procedures

All organometallic manipulations were performed under an atmosphere of N_2 using standard Schlenk line techniques, on a dual vacuum-inlet gas manifold or MBraun UNIlab glovebox, unless stated otherwise. Solvents used were dried by either; reflux over sodium-benzophenone diketyl (THF, Et_2O), over 3 Å molecular sieves (1,4-dioxane), or passage through activated alumina (pentane, hexane, toluene, benzene, CH_2Cl_2) using a MBraun SPS-800 solvent system. Solvents were stored in dried glass ampoules over K mirrors with the exception of THF and CH_2Cl_2 which were stored on pre-dried 3 Å molecular sieves and all thoroughly degassed by passage of a stream of N_2 gas through the liquid. Deuterated solvents for NMR spectroscopy of oxygen or moisture sensitive materials were treated as follows: C_6D_6 and toluene-d_8 were freeze-pump-thaw degassed and dried over a K mirror and CD_2Cl_2 was dried over 3 Å molecular sieves.

6.1.2 Elemental analysis

Elemental microanalyses were conducted by Stephen Boyer at London Metropolitan University, London.

6.1.3 Mass spectrometry

Electron Impact (EI) mass spectra were recorded by Mr Colin Sparrow of the Chemistry Research Laboratory, Oxford, using a Bruker FT-ICR-MS Apex III spectrometer.

6.1.4 IR spectroscopy

IR spectra were recorded on a Nicolet iS5 ThermoScientific spectrometer (range 4000-400 cm^{-1}, resolution 1 cm^{-1}) as KBr discs. Samples were prepared in the glovebox,

mixed and ground with anhydrous KBr, then pressed into discs using an in-house purpose built press and holder, the spectra were recorded immediately.

6.1.5 NMR spectroscopy

^{1}H, ^{13}C and ^{7}Li NMR spectroscopy were performed using; a Bruker AVII 500 MHz with ^{13}C cryoprobe, Varian Mercury VX-Works 300 MHz or Varian Mercury 300 MHz spectrometer and recorded at 298 K unless stated otherwise. ^{1}H and ^{13}C NMR spectra were referenced *via* the residual protio-solvent peak; ^{7}Li were referenced externally to LiCl. Oxygen or moisture sensitive samples were prepared using dried and degassed solvents under an inert atmosphere in a glovebox and were sealed in Wilmad 5mm 505-PS-7 tubes fitted with Young's type concentric stopcocks.

Calculations and modelling of **3.7**'s fluxional behaviour was performed by Dr. Nick Rees of the University of Oxford.

6.2 Single crystal X-ray diffraction

Data were collected and structure determinations and refinement were carried out by Mr Mark Chadwick of the Chemistry Research Laboratory, Oxford, except **2.2**, **2.4** and **3.2** which were undertaken by Dr Andrew Ashley of Imperial College, London.

Crystals were mounted on 0.2 mm MiTeGen MicroMounts using perfluoropolyether oil and cooled rapidly to 150 K in a stream of N_2 using an Oxford Cryosystems Cryostream unit. Diffraction data were measured using an Enraf-Nonius KappaCCD diffractometer (graphite-monochromated MoK_{α} radiation, λ = 0.71073 Å). Intensity data were processed using the DENZO-SMN package. The structure was then solved using the direct-methods program SIR92, which located all non-hydrogen atoms. Subsequent full-matrix least-squares refinement was carried out using the CRYSTALS program suite.[1,2] Full crystallographic data and CIF files may be found in the electronic appendix.

6.3 Ethylene polymerisations

Ethylene polymerisations were conducted with assistance from Dr Ian Casely of the Chemistry Research Laboratory, Oxford.

6.4 Computational methods

Calculations were performed by Dr. Muhsen Al-Ibadi of the Inorganic Chemistry Laboratory, Oxford. All gas phase optimisations were performed with Gaussian09[3] programme package with density functional theory (DFT). Geometries for all intermediates and transition states involved in catalytic cycle were optimised using the PBE1PBE functional,[4] and the SDD basis sets[5,6] was used for Ti. The SVP basis set of Ahlrichs and co-workers was used for the remaining atoms (C, H and O).[7] An extra set of *f*-polarisation functions was added to Ti (αf = 1.506).[8] Unrestricted geometry optimisations were carried out in each case. Vibrational frequency analysis was carried out at the same level to confirm the optimised structures to be ground states (without imaginary frequencies) or transition states (TS) (one imaginary frequency).

6.5 Starting materials

6.5.1 Commercially supplied reagents

All reagents were used as received, unless specified otherwise. All deuterated solvents were supplied by Goss Scientific (minimum 99.5at.%D). Solvents were supplied by either Rathburn or Fisher Scientific (pentane, hexane, benzene, toluene, Et_2O, CH_2Cl_2, THF, 1,4-dioxane). Me_3SnCl, MeLi (1.6 M in Et_2O), KBr (FT-IR grade, >99%), Al^iBu_3, MeMgCl (3.0 M in THF), $PhCH_2MgCl$ (1.0 M in Et_2O), $(C_3H_5)MgCl$ (2.0 M in THF), PhMgCl (2.0 M in THF), H_2 (>99.95%) and 3Å molecular sieves were supplied by Aldrich. Ethylene (CP grade, 99.92%) and CO (CP grade, 99.995%) were supplied by BOC gases. CO_2 (99.995%) was supplied by ARGO international. Silica (EX757) was supplied by PQ Corporation and celite was supplied by Fluka.

6.5.2 Literature preparations

The following compounds were prepared according to published procedures: $Li_2Pn^*(TMEDA)_x$,[9] *cis*-$Pn^*(SnMe_3)_2$,[9] $TiCl_4{\cdot}2THF$,[10] NaCp,[11] $NaCH_2SiMe_3$,[12] $LiCH_2{}^tBu$,[13] Me_2Mg,[14] $[Ph_3C][B(C_6F_5)_4]$,[15] $[PhNMe_2H][B(C_6F_5)_4]$.[16]

6.6 Experimental details for Chapter Two

All experiments were conducted under a N_2 atmosphere using dry solvents.

6.6.1 Improved synthesis of [Pn*TiCl(μ-Cl)]$_2$ (2.1)

Me_3SnCl (6.48 g, 32.53 mmol) in benzene (40 ml) was added to a slurry of $Li_2Pn^*(TMEDA)_x$ (x = 0.099, 3.46 g, 16.35 mmol) in benzene (20 ml) whilst stirring at room temperature. The light tan suspension instantly turned to a dark brown solution with a fine precipitate of LiCl formed and was stirred for a further 16 hours. The suspension was then filtered through Celite on a frit and extracted with toluene (3 x 70 ml) until colourless. Volatiles were reduced to 40 ml *in vacuo*, cooled to −78 °C then transferred to $TiCl_4$·2THF in toluene (20 ml) at −78 °C. The reaction mixture was slowly warmed to room temperature and stirred for a further 16 hours after which it was filtered through celite on a frit and eluted with toluene (3 x 100 ml). The solvent was removed under reduced pressure and the residue subjected to dynamic vacuum (10^{-3} mbar) for 24 hours. The residuum was washed with ice cold (0 °C) pentane (3 x 30 ml) then extracted with hot (90 °C) toluene, filtered *via* cannula and cooled to −35 °C yielding a red-brown crystalline solid which was determined pure by ^{1}H NMR spectroscopy.

Yield = 3.71 g (12.16 mmol, 74.4%).

6.6.2 Synthesis of [Pn*TiMe(μ-Cl)]$_2$ (2.2)

To a stirred solution of **2.1** (0.200 g, 0.328 mmol) in Et_2O (40 ml), MeLi (1.6 M in Et_2O, 0.410 ml, 0.656 mmol) was added *via* syringe at room temperature. The mixture instantly turned dark green and was allowed to stir for 15 minutes after which point the solvent was stripped under vacuum. The residue was washed with pentane before being extracted in toluene and reduced to a minimum volume, which was cooled to −35 °C. A green microcrystalline solid was precipitated, and after removal of the supernatant the solid was washed with −78 °C toluene.

Yield = 0.106 g (0.186 mmol, 56.8%).

6.6.3 Synthesis of [Pn*Ti(μ-Cl)]$_2$(μ-CH_2) (2.3)

Benzene (15 ml) was added to a finger ampoule loaded with **2.2** (0.030 g, 0.053 mmol) and heated to 50 °C for 72 hours. The solution evolved from mint green to a vivid dark magenta and volatiles were stripped under reduced pressure. The residuum

was extracted with hexane in the glovebox, filtered through celite and slow cooled to −35 °C affording a dark red microcrystalline solid.

Yield = 0.014 g (0.025 mmol, 48.0%).

6.6.4 Synthesis of [Pn*Ti(μ-Me)]$_2$(μ-CH$_2$) (2.4)

Method 1: **2.3** + Me_2Mg

To an NMR tube containing **2.3** in C_6D_6 was added an excess of Me_2Mg and a drop of Et_2O. The tube was sonicated for three hours and the solution changed to a darker shade of purple. NMR analysis indicated complete conversion of **2.3** to **2.4**.

Method 2: **2.5** + heat

An NMR aliquot containing **2.5**, C_6D_6 and residual THF taken during the preparation of **2.5** was heated to 50 °C for four days after which time the initial pink solution had transformed to a dark purple. All volatiles were removed under vacuum and subjected to a dynamic vacuum (10^{-3} mbar) for three hours. The residue was extracted with pentane, filtered through celite before removal of the solvent under vacuum and redissolving in C_6D_6 determined **2.4** pure by NMR.

6.6.5 Synthesis of [Pn*TiMe(μ-Me)$_2$]$_2$Mg (2.5)

To a Schlenk tube charged with **2.1** (0.100 g, 0.164 mmol) and Me_2Mg (0.089 g, 1.639 mmol) was added toluene (20 ml) followed by THF (10 ml). The heterogeneous mixture was allowed to stir for 48 hours after which it had turned green-brown in colour. Volatiles were removed *in vacuo* and the residue extracted with hexane to afford a pink solution. On cooling to −35 °C, green crystals were precipitated.

6.6.6 Synthesis of [Pn*TiMe$_3$]Li.(Et$_2$O)$_x$ (2.6)

To a stirred suspension of **2.1** (0.091 g, 0.149 mmol) in Et_2O (30 ml), MeLi (1.6 M in Et_2O, 0.597 ml, 0.955 mmol) was added at −78 °C and allowed to warm to room temperature. The solution immediately turned green and upon warming dark purple then finally at around 0-5 °C deep teal. Solvent was removed under reduced pressure and the residuum washed with ice cold (0 °C) pentane (2 x 20 ml). The product was then extracted with Et_2O and stored as a solution at −35 °C.

6.6.7 Synthesis of Pn*TiMe$_2$ (2.7)

MeMgCl (3.0 M in THF, 0.918 ml, 2.754 mmol) was added to a slurry of **2.1** (0.400 g, 0.656 mmol) in Et_2O (40 ml) whist stirring at −78 °C. The mixture instantly turned green, then red and finally upon warming to room temperature purple. 1,4-dioxane (5 ml) was added to precipitate all magnesium salts,[17,18] and the resulting suspension filtered through celite on a frit and eluted with pentane. The volatiles were removed under vacuum and subjected to a dynamic vacuum (10^{-3} mbar) for five hours. The residue was extracted with hexane and filtered *via* cannula, reduced to minimum volume and the product precipitated as pink block shaped crystals at −78 °C.

Yield = 0.266 g (1.008 mmol, 76.9%).

6.7 Experimental details for Chapter Three

All experiments were conducted under a N_2 atmosphere using dry solvents.

6.7.1 Synthesis of Pn*Ti(CH$_2$Ph)$_2$ (3.1)

$PhCH_2MgCl$ (1.0 M in Et_2O, 2.754 ml, 2.754 mmol), was added to a slurry of **2.1** (0.400 g, 0.656 mmol) in Et_2O (40 ml) whist stirring at −78 °C. The mixture instantly turned dark brown and was allowed to stir for 20 minutes at −78 °C before warming to room temperature. 1,4-dioxane (5 ml) was added to precipitate magnesium salts,[17,18] then all volatiles were stripped under reduced pressure and subjected to a dynamic vacuum (10^{-3} mbar) for six hours. The residuum was extracted with pentane and filtered through celite on a frit before being reduced to minimum volume and cooled to −35 °C to yield a bronze microcrystalline solid

Yield = 0.423 g (1.015 mmol, 77.4%).

6.7.2 Synthesis of Pn*Ti(CH$_2$SiMe$_3$)$_2$ (3.2)

A Youngs tap side arm schlenk was charged with **2.1** (0.400 g, 0.656 mmol) and $NaCH_2SiMe_3$ (0.318 g, 2.885 mmol) to which pentane (40 ml) was added and allowed to stir for 16 hours. The purple suspension was filtered through celite on a frit and eluted with pentane until colourless. The solution was reduced to minimum volume and cooled to −78 °C which yielded a deep purple microcrystalline solid which was collected in two crops.

Yield = 0.385 g (0.942 mmol, 71.8%).

6.7.3 Synthesis of Pn*Ti($CH_2{}^tBu)_2$ (3.3)

To a stirred suspension of **2.1** (0.400 g, 0.656 mmol) in benzene (30 ml), $LiCH_2{}^tBu$ (0.205 g, 2.622 mmol) was added in benzene (30 ml) at room temperature and the mixture instantly turned dark red-purple. The solvent was removed under reduced pressure and the residue subjected to dynamic vacuum (10^{-3} mbar) for six hours. The product was extracted with hexane, reduced to minimum volume and cooled to −78 °C which deposited a microcrystalline red solid.

Yield = 0.360 g (0.956 mmol, 72.9%).

6.7.4 Synthesis of Pn*TiCl($CH_2{}^tBu$) (3.4)

$LiCH_2{}^tBu$ (0.051 g, 0.656 mmol) in benzene (20 ml) was quickly added to **2.1** (0.200 g, 0.328 mmol) in benzene (30 ml) at room temperature whilst stirring giving an instant colour change from dark brown to a dark solution with a purple-red hint. Volatiles were removed under reduced pressure and subjected to a dynamic vacuum (10^{-3} mbar) for five hours. The residuum was extracted with pentane, reduced to minimum volume and cooled to −78 °C precipitating magenta rod and block shaped crystals.

Yield = 0.127 g (0.373 mmol, 56.7%).

6.7.5 Synthesis of [Pn*TiPh(μ-Cl)]$_2$ (3.5)

PhMgCl (2.0 M in THF, 0.164 ml, 0.328 mmol), was added quickly to a solution of **2.1** (0.100 g, 0.164 mmol) in benzene (30 ml) whist stirring at room temperature, resulting in an instant colour change from dark brown to vivid green. After 10 minutes, 1,4-dioxane (5 ml) was added to precipitate any remaining magnesium salts,[17,18] and volatiles were removed under vacuum. The residue was subjected to a dynamic vacuum (10^{-3} mbar) for five hours, washed with pentane (2 x 20 ml) before being extracted with toluene and slow cooled to −35 °C precipitating an emerald green crystalline solid.

Yield = 0.077 g (0.111 mmol, 68.0%).

6.7.6 Synthesis of Pn*TiCl(η^5-Cp) (3.6)

To a schlenk charged with **2.1** (0.100 g, 0.164 mmol) and NaCp (0.029 g, 0.328 mmol) was added −78 °C THF and allowed to stir for 30 minutes. On warming to room temperature the reaction mixture passed through light orange and then red in colour and was stirred for a further hour. Solvent was removed under reduced pressure and subjected to a dynamic vacuum (10^{-3} mbar) for three hours. The residue was extracted with hot (50 °C) hexane, reduced to minimum volume and slow cooled to −35 °C precipitating red crystals.

Yield = 0.091 g (0.273 mmol, 83.4%).

6.7.7 Synthesis of Pn*Ti(η^5-Cp)(η^1-Cp) (3.7)

Benzene (20 ml) was added to a mini schlenk loaded with NaCp (0.072 g, 0.820 mmol) and **2.1** (0.100 g, 0.164 mmol) and sonicated for 3 hours. The suspension was filtered *via* cannula, extracted with benzene (3 x 20 ml) and volatiles then stripped under reduced pressure and subjected to a dynamic vacuum (10^{-3} mbar) for three hours. The residue was extracted with hot (60 °C) hexane, reduced to minimum volume and slow cooled to −35 °C depositing red-orange crystals.

Yield = 0.074 g (0.203 mmol, 61.7%).

6.7.8 Synthesis of Pn*Ti(C_3H_5)$_2$ (3.8)

A schlenk was charged with **2.1** (0.250 g, 0.410 mmol) dissolved in Et_2O (40 ml) and cooled to −78 °C. (C_3H_5)MgCl (2.0 M in THF, 0.901 ml, 1.803 mmol) was added and allowed to stir for 15 minutes before slowly warming to 0 °C by which point the solution had turned dark brown. 1,4-dioxane (5 ml) was added to precipitate magnesium salts,[17,18] then all volatiles were removed *in vacuo* and subjected to a dynamic vacuum (10^{-3} mbar) for one hour. The residue was extracted with hexane and filtered through celite on a frit before being reduced to minimum volume and cooled to −78 °C, depositing yellow-orange needle shaped crystals.

Yield = 0.032 g (0.101 mmol, 12.4%).

6.7.9 Synthesis of Pn*TiPh$_2$ (3.9)

PhMgCl (2.0 M in THF, 0.516 ml, 1.033 mmol), was added slowly to a slurry of **2.1** (0.150 g, 0.246 mmol) in Et_2O (30 ml) whist stirring at −78 °C. The light tan suspension instantly passed through a dark green to a piquant green and was allowed to stir for 30 minutes at −78 °C. The ^{1}H NMR spectroscopy indicated all the **2.1** starting material had been consumed and 1,4-dioxane (5 ml) was added to precipitate magnesium salts.[17,18] The slurry was filtered through celite on a jacketed frit cooled to −78 °C and the product eluted with −78 °C Et_2O. Volatiles were removed under vacuum and subjected to a dynamic vacuum (10^{-3} mbar) for three hours. Above −60 °C the solution turned purple in colour. The residuum was extracted with Et_2O producing a purple-red solution before being reduced to a minimum volume and cooled to −78 °C, precipitating purple needle shaped crystals.

Yield = 0.016 g (0.041 mmol, 8.4%).

6.8 Experimental details for Chapter Four

All experiments were conducted under a N_2 atmosphere using dry solvents.

6.8.1 Synthesis of Pn*Ti(κ^2-O$_2$CMe)$_2$ (4.1)

2.7 (0.058 g, 0.220 mmol) was added to a finger ampoule and dissolved in benzene (20 ml). The pink solution was degassed *via* a freeze-pump-thaw method; freezing the solution into a glass then subjecting it to a dynamic vacuum (10^{-3} mbar) for 20 minutes followed by thawing under a static vacuum. This cycle was completed twice more before CO_2 was admitted to the stirred solution, resulting in an instant colour change through a murky orange-brown to a bright orange. The reaction was allowed to stir for a further 15 hours after which solvent was removed *in vacuo* and subjected to a dynamic vacuum (10^{-3} mbar) for three hours. The residue was extracted with hexane and filtered through celite in the glovebox before being reduced to minimum volume and slow cooled to −35 °C, affording after 2 crops an orange crystalline solid.

Yield = 0.063 g (0.180 mmol, 81.9%).

6.8.2 Synthesis of Pn*Ti(κ^2-$O_2CCH_2Ph)_2$ (4.2)

An identical synthesis to 7.8.1 was undertaken utilising **3.1** (0.064 g, 0.154 mmol). The reaction was much slower taking 40 hours to run to completion as judged by ^{1}H NMR spectroscopy and resulted in a yellow solution. Crystals were precipitated from a concentrated hexane solution, at −35 °C.

Yield = 0.056 g (0.112 mmol, 72.6%).

6.8.3 Synthesis of Pn*Ti(κ^2-$O_2CCH_2SiMe_3)_2$ (4.3)

An identical synthesis to 7.8.1 was undertaken using **3.2** (0.067 g, 0.164 mmol). The reaction required three hours to turn orange in colour but was allowed to react for a further 12 hours before work up. Several crystallisation methods were unsuccessfully attempted but the resulting oil was determined pure by ^{1}H NMR.

6.8.4 Synthesis of Pn*Ti(κ^2-$O_2CCH_2{}^tBu)_2$ (4.4)

An identical synthesis to 7.8.1 was undertaken using **3.3** (0.063 g, 0.168 mmol). The reaction was much slower taking 15 hours to run to completion as judged by ^{1}H NMR spectroscopy and resulted in an orange solution. Similar to 7.8.3 several crystallisation methods were attempted but proved ineffective, the resulting oil was determined pure by ^{1}H NMR.

6.8.5 Synthesis of Pn*Ti[κ^2-O-C(CH_2CMe_3)=C(CH_2CMe_3)-O] (4.5)

3.3 (0.054 g, 0.143 mmol) was added to a finger ampoule and dissolved in benzene (20 ml). The solution was degassed *via* the same freeze-pump-thaw method described in section 7.8.1 (three cycles), followed by introduction of CO. The reaction was allowed to stir for 16 hours after which volatiles were removed under reduced pressure and subjected to a dynamic vacuum (10^{-3} mbar) for three hours. The residue was extracted with hexane, filtered through celite in the glovebox before being reduced to minimum volume and cooled to −35 °C to precipitate an orange crystalline solid.

Yield = 0.017 g (0.040 mmol, 27.6%).

6.8.6 Synthesis of Pn*Ti[κ^2-O-C(CH_2SiMe_3)=C(CH_2SiMe_3)-O] (4.6)

An identical synthesis to 7.8.5 was undertaken utilising **3.2** (0.052 g, 0.127 mmol). The starting material changed from purple through red to an orange colour on admission of CO. Needle crystals were precipitated from a concentrated hexane solution at −35 °C.

Yield = 0.013 g (0.028 mmol, 21.4%).

6.8.7 Synthesis of {Pn*Ti[μ-η^1(O):η^2-$OC(Me)_2$]}$_2$ (4.7)

A partial vacuum was induced to an NMR tube charged with **2.7** (0.013 g, 0.049 mmol) in C_6D_6 by freezing the sealed solution at −78 °C. Carbon monoxide was emitted, the tube sealed and the glass allowed to thaw under an atmosphere of CO. When the glass/solution was mobile the sample was vigorously shaken resulting in the pink solution turning a dark red. NMR analysis indicated the predominant species formed was **4.7**.

6.8.8 Synthesis of [Pn*Ti(μ_2-H)]$_3$(μ_3-H) (4.8)

Benzene (20 ml) was added to a finger ampoule charged with **3.2** (0.050 g, 0.122 mmol). After the purple solution was degassed by the freeze-pump-thaw method described in section 7.8.1, H_2 gas was introduced and the solution allowed to stir for 16 hours at room temperature after which it had turned blue-grey. Solvent was removed under reduced pressure and subjected to a dynamic vacuum (10^{-3} mbar) for four hours. The residuum was extracted with hexane in the glovebox and filtered through celite before being reduced to minimum volume and slow cooled to −35 °C affording large, very dark-purple crystals.

Yield = 0.007 g (0.010 mmol, 23.7%).

6.8.9 Synthesis of (Pn*TiCl)$_2$(μ-O) (4.9)

A similar synthesis to section 7.7.4 was undertaken; $LiCH_2{}^tBu$ (0.026 g, 0.328 mmol) in benzene (15 ml) was quickly added to a stirred solution of **2.1** (0.100 g, 0.164 mmol) in benzene (30 ml) at room temperature. An instant colour change resulted from dark brown to a dark solution with a purple-red hint. Volatiles were removed *in vacuo* and subjected to a dynamic vacuum (10^{-3} mbar) for five hours. The residue was

extracted with wet hexane, reduced to minimum volume and slow cooled to −35 °C precipitating crimson crystals.

Yield = 0.025 g (0.045 mmol, 27.5%).

6.9 Experimental details for Chapter Five

All experiments were conducted under a N_2 atmosphere using dry solvents unless otherwise stated.

6.9.1 Ethylene polymerisations conditions

A generic representative example is detailed below for Pn*TiR_2 (R = Me, CH_2Ph, CH_2SiMe_3 and $CH_2{}^tBu$);

To a Rotaflo ampoule containing a stirrer bar was added Pn*TiR_2 (R = Me, CH_2Ph, CH_2SiMe_3 and $CH_2{}^tBu$; 0.005 g) followed by toluene (25 ml). The ampoule was sealed, cycled onto the schlenk line and briefly degassed to reduce the pressure of the nitrogen atmosphere. The ampoule was subsequently heated to 60 °C with vigorous stirring, creating a good vortex, and pressurised with ethylene gas (2 bar) for 30 minutes. The polymerisation was quenched by removal of the reaction from heat and depressurised by exposure to the atmosphere. The polymer was then filtered and washed with toluene (2 x 15 ml) and pentane (30 ml) and dried overnight in a vacuum oven (50 °C, 1 mbar), yielding the resultant polymer product.

6.9.2 Polymerisations with no activator

The procedure was followed as detailed above (Section 6.9.1);

- R = Me (**2.7**) (0.005 g, 0.019 mmol).

The purple toluene solution of **2.7** remained the same throughout the run, with no discernible change of colour and no polyethylene formed.

Yield = 0.000 g.

- R = CH_2Ph (**3.1**) (0.005 g, 0.013 mmol).

The pale brown solution of **3.1** remained constant throughout the run, with no noticeable change of colour and no polyethylene formed.

Yield = 0.000 g.

- R = CH_2SiMe_3 (**3.2**) (0.005 g, 0.012 mmol).

The initial pale purple toluene solution of **3.2** turned yellow on addition of C_2H_4 and polyethylene was formed.

Yield = 0.016 g.

- R = $CH_2{}^tBu$ (**3.3**) (0.005 g, 0.012 mmol).

The initial brown toluene solution of **3.3** remained constant throughout the run, with no noticeable change of colour and polyethylene was produced.

Yield = 0.002 g.

6.9.3 Polymerisations using $[Ph_3C][B(C_6F_5)_4]$ activator

The same procedure was followed as detailed above (Section 6.9.1) but included the addition of $[Ph_3C][B(C_6F_5)_4]$ at the same time as Pn*TiR_2 in a 1:1 ratio;

- R = Me (**2.7**) (0.005 g, 0.019 mmol); $[Ph_3C][B(C_6F_5)_4]$ (0.017 g, 0.019 mmol).

On addition of $[Ph_3C][B(C_6F_5)_4]$, the initial purple solution of **2.7** turned yellow in colour and precipitated a brown oil. A solid green piece of polyethylene was formed.

Yield = 0.200 g.

- R = CH_2Ph (**3.1**) (0.005 g, 0.013 mmol); $[Ph_3C][B(C_6F_5)_4]$ (0.012 g, 0.013 mmol).

The initial pale brown **3.1**, instantly formed a clear green solution on addition of $[Ph_3C][B(C_6F_5)_4]$. After 10 minutes, a green microcrystalline solid precipitated, leaving a pale yellow solution. No polyethylene was produced.

Yield = 0.000 g.

- R = CH_2SiMe_3 (**3.2**) (0.005 g, 0.012 mmol); $[Ph_3C][B(C_6F_5)_4]$ (0.011 g, 0.012 mmol).

On addition of $[Ph_3C][B(C_6F_5)_4]$ to **3.2**, the initial pale purple solution turned orange in colour. Polyethylene started to form on admission of C_2H_4, which retarded stirring of the heterogeneous mixture. Isolation of the polyethylene yielded a green solid.

Yield = 0.267 g.

- R = $CH_2{}^tBu$ (**3.3**) (0.005 g, 0.012 mmol); $[Ph_3C][B(C_6F_5)_4]$ (0.011 g, 0.012 mmol).

On addition of $[Ph_3C][B(C_6F_5)_4]$, the initial brown solution of **3.3** turned yellow in colour and precipitated a brown oil. Polyethylene was formed.

Yield = 0.012 g.

6.9.4 Polymerisations using $[PhNMe_2H][B(C_6F_5)_4]$ activator

The same procedure was followed as detailed above (Section 6.9.1) but included the addition of $[PhNMe_2H][B(C_6F_5)_4]$ at the same time as Pn*TiR_2 in a 1:1 ratio;

- R = Me (**2.7**) (0.005 g, 0.019 mmol); $[PhNMe_2H][B(C_6F_5)_4]$ (0.015 g, 0.019 mmol).

On addition of $[PhNMe_2H][B(C_6F_5)_4]$ to **2.7**, a purple-brown solution was formed. Pale green polyethylene was produced.

Yield = 0.041 g.

- R = CH_2Ph (**3.1**) (0.005 g, 0.013 mmol); $[PhNMe_2H][B(C_6F_5)_4]$ (0.011 g, 0.013 mmol).

The Identical reactivity is observed as witnessed with using the $[Ph_3C][B(C_6F_5)_4]$ activator; the initial pale brown **3.1**, instantly formed a clear green solution on addition of $[PhNMe_2H][B(C_6F_5)_4]$. After 10 minutes, a green microcrystalline precipitate forms, leaving a pale yellow solution. No polyethylene was produced.

Yield = 0.000 g.

- R = CH_2SiMe_3 (**3.2**) (0.005 g, 0.012 mmol); $[PhNMe_2H][B(C_6F_5)_4]$ (0.010 g, 0.012 mmol).

An identical reactivity is observed as seen with using the $[Ph_3C][B(C_6F_5)_4]$ activator; on addition of $[PhNMe_2H][B(C_6F_5)_4]$ to **3.2**, the initial pale purple solution turned orange in colour. Polyethylene started to form on admission of C_2H_4, which retarded stirring of the heterogeneous mixture. Isolation of the polyethylene yielded a green solid.

Yield = 0.174 g.

- R = $CH_2{}^tBu$ (**3.3**) (0.005 g, 0.012 mmol); $[PhNMe_2H][B(C_6F_5)_4]$ (0.010 g, 0.012 mmol).

On addition of $[PhNMe_2H][B(C_6F_5)_4]$ to **3.3**, a brown solution was formed in conjunction with a dark precipitate. Polyethylene was produced.

Yield = 0.002 g.

6.9.5 Polymerisations using Al^iBu_3 activator

The same procedure was followed as detailed above (Section 6.9.1) but included the addition of Al^iBu_3 at the same time as Pn^*TiR_2 in a 10:1 ratio;

- R = Me (**2.7**) (0.005 g, 0.019 mmol); Al^iBu_3 (0.038 g, 0.189 mmol).

The initial purple toluene solution of **2.7** lightened on addition of Al^iBu_3 and turned pale brown with admission of C_2H_4. No polyethylene was formed.

Yield = 0.000 g.

- R = CH_2Ph (**3.1**) (0.005 g, 0.013 mmol); Al^iBu_3 (0.026 g, 0.133 mmol).

On addition of Al^iBu_3 to **3.1**, the initial pale brown solution turned green in colour. No polyethylene was produced.

Yield = 0.000 g.

- R = CH_2SiMe_3 (**3.2**) (0.005 g, 0.012 mmol); Al^iBu_3 (0.024 g, 0.122 mmol).

The initial pale purple solution turned yellow in colour on addition of Al^iBu_3. Polyethylene was formed.

Yield = 0.005 g.

- R = $CH_2{}^tBu$ (**3.3**) (0.005 g, 0.012 mmol); Al^iBu_3 (0.024 g, 0.120 mmol).

The brown toluene solution of **3.3** remained constant throughout the run, with no discernable change in colour on addition of $Al^{i}Bu_3$ or C_2H_4. Fine white, free flowing granular polyethylene formed.

Yield = 0.139 g.

6.9.6 Polymerisations using H_2 activation

A similar procedure was followed as detailed above (Section 6.9.1) but before the solution was exposed to a C_2H_4 atmosphere, it was degassed *via* the same freeze-pump-thaw method as described in Section 6.8.1 and H_2 (1 bar) was admitted and allowed to stir for 30 minutes. A parallel procedure was then followed.

- R = Me (**2.7**) (0.005 g, 0.019 mmol).

On exposure of **2.7** to a H_2 atmosphere, the initial purple solution gradually turned brown in colour and finally orange following the admission of C_2H_4. No polyethylene was produced.

Yield = 0.000 g.

- R = CH_2Ph (**3.1**) (0.005 g, 0.013 mmol).

The initial pale brown solution of **3.1** turned an orange colour following exposure to H_2. The solution steadily lightened to a yellow-orange after admittance of C_2H_4. No polyethylene was formed.

Yield = 0.000 g.

- R = CH_2SiMe_3 (**3.2**) (0.005 g, 0.012 mmol).

On admission of H_2 to **3.2**, the initial pale purple solution turned light orange in colour and remained constant following exposure to C_2H_4. No polyethylene was produced.

Yield = 0.000 g.

- R = $CH_2{}^{t}Bu$ (**3.3**) (0.005 g, 0.012 mmol).

The initial brown solution of **3.3** remained constant throughout the run, with no discernable change of colour. No polyethylene was formed.

Yield = 0.000 g.

6.10 References for Chapter Six

1. A. Altomare, G. Cascarano, C. Giacovazzo, A. Guagliardi, M. C. Burla, G. Polidori, and M. Camalli, *J. Appl. Crystallogr.*, 1994, 27, 435–435.

2. P. W. Betteridge, J. R. Carruthers, R. I. Cooper, K. Prout, and D. J. Watkin, *J. Appl. Crystallogr.*, 2003, 36, 1487.

3. M. J. Frisch, G. W. Trucks, H. B. Schlegel, G. E. Scuseria, M. A. Robb, G. Cheeseman, J. R. Scalmani, V. Barone, B. Mennucci, G. A. Petersson, H. Nakatsuji, M. Caricato, X. Li, H. P. Hratchian, A. F. Izmaylov, J. Bloino, G. Zheng, J. L. Sonnenberg, M. Hada, M. Ehara, K. Toyota, R. Fukuda, J. Hasegawa, M. Ishida, T. Nakajima, Y. Honda, O. Kitao, H. Nakai, T. Vreven, J. A. Montgomery, Jr., J. E. Peralta, F. Ogliaro, M. Bearpark, J. J. Heyd, E. Brothers, K. N. Kudin, V. N. Staroverov, R. Kobayashi, J. Normand, K. Raghavachari, A. Rendell, J. C. Burant, S. S. Iyengar, J. Tomasi, M. Cossi, N. Rega, J. M. Millam, M. Klene, J. E. Knox, J. B. Cross, V. Bakken, C. Adamo, J. Jaramillo, R. Gomperts, R. E. Stratmann, O. Yazyev, A. J. Austin, R. Cammi, C. Pomelli, J. W. Ochterski, R. L. Martin, K. Morokuma, V. G. Zakrzewski, G. A. Voth, P. Salvador, J. J. Dannenberg, S. Dapprich, A. D. Daniels, Ö. Farkas, J. B. Foresman, J. V. Ortiz, J. Cioslowski, and D. J. Fox, *Gaussian 09, Revision A.02, Gaussian, Inc., Wallingford CT*, 2009.

4. C. Adamo and V. Barone, *The Journal of Chemical Physics*, 1999, 110, 6158.

5. D. Andrae, U. Häußermann, M. Dolg, H. Stoll, and H. Preuß, *Theoretica Chimica Acta*, 1990, 77, 123–141.

6. A. Bergner, M. Dolg, W. Küchle, H. Stoll, and H. Preuß, *Molecular Physics*, 1993, 80, 1431–1441.

7. A. Schäfer, H. Horn, and R. Ahlrichs, *The Journal of Chemical Physics*, 1992, 97, 2571.

8. A. Höllwarth, M. Böhme, S. Dapprich, A. W. Ehlers, A. Gobbi, V. Jonas, K. F. Köhler, R. Stegmann, A. Veldkamp, and G. Frenking, *Chemical Physics Letters*, 1993, 208, 237–240.

9. A. E. Ashley, A. R. Cowley, and D. O'Hare, *Chem. Commun.*, 2007, 1512–4.

10. L. E. Manzer, *Inorg. Syn.*, 1982, 21, 135–140.

11. T. K. Panda, M. T. Gamer, and P. W. Roesky, *Organometallics*, 2003, 22, 877–878.

12. W. Clegg, B. Conway, A. R. Kennedy, J. Klett, R. E. Mulvey, and L. Russo, *European Journal of Inorganic Chemistry*, 2011, 2011, 721–726.

13. B.-H. Chang, H.-S. Tung, and C. H. Brubaker, *Inorganica Chimica Acta*, 1981, 51, 143–148.

14. M. S. Ram, G. P. A. Yap, L. Liable-Sands, A. L. Rheingold, A. Marchaj, and J. R. Norton, *J. Am. Chem. Soc.*, 1997, 119, 1648–1655.

15. J. C. W. Chien, W. M. Tsai, and M. D. Rausch, *J. Am. Chem. Soc.*, 1991, 113, 8570–8571.

16. U. M. Stehling, K. M. Stein, M. R. Kesti, and R. M. Waymouth, *Macromolecules*, 1998, 31, 2019–2027.

17. W. Schlenk and W. Schlenk, *Berichte der deutschen chemischen Gesellschaft (A and B Series)*, 1929, 62, 920–924.

18. J. Langer, S. Krieck, R. Fischer, H. Görls, D. Walther, and M. Westerhausen, *Organometallics*, 2009, 28, 5814–5820.

Chapter Seven

Characterising Data

7.1 General Considerations

Infra-red bands are reported in wavenumbers (cm^{-1}). Elemental analyses are reported as percentages of the total composition. X-ray crystallographic details may be found in the crystallographic information files (CIF) in the electronic appendix, and the appropriate file names are given for each compound. ^{1}H, ^{7}Li and ^{13}C NMR spectra were recorded at 300 MHz, 194 MHz and 75 MHz respectively, at room temperature, unless stated otherwise. The chemical shifts δ, are given in parts per million relative to TMS (^{1}H, ^{13}C, $\delta = 0$) referenced internally to residual protio-solvent resonances or 2M $LiCl_{(aq)}$ (^{7}Li) at 0 ppm respectively. All coupling constants and line widths at half height ($\nu_{½}$) are quoted in hertz (Hz). Labelling of the resonances is either self-evident or in accordance with the relevant crystal structure or figure in the main text. The numbering system used to describe the pentalene ring system is illustrated for clarity below.

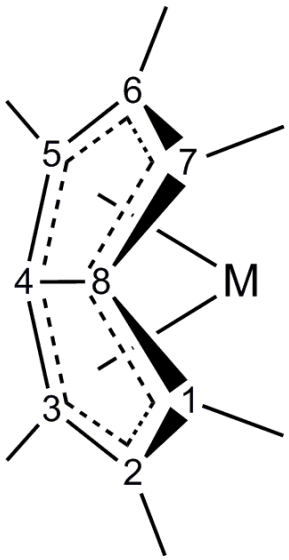

Numbering scheme for the ^{1}H and ^{13}C NMR assignment of η^{8}-Pn* complexes

7.2 Characterising data for Chapter Two

7.2.1 Characterising data for [Pn*TiMe(μ-Cl)]$_2$ (2.2)

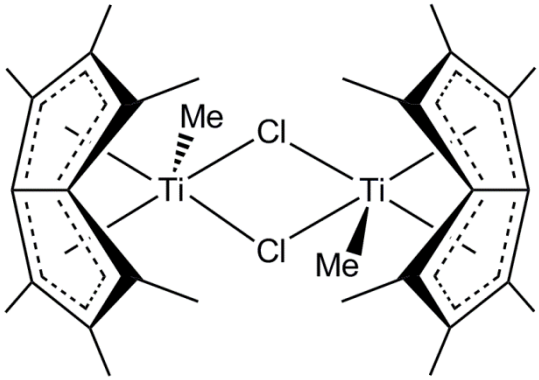

General properties: Mint green crystalline solid, air and thermally sensitive, decomposes to orange-red colour on exposure to air and to **2.3** on heating.

Elemental analysis found (calculated) for $C_{30}H_{42}Ti_2Cl_2$ (MW = 569.29) (%): C 63.16 (63.29), H 7.39 (7.44).

^{1}H NMR (C_6D_6) δ (ppm): 0.38 (Ti*Me*, 6H, s), 1.87 {(**1**,**3**,**5**,**7**)-*Me*$_8$, 24H, s}, 1.89 {(**2**,**6**)-*Me*$_4$, 12H, s}.

^{13}C NMR (C_6D_6) δ (ppm): 10.8 {(**2**,**6**)-*Me*$_4$, q, $^1J_{C\text{-}H}$ = 126.2}, 12.3 {(**1**,**3**,**5**,**7**)-*Me*$_8$, q, $^1J_{C\text{-}H}$ = 126.9}, 37.6 (Ti*Me*, q, $^1J_{C\text{-}H}$ = 118.5), 117.2 (**1**,**3**,**5**,**7**, s), 129.3 (**2**,**6**, s), 131.1 (**4**,**8**, s).

X-ray data: RTC2_2.cif

7.2.2 Characterising data for [Pn*Ti(μ-Cl)]$_2$(μ-CH$_2$) (2.3)

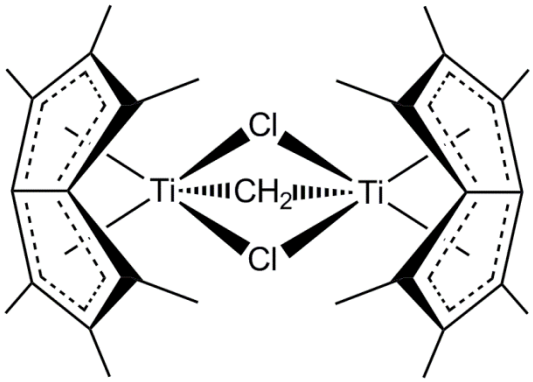

General properties: Purple air-sensitive crystalline solid.

Elemental analysis for $C_{29}H_{38}Ti_2Cl_2$ (MW = 553.25): Satisfactory analysis could not be obtained.

High resolution MS (EI) found (calculated): 552.1308 (552.1310).

MS (EI): *m/z* = 552 (M^+, 10%); 538 (M^+-CH_2, 5%); 518 (M^+-Cl, 10%); 283 (M^+-Pn*-Ti-Cl, 15%); 269 (M^+-Pn*-Ti-Cl-CH_2, 100%).

^{1}H NMR (C_6D_6) δ (ppm): 1.81 {(**1**,**3**,**5**,**7**)-*Me*$_8$, 24H, s}, 2.10 {(**2**,**6**)-*Me*$_4$, 12H, s}, 5.18 (Ti*C*H_2, 2H, s).

^{13}C NMR (C_6D_6) δ (ppm): 11.3 {(**2**,**6**)-*Me*$_4$, q, $^1J_{C\text{-}H}$ = 126.7}, 12.2 {(**1**,**3**,**5**,**7**)-*Me*$_8$, q, $^1J_{C\text{-}H}$ = 126.7}, 115.2 (**1**,**3**,**5**,**7**, s), 132.7 (**2**,**6**, s), 134.3 (**4**,**8**, s), 183.2 (Ti*C*H_2, t, $^1J_{C\text{-}H}$ = 122.9).

X-ray data: RTC2_3.cif

7.2.3 Characterising data for [Pn*Ti(μ-Me)]$_2$(μ-CH_2) (2.4)

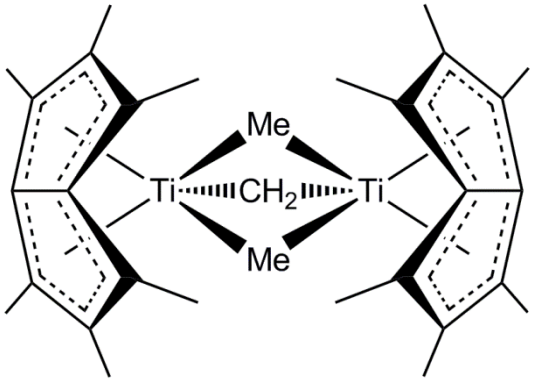

General properties: Dark purple crystalline solid, very air-sensitive.

Elemental analysis for $C_{31}H_{44}Ti_2$ (MW = 512.42): Capricious synthesis prevented analysis.

^{1}H NMR (C_6D_6) δ (ppm): −0.74 (Ti*Me*, 6H, s), 1.88 {(**1**,**3**,**5**,**7**)-*Me*$_8$, 24H, s}, 2.05 {(**2**,**6**)-*Me*$_4$, 12H, s}, 5.23 (Ti*C*H_2, 2H, s).

^{13}C NMR (C_6D_6) δ (ppm): 10.8 {(**2**,**6**)-*Me*$_4$, q, $^1J_{C\text{-}H}$ = 122.7}, 12.3 {(**1**,**3**,**5**,**7**)-*Me*$_8$, q, $^1J_{C\text{-}H}$ = 125.2}, 48.4 (Ti*Me*, q, $^1J_{C\text{-}H}$ = 112.7), 109.6 (**1**,**3**,**5**,**7**, s), 128.8 (**2**,**6**, s), 129.1 (**4**,**8**, s), 180.3 (Ti*C*H_2, t, $^1J_{C\text{-}H}$ = 122.2).

X-ray data: RTC2_4.cif

7.2.4 Characterising data for [Pn*TiMe(μ-Me)$_2$]$_2$Mg (2.5)

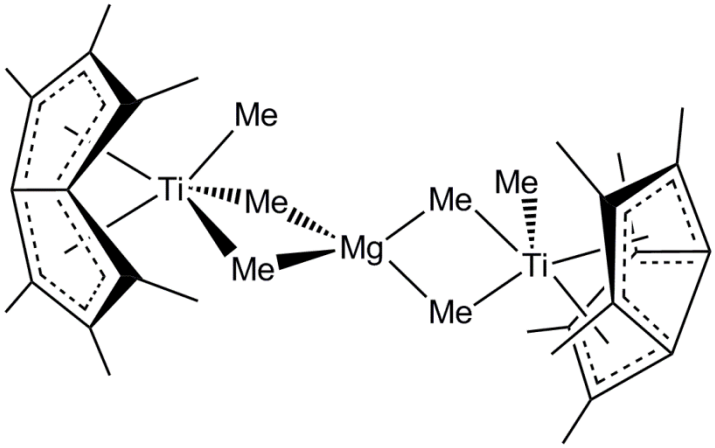

General properties: Green crystalline solid, air and thermally sensitive, decomposes to orange-red colour on exposure to air and to **2.4** on heating.

^{1}H NMR (toluene-*d*$_8$) δ (ppm): −0.37 (Ti*Me*, 18H, br s, $\nu_{½}$ = 83.5), 1.82 {(**2**,**6**)-*Me*$_4$, 12H, s}, 1.89 {(**1**,**3**,**5**,**7**)-*Me*$_8$, 24H, s}.

^{13}C NMR (toluene-*d*$_8$) δ (ppm): 10.8 {(**2**,**6**)-*Me*$_4$, q, $^1J_{C\text{-}H}$ = 126.4}, 12.6 {(**1**,**3**,**5**,**7**)-*Me*$_8$, q, $^1J_{C\text{-}H}$ = 127.1}, 117.2 (**1**,**3**,**5**,**7**, s), 129.8 (**2**,**6**, s), 137.1 (**4**,**8**, s), (Ti*Me* not observed).

X-ray data: RTC2_5.cif

7.2.5 Characterising data for [Pn*TiMe$_3$]Li.(Et$_2$O)$_x$ (2.6)

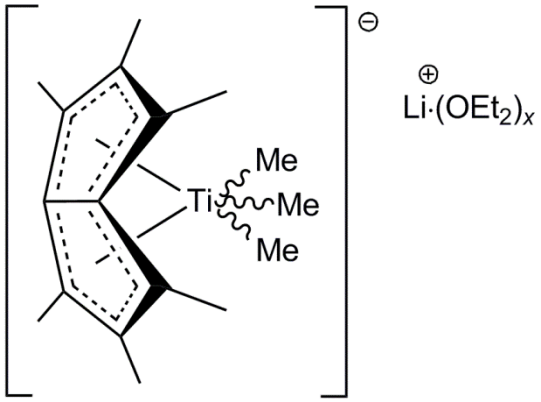

General properties: Teal powder/solution, air-sensitive.

Elemental analysis for $C_{17}H_{27}TiLi(C_4H_{10}O)_x$: Satisfactory analysis could not be obtained.

^{1}H NMR (C_6D_6) δ (ppm): −0.45 (Ti*Me*, 9H, s), 1.02 (OCH_2CH_3, t, $^3J_{H-H}$ = 6.8), 1.96 {(**1**,**3**,**5**,**7**)-*Me*$_4$, 12H, s}, 2.02 {(**2**,**6**)-*Me*$_2$, 6H, s}, 3.18 (OCH_2CH_3, q, $^3J_{H-H}$ = 6.8).

^{13}C NMR (C_6D_6) δ (ppm): 10.5 {(**2**,**6**)-*Me*$_2$, q, $^1J_{C-H}$ = 124.3}, 12.0 {(**1**,**3**,**5**,**7**)-*Me*$_4$, q, $^1J_{C-H}$ = 125.9}, 15.2 (OCH_2CH_3, q, $^1J_{C-H}$ = 124.3), 21.8 (Ti*Me*, q, $^1J_{C-H}$ = 110.0), 65.6 (OCH_2CH_3, t, $^1J_{C-H}$ = 136.9), 109.6 (**1**,**3**,**5**,**7**, s), 127.3 (**4**,**8**, s), 130.2 (**2**,**6**, s).

^{7}Li NMR (194 MHz, C_6D_6) δ (ppm): −0.1 (s).

7.2.6 Characterising data for Pn*TiMe$_2$ (2.7)

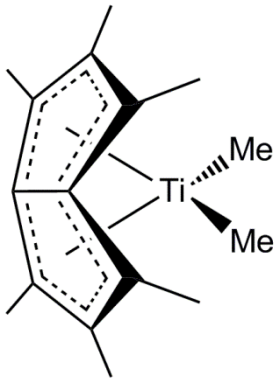

General properties: Pink crystalline solid, extremely air sensitive, turns red on decomposition.

Elemental analysis found (calculated) for $C_{16}H_{24}Ti$ (MW = 264.23) (%): C 72.61 (72.73), H 9.25 (9.16).

IR (KBr) cm^{-1}: 2944 (m), 2905 (m), 2870 (m), 1457 (br), 1378 (s), 1097 (m), 1021 (s), 870 (m), 797 (m), 764 (m), 689 (m), 668 (m).

^{1}H NMR (C_6D_6) δ (ppm): 0.15 (Ti*Me*, 6H, s), 1.78 {(**2**,**6**)-*Me*$_2$, 6H, s}, 1.89 {(**1**,**3**,**5**,**7**)-*Me*$_4$, 12H, s}.

^{13}C NMR (C_6D_6) δ (ppm): 11.0 {(**2**,**6**)-*Me*$_2$, q, $^1J_{C-H}$ = 126.8}, 12.7 {(**1**,**3**,**5**,**7**)-*Me*$_4$, q, $^1J_{C-H}$ = 126.0}, 41.1 (Ti*Me*, q, $^1J_{C-H}$ = 114.8), 117.5 (**1**,**3**,**5**,**7**, s), 129.8 (**2**,**6**, s), 137.4 (**4**,**8**, s).

X-ray data: RTC2_7.cif

7.3 Characterising data for Chapter Three

7.3.1 Characterising data for Pn*Ti(CH_2Ph)$_2$ (3.1)

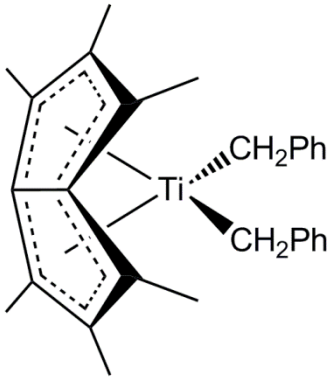

General properties: Bronze crystalline solid, air-sensitive.

Elemental analysis found (calculated) for $C_{28}H_{32}Ti$ (MW = 416.42) (%): C 80.57 (80.76), H 7.82 (7.75).

IR (KBr) cm^{-1}: 3058 (m), 3011 (m), 2978 (m), 1590 (s), 1559 (m), 1479 (s), 1381 (m), 1208 (s), 1093 (m), 1027 (s), 936 (m), 877 (m), 801 (m), 744 (s), 693 (m), 669 (m).

^{1}H NMR (C_6D_6) δ (ppm): 1.69 {(**2**,**6**)-*Me*$_2$, 6H, s}, 1.75 {(**1**,**3**,**5**,**7**)-*Me*$_4$, 12H, s}, 1.82 (TiC*H*$_2$, 4H, s), 6.83 (*o*-Ph, 4H, d), 6.90 (*p*-Ph, 2H, t), 7.13 (*m*-Ph, 4H, t).

^{13}C NMR (C_6D_6) δ (ppm): 10.9 {(**2**,**6**)-*Me*$_2$, q, $^1J_{C\text{-}H}$ = 126.7}, 12.5 {(**1**,**3**,**5**,**7**)-*Me*$_4$, q, $^1J_{C\text{-}H}$ = 127.8}, 68.1 (Ti*C*H$_2$, t, $^1J_{C\text{-}H}$ = 120.9), 117.2 (**1**,**3**,**5**,**7**, s), 121.8 (*p*-Ph), 126.4 (*o*-Ph), 128.9 (*m*-Ph), 129.8 (**2**,**6**, s), 136.1 (**4**,**8**, s), 148.8 (*ipso*-Ph, s).

X-ray data: RTC3_1.cif

7.3.2 Characterising data for Pn*Ti(CH_2SiMe_3)$_2$ (3.2)

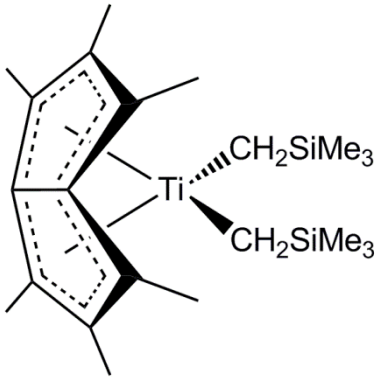

General properties: Deep purple crystalline solid, extremely air-sensitive.

Elemental analysis found (calculated) for $C_{22}H_{40}TiSi_2$ (MW = 408.59) (%): C 64.49 (64.67), H 9.67 (9.87).

^{1}H NMR (C_6D_6) δ (ppm): −0.15 (TiC*H*$_2$, 4H, s), 0.25 (Si*Me*$_3$, 18H, s), 1.84 {(**2**,**6**)-*Me*$_2$, 6H, s}, 1.87 {(**1**,**3**,**5**,**7**)-*Me*$_4$, 12H, s}.

^{13}C NMR (C_6D_6) δ (ppm): 4.0 (Si*Me*$_3$, q, $^1J_{C\text{-}H}$ = 116.1), 11.6 {(**2**,**6**)-*Me*$_2$, q, $^1J_{C\text{-}H}$ = 127.2}, 13.2 {(**1**,**3**,**5**,**7**)-*Me*$_4$, q, $^1J_{C\text{-}H}$ = 126.8}, 56.4 (Ti*C*H$_2$, t, $^1J_{C\text{-}H}$ = 105.3), 116.9 (**1**,**3**,**5**,**7**, s), 130.1 (**2**,**6**, s), 137.0 (**4**,**8**, s).

X-ray data: RTC3_2.cif

7.3.3 Characterising data for Pn*Ti($CH_2{}^tBu$)$_2$ (3.3)

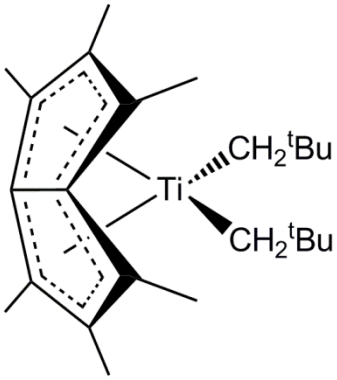

General properties: Red air-sensitive crystalline solid, decomposes upon heating.

Elemental analysis for $C_{24}H_{40}Ti$ (MW = 376.44): Satisfactory analysis could not be obtained due to thermal sensitivity of product.

^{1}H NMR (C_6D_6) δ (ppm): 0.77 (TiC*H*$_2$, 4H, s), 1.21 (C*Me*$_3$, 18H, s), 1.79 {(**2**,**6**)-*Me*$_2$, 6H, s}, 2.00 {(**1**,**3**,**5**,**7**)-*Me*$_4$, 12H, s}.

^{13}C NMR (C_6D_6) δ (ppm): 11.1 {(**2**,**6**)-*Me*$_2$, q, $^{1}J_{C\text{-}H}$ = 126.4}, 13.6 {(**1**,**3**,**5**,**7**)-*Me*$_4$, q, $^{1}J_{C\text{-}H}$ = 127.2}, 35.4 (C*Me*$_3$, q, $^{1}J_{C\text{-}H}$ = 124.0), 35.6 (*C*Me$_3$, s), 90.7 (Ti*C*H$_2$, t, $^{1}J_{C\text{-}H}$ = 111.2), 115.6 (**1**,**3**,**5**,**7**, s), 128.6 (**2**,**6**, s), 134.1 (**4**,**8**, s).

X-ray data: RTC3_3.cif

7.3.4 Characterising data for Pn*TiCl(CH$_2$^{t}Bu) (3.4)

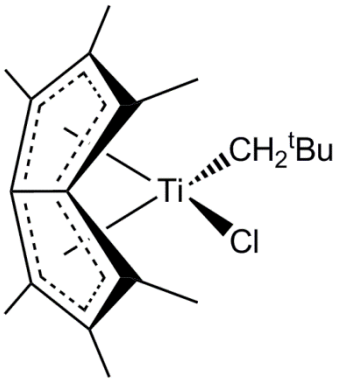

General properties: Red-purple crystalline solid, air-sensitive.

Elemental analysis found (calculated) for $C_{19}H_{29}TiCl$ (MW = 340.75) (%): C 66.85 (66.97), H 8.45 (8.58).

^{1}H NMR (C_6D_6) δ (ppm): 0.58 (TiC*H*$_2$, 2H, s), 1.33 (C*Me*$_3$, 9H, s), 1.64 {(**2**,**6**)-*Me*$_2$, 6H, s}, 1.79 {(**3**,**5**)-*Me*$_2$, 6H, s}, 1.97 {(**1**,**7**)-*Me*$_2$, 6H, s}.

^{13}C NMR (C_6D_6) δ (ppm): 10.9 {(**2**,**6**)-*Me*$_2$, q, $^{1}J_{C\text{-}H}$ = 126.7}, 12.7 {(**3**,**5**)-*Me*$_2$, q, $^{1}J_{C\text{-}H}$ = 127.9}, 13.0 {(**1**,**7**)-*Me*$_2$, q, $^{1}J_{C\text{-}H}$ = 127.9}, 34.4 (*C*Me$_3$, s), 34.8 (C*Me*$_3$, q, $^{1}J_{C\text{-}H}$ = 125.9), 83.5 (Ti*C*H$_2$, t, $^{1}J_{C\text{-}H}$ = 116.3), 119.1 (**3**,**5**, s), 122.1 (**1**,**7**, s), 130.9 (**2**,**6**, s), 136.0 (**8**, s), 141.0 (**4**, s).

X-ray data: RTC3_4.cif

7.3.5 Characterising data for [Pn*TiPh(μ-Cl)]$_2$ (3.5)

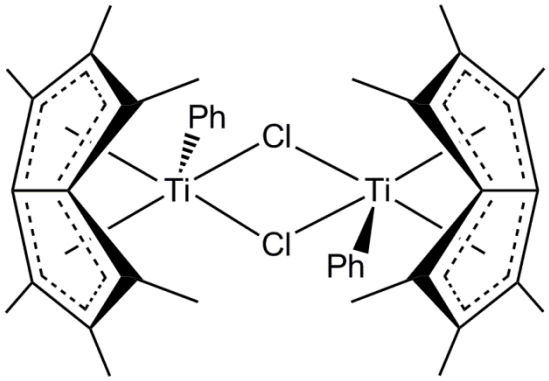

General properties: Bright green crystalline solid, air-sensitive, turns orange-red on decomposition.

Elemental analysis found (calculated) for $C_{40}H_{46}Ti_2Cl_2$ (MW = 693.43): C 69.14 (69.28), H 6.60 (6.69).

^{1}H NMR (CD_2Cl_2) δ (ppm): 1.60 {(**1**,**3**,**5**,**7**)-*Me*$_8$, 24H, br s, $\nu_{½}$ = 3.7}, 2.10 {(**2**,**6**)-*Me*$_4$, 12H, s}, 6.87 (*p*-Ph, 2H, t), 6.89 (*m*-Ph, 4H, t), 7.11 (*o*-Ph, 4H, d).

^{13}C NMR (CD_2Cl_2) δ (ppm): 10.7 {(**2**,**6**)-*Me*$_4$, q, $^1J_{C\text{-}H}$ = 127.2}, 12.8 {(**1**,**3**,**5**,**7**)-*Me*$_8$, q, $^1J_{C\text{-}H}$ = 128.0}, 120.4 (**1**,**3**,**5**,**7**, br s, $\nu_{½}$ = 10.1), 125.1 (*p*-Ph, d, $^1J_{C\text{-}H}$ = 165.3), 125.8 (*m*-Ph, d, $^1J_{C\text{-}H}$ = 159.6), 128.5 (**4**,**8**, s), 131.8 (**2**,**6**, s), 137.9 (*o*-Ph, d, $^1J_{C\text{-}H}$ = 153.9), 187.6 (*ipso*-Ph, s).

X-ray data: RTC3_5.cif

7.3.6 Characterising data for Pn*TiClCp (3.6)

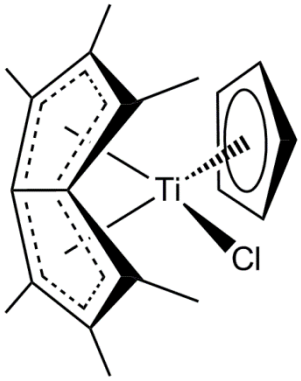

General properties: Red crystalline solid, air-sensitive.

Elemental analysis found (calculated) for $C_{19}H_{23}TiCl$ (MW = 334.71) (%): C 68.01 (68.18), H 6.77 (6.93).

High resolution MS (EI) found (calculated): 334.0953 (334.0968).

MS (EI): *m/z* = 334 (M^+, 25%); 299 (M^+-Cl, 100%); 269 (M^+-Cp, 95%).

^{1}H NMR (C_6D_6) δ (ppm): 1.51 {(**2**,**6**)-*Me*$_2$, 6H, s}, 1.64 {(**3**,**5**)-*Me*$_2$, 6H, s}, 2.19 {(**1**,**7**)-*Me*$_2$, 6H, s}, 5.38 (*Cp*, 5H, s).

^{13}C NMR (C_6D_6) δ (ppm): 10.9 {(**2**,**6**)-*Me*$_2$, q, $^1J_{C\text{-}H}$ = 126.0}, 13.7 {(**3**,**5**)-*Me*$_2$, q, $^1J_{C\text{-}H}$ = 127.2}, 13.9 {(**1**,**7**)-*Me*$_2$, q, $^1J_{C\text{-}H}$ = 127.2}, 110.6 (*Cp*, d, $^1J_{C\text{-}H}$ = 173.6), 114.3 (**3**,**5**, s), 117.7 (**4**, s), 121.1 (**1**,**7**, s), 122.3 (**2**,**6**, s), 129.2 (**8**, s).

X-ray data: RTC3_6.cif

7.3.7 Characterising data for Pn*Ti(η^5-Cp)(η^1-Cp) (3.7)

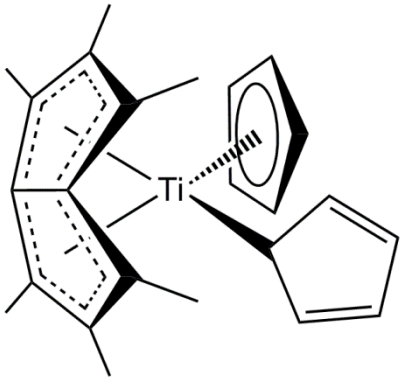

General properties: Red air-sensitive crystalline solid.

Elemental analysis found (calculated) for $C_{24}H_{28}Ti$ (MW = 364.35) (%): C 78.93 (79.12), H 7.69 (7.75).

MS (EI): 299 (M^+-Cp, 100%); 186 (M^+-2Cp-Ti, 100%).

^{1}H NMR (C_6D_6) δ (ppm): 1.48 {(**2**,**6**)-*Me*$_2$, 6H, s}, 1.69 {(**3**,**5**)-*Me*$_2$, 6H, s}, 2.17 {(**1**,**7**)-*Me*$_2$, 6H, s}, 4.61 (*η^5-Cp*, 5H, s), 6.02 (*η^1-Cp*, 5H, br s, $\nu_{½}$ = 36.1).

^{1}H NMR (toluene-*d*$_8$) δ (ppm): 1.52 {(**2**,**6**)-*Me*$_2$, 6H, s}, 1.72 {(**3**,**5**)-*Me*$_2$, 6H, s}, 2.17 {(**1**,**7**)-*Me*$_2$, 6H, s}, 4.55 (*η^5-Cp*, 5H, s), 5.90 (*η^1-Cp*, 5H, br s, $\nu_{½}$ = 37.5).

^{1}H NMR (toluene-d_8, 193 K) δ (ppm): 1.40 {(**2**,**6**)-*Me*$_2$, 6H, s}, 1.57 {(**3**,**5**)-*Me*$_2$, 6H, s}, 2.19 {(**1**,**7**)-*Me*$_2$, 6H, s}, 4.04 (*ipso*-η^1-*Cp*, 1H, br s, $\nu_{½}$ = 8.8), 4.57 (η^5-*Cp*, 5H, s), 6.32 (α-η^1-*Cp*, 2H, br s, $\nu_{½}$ = 11.5), 7.05 (β-η^1-*Cp*, 2H, br s, $\nu_{½}$ = 12.1).

^{13}C NMR (C_6D_6) δ (ppm): 10.8 {(**2**,**6**)-*Me*$_2$, q, $^1J_{C\text{-}H}$ = 126.7}, 13.2 {(**1**,**7**)-*Me*$_2$, q, $^1J_{C\text{-}H}$ = 127.4}, 14.0 {(**3**,**5**)-*Me*$_2$, q, $^1J_{C\text{-}H}$ = 126.7}, 110.1 (η^5-*Cp*, d, $^1J_{C\text{-}H}$ = 177.4), 110.3 (η^1-*Cp*), 112.2 (**3**,**5**, s), 114.9 (**4**, s), 115.1 (**1**,**7**, s), 121.4 (**2**,**6**, s), 122.7 (**8**, s).

^{13}C NMR (toluene-d_8) δ (ppm): 10.8 {(**2**,**6**)-*Me*$_2$, q, $^1J_{C\text{-}H}$ = 127.6}, 13.1 {(**1**,**7**)-*Me*$_2$, q, $^1J_{C\text{-}H}$ = 126.8}, 13.9 {(**3**,**5**)-*Me*$_2$, q, $^1J_{C\text{-}H}$ = 126.1}, 110.0 (η^5-*Cp*, d, $^1J_{C\text{-}H}$ = 174.2), 110.4 (η^1-*Cp*), 112.0 (**3**,**5**, s), 114.9 (**4**, s), 115.0 (**1**,**7**, s), 121.3 (**2**,**6**, s), 122.7 (**8**, s).

^{13}C NMR (toluene-d_8, 193 K) δ (ppm): 10.6 {(**2**,**6**)-*Me*$_2$, q, $^1J_{C\text{-}H}$ = 126.8}, 13.2 {(**1**,**7**)-*Me*$_2$, q, $^1J_{C\text{-}H}$ = 127.6}, 13.8 {(**3**,**5**)-*Me*$_2$, q, $^1J_{C\text{-}H}$ = 126.8}, 61.0 (*ipso*-η^1-*Cp*, d, $^1J_{C\text{-}H}$ = 140.0), 109.6 (η^5-*Cp*, d, $^1J_{C\text{-}H}$ = 172.6), 112.1 (**3**,**5**, s), 114.4 (**4**, s), 114.6 (**1**,**7**, s), 119.1 (β-η^1-*Cp*, d, $^1J_{C\text{-}H}$ = 159.5), 121.0 (**2**,**6**, s), 121.8 (**8**, s), 135.0 (α-η^1-*Cp*, d, $^1J_{C\text{-}H}$ = 157.9).

X-ray data: RTC3_7.cif

7.3.8 Characterising data for Pn*Ti(C_3H_5)$_2$ (3.8)

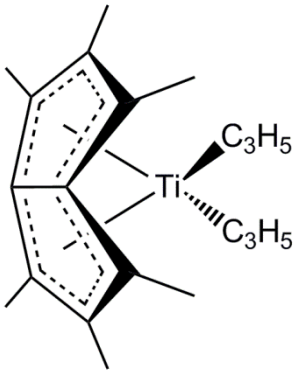

General properties: Orange-yellow crystalline solid, highly air and thermally sensitive.

Elemental analysis for $C_{20}H_{28}Ti$ (MW = 316.30): Could not be obtained due to extreme air and thermal sensitivity of product.

High resolution MS (EI) found (calculated): 316.1672 (316.1670).

MS (EI): *m/z* = 316 (M^+, 30%); 234 {M^+-2(C_3H_5), 100%}.

^{1}H NMR (C_6D_6) δ (ppm): 1.48 {(**2**,**6**)-*Me*$_2$, 6H, s}, 1.86 {(**1**,**3**,**5**,**7**)-*Me*$_4$, 12H, s}, 2.44 (C*H*$_2$CHC*H*$_2$, 8H, d, $^{3}J_{H\text{-}H}$ = 12.3), 4.81 (CH_2CHCH_2, 2H, q, $^{3}J_{H\text{-}H}$ = 12.3).

^{13}C{^{1}H} NMR (C_6D_6) δ (ppm): 10.3 {(**2**,**6**)-*Me*$_2$}, 13.4 {(**1**,**3**,**5**,**7**)-*Me*$_4$}, 65.9 (*C*H_2CH*C*H_2), 107.5 (**1**,**3**,**5**,**7**), 115.7 (**4**,**8**), 126.9 (**2**,**6**), 141.4 (CH_2*C*HCH_2).

7.3.9 Characterising data for Pn*TiPh$_2$ (3.9)

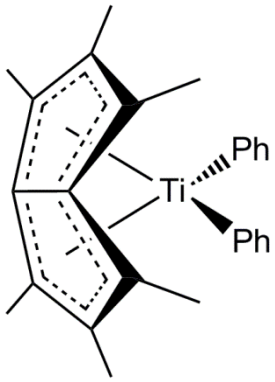

General properties: Exceptionally thermal and air-sensitive purple crystalline solid, both in solid state and solution. Decomposes to a red-brown colour.

Elemental analysis for $C_{26}H_{28}Ti$ (MW = 316.30): Could not be obtained due to extreme air and thermal sensitivity of product.

^{1}H NMR (C_6D_6) δ (ppm): 1.92 {(**2**,**6**)-*Me*$_2$, 6H, s}, 1.93 {(**1**,**3**,**5**,**7**)-*Me*$_4$, 12H, s}, 7.03 (*p*-Ph, 2H, t), 7.16 (*m*-Ph, 4H, t), 7.42 (*o*-Ph, 4H, d).

7.4 Characterising data for Chapter Four

7.4.1 Characterising data for Pn*Ti(κ^2-O$_2$CMe)$_2$ (4.1)

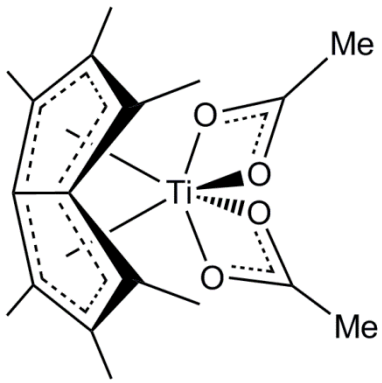

General properties: Orange-yellow crystalline solid.

Elemental analysis found (calculated) for $C_{18}H_{24}TiO_4$ (MW = 352.25) (%): C 61.36 (61.38), H 6.76 (6.87).

High resolution MS (EI) found (calculated): 352.1150 (352.1154).

MS (EI): *m/z* = 352 (M^+, 10%); 292 (M^+-O_2CMe, 100%).

IR (KBr) cm^{-1}: 2991 (m), 2947 (m), 2914 (m), 2859 (w), 1541 (s), 1473 (s), 1378 (m), 1261 (m), 1101 (m), 1018 (m), 949 (s), 798 (s), 706 (m), 689 (s), 668 (m).

^{1}H NMR (toluene-d_8) δ (ppm): 1.72 {(**2**,**6**)-*Me*$_2$, 6H, s}, 1.78 (O_2C*Me*, 6H, s), 1.80 {(**3**,**7**)-*Me*$_2$, 6H, br s, $\nu_{½}$ = 80.7}, 2.01 {(**1**,**5**)-*Me*$_2$, 6H, br s, $\nu_{½}$ = 108.0}.

^{1}H NMR (toluene-d_8, 263 K) δ (ppm): 1.72 {(**2**,**6**)-*Me*$_2$, 6H, s}, 1.78 (O_2C*Me*, 6H, s), 1.79 {(**3**,**7**)-*Me*$_2$, 6H, s}, 2.05 {(**1**,**5**)-*Me*$_2$, 6H, s}.

^{1}H NMR (toluene-d_8, 343 K) δ (ppm): 1.72 {(**2**,**6**)-*Me*$_2$, 6H, s}, 1.77 (O_2C*Me*, 6H, s), 1.88 {(**1**,**3**,**5**,**7**)-*Me*$_4$, 12H, br s, $\nu_{½}$ = 2.2}.

^{13}C NMR (toluene-d_8) δ (ppm): 10.0 {(**2**,**6**)-*Me*$_2$, q, $^1J_{C\text{-}H}$ = 127.3}, 11.4 {(**1**,**3**,**5**,**7**)-*Me*$_4$, q, $^1J_{C\text{-}H}$ = 125.3}, 22.8 (O_2C*Me*, q, $^1J_{C\text{-}H}$ = 127.3), 119.0 (**3**,**7**, br s, $\nu_{½}$ = 31.6), 120.9 (**1**,**5**, br s, $\nu_{½}$ = 20.5), 133.3 (**2**,**6**, s), 133.5 (**4**,**8**, s), 188.5 (O_2*C*Me, s).

^{13}C NMR (toluene-d_8, 263 K) δ (ppm): 9.9 {(**2**,**6**)-*Me*$_2$, q, $^1J_{C\text{-}H}$ = 126.6}, 11.4 {(**1**,**5**)-*Me*$_2$, q, $^1J_{C\text{-}H}$ = 128.4}, 11.5 {(**3**,**7**)-*Me*$_2$, q, $^1J_{C\text{-}H}$ = 126.6}, 22.9 (O_2C*Me*, q, $^1J_{C\text{-}H}$ = 126.7), 118.9 (**3**,**7**, s), 120.9 (**1**,**5**, s), 133.2 (**2**,**6**, s), 133.3 (**4**,**8**, s), 188.5 (O_2*C*Me, s).

^{13}C NMR (toluene-d_8, 343 K) δ (ppm): 10.0 {(**2**,**6**)-*Me*$_2$, q, $^1J_{C\text{-}H}$ = 125.2}, 11.4 {(**1**,**3**,**5**,**7**)-*Me*$_4$, q, $^1J_{C\text{-}H}$ = 126.9}, 22.8 (O_2C*Me*, q, $^1J_{C\text{-}H}$ = 126.9), 120.3 (**1**,**3**,**5**,**7**, br s, $\nu_{½}$ = 8.7), 133.5 (**2**,**6**, s), 133.8 (**4**,**8**, s), 188.5 (O_2*C*Me, s).

X-ray data: RTC4_1.cif

7.4.2 Characterising data for Pn*Ti(κ^2-O_2CCH_2Ph)$_2$ (4.2)

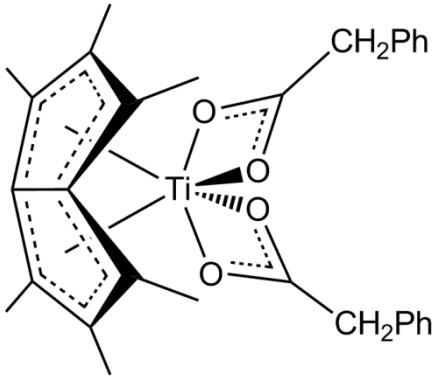

General properties: Orange-yellow crystalline solid.

Elemental analysis found (calculated) for $C_{30}H_{32}TiO_4$ (MW = 504.44) (%): C 71.32 (71.43), H 6.42 (6.39).

High resolution MS (EI) found (calculated): 504.1783 (504.1780).

MS (EI): *m/z* = 504 (M^+, 20%); 368 (M^+-O_2CCH_2Ph, 100%).

IR (KBr) cm^{-1}: 3054 (m), 3036 (m), 2989 (m), 2908 (m), 1538 (s), 1458 (m), 1380 (m), 1280 (m), 1162 (m), 1076 (m), 946 (m), 862 (m), 797 (m), 716 (m), 669 (m).

^{1}H NMR (toluene-d_8) δ (ppm): 1.59 {(**2**,**6**)-Me_2, 6H, s}, 1.60 {(**3**,**7**)-Me_2, 6H, br s, $\nu_{½}$ = 153.7}, 2.09 {(**1**,**5**)-Me_2, 6H, br s, $\nu_{½}$ = 148.7}, 3.37 (O_2CCH_2Ph, 4H, br s, $\nu_{½}$ = 6.7), 7.04 (*p*-Ph, 2H, t), 7.09 (*m*-Ph, 4H, t), 7.18 (*o*-Ph, 4H, d).

^{1}H NMR (toluene-d_8, 263 K) δ (ppm): 1.54 {(**3**,**7**)-Me_2, 6H, s}, 1.58 {(**2**,**6**)-Me_2, 6H, s}, 1.99 {(**1**,**5**)-Me_2, 6H, s}, 3.34, 3.42 (O_2CCH_2Ph, 4H, ABq, $^2J_{H\text{-}H}$ = −14.1), 7.06 (*p*-Ph, 2H, t), 7.10 (*m*-Ph, 4H, t), 7.19 (*o*-Ph, 4H, d).

^{1}H NMR (toluene-d_8, 343 K) δ (ppm): 1.60 {(**2**,**6**)-Me_2, 6H, s}, 1.88 {(**1**,**3**,**5**,**7**)-Me_4, 12H, br s, $\nu_{½}$ = 4.2}, 3.36 (O_2CCH_2Ph, 4H, s), 7.03 (*p*-Ph, 2H, t), 7.08 (*m*-Ph, 4H, t), 7.18 (*o*-Ph, 4H, d).

^{13}C NMR (toluene-d_8) δ (ppm): 9.9 {(**2**,**6**)-Me_2, q, $^1J_{C\text{-}H}$ = 127.7}, 11.3 {(**1**,**3**,**5**,**7**)-Me_4, q, $^1J_{C\text{-}H}$ = 127.7}, 43.9 (O_2CCH_2Ph, t, $^1J_{C\text{-}H}$ = 128.4), 119.7 (**3**,**7**, br s, $\nu_{½}$ = 40.8), 120.9 (**1**,**5**, br s, $\nu_{½}$ = 32.0), 126.8 (*p*-Ph), 128.4 (*m*-Ph), 129.9 (*o*-Ph), 133.4 (**2**,**6**, s), 133.7 (**4**,**8**, s), 135.4 (*ipso*-Ph), 188.6 (O_2CCH_2Ph, s).

^{13}C NMR (toluene-d_8, 263 K) δ (ppm): 9.8 {(**2**,**6**)-*Me*$_2$, q, $^1J_{C\text{-}H}$ = 126.3}, 11.2 {(**3**,**7**)-*Me*$_2$, q, $^1J_{C\text{-}H}$ = 127.4}, 11.3 {(**1**,**5**)-*Me*$_2$, q, $^1J_{C\text{-}H}$ = 127.4}, 43.8 (O_2CCH_2Ph, t, $^1J_{C\text{-}H}$ = 128.6), 119.5 (**3**,**7**, s), 120.9 (**1**,**5**, s), 126.8 (*p*-Ph), 128.1 (*o*-Ph), 128.4 (*m*-Ph), 133.4 (**4**,**8**, s), 133.5 (**2**,**6**, s), 135.3 (*ipso*-Ph), 188.6 (O_2CCH_2Ph, s).

^{13}C NMR (toluene-d_8, 343 K) δ (ppm): 9.9 {(**2**,**6**)-*Me*$_2$, q, $^1J_{C\text{-}H}$ = 127.1}, 11.2 {(**1**,**3**,**5**,**7**)-*Me*$_4$, q, $^1J_{C\text{-}H}$ = 127.6}, 44.0 (O_2CCH_2Ph, t, $^1J_{C\text{-}H}$ = 129.1), 120.6 (**1**,**3**,**5**,**7**, br s, $\nu_{½}$ = 2.9), 126.9 (*p*-Ph), 128.5 (*m*-Ph), 130.0 (*o*-Ph), 133.6 (**2**,**6**, s), 134.0 (**4**,**8**, s), 135.6 (*ipso*-Ph), 188.6 (O_2CCH_2Ph, s).

X-ray data: RTC4_2.cif

7.4.3 Characterising data for Pn*Ti(κ^2-$O_2CCH_2SiMe_3$)$_2$ (4.3)

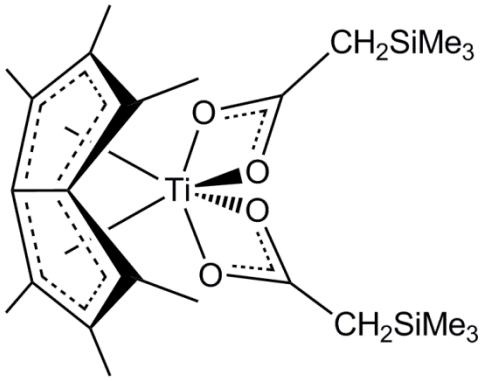

General properties: Orange-yellow oil.

High resolution MS (EI) found (calculated): 496.1954 (496.1945).

MS (EI): *m/z* = 496 (M^+, 10%); 349 (M^+-$O_2CCH_2SiMe_3$, 50%).

IR (KBr) cm^{-1}: 2999 (m), 2953 (m), 2911 (m), 2879 (m), 1551 (s), 1477 (s), 1387 (m), 1221 (m), 1101 (m), 949 (m), 798 (m), 756 (m), 689 (s).

^{1}H NMR (toluene-d_8) δ (ppm): 0.11 ($O_2CCH_2SiMe_3$, 18H, s), 1.76 {(**2**,**6**)-*Me*$_2$, 6H, s}, 1.79 ($O_2CCH_2SiMe_3$, 4H, s), 1.89 {(**3**,**7**)-*Me*$_2$, 6H, br s, $\nu_{½}$ = 77.7}, 2.03 {(**1**,**5**)-*Me*$_2$, 6H, br s, $\nu_{½}$ = 104.3}.

^{1}H NMR (toluene-d_8, 263 K) δ (ppm): 0.10 ($O_2CCH_2SiMe_3$, 18H, s), 1.74 {(**2**,**6**)-*Me*$_2$, 6H, s}, 1.79 ($O_2CCH_2SiMe_3$, 4H, s), 1.86 {(**3**,**7**)-*Me*$_2$, 6H, s}, 2.06 {(**1**,**5**)-*Me*$_2$, 6H, s}.

^{1}H NMR (toluene-d_8, 343 K) δ (ppm): 0.09 ($O_2CCH_2Si\mathit{Me}_3$, 18H, s), 1.75 {(**2**,**6**)-Me_2, 6H, s}, 1.76 ($O_2CC\mathit{H}_2SiMe_3$, 4H, s), 1.92 {(**1**,**3**,**5**,**7**)-Me_4, 12H, s}.

^{13}C NMR (toluene-d_8) δ (ppm): −1.0 ($O_2CCH_2Si\mathit{Me}_3$, q, $^{1}J_{C\text{-}H}$ = 119.7), 10.1 {(**2**,**6**)-Me_2, q, $^{1}J_{C\text{-}H}$ = 127.1}, 11.5 {(**1**,**5**)-Me_2, br q, $\nu_{½}$ = 47.9}, 11.8 {(**3**,**7**)-Me_2, br q, $\nu_{½}$ = 46.5}, 29.1 ($O_2C\mathit{C}H_2SiMe_3$, t, $^{1}J_{C\text{-}H}$ = 124.3), 118.8 (**3**,**7**, br s, $\nu_{½}$ = 22.4), 120.1 (**1**,**5**, br s, $\nu_{½}$ = 24.6), 132.7 (**2**,**6**, s), 132.8 (**4**,**8**, s), 189.8 ($O_2\mathit{C}CH_2SiMe_3$, s).

^{13}C NMR (toluene-d_8, 263 K) δ (ppm): −1.1 ($O_2CCH_2Si\mathit{Me}_3$, q, $^{1}J_{C\text{-}H}$ = 119.4), 10.1 {(**2**,**6**)-Me_2, q, $^{1}J_{C\text{-}H}$ = 125.2}, 11.4 {(**1**,**5**)-Me_2, q, $^{1}J_{C\text{-}H}$ = 126.1}, 12.0 {(**3**,**7**)-Me_2, q, $^{1}J_{C\text{-}H}$ = 126.7}, 29.0 ($O_2C\mathit{C}H_2SiMe_3$, t, $^{1}J_{C\text{-}H}$ = 122.1), 118.7 (**3**,**7**, s), 120.1 (**1**,**5**, s), 132.6 (**4**,**8**, s), 132.8 (**2**,**6**, s), 189.9 ($O_2\mathit{C}CH_2SiMe_3$, s).

^{13}C NMR (toluene-d_8, 343 K) δ (ppm): −0.9 ($O_2CCH_2Si\mathit{Me}_3$, q, $^{1}J_{C\text{-}H}$ = 120.2), 10.1 {(**2**,**6**)-Me_2, q, $^{1}J_{C\text{-}H}$ = 126.0}, 11.6 {(**1**,**3**,**5**,**7**)-Me_4, q, $^{1}J_{C\text{-}H}$ = 128.6}, 29.3 ($O_2C\mathit{C}H_2SiMe_3$, t, $^{1}J_{C\text{-}H}$ = 120.9), 119.7 (**1**,**3**,**5**,**7**, br s, $\nu_{½}$ = 6.2), 132.9 (**2**,**6**, s), 133.0 (**4**,**8**, s), 189.9 ($O_2\mathit{C}CH_2SiMe3$, s).

X-ray data: RTC4_3.cif

7.4.4 Characterising data for Pn*Ti(κ^2-$O_2CCH_2{}^tBu)_2$ (4.4)

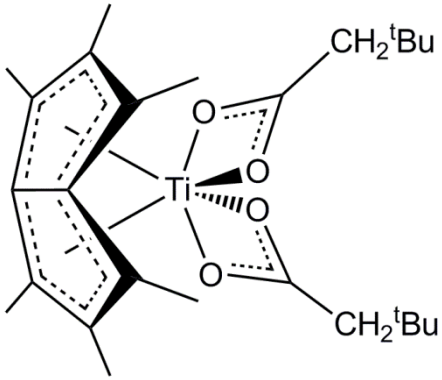

General properties: Yellow oil.

High resolution MS (EI) found (calculated): 464.2409 (464.2406).

MS (EI): *m/z* = 464 (M^+, 30%); 349 (M^+-$O_2CCH_2CMe_3$, 100%).

IR (KBr) cm^{-1}: 2958 (m), 2917 (m), 2867 (m), 1526 (s), 1457 (s), 1363 (m), 1261 (s), 1098 (s), 1022 (s), 798 (s), 751 (m), 668 (m).

^{1}H NMR (toluene-d_8) δ (ppm): 1.04 ($O_2CCH_2C\mathit{Me}_3$, 18H, s), 1.74 {(**2**,**6**)-Me_2, 6H, s}, 1.84 {(**3**,**7**)-Me_2, 6H, br s, $\nu_{½}$ = 130.0}, 2.01 {(**1**,**5**)-Me_2, 6H, br s, $\nu_{½}$ = 130.4}, 2.11 ($O_2CC\mathit{H}_2CMe_3$, 4H, s).

^{1}H NMR (toluene-d_8, 263 K) δ (ppm): 1.05 ($O_2CCH_2C\mathit{Me}_3$, 18H, s), 1.73 {(**2**,**6**)-Me_2, 6H, s}, 1.82 {(**3**,**7**)-Me_2, 6H, s}, 2.05 {(**1**,**5**)-Me_2, 6H, s}, 2.11 ($O_2CC\mathit{H}_2CMe_3$, 4H, s).

^{1}H NMR (toluene-d_8, 343 K) δ (ppm): 1.04 ($O_2CCH_2C\mathit{Me}_3$, 18H, s), 1.75 {(**2**,**6**)-Me_2, 6H, s}, 1.91 {(**1**,**3**,**5**,**7**)-Me_4, 12H, s}, 2.11 ($O_2CC\mathit{H}_2CMe_3$, 4H, s).

^{13}C NMR (toluene-d_8) δ (ppm): 10.0 {(**2**,**6**)-Me_2, q, $^1J_{C\text{-}H}$ = 127.4}, 11.6 {(**1**,**3**,**5**,**7**)-Me_4, br q, $\nu_{½}$ = 35.7}, 29.9 ($O_2CCH_2C\mathit{Me}_3$, q, $^1J_{C\text{-}H}$ = 124.4), 30.4 ($O_2CCH_2\mathit{C}Me_3$, s), 50.3 ($O_2C\mathit{C}H_2CMe_3$, t, $^1J_{C\text{-}H}$ = 125.4), 119.0 (**3**,**7**, br s, $\nu_{½}$ = 23.5), 120.6 (**1**,**5**, br s, $\nu_{½}$ = 19.6), 133.2 (**2**,**6**, s), 133.3 (**4**,**8**, s), 189.9 ($O_2\mathit{C}CH_2CMe_3$, s).

^{13}C NMR (toluene-d_8, 263 K) δ (ppm): 10.1 {(**2**,**6**)-Me_2, q, $^1J_{C\text{-}H}$ = 126.9}, 11.4 {(**1**,**5**)-Me_2, q, $^1J_{C\text{-}H}$ = 126.9}, 11.8 {(**3**,**7**)-Me_2, q, $^1J_{C\text{-}H}$ = 128.1}, 29.8 ($O_2CCH_2C\mathit{Me}_3$, q, $^1J_{C\text{-}H}$ = 124.5), 30.4 ($O_2CCH_2\mathit{C}Me_3$, s), 50.1 ($O_2C\mathit{C}H_2CMe_3$, t, $^1J_{C\text{-}H}$ = 126.5), 118.9 (**3**,**7**, s), 120.5 (**1**,**5**, s), 133.1 (**2**,**6**, s), 133.1 (**4**,**8**, s), 189.9 ($O_2\mathit{C}CH_2CMe_3$, s).

^{13}C NMR (toluene-d_8, 343 K) δ (ppm): 10.1 {(**2**,**6**)-Me_2, q, $^1J_{C\text{-}H}$ = 127.2}, 11.5 {(**1**,**3**,**5**,**7**)-Me_4, q, $^1J_{C\text{-}H}$ = 127.8}, 30.1 ($O_2CCH_2C\mathit{Me}_3$, q, $^1J_{C\text{-}H}$ = 125.6), 30.4 ($O_2CCH_2\mathit{C}Me_3$, s), 50.6 ($O_2C\mathit{C}H_2CMe_3$, t, $^1J_{C\text{-}H}$ = 125.6), 120.1 (**1**,**3**,**5**,**7**, br s, $\nu_{½}$ = 7.5), 133.3 (**2**,**6**, s), 133.5 (**4**,**8**, s), 190.0 ($O_2\mathit{C}CH_2CMe_3$, s).

7.4.5 Characterising data for Pn*Ti[κ^2-O-C(CH$_2$CMe$_3$)=C(CH$_2$CMe$_3$)-O] (4.5)

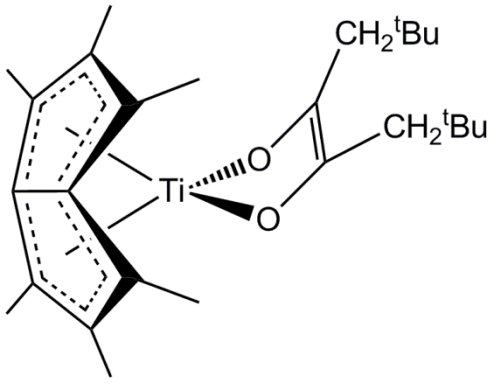

General properties: Orange air-sensitive crystalline solid.

Elemental analysis for $C_{26}H_{40}TiO_2$ (MW = 432.46): Could not be obtained due to extreme solubility of product.

High resolution MS (EI) found (calculated): 432.2503 (432.2508).

MS (EI): *m/z* = 432 (M^+, 15%); 375 (M^+-CMe_3, 100%); 319 {M^+-2(CMe_3), 20%}.

^{1}H NMR (C_6D_6) δ (ppm): 1.24 (CH_2CMe_3, 18H, s), 1.55 {(**2**,**6**)-Me_2, 6H, s}, 1.94 {(**1**,**3**,**5**,**7**)-Me_4, 12H, s}, 2.16 (CH_2CMe_3, 4H, s).

^{13}C NMR (C_6D_6) δ (ppm): 10.3 {(**2**,**6**)-Me_2, q, $^1J_{C\text{-}H}$ = 126.6}, 11.6 {(**1**,**3**,**5**,**7**)-Me_4, q, $^1J_{C\text{-}H}$ = 127.4}, 30.9 (CH_2CMe_3, q, $^1J_{C\text{-}H}$ = 125.3), 32.6 (CH_2CMe_3, s), 44.1 (CH_2CMe_3, t, $^1J_{C\text{-}H}$ = 123.5), 114.7 (**1**,**3**,**5**,**7**, s), 132.7 (**2**,**6**, s), 135.6 {[O-$C(CH_2CMe_3)$=$C(CH_2CMe_3)$-O], s}, 139.0 (**4**,**8**, s).

X-ray data: RTC4_5.cif

7.4.6 Characterising data for Pn*Ti[κ^2-O-C(CH_2SiMe_3)=C(CH_2SiMe_3)-O] (4.6)

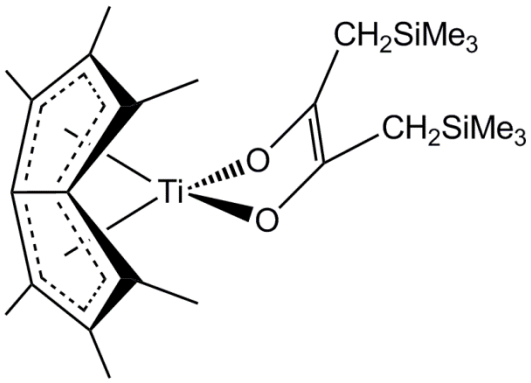

General properties: Orange crystalline solid, air-sensitive.

Elemental analysis for $C_{24}H_{40}TiO_2Si_2$ (MW = 464.61): Could not be obtained due to extreme solubility of product.

High resolution MS (EI) found (calculated): 464.2059 (464.2046).

MS (EI): *m/z* = 464 (M^+, 10%); 375 (M^+-$SiMe_3$, 10%).

^{1}H NMR (C_6D_6) δ (ppm): 0.25 (CH_2SiMe_3, 18H, s), 1.58 {(**2**,**6**)-Me_2, 6H, s}, 1.64 (CH_2SiMe_3, 4H, s), 1.96 {(**1**,**3**,**5**,**7**)-Me_4, 12H, s}.

^{13}C NMR (C_6D_6) δ (ppm): −0.3 ($CH_2Si\mathit{Me}_3$, q, $^1J_{C\text{-}H}$ = 118.5), 10.3 {(**2**,**6**)-Me_2, q, $^1J_{C\text{-}H}$ = 126.1}, 11.6 {(**1**,**3**,**5**,**7**)-Me_4, q, $^1J_{C\text{-}H}$ = 126.1}, 21.4 ($\mathit{C}H_2SiMe_3$, t, $^1J_{C\text{-}H}$ = 118.5), 114.2 (**1**,**3**,**5**,**7**, s), 132.5 (**2**,**6**, s), 132.9 {[O-C(CH_2SiMe_3)=C(CH_2SiMe_3)-O], s}, 138.8 (**4**,**8**, s).

7.4.7 Characterising data for {Pn*Ti[μ-η^1(O):η^2-OC(Me)$_2$]}$_2$ (4.7)

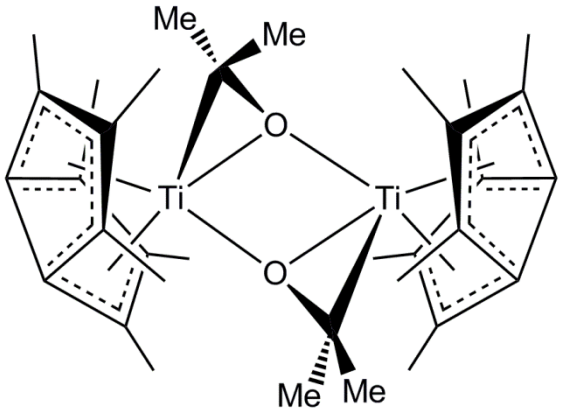

General properties: Orange-red air-sensitive crystalline solid.

Elemental analysis for $C_{34}H_{48}Ti_2O_2$ (MW = 584.48): Could not be obtained due to small scale of reaction and problems with large scale synthesis.

High resolution MS (EI) found (calculated) for Pn*TiOC(Me)$_2$: 292.1308 (292.1307).

MS (EI): *m/z* = 292 (M^+/2, 5%); 186 (M^+/2-Ti-OC(Me)$_2$, 30%).

^{1}H NMR (C_6D_6) δ (ppm): 1.13 (OCMe_2, 12H, s), 1.82 {(**2**,**6**)-Me_4, 12H, s}, 2.02 {(**1**,**7**)-Me_4, 12H, s}, 2.14 {(**3**,**5**)-Me_4, 12H, s}.

^{13}C NMR (C_6D_6) δ (ppm): 11.2 {(**2**,**6**)-Me_4, q, $^1J_{C\text{-}H}$ = 126.3}, 13.2 {(**1**,**7**)-Me_4, q, $^1J_{C\text{-}H}$ = 126.3}, 13.4 {(**3**,**5**)-Me_4, q, $^1J_{C\text{-}H}$ = 125.7}, 29.6 (OCMe_2, q, $^1J_{C\text{-}H}$ = 126.6), 90.1 (OCMe$_2$, s), 110.5 (**1**,**7**, s), 113.7 (**3**,**5**, s), 124.1 (**2**,**6**, s), 127.9 (**4**, s), 128.9 (**8**, s).

X-ray data: RTC4_7.cif

7.4.8 Characterising data for [Pn*Ti(μ$_2$-H)]$_3$(μ$_3$-H) (4.8)

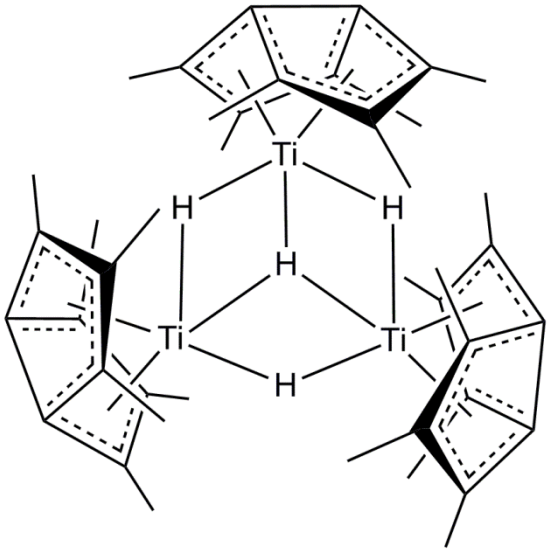

General properties: Dark purple crystalline solid, very air-sensitive.

Elemental analysis for $C_{42}H_{58}Ti_3$ (MW = 706.51): Could not be obtained due to extreme air sensitivity of product.

^{1}H NMR (C_6D_6) δ (ppm): −2.91 (Ti*H*, 4H, br s, $\nu_{½}$ = 6.5), 2.15 {(**2**,**6**)-*Me*$_6$, 18H, s}, 2.30 {(**1**,**3**,**5**,**7**)-*Me*$_{12}$, 36H, s}.

^{13}C{^{1}H} NMR (C_6D_6) δ (ppm): 12.5 {(**2**,**6**)-*Me*$_2$}, 15.7 {(**1**,**3**,**5**,**7**)-*Me*$_4$}, 112.9 (**1**,**3**,**5**,**7**), 122.6 (**2**,**6**), (**4**,**8**, not observed).

X-ray data: RTC4_8.cif

7.4.9 Characterising data for $(Pn^*TiCl)_2(\mu\text{-}O)$ (4.9)

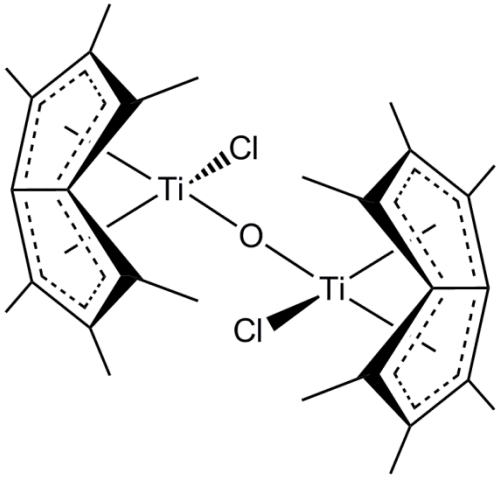

General properties: Crimson crystalline solid.

High resolution MS (EI) found (calculated): 554.1108 (554.1102).

MS (EI): *m/z* = 554 (M^+, 5%); 519 (M^+-Cl, 5%); 269 (M^+-Pn*-Ti-Cl-O, 5%).

^{1}H NMR (C_6D_6) δ (ppm): 1.79 {(**2**,**6**)-*Me*$_4$, 12H, s}, 2.01 {(**1**,**3**,**5**,**7**)-*Me*$_8$, 24H, s}.

^{13}C NMR (C_6D_6) δ (ppm): 10.9 {(**2**,**6**)-*Me*$_4$, q, $^1J_{C\text{-}H}$ = 127.2}, 12.7 {(**1**,**3**,**5**,**7**)-*Me*$_8$, q, $^1J_{C\text{-}H}$ = 127.2}, 122.6 (**1**,**3**,**5**,**7**, s), 130.3 (**2**,**6**, s), 139.1 (**4**,**8**, s).

X-ray data: RTC4_9.cif